IPP Max-Planck-Institut für Plasmaphysik

Annual Report 1998

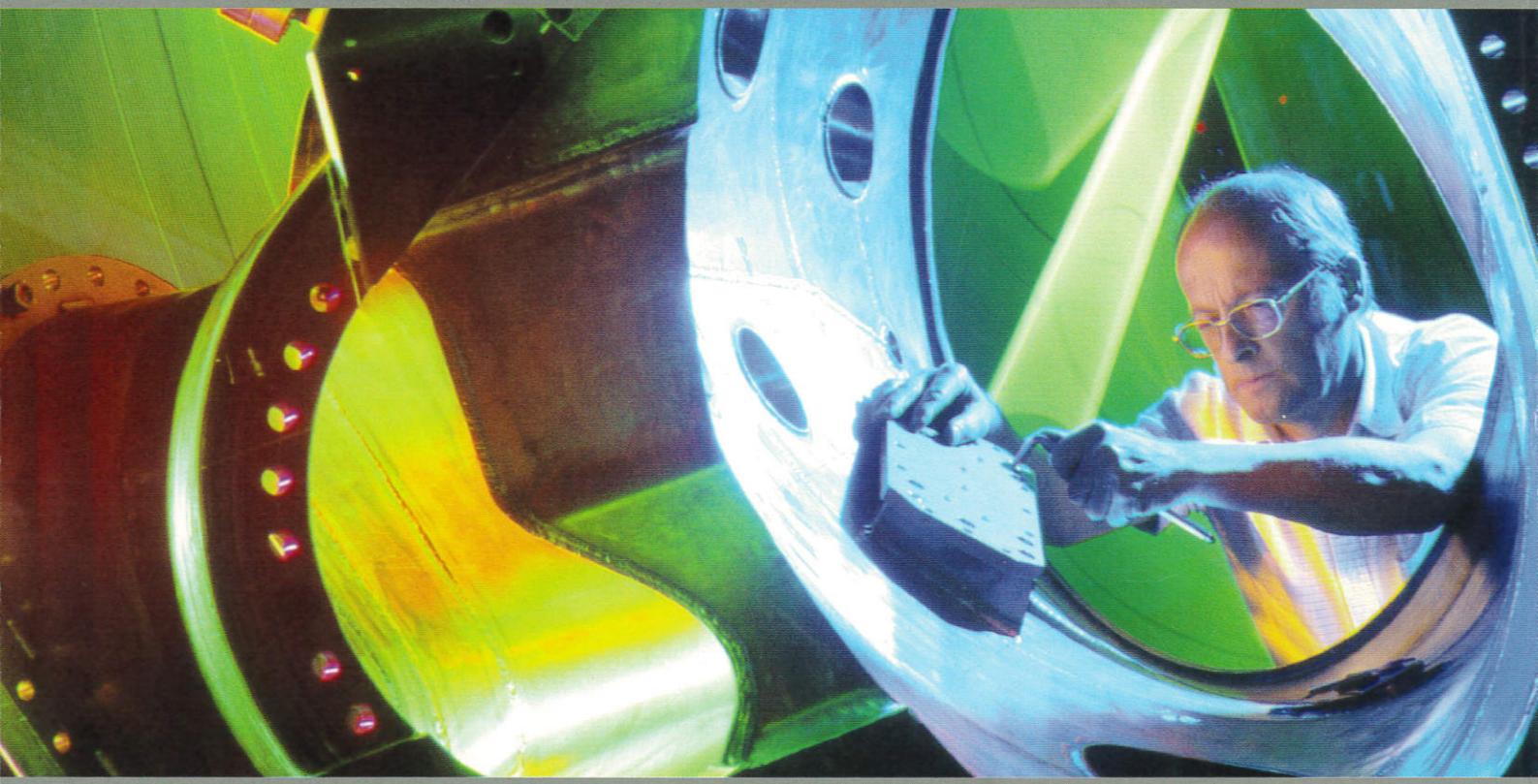

COVER ILLUSTRATION

In 1998 the stellarator experiment WENDELSTEIN 7-AS was equipped with a set of ten coils inside the torus vessel for improved control of the plasma boundary island geometry. The picture shows assembling a support structure for one of these coils in a torus model.
(Photo: Peter Ginter)

IPP

Max-Planck-Institut
für Plasmaphysik

EURATOM Association

Annual Report 1998

CONTENTS

PREFACE

Max-Planck-Institut für Plasmaphysik is investigating the two main types of fusion devices, the tokamak and the stellarator. The aim of the ASDEX Upgrade divertor tokamak is to realize a reactor-compatible divertor and study reactor-relevant plasma edge physics as well as particle and energy transport in the bulk plasma. Experiments are strongly focused on preparations for ITER: Originally mainly concerned with studies of divertor behaviour and control issues relating to ITER, ASDEX Upgrade is now also contributing to the basic understanding of instabilities and particle and energy transport in the plasma core. The new closed divertor, which is similar to that proposed for ITER, has reduced the heat load by a factor of more than two compared with the previous open divertor. In 1998 ASDEX Upgrade entered the field of "advanced tokamak" experiments: Stationary operation of a discharge combining H-mode with an internal confinement barrier was achieved for the first time. The extended heating capacity has allowed the investigation of beta-limits, which has demonstrated the basic possibility of stabilizing the neoclassical tearing modes by ECRH.

During a seven-month opening period at the WENDELSTEIN 7-AS stellarator in 1998 ten control coils were installed in the plasma vessel. As first step for divertor experiments in WENDELSTEIN 7-AS, the coils are to control resonant field structures at the plasma edge: natural magnetic islands can be enlarged, decreased or compensated. First experiments show a clear dependence of the energy content on the effective radius of the last closed flux surface. The ECRH heating power was increased by a third 140 GHz gyrotron. Thus, very high local power densities were available for current drive and heating. Central electron temperatures could be increased to 5.7 keV. Also the ICRH antenna was replaced by a new double-strap antenna in order to define the appropriate experimental antenna for WENDELSTEIN 7-X.

The follow-up experiment for demonstrating the reactor relevance of the Advanced Stellarator principle, WENDELSTEIN 7-X, will be a 5-period Helias configuration with helical divertor and superconducting coil assembly. It is to be operated at the Greifswald Branch Institute of IPP, the topping-out ceremony for its new buildings having taken place in August 1998. Technical development for WENDELSTEIN 7-X has concentrated on an advanced conductor, which was delivered by industry. Its sucessful electromagnetic testing was followed by placement of the order for the magnet system at the end of 1998. At the Low Temperature Laboratory of CEA at Saclay, where the cryogenic acceptance tests of the superconducting coils will be performed, design and setup of the test facility have started. The DEMO cryostat is approaching completion. The DEMO coil, an original-sized superconducting magnet, was manufactured and delivered to Forschungszentrum Karlsruhe to be tested in the TOSKA facility. Forschungszentrum Karlsruhe will also contribute the complete ECRH system for WENDELSTEIN 7-X.

On the national level, IPP coordinates its research effort with Forschungszentrum Karlsruhe within the "Entwicklungsgemeinschaft Kernfusion" and also with Forschungszentrum Jülich. IPP also closely cooperates with a number of German universities, the collaboration with the Universitiy of Stuttgart being particularly intensive. Cooperation with the University of Greifswald is in development. The research conducted at IPP is part of the European fusion programme: IPP is involved in JET, the joint European experiment. The ASDEX Upgrade tokamak and the stellarator concept of the WENDELSTEIN experiments provide essential information for preparing the next steps in the overall European programme. Furthermore, IPP acts as host to NET, the European reactor study group, which has been working at Garching since 1983.

Coordination of research is also worldwide in extent. IPP is party to two Implementing Agreements: the one - with the USA - covering cooperation on the ASDEX Upgrade divertor tokamak; the other - with the USA, Japan, Australia and Russia - regulating cooperation in the joint stellarator programme, to which the WENDELSTEIN experiments make a major contribution. From 1988 IPP provided the technical site for the American-European-Japanese-Soviet group responsible for the design of ITER, the International Thermonuclear Experimental Reactor. After completion of the conceptual design, IPP was also chosen in 1992 - together with the fusion laboratories in Naka and San Diego - as site for the ITER Engineering Design Phase. This was completed in July 1998 with the Final Design Report. The physics part of it was written by the different Expert Groups with strong participation of IPP scientists. The ITER partners having decided to investigate a reduced-objective, reduced-cost version, IPP is still one of the hosts for the detailed technical design activities scheduled for the three-year period from 1998 to 2001.

Klaus Pinkau

Projects

TOKAMAKS

A large part of the capacity at IPP is devoted to investigating confinement in the tokamak configuration. IPP pioneered the divertor principle with the ASDEX tokamak, which demonstrated the favourable impurity control capabilities of this configuration and discovered the so-called H-regime of improved energy confinement. The divertor configuration has also been adopted for ITER, and ASDEX Upgrade, IPP's successor experiment to ASDEX, closely resembles a scaled-down version of ITER.

As a consequence, experiments on ASDEX Upgrade are strongly focused on the critical R&D tasks for ITER. Originally, this implied mainly studies of divertor behaviour and control issues relating to its ITER-like configuration. With the enhancement and diversification of its heating and particle control systems and the extension of its diagnostic capabilities, ASDEX Upgrade is now in addition also strongly contributing to the basic understanding of magnetohydrodynamic instabilities and particle and energy transport in the plasma core. After detection of the strong correlation of the properties of the plasma edge and core this extension of the research to core physics has become even more important. In addition ASDEX Upgrade entered in 1998 the field of socalled "advanced tokamak" experiments. After a very short time of operation for the first time a discharge with a H-mode barrier and an internal confinement barrier was established stationary for about 40 energy confinement times.

In all areas the experimental work is accompanied by strong theoretical effort, with, in particular, IPP's divertor theory effort also constituting the main modelling input to the ITER design. First-principle-based fluid turbulence studies for clarifying transport in the outer regions of the bulk plasma are a further area of excellence of IPP. MHD stability phenomena have become a further focal point of our theoretical efforts due to the increasing importance of high-β scenarios for ASDEX Upgrade and steady-state tokamak reactor operation.

During 1998, ASDEX Upgrade operated with the extended NBI heating power capability of $P_H \leq 20$ MW. With this heating power, the characteristic number P_H/R_0 is the highest in Europe and comes closer to the ITER value. ECRH was operated with heating powers of 0.8 MW and ICRH up to 5.7 MW. The operation with a high-field-side pellet injector system, which has achieved outstanding results.

One focal point of the ASDEX Upgrade activities in 1998 was the investigation of the new LYRA divertor. This divertor with its narrow "W" shape is very similar in its relative dimensions to the proposed ITER divertor. The Lyra divertor heat load is reduced by more than a factor of two compared with the previous open divertor under comparable conditions.

Outstanding physics results of ASDEX Upgrade in 1998 were:

- A reduction of the divertor heat load in the LYRA divertor was observed. It could be related to an increase of the divertor radiation by carbon and hydrogen.
- Another focal point was the operation at high density close to the Greenwald limit. High density discharges were characterized by temperature and density at the plasma boundary. An extension of the operation regime was obtained by pellet injection from the high field side.
- The extended heating capacity allowed the investigation of β-limits practically under all conditions. A special investigation was devoted to the neoclassical tearing modes, which turn out to be one of the dominant limiting factors for ITER. The principal possibility to stabilize these modes by ECRH was demonstrated.
- ASDEX Upgrade started in 1998 with the investigation of advanced scenarios with reversed or flat q-profiles. The most outstanding result was the establishment of a H-mode discharge in combination with internal transport barrier stationary for about 40 energy confinement times.

In the near future (1999 and 2000) ASDEX Upgrade will have the capacity to operate with higher triangularity, a NBI system with 100 kV beam energy and start first current drive experiment with our ICRH system. For the following time period the NBI system will partly by turned into the tangential direction for current drive, the reactive power ov the power supply will be compensated to allow longer pulses, and the divertor will be adopted to higher triangularity.

ASDEX Upgrade maintains fruitful collaborations with the following institutions: Forschungszentrum Jülich; Inst. für Plasmaforschung, University of Stuttgart; University of Kiel; University of Magdeburg; University of Düsseldorf; University of Augsburg University of Bayreuth; Culham Lab., Abingdon, UK; Centro de Fusão Nuclear, Lisbon, Portugal; University College, Cork, Ireland; Inst. Allgemeine Physik, TU Vienna, Austria; NCSR Demokritos, Athens, Greece; IESL-FoRTH, Heraklion, Greece; CRPP, École Polytechnique, Lausanne, Switzerland; CEA Cadarache, France; Istituto di Fisica del Plasma, CNR Milano, Italy; CREATE Group, Naples, Italy; University of Strathclyde, Scotland; FOM-Inst. voor Plasmafysica, Rijnhuizen, Netherlands; VTT Energy, Helsinki, Finland; Research Inst. for Particle and Nuclear Physics, Budapest, Hungary; Inst. of Applied Physics, Nizhni Novgorod, Russia; I.V.Kurchatov Institute of Atomic Energy, Moscow, Russia; Ioffe Institute, St. Petersburg, Russia; Technical University of Applied Physics, St. Petersburg, Russia; St.P.T.U., St. Petersburg, Russia; PPPL, Princeton, USA; GA, San Diego, USA; MIT, Cambridge, USA; Oak Ridge National Lab., Oak Ridge, USA; Sandia Labs, Livermore and Albuquerque, USA; N.Y. University, Courant Institute, USA; University of Toronto, Canada; Institute for Plasma Research, BHAT, Gandhinagar, India; Institute of Plasma Physics, Hefei, China; Korea Basic Science Institute, Yusung, Korea; National Institute for Fusion Science, Nagoya, Japan; University of Yokohama, Japan.

Besides operating its own tokamak ASDEX Upgrade, the IPP is involved in JET, the Joint European Torus at Culham (UK) since many years. In 1998, JET began with a month of operations to complete urgent ITER Physics Studies in hydrogen and deuterium. The aim was to reduce the uncertainties in extrapolations to ITER. The third stage of the JET divertor programme then started early in February 1998 with a four month shutdown for the exchange, by remote handling without manned intervention in the vessel, of the Mark IIA divertor for the Gas Box divertor (Mark IIGB). This shutdown was highly successful and provided a clear demonstration of remote handling as a method of maintenance, repair and upgrading of fusion devices. The shutdown was completed as planned at the end of May, the first plasma pulse was obtained in early July. The new divertor geometry lead to improved deuterium exhaust, more symmetric detachment and a somewhat higher density limit. Access to the H-mode has been found to be dependent on divertor geometry.

Transiently high performance has been more difficult to achieve with the Mark IIGB divertor largely due to the earlier onset of an H-mode. On the other hand, steady state operation has been easier and the ELMs have been more benign. The duration of the high performance phase has been extended by preventing excessive edge pressures by injecting krypton, argon or neon impurities to increase the edge radiation. In this way, steady state discharges with double transport barriers have been achieved for 4-5s using a continuous bleed of argon. The confinement enhancement factor relative to the ITER 89 scaling law is up to 3 and the normalised plasma pressure β_N up to 2.5 for an edge safety factor $q_{95} = 3.3$ which is a reactor relevant domain.

The IPP participates in the scientific exploitation of the JET experiment as well as gives advice and support for the design and operation of many JET plasma diagnostic systems. The cooperation with JET is organised within four Task Agreements. Besides the activities on both tokamaks to find an optimised conventional plasma discharge scenario for the next-step device ITER, a new Task Agreement Study of Advanced Tokamak Scenarios has been called into being. Within this Task Agreement the IPP contributes to the development and optimisation of JET configurations with optimised shear leading to the formation of internal transport barriers. The IPP gives support to JET especially to develop fuelling schemes by Pellet injection for such discharges as well as to control the transport barrier with edge radiation. These experimental activities are accompanied by MHD stability analysis as well as by transport code modelling.

The results of JET, IPP and, in general, the world-wide tokamak programme formed the groundwork for planning an experimental reactor as a next step. The European Union, Japan, the USA and Russia have agreed to prepare this next step as a joint venture. The EDA effort was completed in July 1998 and its results were documented in the Final Design Report. The physics part was written by the different expert groups with strong participation of IPP scientists.
After completation of the engineering design activity, the ITER partners have decided to investigate a reduced objective, reduced cost version, and to carry through its detailed technical design during a three-years period 1998–2001. The USA has decided to participate only in the first year of this effort. These studies, initiated in 1998, have shown that a device, capable to reach Q = 10 (i.e. a 10–fold amplification of the externally supplied heating power by fusion reactions) could be constructed for about 50% of the cost of the FDR-ITER, using the same physics assumptions which predict full ignition for the latter device. This performance would suffice to satisfy a strategic aim of ITER, namely to constitute a single device generation before demonstration of long pulse tokamak operation with controlled plasma current profiles ("advanced mode" operation - see section on ASDEX Upgrade) and has, furthermore, pointed out an operation scenario, where also the reduced size of ITER could reach full ignition. On of the main differences between the FDR and the reduced size ITER consists thus in the fusion power level whereas the FDR-device would have arrived in the range of full power-producing reactors (1.5 GW thermal), the reduced size ITER is rated at approximately 500 MW.

ASDEX UPGRADE PROJECT

(Head of Project: Dr. Otto Gruber)

Experimental Plasma Physics Division E1: C. Aubanel, H. Bauer, K. Behler, M. Bessenrodt-Weberpals, H. Blank, H.-S. Bosch, R. Brückner, B. Brüsehaber, K. Büchl, A. Buhler, A. Cierpka, C. Dorn, R. Drube, J. Ernesti, H.-U. Fahrbach, J.C. Fuchs, K. Förster, O. Gehre, J. Gernhardt, D. Gonda, O. Gruber, E. Gubanka, A. Gude, G. Haas, M. Harnau, G. Herppich, A. Herrmann, H. Hohenöcker, G. Hussong, T. Härtl, D. Jacobi, S. Kamm, E. Kaplan, M. Kaufmann, H. Klement, H. Kollotzek, B. Kurzan, G. Kölbl, P.T. Lang, R.S. Lang, A. Lorenz, H. Maier, M. Maraschek, K.F. Mast, K. Mattes, D. Meisel, R. Merkel, V. Mertens, H. Murmann, H.W. Müller, M. Münch, G. Neu, E. Oberlander, M. Pflug, G. Prausner, G. Raupp, G. Reichert, V. Rohde, H. Röhr, M. Sator, H.-B. Schilling, G. Schramm, G. Schrembs, S. Schweizer, U. Seidel, S. Sesnic, Ch. Sihler, K.-H. Steuer, A. Stimmelmayr, J. Stober, B. Streibl, W. Suttrop, W. Treutterer, M. Troppmann, W. Ullrich, M. Ulrich, G. Weber, R. Wolf, D. Zasche, T. Zehetbauer

Guests in Division E1: S.M. Egorov, Technical University, Plasma Physics Department, St. Petersburg, CIS;
P. Fu, L. Hu, Y. Zhu, Academia Sinica, Hefei, China;
S. Saarlema, VTT, Finland;
H. Weitzner, N.Y. University, USA;

Tokamak Physics Division: G. Becker, A. Bergmann, D. Biskamp, K. Borrass, M. Brambilla, A. Carlson, D. Correa-Restrepo, D. Coster, W. Feneberg, S. Günter, K. Hallatschek, B. Janauschek, F. Jenko, O. Kardaun, K. Lackner, D. Lortz, P. Martin, R. Meyer-Spasche, J. Neuhauser, G. Pautasso, A.G. Peeters, S. Pinches, W. Sandmann, S. Schade, R. Schneider, W. Schneider, E. Schwarz, J. Schweinzer, B. Scott, H. Tasso, Ch. Tichmann, R. Wunderlich, H.P. Zehrfeld, A. Zeiler

Guests in Tokamak Physics Division: B. Braams, New York University, N.Y., USA;
S. Kalvin, G. Veres, KFKI, Budapest, Hungary;
V. Rozhansky, A. Ushakov, S. Voskoboynikov, LPI, St. Petersburg, CIS;
R. Brandenburg, IAP, Vienna, Austria;
A. Celani, CNR, Italy;
J.-H. Han, KBSI, Korea;
J. Drake, Institute of Plasma Research, Maryland, USA;
I. Bandophodaya, Gandhinagar, India;
Khudoleev, IOFFE, St. Petersburg, CIS;
Q. Yu, Academia Sinica, Hefei, China;

Experimental Plasma Physics Division E4: A. Bard, K. Behringer, D. Bolshukhin, S. de Peña Hempel, R. Dux, W. Engelhardt, J. Fink, J. Gafert, A. Geier, A. Kallenbach, H. Meister, R. Neu, R. Pugno, H. Salzmann, D. Schlögl.

Technology Division: W. Becker, M. Beckmann, F. Braun, H. Brinkschulte, M. Ciric, H. Faugel, R. Fritsch, D. Hartmann, B. Heinemann, F. Hofmeister, W. Kraus, F. Leuterer, F. Monaco, M. Münich, J.-M. Noterdaeme, S. Obermayer, F. Probst, S. Puri, R. Riedl, F. Ryter, W. Schärich, E. Speth, A. Stäbler, O. Vollmer, F. Wesner, R. Wilhelm, K. Wittenbecher.

Berlin Division: G. Fussmann, H. Kastelewicz, M. Laux, U. Wenzel.

Computer Science Division: H. Friedrich, P. Heimann, F. Hertweck, J. Maier, M. Pacco-Düchs, U. Schneider-Maxon, C. Tichmann, R. Tisma, M. Zilker, H. Richter.

Surface Physics Division: K. Krieger, J. Roth, A. Tabasso.

Stellarator Division: H. Greuner.

Central Technical Services: M. Balden, R. Ammer, H. Eixenberger, F. Gresser, E. Grois, M. Kluger, H. Kosniowski, J. Kutsch, R. Kutzner, S. Mukherjee, J. Perchermeier, R. Zickert

University of Cork, Ireland: P. McCarthy.

IPF University of Stuttgart: I. Altmann, G. Dodel, W. Förster, J. Gafert, G. Gantenbein, K. Hirsch, E. Holzhauer, H. Jentschke, P.G. Schüller, K. Schmidtmann, U. Schumacher, J.P. Meskat, G.A. Müller, B. Plaum, H. Zohm.

IPP Kernforschungszentrum Jülich: H. Euringer, J. Linke, M. Sauer, M. Scherer, R. Uhlemann.

Centro de Fusão Nuclear, Lisbon, Portugal: L. Cupido, V. Grossmann, C. Loureiro, M.-E. Manso, L. Meneses, I. Nunes, J. Santos, F. Serra, A. Silva, P. Varela, S. Vergamoto.

NCSR Demokritos, Athens, Greece: G. Kyriakakis, P. Theodoropoulos, N. Tsois, P. Xantopoulos.

TEKES (HUT and VTT), Finland: J.A. Heikkinen, T. Kiviniemi, T. Kurki-Suonio.

University of Augsburg: B. Heger, H. Paulin, U. Fantz.

1. OVERVIEW

1.1 Scientific Aims and Operation

The ASDEX Upgrade non-circular tokamak programme has largely been concerned with edge and divertor physics in the high-power H-mode regime with the aim of identifying and optimizing ways for safe power exhaust and particle control (ash removal). Additionally, during the last few years, core physics, confinement and performance related, have played an increasingly important role. Especially edge-core interaction has been the subject of pioneering work in ASDEX Upgrade. The edge operational diagram introduced by ASDEX Upgrade characterizes different edge operating conditions for L- and H-mode in connection with the ballooning and density limits. MHD stability and β limits as well as the avoidance and mitigation of disruptions have been further main topics. Investigation of scenarios and physics of advanced tokamak plasma concepts has also just started.

Here the similarity of ASDEX Upgrade to ITER in poloidal field coil system and divertor configuration makes it particularly suited to testing control strategies for shape, plasma performance and mode stabilization. Additionally, the similarity in cross-section to other divertor tokamaks is important in determining size scalings for core and edge physics. This collaborative work, including extrapolation to ITER parameters, has continued with emphasis on the confinement scaling and L-H transition.

The physics programme of 1998 was based on the conclusions and findings of the last years and the ITER requirements. A strong reduction of maximum heat flux to the target plates was found in the closed divertor II LYRA and modelled with the B2–Eirene code. The onset condition of neoclassical tearing limiting the achievable β and their feedback stabilization by using phased ECR heating and current drive was another main item. Emphasis was placed on high density operation close to the Greenwald density with gas-puffing and pellet injection from the high field side, and the H-mode confinement degradation approaching this density limit.

For the first time, scenarios and physics of advanced tokamak plasma concepts leading to stationary operation and enhanced performance were investigated. These "advanced tokamak" concepts are characterized by a high fraction of bootstrap current and external current drive. Alignment of the internal transport barrier with the optimal shear profile and the compatibility of this new idea with stationary operation at high power and, simultaneously, a cold divertor will be one of the key elements of the ASDEX Upgrade programme.

Finally, the ASDEX Upgrade programme is imbedded in a framework of national (IPF Stuttgart, University of Augsburg, see also section University contributions to IPP programme) and international collaborations (see section International Cooperation).

In 1998 ASDEX Upgrade has been operated with the Div II installation, "LYRA", and with a cryopump (100 m^3/s pumping speed, see section 2). While Div I used flat target plates (covered with fine-grain graphite) close to the X-point to benefit from the large flux expansion there, Div II has vertical, lyra-shaped targets to reflect the neutrals created at the target preferentially towards the power-conducting sheath close to the separatrix, and to make the target heat load distribution as homogeneous as possible. This closed divertor is capable of handling heating powers up to 20 MW or P/R of 12 MW/m.

At the same time, the heating systems were substantially upgraded. For neutral beam injection of D^0 at 60 keV, two injector boxes provide a total NBI power of 20 MW in D^0 and 14 MW in H^0. The scaling parameter P/R for divertor discharges now reaches values of about 12 MW/m. This heating power allowed β limit and MHD stability studies with toroidal fields of up to 3 T and extended H-mode studies in hydrogen. In the shut down period from mid August to end November the beam energy of the second injector was upgraded to 100 kV in deuterium. The ICRH system was equipped with 3 db couplers to enhance the system efficiency in ELMy plasmas, allowing now coupling of the full power of 5.7 MW (see section 5). The ECRH system consists of two gyrotrons with a power of 0.8 MW for 2 s, allowing stabilization of neoclassical modes (see section 4), and transport studies. The pellet injection system was modified to allow pellet injection from the high-field side (HFS) now also with a centrifuge (see section 5).

1.2 Summary of Main Results

The most important observation in the Div II geometry is a strongly distributed power flux to the surrounding structures both during ELM and ELM-free phases. Even with a heating power of 20 MW the maximum local heat flux density in the strike point region stays below 5 MW/m^2. The origin of this reduction by more than a factor of about two compared with Div I is a larger fraction of divertor radiation (up to 50% of the heating power) due to increased cooling by hydrogen and carbon radiation in this divertor geometry. This result is in agreement with B2–Eirene simulations and may have a strong influence on future divertor designs (section 2).

At medium densities in the H-mode, the type-I ELM behaviour shows no dependence on the heating method (NBI, ICRH). ASDEX Upgrade-JET dimensionless identity experiments showed compatibility of the L-H transition with core physics constraints, while in the H-mode confinement inconsistencies with the invariance principle were established (section 8). At high densities close to the Greenwald density the influence of divertor detachment on separatrix parameters and increasing edge transport lead to limited edge densities and, due to MHD limited edge pressures, finally temperatures below the critical edge temperature for H-mode. This results in an upper H-mode density limit with gas-puff refuelling. The H-mode confinement degradation approaching this density limit is caused by the ballooning mode limited edge pressures in combination with a "stiff" temperature profiles relating core and edge temperatures. Repetitive high-field side pellet injection allows for H-mode operation well above the Greenwald density, and moreover higher confinement than with gas fuelling is found up to the highest densities (section 5).

Neoclassical tearing modes limit the achievable β depending on the collisionality at the resonant surface. In agreement with the polarization current model the onset β is found to be proportional to the ion gyro-radius in the collisionless regime, while higher collisionalities are stabilizing. The fractional energy loss connected with saturated modes at high pressures is about 25%. Reduction of neoclassical mode amplitude and increase of β was demonstrated by using phased ECR heating and current drive in the islands O-point (section 4).

Most remarkable results were achieved in advanced tokamak scenarios showing strongly reduced core transport with flat shear profiles and $q(0) \geq 1$ or with reversed shear and $q_{min} > 2$. These shear profiles were created by freezing the current profile with "early" heating during current ramp-up, which was followed by stronger central heating with up to 10 MW NBI in the flattop. A stationary H-mode scenario with internal transport barriers for ions, electrons, particles and toroidal momentum, $H_{ITER-89P} = 2.4$ and $\beta_N = 2.0$ was maintained for 40 confinement times and several internal skin times. The highest $n_i T_i \tau_i$ values of 8×10^{19} keV s m-3 (for 1 s) observed so far in ASDEX Upgrade were obtained in these discharges. Attempts to increase β_N were limited by either (3,2) neoclassical tearing modes in the case of flat q profile or (2,1) mode with reversed shear profile when approaching $q_{min} = 2$ (section 3).

1.3 ASDEX Upgrade Programme in 1999

Next year the main emphasis will be on the influence of the plasma shape triangularity on both "conventional" H-mode and "advanced" tokamak scenarios. Higher triangularities are advantageous for both scenarios in terms of higher confinement, enhanced MHD stability and, therefore, higher β values. These equilibria can be already run in the Div II with the outer strike point on the roof baffle, which was modified in the summer shutdown 1998 to use tilted CFC tiles. In parallel, the ICRH antennae were moved toroidally outward to allow separatrix triangularities up to δ = 0.45. In these configurations plasma currents up to 1 MA are possible according to poloidal field and power supply capabilities.

Core physics studies will continue with the investigation of plasma performance (energy and particle transport, MHD-instabilities and their stabilization using ECRH and ECCD). Regarding energy transport the relation between core and edge and their reciprocal influences, profile resilience, transport barrier physics, dimensionless scalings (manly in connection with JET) and heat wave studies are envisaged. Particle transport and density limits remain a substantial part of our effort, including the promising refuelling by pellet injection from the high field side.

While these high δ plasma shapes will suffer from the more perpendicular inclination of the SOL to the target (similar to Div I) and a reduced pumping capability, an adaptation of the divertor to the higher triangular plasma shapes is envisaged for 2000/1. In parallel, the provision for off-axis current drive is made to sustain and control flat or reversed shear profiles in advanced mode operation. This can be achieved in a flexible way by mode conversion CD (available at the beginning of 2000 with our ICRH system) and NBCD using tangential injection (preferential support for turning one of the existing injectors was approved in 1998). To get stationarity on the transport and MHD time scales and to approach the skin time, a flattop time of 10 s should be sufficient, requiring a reactive power compensation for the generator EZ3 (preferential support was approved in 1998).

In the following sections 2-6 the topics divertor physics, advanced tokamak operation, neoclassical tearing modes and their stabilization, H-mode operation at high densities and ICRH heating are presented. In section 7 the ASDEX Upgrade technical systems, control, data processing and heating systems are described. Section 8 deals with additional results concerning the plasma core, while section 9 is particularly devoted to the SOL/divertor conditions. The progress in diagnostic development is given in section 10.

2. DIVERTOR TARGET LOAD AND CARBON RADIATION

After more than one year of operation of the new divertor (LYRA) on ASDEX Upgrade, it is appropriate to take this opportunity to review its performance. With the doubling of the NBI heating power to 20 MW, it was expected that the old divertor configuration (Div I/Fig. 2.1, top) would not be able to handle the increased heating power without unduly compromising operational flexibility. It was in this light that the new

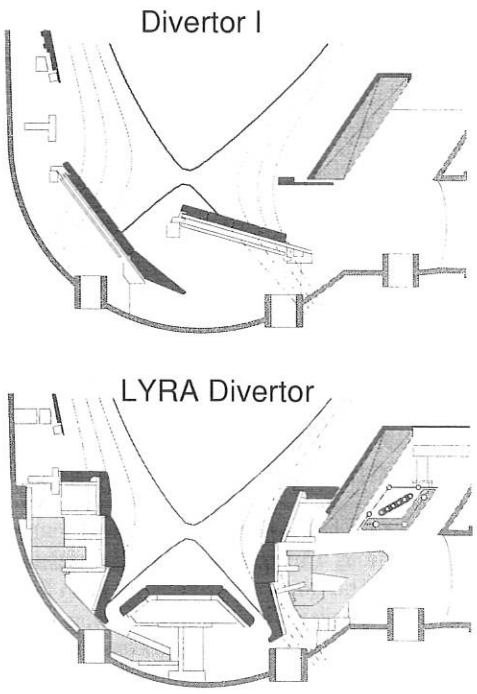

FIG. 2.1: Poloidal cross-section of ASDEX Upgrade with Div I (top) and Div II in the LYRA configuration (bottom). Div II consists of the so-called inner and outer retention, transition and strike point modules (from top to bottom), with the roof baffle in between.

divertor was designed. Since it incorporated some of the features of the proposed ITER divertor design, its performance would also be a way of verifying the design and the methodology behind it. The old divertor used fine-grain graphite target plates. The inner target was nearly perpendicular to the flux surfaces, and the outer target was positioned near the X-point (to benefit from flux expansion) and was inclined so that neutrals generated at the separatrix strike point by recycling were reflected away from the strike point towards the pumping duct. The new divertor (Fig. 2.1, bottom) uses CFC target plates aligned so that generated neutrals are reflected towards the high-power zone near the separatrix, and pumping is done through the private flux region. With more than a year's results analysed, the new divertor has performed exceptionally well - even better than expected in some ways: at the same input power and line-averaged density, there is a factor of more than two decrease in the target power flux density; the target power density for a 15 MW shot with the new divertor configuration is only marginally higher than a 5 MW shot with the old divertor configuration (Fig. 2.2). In order to try and understand the reason for this, a series of shots was performed and subsequently modelled with B2-Eirene. The shot sequence is identified in Fig. 2.4. Time traces for the reference discharge are shown in Fig. 2.5. This choice of experimental conditions was made

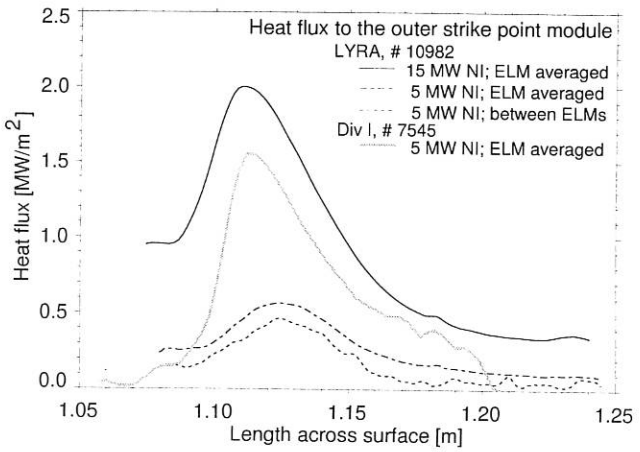

FIG. 2.2: Heat flux to the outer strike point module measured by infrared thermography.

to explore the effects of: (1) geometry (old versus new divertor); (ii) input power (variation by a factor of six); (iii) plasma current; and (iv) density.The B2-Eirene simulation results reproduced the experimental results well (Fig. 2.6) and provided an explanation for the better than expected behaviour in the new divertor configuration. The main part of the explanation for the better than expected performance is to be found in the increased divertor radiation seen with the LYRA divertor. Whereas the main chamber radiation remained nearly constant, the radiation in the divertor region approximately doubled when going from the old to the new divertor configuration (Fig. 2.3). If the plasma temperature at the target is near (or below) 2 eV, then the hydrogen or deuterium particle flux is nearly proportional to the target energy flux, though there is a flux dependence at the highest flux levels. This target energy flux is equal to the input energy flux (provided mainly by NBI) less the radiated energy.

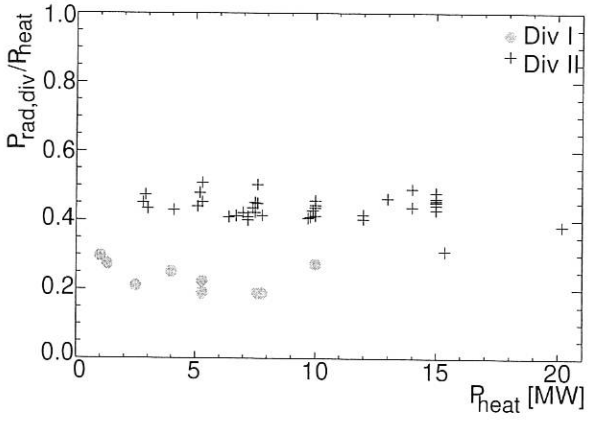

FIG. 2.3: The fraction of radiation losses inside the divertor is doubled for the LYRA divertor.

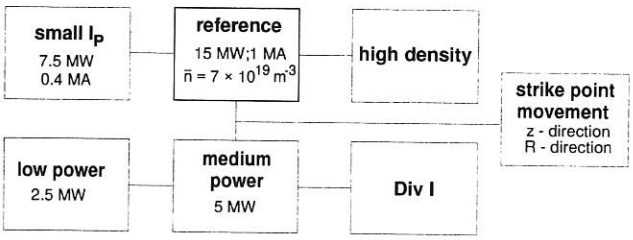

FIG. 2.4: Scheme of the parameter variation for ELMy H-mode conditions. The reference discharge has the toroidal field $B_t = -2.5\ T$ and plasma current $I_p = 1\ MA$, $q_{95} = 4$.

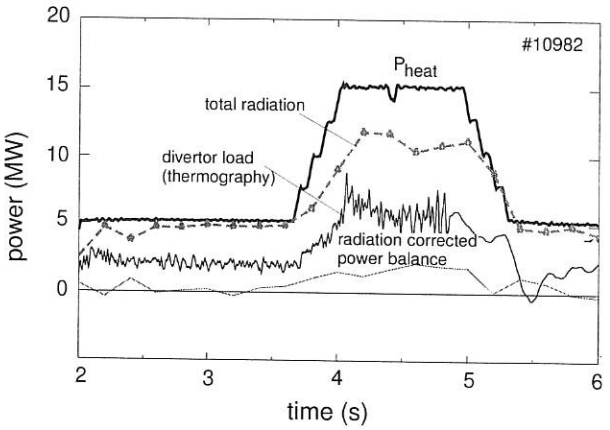

FIG. 2.5: Time traces of the reference discharge with two heating power plateaus at 5 and 15 MW. $D^0 \rightarrow D^+$ NBI, $I_p = 1\ MA$, $B_t = -2.5T$, $q_{95} = 4$.

The energy radiated in the divertor is a function of the electron density, the electron temperature and the number of radiating atoms or ions. In the 2 eV temperature range most of the carbon impurities arise from chemical sputtering and not physical sputtering, and are released in direct proportion to the incident hydrogen or deuterium flux, and hence to the energy flux. The carbon produced then radiates in the divertor, lowering the energy flux to the targets and resulting in the divertor radia-

tion being approximately proportional to the input power (Fig. 2.7). This mechanism would, of course, apply to both the new and old divertor configurations. Why the difference? As mentioned earlier, the new divertor configuration reflects recycling neutrals towards the separatrix, usually the part of the plasma carrying the highest power flux density. These neutrals provide additional losses in this region and also raise the density. This lowers the temperature at the target close to the separatrix and brings us into the favourable sub-2 eV temperature regime. In contrast to this, the old divertor configuration directed the neutrals away from the separatrix. The LYRA divertor would thus be expected to be in the favourable regime for a wider range of experimental conditions than the old divertor configuration, an expectation supported by the modelling shown in Fig. 2.8 The new divertor has performed very well with reduced target power fluxes in comparison with the old configuration, which can be ascribed to increased divertor radiation. A carefully crafted experimental campaign in conjunction with modelling provided an explanation for the increased radiation in terms of impurity radiation caused by chemically sputtered carbon and the lowered temperatures at the target arising from target inclination.

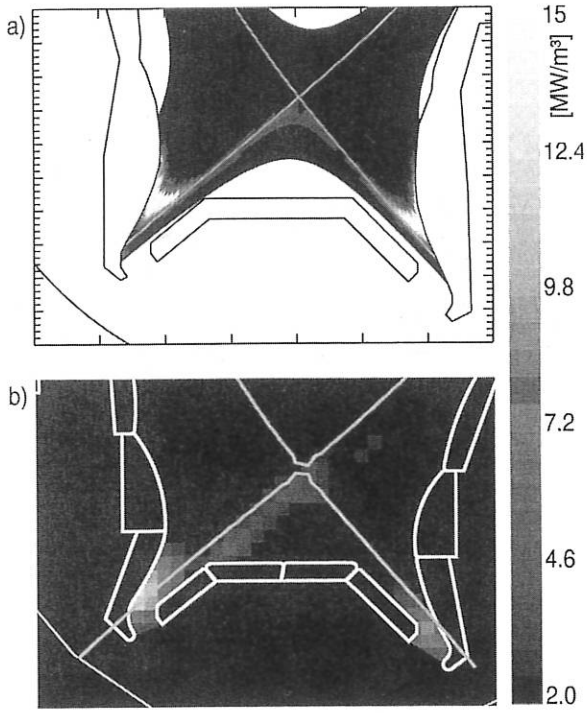

FIG. 2.6: a) B2-Eirene modelling of the radiation pattern predicts radiation bands between the X-point and strike points. b) Reconstructed radiation pattern using virtual lines of sight during vertical shift of the plasma reveals a narrow radiation zone from the inner strike point to the X-point. A corresponding band at the outer strike point cannot be detected due to missing bolometer lines of sight. $P_{heat} = 5$ MW.

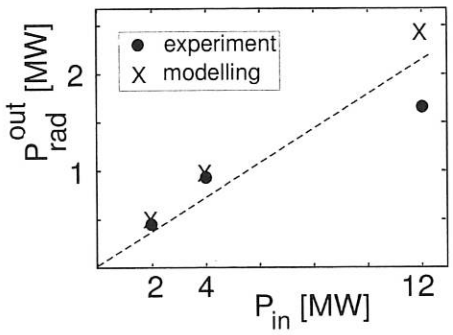

FIG. 2.7: Divertor radiation versus input power from the experiment and the B2-Eirene modelling with deuterium and carbon.

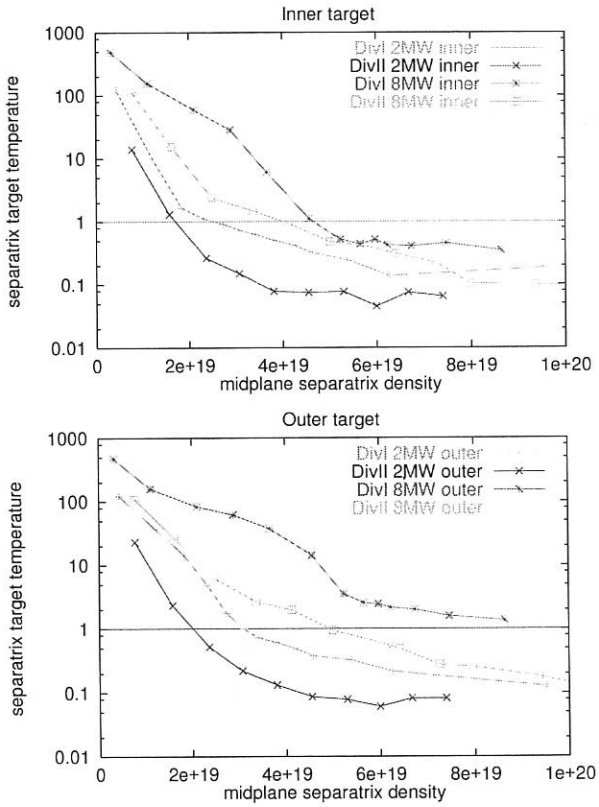

FIG. 2.8: B2-Eirene modelling results showing the predicted separatrix target temperature as a function of the upstream density for the inner and outer divertors for pure hydrogen simulations of both the old and new divertor configurations.

3. ADVANCED TOKAMAK OPERATION

3.1 Introduction

Improved confinement relating to modification of the current profile was observed in several tokamaks. Common to these regimes of operation is the flattening of the central current profile corresponding to a zero or even negative value of the central magnetic shear ($s = \frac{r}{q}\frac{dq}{dr}$, where q is the safety factor). There is increasing evidence that, in addition to magnetic shear

stabilization, a combination with $\mathbf{E} \times \mathbf{B}$ shear stabilization is required for initiating internal transport barriers (ITB). In most experiments additional heating in the current ramp phase is used to reduce current diffusion and hence generate a broad or hollow current profile with q > 1. Two types of discharges with ITBs can be distinguished: (1) By avoiding an early H-mode transition ITBs are established with edge plasma parameters comparable to L-mode. (2) The second regime of operation combines improved core confinement with an H-mode edge.

On ASDEX Upgrade, various operating scenarios have been investigated to achieve improved core confinement by modifying the current density profile by means of early additional heating in the current ramp at low initial density ($\overline{n}_e < 3 \times 10^{19} m^{-3}$), thereby strongly increasing the central electron temperature. While the current is still penetrating into the plasma, starting from a skin current profile, reduction of the current diffusion due to decreased resistivity leads to flat or even inverted q-profile.

In discharges with limiter configuration, to avoid the H-mode transition, ITBs with plasma edge parameters comparable to L-mode were obtained transiently, which are distinguished by steep pressure gradients in the barrier region. At a neutral beam power of 5 MW central ion temperatures of up to 15 keV have been reached, corresponding to ion thermal conductivities at neoclassical level. Discharges with improved core confinement and H-mode edge, which exhibit more moderate gradients, but under steady-state conditions, have been produced. Central values of T_i = 10 keV and T_e = 6.5 keV could be maintained for 6 s, only limited by the given duration of the neutral beam injection, which corresponds to 40 confinement times or 2.5 resistive time scales for internal current diffusion. In this regime of operation, not only the ion thermal conductivity approaches the neoclassical value, but also the electron transport is significantly reduced.

3.2 Improved Core Confinement with L-Mode Edge

Applying 5 MW of neutral beam heating in a current ramp of 1 MA/s, which is the maximum possible at ASDEX Upgrade, and at the same time avoiding the H-mode transition by using a limiter configuration, produced ITBs obtained reaching central values of T_e = 5 keV and T_i = 15 keV. The confinement enhancement factor of $H_{ITER89-P}$ = 1.9 and normalized beta of β_N = 1.6 are limited by the radial extent of the barrier region ($\rho_{tor} \leq 0.5$). In Fig. 3.1 the profiles of temperature, density, and toroidal rotational velocity of such a discharge with L-mode edge and ITB are shown. Associated with the high ion temperatures are rotational velocities of up to 370 km/s.

Transport analysis with the ASTRA 1–1/2–D code gives ion thermal conductivities at neoclassical values in the plasma core (Fig. 3.2a). The plateau in T_i leads to a rise of χ_i towards the plasma center, the uncertainty of which is large (50%), since it sensitively depends on the T_i gradient in the centre. The electron thermal conductivity is larger than χ_i, reflected in the large difference between T_i and T_e, which is only partly caused by the stronger NBI heating of the ions. The q-profile, inferred

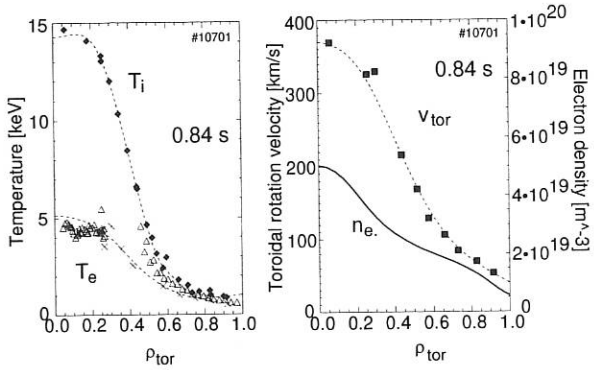

FIG. 3.1. Radial profiles of ion and electron temperatures (ECE and Thomson scattering), electron density, toroidal rotational velocity (v_{tor}) of discharge with ITB and L-mode edge, and 5 MW of NBI. The time point chosen is at maximum performance just before termination of the ITB.

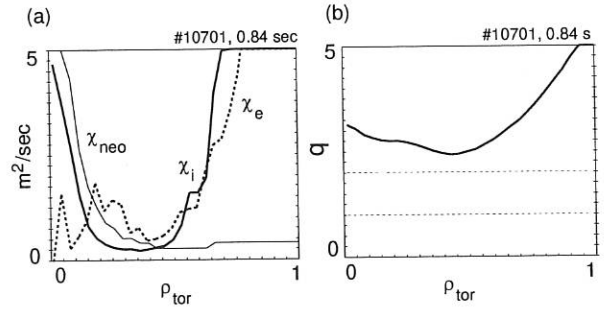

FIG. 3.2: (a) Ion and electron thermal conductivities ($\chi_{i,e}$) for discharge of Fig. 3.1 vs. normalized toroidal flux radius. Also shown is the neoclassical ion thermal conductivity (χ_{neo}). (b) Profile of safety factor.

from the transport calculations, exhibits a negative central shear region (Fig. 3.2b). Since the absolute value of the calculated q in a non-stationary plasma depends on the initial conditions, they were adjusted so that the minimum of the q-profile reaches 2 when the (2,1) mode appears.

The radial electric field, which is associated with a reduction of turbulence through sheared $\mathbf{E} \times \mathbf{B}$ flow stabilization and a subsequent improvement of confinement, was inferred from measurement of the toroidal and poloidal rotational velocities and the pressure gradient of helium using charge exchange recombination spectroscopy (CXRS). In Fig. 3.3 the formation of the ITB is illustrated. The onset of core transport enhancement at 0.761 s is accompanied by a localized spontaneous excursion of the radial electric field at $\rho \approx 0.6$ which originates from a reversal of the poloidal flow velocity. This indicates describes the change of E_r to be a causal element of the confinement bifurcation. As the flow reversal subsequently relaxes and the transport barrier moves outward (0.797 s), the diamagnetic contribution to the radial electric field cannot compensate the toroidal velocity term any longer, leading to an increase of E_r at $\rho \approx 0.2$.

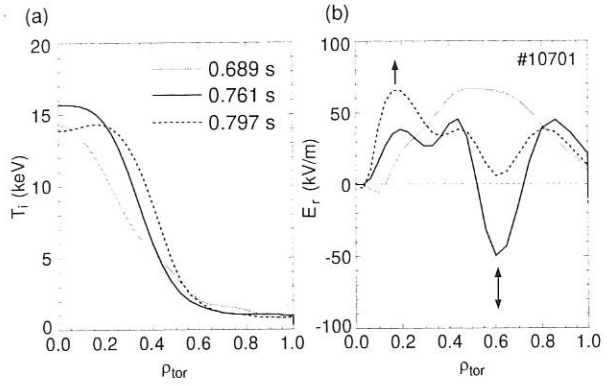

FIG. 3.3: (a) Temporal evolution of ion temperature profiles (T_i) and (b) corresponding radial electric field (E_r), derived from CXRS.

The ITBs were only of a transient nature, usually terminated by (2,1) modes, radiation collapse due to large impurity influxes, or both. By increasing the toroidal magnetic field the onset of the (2,1) mode could be delayed in time, while the ratio $B_{tor}/I_p \sim q_{95}$ stayed constant (Fig. 3.4). This indicates that, due to the constantly penetrating current, as soon as a q = 2 surface is formed, the large pressure gradients become unstable.

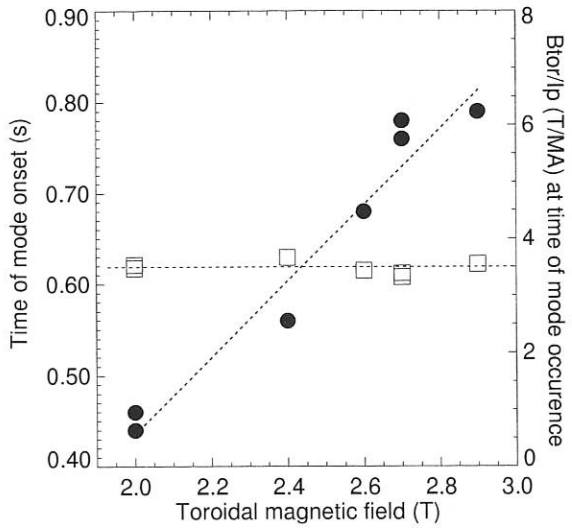

FIG. 3.4: Dependence of the onset of the (2,1) mode on the toroidal magnetic field (dots). The ratio B_{tor}/I_p (squares) stays constant.

3.3 Stationary Improved Core Confinement with H-Mode edge

A stationary regime of operation were found which shows improved core confinement of both electrons and ions in combination with an H-mode edge. In Fig. 3.5 the main plasma parameters of such a discharge are illustrated. During the current ramp of 1 MA/s moderate neutral beam heating of 2.5 MW is applied. At 1 s the X-point is formed and the L-H transition occurs. After reaching the current flat-top, the NBI power is raised to 5 MW and the line-averaged density is kept at 4×10^{19} m^{-3}. While during the current ramp at heating power 2.5 MW electron and ion temperatures increase at the same rate, T_i reaches almost twice the value of T_e when the heating power is doubled.

Central values of T_i = 10 keV and T_e = 6.5 keV, $H_{ITER89-P}$ = 2.4, and β_N = 2 are maintained for 6 s, only limited by the prescribed duration of the NBI. This corresponds to 40 confinement times or 2.5 resistive time scales for internal current redistribution, which here is the time for a current perturbation to diffuse over half of the minor radius. Current profiles from an equilibrium reconstruction using the 8-channel motional Stark effect (MSE) polarimeter are not yet available, since the implementation of the MSE data in the equilibrium code has to be completed first. However, the MSE data show that the current profile remains stationary shortly after the full neutral beam power is applied. In addition, the measured loop voltage is also stationary within 10%. The profiles of plasma temperature, density, and rotational velocity (Fig. 3.6) show, in addition to

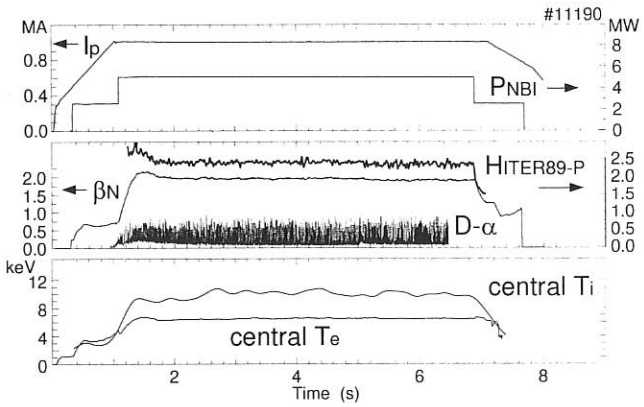

FIG. 3.5: Time evolution of plasma current (I_p), neutral beam heating power (P_{NBI}), H-factor ($H_{ITER89-P}$), normalized β (β_N), divertor D_α radiation, and central electron and ion temperatures ($T_{e,i}$) for a stationary discharge with ITB and H-mode edge. The toroidal magnetic field is B_{tor} = 2.5 T.

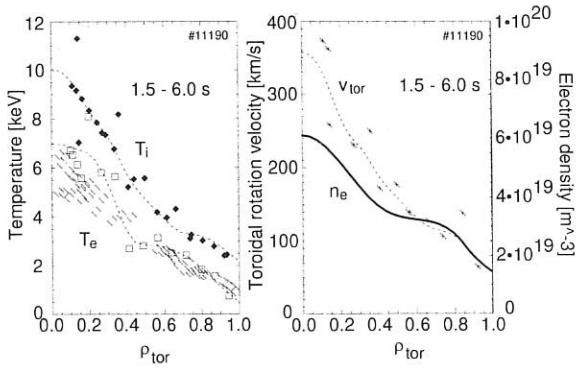

FIG. 3.6: Radial profiles of ion and electron temperatures, electron density, and toroidal rotational velocity (v_{tor}) of the discharge presented in Fig. 3.5. The profiles are the average from 1.5 to 6 s, covering most of the 5 MW heating phase.

the H-mode pedestal, an increase starting at $\rho_{tor} = 0.6$, which, compared with ASDEX Upgrade transport barriers with L-mode edge, is less pronounced. The density peaking is $n_{e0}/\bar{n}_e = 1.5$.

The only MHD activity observed in the core of the plasma are strong (1,1) fishbones which start at 1.1 s and accompany the whole 5 MW heating phase, indicating that a q = 1 surface is present in the plasma. The plasma edge is that of an ELMy H-mode, as seen on the D_α-trace.

The fishbone oscillations seem to behave like a resistive MHD instability. Similarly to sawteeth, but on a much faster time scale, the soft X-ray (SXR) profiles from a 1-D deconvolution of the line-integrated SXR emissivities show a relaxation oscillation expelling energy and possibly also impurities. This is confirmed by T_e measurements using electron cyclotron emission. The fishbones change the temperature of the background plasma on a much faster time scale ($\approx$ 1 ms) than would follow from the redistribution of the fast particles, and consequently of the heating power. The magnetic reconnection due to fishbones would also explain that, despite q being in the vicinity of one, sawteeth do not appear, since the fishbones oscillations could serve as a mechanism for keeping q at one.

When the beam power was increased, β_N was limited by the occurrence of (3,2) neoclassical tearing modes, the onset of which was always preceded by a fishbone. Due to the low density the (3,2) modes were usually followed by (2,1) modes, which ultimately lock. Considering that sawteeth are not present, the second harmonic of a (1,1) fishbone acts as a seed island for the initiation of (3,2) neoclassical tearing modes. The β-limit is close to $\beta_N = 2.2$. At 6.25 MW of NBI $\beta_N = 2.2$ could still be maintained for a duration of 1 s, after which, due to the proximity to the β-limit, a (3,2) mode occurred.

A major concern regarding stationary plasma operation with improved confinement is the behaviour of the impurity content. From spectroscopic data the main impurities have been identified as helium (He: 5%), carbon (C: 2.5%), oxygen (O: 1.2%), and silicon (Si: $\approx$ 0.3%) after siliconization of the vacuum vessel. Charge exchange recombination spectroscopy yields a flat concentration profile of carbon, and the 1–D deconvolution of SXR measurements indicates no temporal accumulation of impurities in the centre. Neglecting the presence of elements with Z larger than Si, an upper limit of Z_{eff} can be inferred from SXR emissivities by using the STRAHL impurity transport code. The calculation assumes flat profiles for the concentration of He, C and O and fits the Si profile to the measured SXR emissivity. The resulting Z_{eff} profile is slightly peaked in the centre (Fig. 3.7) and quasi-stationary from 2 s until the end of the 5 MW heating phase. The peaking of the electron density is partly caused by the impurities, but nevertheless, the deuteron density also increases towards the plasma centre. The steady-state is possibly caused by the strong fishbone activity expelling, similarly to sawteeth, impurities from the plasma core.

Energy transport was analyzed with the ASTRA 1–1/2–D code. Besides electron density and ion and electron temperature profiles, profiles of radiated power and Z_{eff} were incorporated in the study. In Fig. 3.8 the resulting ion and electron thermal conductivities are shown. In the central regions of the plasma

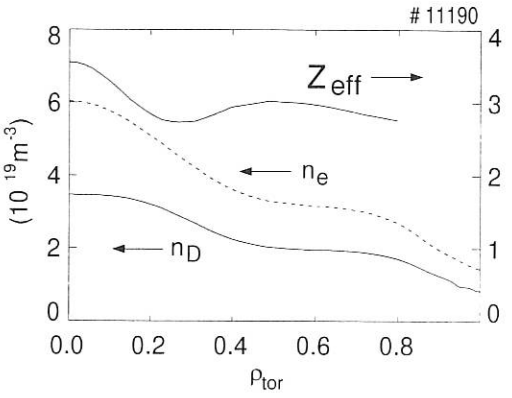

FIG. 3.7: Radial profiles of electron, deuteron density, and Z_{eff} at 4 s of discharge #11190. The Z_{eff} profile represents an upper limit.

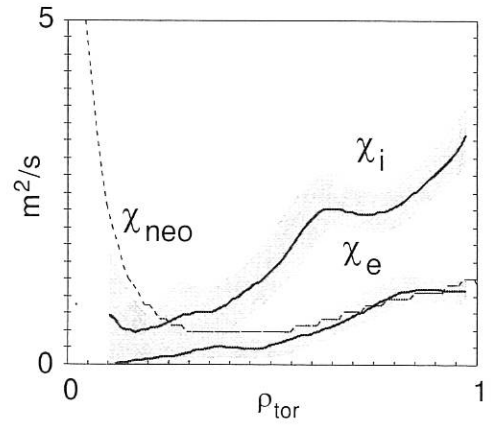

FIG. 3.8: Ion and electron thermal conductivities at 2.5 s of the discharge of Fig. 3.5 vs. normalized toroidal flux radius. Also shown is the neoclassical ion thermal conductivity.

χ_i drops to neoclassical values, but also χ_e is at a low level, indicating that the transport reduction is not limited to the ions.

Considering that no sawteeth have been observed, a mechanism associated with the fishbone activity is required to keep q at or just above one. In the ASTRA calculations this was simulated using Kadomtsev reconnection, which redistributes the central current as soon as q drops below one. The resulting q-profile (Fig. 3.9a) is flat in the centre with $q \approx 1$ inside $\rho_{tor} = 0.2$, which is consistent with the location of the (1,1) fishbone mode derived from the SXR oscillations. Without this mechanism a stationary current profile is not attained in the transport calculation. The safety factor continuously drops in conjunction with expansion of the q = 1 surface, reaching values below 0.8 after 4.4 s of the discharge. In addition to the absence of sawteeth, this behaviour contradicts the observations of a constant position of the (1,1) fishbone mode and constant MSE polarization angles. The composition of the current density profile from ASTRA, which solves the current diffusion equation using the experimental temperature and Z_{eff} evolution, is illustrated in Fig. 3.9b. The total current profile is flat in the

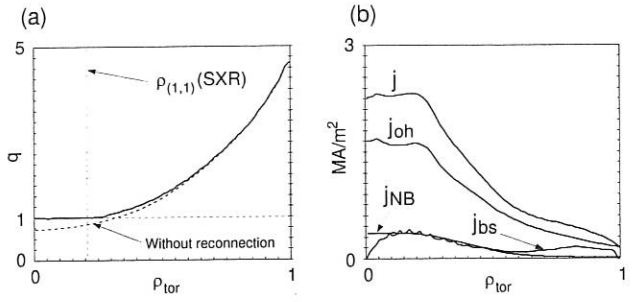

FIG. 3.9: (a) q-profile from ASTRA with (solid line) and without (dashed line) Kadomtsev reconnection. In the latter case q_0 clearly drops below unity. $\rho_{(1,1)}$(SXR) indicates the radial location of the (1,1) mode from the soft X-ray diagnostic. (b) Toroidal current profile and its composition.

centre, but still monotonic, which is supported by the bootstrap current having its maximum close to the centre due to a smaller pressure gradient as compared with internal transport barriers with L-mode edge. The total plasma current consists of 70% ohmic current, 10% current drive from NBI, and 20% bootstrap current, the small bootstrap current fraction corresponding to relatively moderate values of β_N and q_{95}.

Both raising the density and reducing the heating power resulted in deterioration of the confinement which is accompanied by the appearance of sawtooth oscillations when T_i approaches T_e. A discharge where the line-averaged density was increased from 4.2×10^{19} m^{-3} to 5.8×10^{19} m^{-3} is shown in Fig. 3.10. Until 2.3

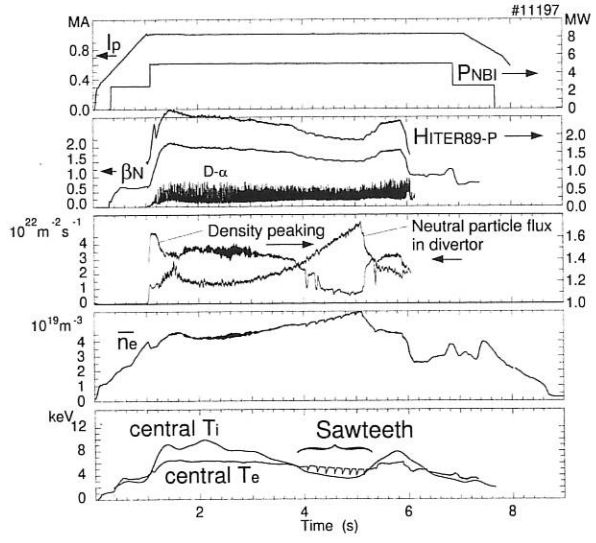

FIG. 3.10: I_p, P_{NBI}, H-factor, β_N, D_α-signal, density peaking factor, neutral particle flux in the divertor, line-averaged density, and central temperatures of a discharge where after the formation of the ITB the density was increased.

s the plasma parameters resemble those of the discharge shown in Fig. 3.5. Associated with the increase of the density was an increase of the neutral particle flux in the divertor, representing a particle source for the main plasma, and a simultaneous reduction of the density peaking. The central ion temperature and the toroidal rotation velocity decreased by more than a factor of two. The effect on T_e is less prominent since, with the drop of T_i, more power goes into the electrons. The amplitude of the fishbone oscillations also decreases. It is seen from the β_N- and $H_{ITER\text{-}89P}$-traces that the confinement drops, which means, since the power is kept constant, that the temperature decrease is stronger than the corresponding density increase. It is interesting to note that, after decreasing the density is again decreased, the ITB partially recovers, although it is finally terminated by a (3,2) mode. This suggests that the stability of the regime could not be entirely recovered. The influence of the neutral particle flux has also been observed in cases where the cryopump, which has been used in the discharges described so far, was not in operation. After the NBI power is increased to 5 MW, an ITB is formed transiently lasting only 100 ms. While the density is 15% higher than in the cases where the ITB could be sustained, the neutral particle flux is a factor of about three higher.

3.4 Summary

Different scenarios with improved core confinement due to modification of the current profile by neutral beam heating have been attained on ASDEX Upgrade.

ITBs with L-mode edge show steep pressure gradients and mainly reduced ion transport at neoclassical levels in the plasma core ($\rho_{tor} < 0.5$). $H_{ITER89\text{-}P} = 1.9$ and $\beta_N = 1.6$ are limited by the radial extent of the improved confinement region. The ITB is terminated by the occurrence of (2,1) modes.

A stationary H-mode discharge with improved core confinement where both ion and electron transport are reduced has been produced. $H_{ITER89\text{-}P} = 2.4$ and $\beta_N = 2$ could be maintained for 6 s, corresponding to 40 confinement times or 2.5 time scales for internal current redistribution. These discharges resulted in the highest $n_{D,0}T_{i,0}\tau_E$ so far observed on ASDEX Upgrade (7.5×10^{19} keV s m^{-3} for 6 s and 8×10^{19} keV s m^{-3} for 1 s). Fishbones, acting like a resistive MHD instability, seem to play a dominant role in sustaining a current profile required for stability of the improved confinement plasma.

4. MHD STABILITY BEHAVIOUR AND STABILIZATION METHODS

Due to its high and flexible additional heating power, ASDEX Upgrade can explore pressure limiting MHD phenomena under a wide range of discharge parameters. The capability to carry out these investigations over a broad range of B_t is particularly valuable for the neo-classical MHD modes, where an explicit B_t dependence of the critical β values is postulated by one theory and was found also in our experiments. The flexibility in our heating system - with two sets of NBI sources corresponding to significantly different pitch-angle distribution of the ionized fast particles, and a significant amount of ICRH power - allows us also to study in a systematic way fast particle driven MHD instabilities. Finally the availability of ECR power with

a controllable injection geometry has allowed us to carry out first successful experiments concerning the active stabilization of neo-classical tearing modes with phase controlled localized heating and current dirve. Of equal importance to the success of these investigations was our suit of relevant diagnostic systems, to which we have added recently (but started only to exploit) also an MSE system for the determination of current profiles, and the strong build-up of our MHD modelling capability.
These capabilities of ASDEX Upgrade and the growing realization that MHD phenomena put the most serious performance constraint onto the operation of ITER and power producting reactors has made the MHD studies one of the focal points of our scientific programme.

4.1 Neoclassical Tearing Modes

4.1.1 *General behaviour of neoclassical tearing modes*

During the last year of experiments with increased heating power of up to 20 MW NBI, the neoclassical tearing modes have been the major limitation for the maximum achievable β, e.g. $\beta_N = \beta_t/(I_p/(aB_T))$. Mainly the (3/2) neoclassical tearing mode is of concern for ASDEX Upgrade. For the plasma shapes and current profiles considered on ASDEX Upgrade the tearing mode parameter Δ' is assumed to be negative and the tearing mode should therefore be linearly stable. A code for determining Δ' in full toroidal geometry with arbitrary shaping was developed and will be used in the future together with improved knowledge of the current profile from the Motional Stark Effect (MSE) diagnostic. Besides the Δ' term, neoclassical tearing modes are mainly governed and driven by the lack of helical bootstrap current over an already existing small island, the so-called seed island. The seed island provides flattening of the pressure profile across the island, resulting in a reduction of bootstrap current. The flattening is caused by the larger heat conductivity parallel to the magnetic field in relation to the perpendicular heat conductivity ($\chi_\parallel \gg \chi_\perp$). For small islands this flattening is incomplete due to the still finite $\chi_\parallel/\chi_\perp$ ratio ($\chi_\parallel/\chi_\perp$ model), and therefore the destabilization is reduced. The second stabilizing effect arises from the ion polarization current, which is driven by the time-varying electric field induced by the rotating island itself. In the collisionless case ($\bar{\nu}_{ii} \ll 1$) this stabilizing current consists only of the trapped particles, whereas in the collisional case ($\bar{\nu}_{ii} \gg 1$) the number of particles affected is increased by a factor $\epsilon^{-3/2}$. The stabilizing effect of the ion polarization current is proportional to the function $g(\epsilon, \nu_{ii})$, which depends on the normalized ion-ion collision frequency $\bar{\nu}_{ii} = \nu_{ii}/m\epsilon\omega_e^*$.

$$g(\epsilon, \nu_{ii}) = \begin{cases} \epsilon^{3/2}, & \bar{\nu}_{ii} = \nu_{ii}/m\epsilon\omega_e^* \ll 1 \\ 1, & \bar{\nu}_{ii} = \nu_{ii}/m\epsilon\omega_e^* \gg 1 \end{cases}$$

In order to decide which of the stabilizing effects is most important, the dependence of the onset of neoclassical tearing modes, namely the relevant maximum achieved local $\beta_p = p(q = 3/2)/(B_p^2(q = 3/2)/2\mu_0)$, was investigated for the collisionless case. In order to have similar seed island sizes, only cases with sawtooth crashes providing the seed island were used. For small islands the polarization current model would lead to $\beta_{p,onset}^{pol} \sim \sqrt{g(\epsilon, \nu_{ii})} \cdot \rho_{p,i}$. The $\chi_\perp/\chi_\parallel$ model with the assumption of gyro Bohm scaling for the radial transport and Spitzer heat conductivity for the parallel transport gives $\beta_{p,onset}^{\chi} \sim \nu_*^{0.5}\rho_{p,i}^*$, where ν_* describes the usual collisionality $\nu_* \sim na/T_i^2$. For the collisionless case, which is valid if the modes are not located near the plasma edge, one finds a linear dependence of the local β_p at the $q = 3/2$ surface on the normalized poloidal ion gyro radius $\rho_{p,i}^*$. The experimental data for $q_{95} \approx 4$ give a scaling as $\beta_p^{onset} \sim \rho_{p,i}^{*1.02} \cdot \bar{\nu}_{ii}^{-0.02}$ (Fig. 4.1) in favour of the ion polarization current model. Apart

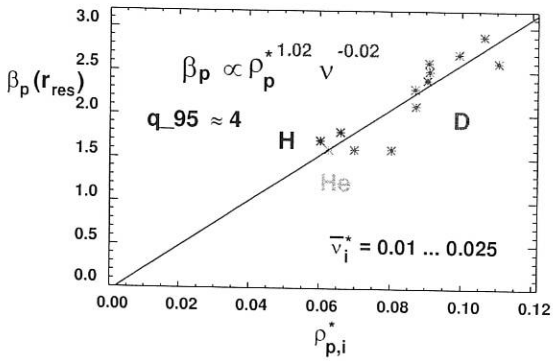

FIG. 4.1: β_p at the rational surface at the mode onset vs ρ_p^* for collisionless plasmas ($\bar{\nu}_{ii} = 0.01 \ldots 0.025$, $q_{95} = 4 \ldots 4.4$). A fit to the experimental data leads to $\beta_p \propto \rho_p^{*1.02}\bar{\nu}_{ii}^{-0.02}$. The isotope effect following from this scaling law can also be seen.

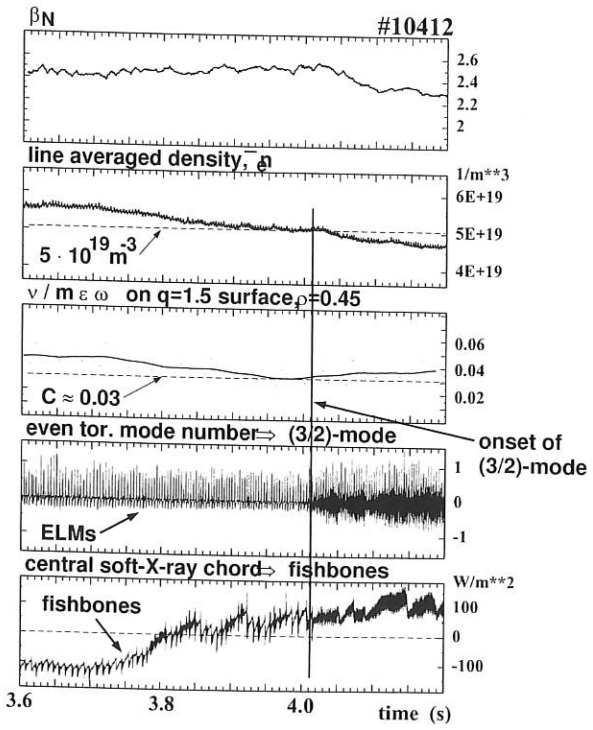

FIG. 4.2: Dependence of the excitation of the neoclassical (3/2)-mode on the collisionality alone. β_N remains constant while the density and $\nu_{ii}/m\epsilon\omega_e^*$ slowly fall until there thresholds are reached.

from sawtooth crashes, fishbones can also produce seed islands for excitation of neoclassical tearing modes. In this case and in cases with no observable seed island β reaches its highest values with respect to the scaling with the poloidal ion gyro radius $\beta_p^{onset} \sim \rho_{p,i}^*$. On the other hand, one would expect a clear dependence of the onset of these modes on the local normalized collision frequency $\bar{\nu}_{ii} = \nu_{ii}/m\epsilon\omega_e^*$ at the resonant surface of the mode. The experimental data have indeed shown as a second necessary condition for the onset of this type of mode a sufficiently small collisionality at the corresponding resonant surface. With constant β, the collisionality was decreased by reducing the density until a neoclassical mode is excited (Fig. 4.2). A possible way to avoid excitation of a neoclassical tearing mode lies therefore in increasing the normalized local collisionality and hence increasing the stabilizing polarization current at the $q = 3/2$ surface (Eq. (1)). This threshold in the line-averaged density $\bar{n}_e$ for the (3/2)-mode was experimentally determined for a typical discharge with $B_t = 2.0T$, $I_p = 1.0MA$, $q_{95} = 3.2$ and a neutral beam heating power of up to 15 MW. Figure 4.3 shows two similar discharges with only slightly different densities and a maximum $\beta_{N,max} \approx 2.55$. For $\bar{n}_e = 8 \cdot 10^{19}\ m^{-3}$ a (3/2)-mode appears and deteriorates the confinement, visible on the drop of β_N, whereas at $\bar{n}_e = 8.5 \cdot 10^{19}\ m^{-3}$, and therefore increased collisionality, the mode cannot be excited any longer. On the other hand, a reduction of the density and hence the collisionality below the value for the possible excitation of the (3/2)-mode leads to additional destabilization of the (2/1) neoclassical tearing mode once the (3/2)-mode has been excited. Consequently the (2/1)-mode can be kept stable by keeping the (3/2)-mode stable by sufficiently high collisionality.

4.1.2 *Stabilization of neoclassical tearing modes with ECCD*

In a reactor $\bar{\nu}_{ii}$ is no longer a free parameter in order to avoid modes of these types. Another approach to controlling already excited neoclassical tearing modes is therefore to replace the lack of helical bootstrap current by an externally driven current. This has been successfully shown at ASDEX Upgrade for the first time in cooperation with IPF-Stuttgart. The current is externally driven by electron cyclotron current drive (ECCD). The power of the ECRH and hence the driven current should only be applied in the O-point of the island, where the bootstrap current is missing. The ECRH power was therefore modulated by measuring the phase of an n = 2 combination of Mirnov coils and adjusting the relative phase of the ECRH antenna correspondingly. The deposition of the ECRH and the island position were determined by ECE measurement. With only 5-10% of the total NBI heating power of 10 MW, 25% of the β loss caused by the (3/2)-mode could be recovered and the mode amplitude was significantly reduced (see also section, "University Contributions to IPP Programme", IPF Stuttgart). In Fig. 4.4 the difference between O- and X-point injection is shown. In the O-point case a reduction of the mode amplitude

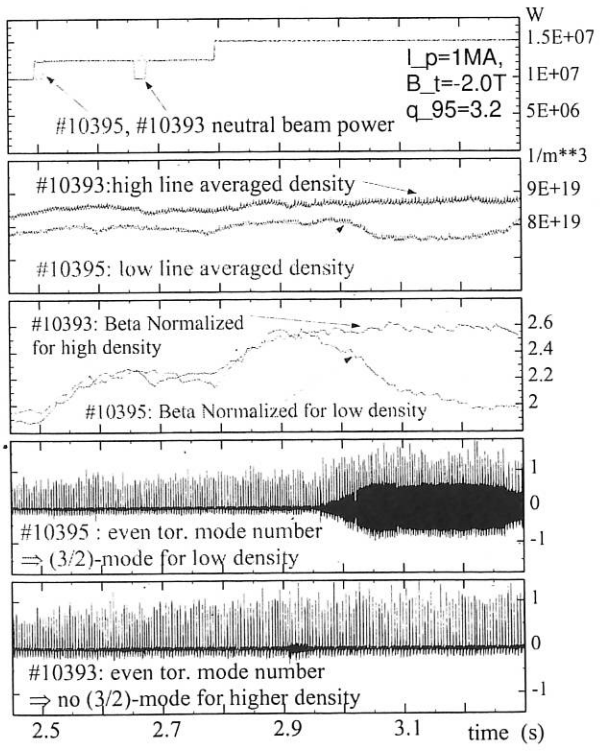

FIG. 4.3: Comparison between two similar discharges ($B_t = 2.0T$, $I_p = 1.0MA$, $q_{95} = 3.2$) with only slightly different densities. In #10395 with $\bar{n}_e = 8 \cdot 10^{19}\ m^{-3}$ the (3/2)-mode appears, whereas in #10393 with $\bar{n}_e = 8.5 \cdot 10^{19}\ m^{-3}$ the (3/2)-mode is not excited.

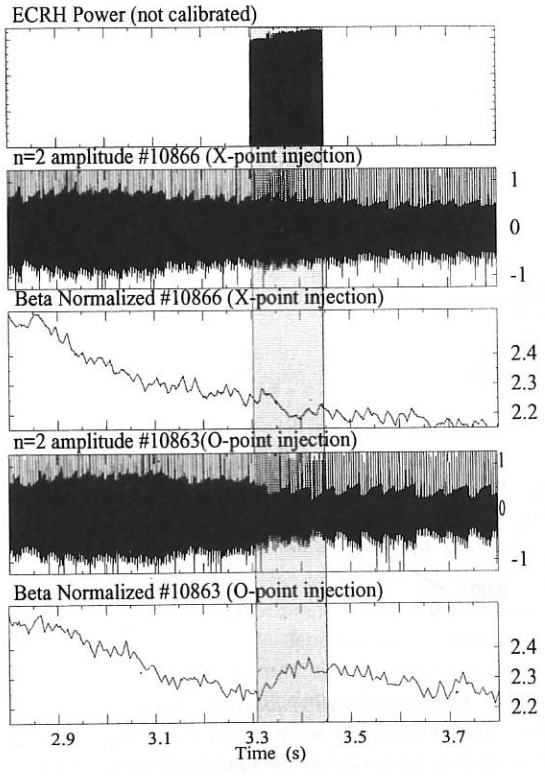

FIG. 4.4: Effect of a driven current in the O-point and the X-point of the island. For the O-point recovery of β and reduction of the mode amplitude could be observed, whereas for the X-point a further loss in β could be measured.

and recovery of β can be seen, whereas in the X-point case even a further decrease in β can be observed without a clear influence on the mode amplitude. The reduced effect for the X-point case points towards the possibility of stabilizing the mode with DC current drive alone. This will be a point for further investigations. Theoretical calculations show that the additional heating by ECRH also increases the current through the reduction of the resistivity. Both effects together should make it possible to stabilize the mode completely in the future, when twice the ECRH power is available.

4.1.3 *Confinement degradation due to neoclassical tearing modes*

We studied the scaling of the observed confinement degradation with a combined nonlinear tearing mode and transport code in comparison with experimental results. In the simulations we consider nonlinear growth of neoclassical magnetic islands, including self-consistent evaluation of the bootstrap current density and the increased heat transport across the island. The growth time as well as the saturated island size predicted by the code agree well with the experimental observations. Consistently with the analytical theory for the effect of islands on global confinement time, our simulations indicate a linear dependence of confinement degradation on the island width. Combining this with the dependence of the island width on the plasma pressure resulting from our calculations of the confinement deterioration due to an island of width w leads to the predicted saturation in the confinement degradation for large β. After correcting an observed density decrease of typically 10% at the mode onset, good agreement of experiments with $q_{95} \approx 3$ with the simulation could be found. For large bootstrap current densities at the rational surface the degradation in energy confinement saturates at about 25% of the plasma energy.

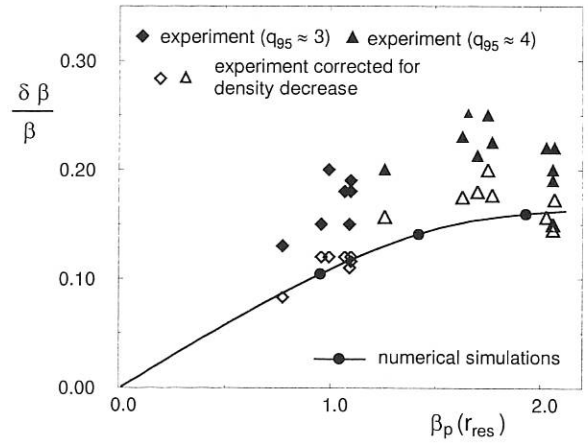

FIG. 4.5: Confinement degradation versus β_p at the rational surface. The simulations were carried out for $q_{95} \approx 3$. The blank symbols correspond to the measured values corrected for the decreased density after the mode onset.

4.2 Fast-particle-driven MHD

A large population of suprathermal ions, such as associated with ICRH, NBI or α-particle heating, can strongly modify the stability of MHD modes. They can tap their energy and give rise to their spatial redistribution and possibly to a significant loss of heating efficiency. Two of the most frequently observed modes in ASDEX Upgrade are the fishbone and the TAE (toroidicity-induced Alfvén eigenmode). The TAEs are modelled with the Castor code to identify the spectrum of excitable Alfvén waves and the Hagis code to study the nonlinear interaction of these modes with the fast-particle population. The Hagis code follows the guiding centres of an ensemble of fast particles to evolve self-consistently their distribution and the spectrum of TAE present. For TAEs the effect of the fast particles is to modify perturbatively the amplitude and frequency of the linear wave. The evolution equations for each eigenmode are derived from a Lagrangian formulation in which wave-particle interactions are included. The NBI system in ASDEX Upgrade produces a population of energetic particles with a characteristic birth energy of ~ 60 keV and a typical slowing-down time of around 75 ms. The distribution of these beam particles was calculated by solving for the bounce averaged fast ion distribution function with the Fpp code. Fpp-3D is based upon the 3D Fokker Planck theory of "banana regime" neoclassical effects in tokamaks. Based on such a fast-ion distribution, Fig. 4.6 shows the predicted evolution of the experimentally observed $n = 4$ TAE driven by the neutral beam, which could be perfectly identified by the Castor code. The system assumed a beam tangency of 93 cm and co-injection of 12.5 MW. The continuum damping rate calculated for this mode by Castor is $\gamma_d \simeq 3 \times 10^{-6} \tau_A$, which was negligible in comparison with the drive from the beam particles.

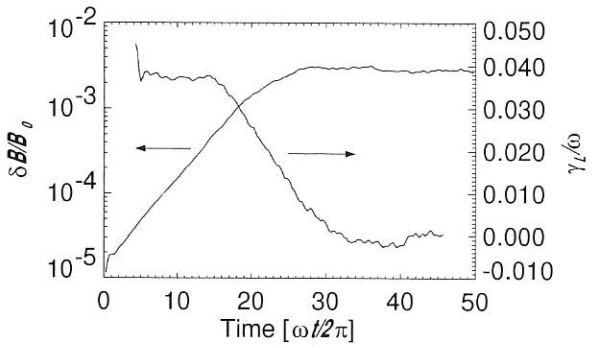

FIG. 4.6: Evolution of an n = 4, m = 3.4 TAE calcualted by the Hagis code.

5. H-MODE OPERATION AT HIGH DENSITY

5.1 High Density H-Mode Operation

In order to achieve sufficient fusion power and limit the power load to the target plates, a fusion reactor must safely operate at rather high plasma density while retaining sufficiently high energy confinement. In practice, this means operation in the

vincinity of the empirical ''Greenwald limit'' maintaining the H-mode. Both the H-L transition and the L-mode density limit form important boundaries in tokamak operation. A systematic investigation of the H-mode density limit was performed in the new DV-II closed divertor configuration. Recent experiments covering a significantly enlarged parameter space compared earlier studies confirm earlier findings when approaching the Greenwald density.

With pellet injection from the magnetic high-field side, extension of the operation space can be achieved, giving at least transient access to operation at densities well beyond the Greenwald limit without loss of confinement. A distinguished progress in the understanding of the mechanism for both the H-mode and the density limit was achieved by introducing boundary parameters in the description of both limits. Whereas their driving physical processes are probably different, both limits are believed to be governed by edge physics. In the following we discuss first global parameter dependences of gas-fuelled and pellet-fuelled discharges and then present the edge parameter behaviour.

5.1.1 High-density H-mode parameter dependences

The H-mode is generally accessible when the input heating power P_{heat} exceeds a certain limit depending on the density and magnetic field $P_{heat}^{L\rightarrow H} = c \times \bar{n}_e B_t$, where the constant c depends primarily on the ion species and ion ∇B drift direction. The H-L back-transition shows the same parameter dependences but happens at medium densities at about half the L-H threshold power. During density build-up of H-mode plasmas up to the non-disruptive H-mode density limit the discharge normally undergoes the following phases: the ELM frequency rises and at high density the ELM type reverts from type-I to type-III. The density at the separatrix n_e^{sep} increases monotonically with $\bar{n}_e$ but tends to saturate in the high-density phase despite increasing neutral particle flux. Divertor detachment first sets in between type-I ELMs at high densities and intensifies markedly during the type-III ELM phase. It is generally found that H-mode confinement depends on the plasma density. Near the Greenwald density limit the confinement degrades down to L-mode levels. After back-transition into L-mode the density profile peaks slightly and a MARFE grows at the X-point into the bulk, finally leading to disruption.

Earlier experiments in ASDEX Upgrade, performed at one particular plasma current, had shown the L-H threshold power to deviate dramatically from the $\bar{n}_e B_t$ scaling when approaching the Greenwald limit. The H-mode density limit is found to become nearly independent of P_{heat} and the hysteresis vanishes. To improve confidence in the validity of this observation, experiments mapping out the H-L transition with a large variation of I_p, B_t and P_{heat} were performed. The expanded parameter range was used to deduce scalings and probably identify theoretical density limit models. Figure 5.1 shows the measured heating power dependence of H- and L-mode density limit, as a function of normalized density. The power is in first approximation normalized to $P_{thr}(\bar{n}_e = \bar{n}_e^{GW}) \propto \bar{n}_e^{GW} B_t \propto I_p^2 q_{95}$ to reflect the L-H transition power threshold found at medium densities ($P_{thr} \propto \bar{n}_e B_t$) extrapolated to the Greenwald density.

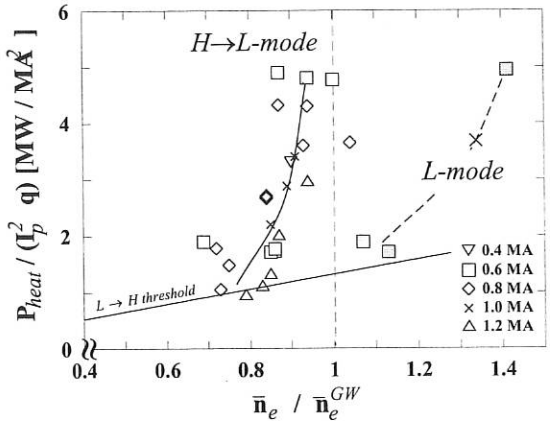

FIG. 5.1: The operation diagram shows the strong derivation of the power needed to achieve H-mode from the usual $P_{heat} \propto \bar{n}_e B_t$ scaling colse below $\bar{n}_e^{GW}$

Figure 5.1 clearly confirms that the earlier findings also hold for the significantly enlarged parameter space. It is interesting to note that the increase of I_p by a factor of 3 yields roughly the same normalized densities $\bar{n}_e/\bar{n}_e^{GW}$, i.e. at 1.2 MA three times as high a line-averaged density as at 0.4 MA. This is noticeable since the large density variation implies, in parallel, strong modification of the particle fuelling profiles for both recycling and NBI heating sources. It can be pressumed that the particle fuelling profile shape has no strong effect on the loss of the H-mode. Normally, with gas puffing alone the Greenwald limit is not exceeded.To get a deeper insight into the H-mode limit physics we performed a detailed fit to the database. The experiments are well described by the empirical regression fit

$$\bar{n}_e^{exp} = 5.0 \frac{q_\perp^{0.15} B_t^{0.61}}{(q_\psi R)^{0.95}}$$

$[10^{20} m^{-3},\ MW\ m^{-2},\ T]$, where $q_\perp = P_{sep}/S$ and S is the plasma surface. This is remarkably close to the following scaling proposed by Borrass et al.:

$$\bar{n}_e^{BLS} = 4.14 \frac{q_\perp^{0.09} B_t^{0.53}}{(q_\psi R)^{0.88}},$$

which relates the H-mode density limit to divertor detachment. Our findings were also compared with the Greenwald scaling. While the first two scalings virtually coincide on the existing database, the deviations from the Greenwald scaling can be reliably assessed. This is particularly true of the B_t dependence, which is clearly weaker than in the Greenwald scaling. In edge-based models, the B_t dependence is directly related to the B_t dependence of the underlying transverse scrape-off layer transport. The wide B_t variation in the present database offers for the first time the possibility to discriminate between various alternative transport models.

5.1.2 Extension of operational limits by pellet injection

Pellets injected into a hot plasma sublimate and a neutral gas cloud is formed around the pellet. Due to the incoming electron heat flux the gas is ionized and the plasmoid of cold,

dense gas expands along the magnetic field lines. Since the heating electrons are much faster than the expanding plasmoid ions, the plasmoid acts as an energy sponge and a localized high-β plasmoid is formed. This plasmoid, diamagnetic with respect to the surrounding plasma, is subject to a curvature drift force directed to the low magnetic field side (LFS). In recent experiments, this high-β drift was measured for the first time highly resolved in radius and time. Measured drift velocities are in the range up to 10^3 to 10^4 m/s, as predicted by theoretical models. It became clear that particles are lost on a μs time scale in the case of LFS pellet injection due to the outward directed drift. However, pellet injection from the magnetic high field side (HFS) causes a high-β drift towards the plasma centre, avoiding these fast-particle losses. Consequentely, all further pellet refuelling experiments were performed from the HFS. The main aim of our experiments was to demonstrate density feedback steady-state operation close to or even beyond $\bar{n}_e^{GW}$ with clear H-mode characteristics. The target plasma conditions were varied mainly by changing the external gas-puff rate, pumping speed (e.g. by cryopumping) and the preprogrammed density $\bar{n}_e^{set}$. In the course of the experiments it was found that the global confinement characteristics of purely gas refuelled discharges were preserved during the pellet fuelling phase. The actual peak density $\bar{n}_e$, for example, decayed after each pellet towards the equilibrium value $\bar{n}_e^{equ}$ found in equivalent discharges without pellet injection. The density evolution after injection of a pellet can be described by exponential decay consisting of two time constants. The fast decaying component of 10 ms specifies that the loss of approximately half of the pellet mass is caused by additionally induced ELMs. The slow component of 120 ms corresponds to the usual bulk particle confinement.

Injection at a sufficiently high pellet frequency can raise the density to the required level $\bar{n}_e^{set}$. The density enhancement $\Delta = \bar{n}_e^{set} - \bar{n}_e^{equ}$, however, determines the required pellet particle flux, irrespectively of the initial plasma conditions. The approximately linear increase of the required pellet particle flux Φ with density increment Δ indicates that particle confinement remains nearly unchanged.

On the other hand, it was found in earlier studies, that HFS injection increases the bulk density, while the separatrix region does not significantly change. The reduced particle losses associated with HFS injection yield a clear gain in plasma stored energy W_{MHD} in contrast to experiments with LFS injection, as demonstrated in Fig. 5.2. The improvements are most pronounced at low heating powers. However, the confinement is still degraded with respect to extrapolations gained from scaling laws such as the ITERH92-P scaling, represented by the solid curves in Fig. 5.2. Notably, it should be mentioned that pellets can trigger neoclassical tearing modes with detrimental effect on τ_E. These modes are not observed in gas-fuelled high-density discharges. A key element to understanding the behaviour of HFS pellet-refuelled discharges described so far seems to be the evolution of density and temperature profiles. The measured evolution of electron density profiles with ms temporal resolution gives no indication of a significant change of the gradient in the boundary region even for the time shortly after pellet injection. During the phase of fast density decay the loss from the plasma corresponds to a particle flux of about

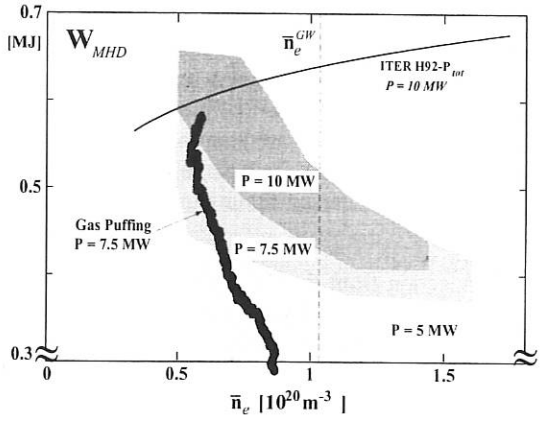

FIG. 5.2: Plasma stored energy W_{MHD} vs. $\bar{n}_e$ of stationary HFS pellet-fuelled H-mode discharges with different P_{heat}. For comparison, the trajectory of a gas-fuelled discharge is included. The curves correspond to energy contents calculated by the ITERH92–P scaling.

$\Phi \approx 10^{22}$/s crossing the edge region. The excess density beyond that of purely gas-fuelled discharges is caused by radial broadening of the edge gradient zone into the plasma core. The central part of the profile remains almost flat. The evolution of the electron temperature profile close to the plasma edge behaves like that of related gas-puffed discharges. A significant difference is observed, however, in the core region. In gas-fuelled H-mode discharges with saturated edge pressure gradients (e.g. type-I ELMy H-mode) the T_e profiles show remarkable resilience. When pellet injection sets in, the bulk temperatures drop below the according values. This contributes at least partly to the degradation of the plasma energy when $\bar{n}_e$ is increased. In next-step experiments we increase the pellet injection velocity and hence the penetration depths. This might reduce the pellet-induced ELMs.

5.1.3 Density limits in edge parameters

The plasma edge, in particular the region near the separatrix, affects confinement and stability in various ways. Operational limits, e.g. the boundary between L- and H-mode confinement regimes, can be mapped out in edge parameters, in particular edge temperature and pressure gradient. With the focus on the H-mode boundary for densities approaching the Greenwald limit, global and local parameters are compared with respect to a change in confinement behaviour. In this density regime, where the H-mode power threshold strongly increases above the $\bar{n}_e B_t$ scaling valid at low and medium densities, differences becomes especially apparent between local and global scalings. Whereas the edge parameter threshold scaling was found to be relatively robust, e.g. the critical edge temperature for the H-mode transition did not change even with changed divertor geometry or when operating with the newly installed cryopump, global scalings can be affected by heat and particle transport. With upgrading to 20 MW neutral beam heating, a series of high edge density experiments with gas-puff fuelling were carried out. It was found that high edge densities can be achieved only if the heating power is increased proportionally to the total neutral gas influx (external gas flux plus wall recy-

cling). The operational space at high density and high heating power is mapped out by the trajectories shown in Fig. 5.3: a) in global engineering parameters, heating power vs. neutral gas influx; b) in local edge parameters, electron temperature and density at $r = a - 1$ cm (in the gradient zone). Stable operation at high densities is achieved above the boundary labelled ''HL'', which denotes the H- to L back-transition. At high edge densities, the back-transition is manifested in a fast drop of the edge temperature gradient, effectively destroying the edge transport barrier. If fuelling is continued, the edge temperature can drop further, leading to tearing mode formation and a disruption, which can be avoided if the heating power is increased to above the ''HL'' boundary. In the new DV-II divertor, at high density the ''HL'' boundary almost coincides with the onset of strike point detachment during type III ELMs both in global and edge parameters. Although a particle flux to the divertor plates is observed during ELMs, the pressure balance at the separatrix between the divertor target plate and midplane is lost in between and during ELMs. If the heating power is much in excess of the H-mode threshold, the edge temperature increases. If the pressure gradient imposed by ELMs (''MHD'' boundary) is reached, a further increase of the edge temperature is accompanied by a reduction of the edge density. At sufficiently high edge temperature, small type III ELMs vanish and type I ELMs occur. Type I ELMs are characterized by lower ELM frequency and larger momentary heat flux during the ELM event. While detachment can be maintained during type III ELMs, during type I ELMs detachment has not been observed to date even at high edge densities, and thus a large fraction of the type I ELM energy can be expected to be deposited on the divertor target, which might

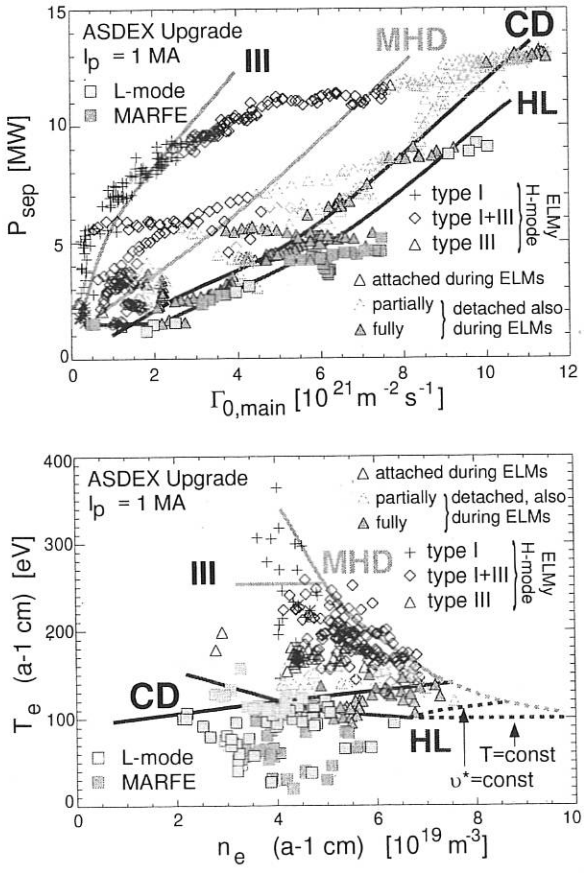

FIG. 5.3: Operational space at high densities: a) in global engineering parameters, separatrix power vs. main chamber neutral gas flux, b) in local parameters, edge density and edge temperature (taken at r = a - 1 cm).

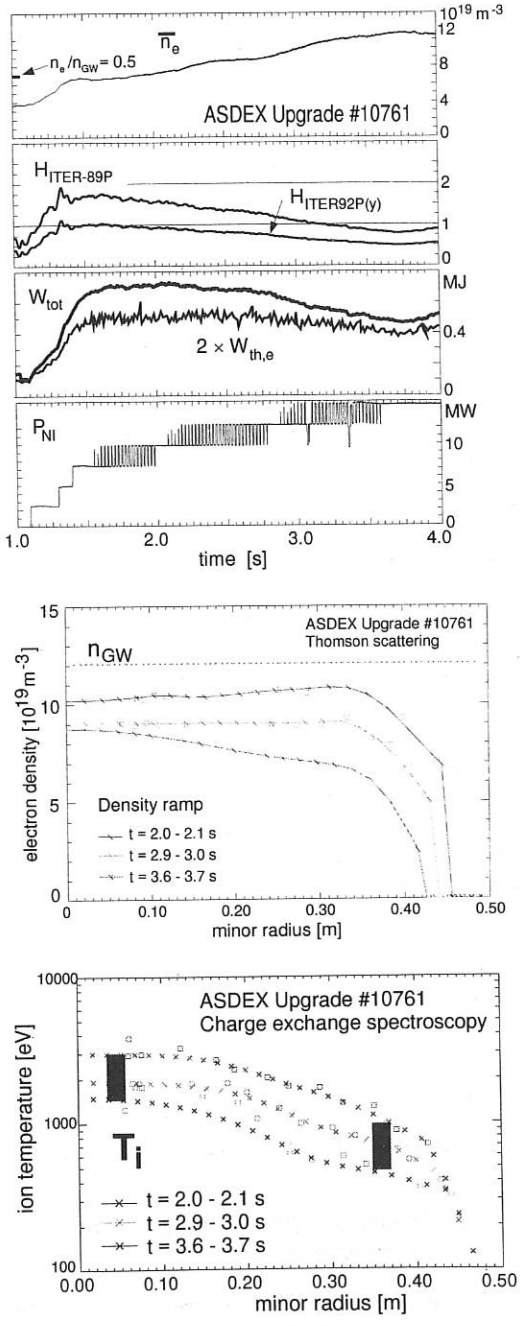

FIG. 5.4: a) Time traces, b) electron density and c) ion temperature profiles of an H-mode density ramp-up experiment. As the density is enhanced, the increasing edge density causes an edge temperature drop. Core temperatures fall proportionally and, together with a flat density profile, the stored energy decreases.

lead to an unacceptable peak power load in a reactor-sized plasma. As can be seen from Fig. 5.3b), the edge ''MHD'' pressure gradient boundary approaches the ''HL'' boundary for maintaining the edge transport barrier and avoiding radiation instability, leaving a narrow space for stable H-mode operation at high density. The intersection of the ''MHD'' and ''HL'' boundaries formally defines a maximum edge density for H-mode operation, but this value is not achieved experimentally even with high heating power. Instead, at high edge densities a reduction of edge gradients with the onset of detachment is observed. Approaching the H-L transition, the edge density does not increase any more despite the increasing neutral gas flux, and at the same time the edge temperature gradient drops, coinciding with a reduced edge pressure gradient. Correspondingly, estimates exhibit a strongly increasing effective heat diffusivity in the pedestal region. From the edge measurement it is difficult to infer scaling of this ''transport limit'' boundary. Possibilities are a T = const. or collisionality boundary ν^* const. A density ramp experiment performed this way is illustrated in Fig. 5.4. Even with increased heating power the confinement decreases to L-mode levels when the Greenwald limit is approached. The origin for this degradation can be inferred from the profiles, taken at 3 different times. With increased gas puffing, mainly the edge density increases. The limitation of the edge pressure gradient leads to an edge temperature decrease. The T_e profile resilience causes the core temperature to decrease as well. The temperature scale length $L_T = T/T'$ has a lower limit, which is reached at high heating powers that usually lead to H-mode. The density profiles in gas-puffed H-modes are typically flat, and the density peaking decreases with increasing gas puff, i.e. the core density increases more slowly than the edge density. Therefore, if the temperature reduction in the core cannot be compensated with a density increase by the same factor, the core pressure and the stored energy must decrease.
Further experiments with enlarged triangularity will show whether the high-density operation space expanded and the confinement degradation mitigated.

6. ICRH RESULTS

6.1 Ion Cyclotron Resonance frequency (ICRF) heating

6.1.1 *Modification to the ICRF system and improvements in operation*

The ICRF system of ASDEX Upgrade includes 4 generators with originally a nominal tube output of 2 MW each, powering 4 double-loop antennas. The frequency range (30-120 MHz, full power up to 80 MHz) allows the application of minority, second-harmonic and mode-conversion heating to mixed H and D plasmas for the magnetic fields used on ASDEX Upgrade. A basic problem in the ion resonance frequency domain is the change in antenna impedance due to plasma variations, resulting in power reflections back to the generators, which react with power reduction or even with cut-off and self-oscillation. This strongly limits the reliably achievable power, particularly in the case of "type 1 ELMs" during H-mode plasmas, which are too fast for active feedback compensation. At ASDEX Upgrade this problem has been solved by combining the 4 generators and antennas with 3-dB hybrids to two equal "double systems" (Fig. 6.1). The couplers reduce, in a purely passive way, the sensitivity of the ICRF system to fast coupling changes such as occur in the presence of ELMs. The basic circuitry (without current drive option) was completed in 1997 and is described in the Annual Report 1997. First results using this improved system were obtained in 1998. The 3-dB couplers operated as expected and permitted full-power operation of the system (5.7 MW at the antenna, 6.8 MW generator output) as well as routine operation at 4 MW. Experiments at higher heating power thus became possible.

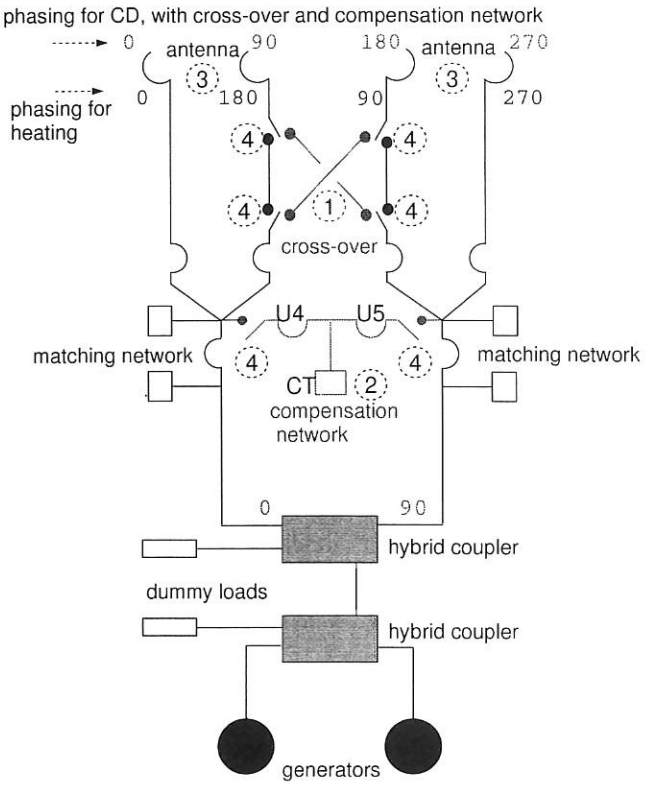

FIG. 6.1: Circuit diagram of one of the two ICRF heating and current drive double systems at ASDEX Upgrade. The diagram also includes the additional changes that are necessary for current drive: cross-over feeding of antenna straps (1) and compensation (2) for the mutual coupling between antenna straps (3), containing two line stretchers U4 and U5 and the stub tuner CT, which can be switched on by coaxial switches (4), will be installed in 1999.

6.1.2 *Experimental results*

The ICRF-related experiments were concentrated along two lines: 1. The new capabilities were used to compare at high power the effect of the localization of the heating power and its distribution among species on the discharge parameters, in particular sawteeth and ELMs. 2. Pilot experiments were

performed to check as far as possible, with the present system, the physics issues of current drive.

6.1.3 Comparison at high power

Comparing ICRF heating and NI at typically 5 MW (3 times above the H-mode threshold), we observed differences in the density and temperature profiles, and in the sawtooth behaviour, reflecting the differences in refuelling and power deposition. On the other hand, no differences were found in the plasma energy content (except when the discharge evolves differently) and ELM parameters. The global (bulk + divertor) bolometric radiation in unseeded plasmas is similar for ICRF and NI ($P_{rad}/P_{tot} = 0.7$), as is the concentration of O and C impurities. This reflects the understanding that, whereas sawteeth are sensitive to localization of the power deposition as well as to the distribution of power between electrons and ions, the total energy, global radiation and ELMs seem to be sensitive to the total power only (for the same boundary conditions, such as gas puff rate etc.). We used for ICRF heating a H minority in D, with a central position of the resonance layer, f = 30 and 31.6 MHz ($B_t = 2.1$T, $I_p = 1$ MA), and for NI 60 keV D. The differences in the profiles are larger at the top of the sawteeth. At the same line-averaged density (typ. 5×10^{19} m^{-3}), the density profile is flatter with ICRF (and increasingly so with higher density), indicating refuelling from the edge. The maximum central electron temperature is higher with ICRF (5.5 keV versus 4 keV for NI, see Fig. 6.2) and the profile more peaked: the ratio $T_{e\ ICRF}/T_{e\ NI}$ decreases from 1.4 centre, to 1.25 at r/a = 0.4, and is close to 1 at r/a = 1. At the bottom of the sawteeth, the differences are smaller. The higher average electron temperature and sawtooth amplitude with ICRF exist simultaneously with a shorter sawtooth period (82 ms versus 120 ms with NI). This is due not only to the faster initial central heating rate (58 eV/ms versus 22 eV/ms), but also to the shorter period during which the electron temperature is saturated. For minority heating, the sawtooth period increases with increasing power

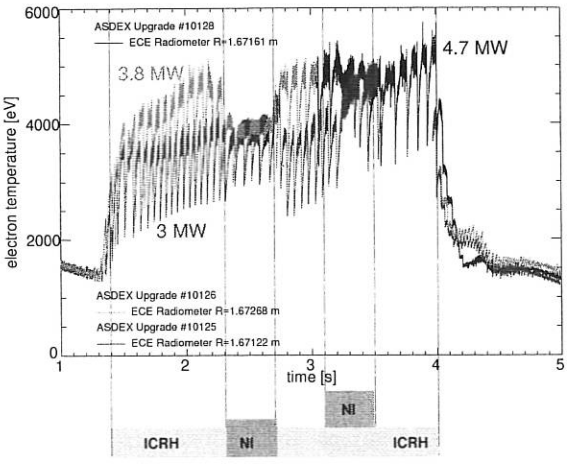

FIG. 6.2: Central electron temperature for three discharges, with increasing levels of ICRF power (3 MW, 3.8 MW, 4.7 MW). Each discharge has, during the times indicated, 5 MW NI (in the first phase alone, in the second phase in combination with ICRF).

(from 48 ms at 3 MW to 82 ms at 4.7 MW). When the position of the minority resonance layer is varied, a more central position of the resonance layer results in a longer sawtooth period. Two competing mechanisms play a role: on the one hand, the localization of the electron heating and resultant change in current profile and, on the other, the stabilizing effect of fast particles. The latter can be separated by using mode conversion heating (He_3 in H): the power goes directly and very locally to the electrons and no stabilizing effect due to fast particles occurs; under certain conditions the sawtooth period can then even be made to decrease with increasing ICRF power and the influence of the localization of the power can be analyzed. Because current

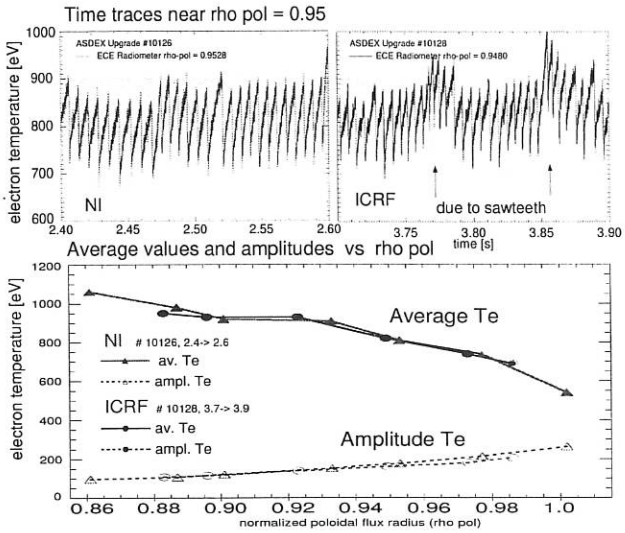

FIG. 6.3: Top: time traces of the edge electron temperature with NI and ICRF near the separatrix: the ELM frequency, and electron temperature variation due to the ELMs is the same for NI and ICRF. Bottom: average temperature and amplitude of the variation due to ELMs in the neighbourhood of the separatrix. Triangles for NI, circles for ICRF.

drive requires an asymmetric (directional) antenna spectrum, and the present system configuration only permits a symmetric spectrum, technical changes have first to be implemented to actually allow an asymmetric antenna spectrum and perform current drive experiments. However, pilot experiments can and have been performed with a symmetric spectrum to answer two fundamental questions: First, is it possible to couple efficiently to the electrons, on and off-axis? Second, does a spectrum that is less favourable concerning impurity production than the optimal one used for heating still not lead to impurity problems, in particular without Faraday screen? With different heating scenarios, it was demonstrated that coupling to the electrons is possible. Under the conditions envisaged for FWCD (fast-wave current drive, no ion resonance in the plasma), central heating of the electrons, while at the same time avoiding resonant ion heating at the edge, was shown. Similarly, under conditions of MCCD (mode conversion current drive, two ion species), coupling to the electrons off-axis was measured. The heating of the electrons was more efficient than in the case of FW electron heating. The measurement of the power deposition profile on the electrons, previously done for He_3 in H,

was extended to He_3 in D. It was also shown that, by varying the He_3 concentration, the position of the power deposition moves across the plasma radius, thereby strongly influencing the sawtooth behaviour. This provides a first indication that it should be possible to dynamically control the position of the driven current during the discharge as required for ITB control. It was demonstrated that an antenna spectrum, symmetric but less favourable concerning impurity production than that for current drive, still does not lead to impurity problems. The symmetric antenna spectrum typically used for heating in ASDEX Upgrade is produced by currents in the two antenna straps, which are 180° out of phase. It is known that this spectrum is the least likely to produce impurities. An (asymmetric) current drive spectrum will be generated by currents which are 90° out of phase. Impurity production could be larger under those conditions. To test the issue, heating experiments were performed under the (for impurity production) even more stringent conditions of current completely in phase, for an antenna without Faraday screen. The impurity concentration was only slightly increased. Impurity production is thus not expected to be a problem with a current drive spectrum.

6.1.4 *Reconfiguration of the antenna for higher triangularity*

During the summer 1998 opening, the four antennas were modified to allow plasma cross-sections with higher triangularity. This included shifting of the antenna housings towards the vessel wall, new cooling-water piping, and exchange of the antenna loops and some other elements by new parts with different geometry. The new antenna shape provides the maximum freedom for plasma shaping with this antenna type. Further increased plasma triangularity, as planned for future experiments, calls for a new antenna concept, studies of which have been started in co-operation with Oak Ridge National Laboratory.

6.1.5 *Plans for current drive*

Power has so far been applied on ASDEX Upgrade for plasma heating using a toroidally symmetric wave spectrum. Ion Cyclotron Current Drive is planned, mainly for current profile shaping in "advanced tokamak" experiments with internal transport barriers. In this case, a directional (asymmetric) wave spectrum must be launched, and the power must be deposited on the plasma electrons. This requires a modification of the RF system which was developed in 1998 and is to be installed in 1999. For current drive, the required phase difference between antenna loops can be provided by utilizing the 90° phase between the outputs of the 3-dB hybrids with the help of "cross-over feeding" of the antennas. The characteristics of this circuitry were studied. Calculations show that the mutual coupling between loops must be taken into account and compensated to avoid unacceptable phase variations and a power imbalance between the antenna straps in this asymmetric antenna operation. This can be achieved passively by compensating circuitry shown in Fig. 6.1.

7. TECHNICAL SYSTEMS

After Div II was installed, operation of the experiment restarted in April 1997 and lasted until August 1998. During this time spell there were 138 days of experimentation with 2.650 discharges and technical test shots. The vacuum vessel was opened in early August to modify the ICRH antenna contour for plasma shapes with high tiangularity (δ). For a bottom triangularity $\delta_{bot} > 0.3$ the separatrix at present hits the roof baffle of Div II. As intermediate solution for experiments up to $\delta_{bot} \approx 0.5$ the roof baffle was hardened with carbon-fibre-reinforced edge-shaded tiles to increase the discharge duration for the resulting higher heat load on the roof. The concept for a more versatile divertor (Div IIb) covering the triangularity range $0.3 < \delta_{bot} < 0.5$ under high-recycling conditions and low heat load was established towards the end of 1998. Operation of Div IIb is scheduled for early 2001 together with a rotation of the second neutral-beam injector (NI2) to achieve a higher current drive efficiency. As a first step towards this goal, the acceleration voltage of the NI2 injector was upgraded to 100 kV for deuterium in 1999.

The non-brazed steady-state target developed in 1997 was subjected in summer 1998 to 300 cycles at 10 MW/m^2 with a 20-second duration. No signs of fatigue were detected. The first 30 MVAr module of the reactive power compensation for generator EZ3 was commissioned in autumn. First numerical computations with an approved dynamic generator model have shown the feasibility of running the two 10 kV fly-wheel generators EZ3 and EZ4 synchronously in parallel.

7.1 Parallel Operation of EZ3 and EZ4

The two synchronous generators at present feed the poloidal field (PF) coils and the additional heating systems via two independent grids. Load sharing has therefore to be arranged in a complicated way to be consistent with the available flywheel energy and the apparent power of the generators. Since the main parameters of EZ3 and EZ4 - grid voltage and speed change for unloading the flywheels - are identical, it is in principle possible to switch the generators in parallel, hence to feed the whole load via a common grid. The synchronous unloading of the flywheels would then be guaranteed. Proper sharing of the apparent power could be achieved by suitable voltage controllers. First numerical computations with SIMPLORER have confirmed this concept and indicate that intense load changes will not violate synchronism. Figure 7.1 shows the load changes impressed in the active and reactive power and the small changes of the grid voltage resulting from the control of the exciter currents. The maximum rotor angles relative to the common grid for EZ3 and EZ4 are only 22 and 15 degrees, respectively. Figure 7.2 shows the transient behaviour of the individual generator currents and the load current on the common grid. Steady-state conditions are established within 1.5 s. The resultant current sharing is in good agreement with the apparent power ratio of the two generators. Further computations with regard to stability limits and assessment of saturation effects with the code EMTP will follow.

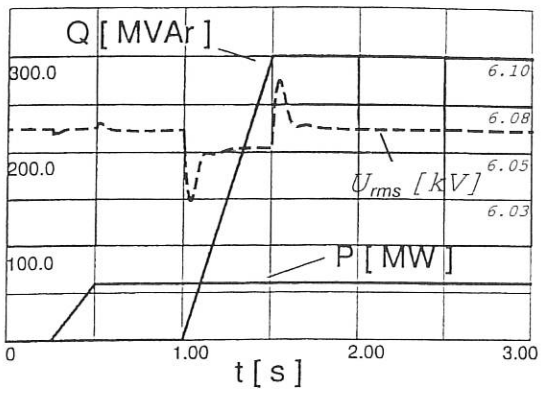

FIG. 7.1: Impressed total active and reactive load and resulting voltage response for EZ3 and EZ4 in parallel.

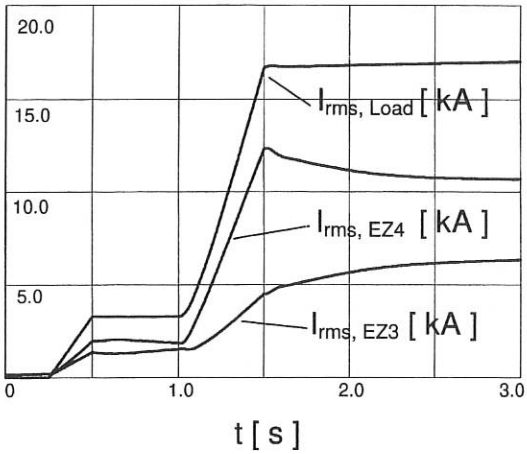

FIG. 7.2: Transient current response for EZ3 and EZ4 in parallel for the impressed load of Fig. 7.1.

7.2 Reactive Power Compensation (RPC)

The commissioning tests of the first 30 MVAr / 100 Hz RPC module showed that the consecutive initiation of the two 15 MVAr capacitor units during plasma ramp-up is effectively controlled by the reactive power measured on the EZ3 generator bus. The switching action, performed by phase-synchronized vacuum switches with zero voltage closing control, is achieved within the projected tolerance of 0.5 ms. The calculated surges on the generator bus and capacitors were confirmed for synchronized as well as alternative 3-pole switching. The purpose of the RPC modules is to reduce the generator current, i.e. the apparent power. Due to the small power factor, which is usually a consequence of fast PF-coil current control with thyristors, RPC is very effective. Figure 7.3 shows one of the first RPC module commissioning tests for a particular situation. The generator is loaded in such a way that the reactive power is almost completely compensated by the RPC module. The switch-on of the second RPC unit distinctly shows the resulting reduction of the generator phase current. Operation of a further three 30 MVAr RPC modules (EURATOM Preferential Support) is scheduled for late 2000.

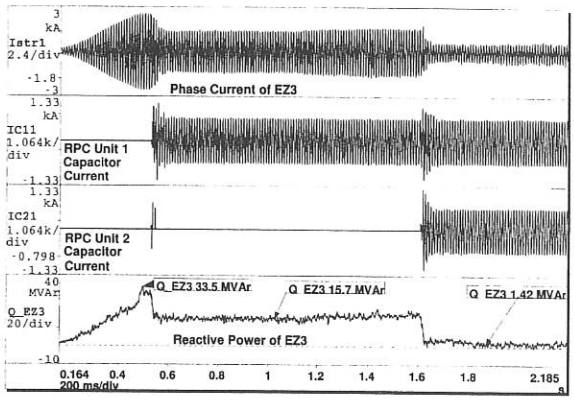

FIG. 7.3: Reactive power compensation with module 1.

7.3 Machine Protection System

The machine and discharge control systems of ASDEX Upgrade are integrated with a common machine protection system. The protection system was upgraded to cover the increased operational range:

1. For better control of closed divertor and advanced tokamak configurations, the poloidal coil systems in-line operated ohmic coil segments had been split up into central column and upper and lower coils, with individual power supplies. The real-time coil monitor was enhanced to initiate soft discharge termination in case of excessive mechanical overloads.
2. The coil current monitor was restructured to take account into the individual current limits of coils, thyristors and transmission lines, depending on the power supplies and cross-bar settings. Protection layers and current limits were re-designed for hierarchical onset of shape controller set value clipping, thyristor current clipping, soft discharge termination and machine pulse stop.
3. For improved protection of generators and coils in case of failures in the internal control system of the power supplies, the real-time coil monitor was enhanced to intervene immediately on the level of power breakers in case of inadequate current ramp-down.

7.4 Data Processing

Most of the work of the data acquisition and processing group was sirected at maintaining and upgrading the current DAQ, analysis and archival systems. Noteworthy topics are:

1. Replacement of two file servers by dual processor Sun UltraSPARC 60/300 PCI systems.
2. Acquisition of three fibre channel disk arrays as RAID file systems for doubling the available user and archive disk space. This was required to manage the data acquired and processed by the now up to 220 diagnostics (raw and processed), which deliver 550 MBytes of data per shot on a regular basis.
3. Rebuilding of the whole ASDEX Upgrade office network as a structured FastEthernet with a GigabitEthernet back-

bone. Not only will the GigabitEthernet backbone, going into operation in 1999, appreciably increase the access speed to the archived ASDEX Upgrade files stored in the computer centre, but also the ASDEX Upgrade environment will benefit from faster access to the German high-speed research network (DFN).

4. The diagnostic software and diagnostic supervision control software (DUT) were extended to start and operate diagnostics remotely from the DUT control application at a central desktop.

7.5 Neutral Injection

7.5.1 *Commissioning of the second injector*

Since Dec. 1997 the neutral beam injection system of ASDEX Upgrade consists of two beam-lines: conventional arc sources are used for the first beam-line, whereas the second beamline is equipped with new RF sources. These two beamlines have achieved injection powers of 14 MW with 55 keV H^0 and 20 MW with 60 keV D^0 (Fig. 7.4), respectively. During the course of the experiments, the RF sources proved to be as reliable and efficient as the arc sources of the first injector. Measurements of the beam composition via Doppler shift spectroscopy in the neutralizers showed an increase of the full-energy component by about 10%; this was confirmed by Doppler shift measurements in the duct during injection into the empty torus (i.e. without plasma and magnetic field). During shut down in autumn 1998, the RF ion sources were upgraded to 100 kV deuterium injection by increasing the gap between the plasma and acceleration grid from 8.0 mm to 15.4 mm. This changes the perveance; hence the beam current is lower at a given voltage, again limiting the injected power at 100 kV to 2.5 MW per beam. The sources were high-potted to 100 kV at the testbed, and - because D^0 operation is not possible there - conditioned up to 70 kV hydrogen operation; presently, they are being further conditioned up to the full power level at the second injector.

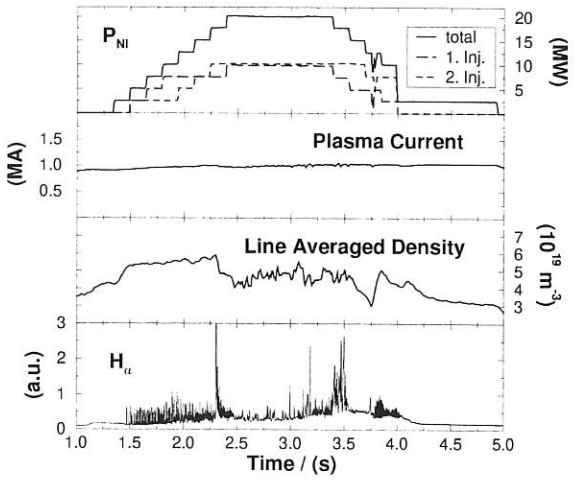

FIG. 7.4: 20 MW neutral injection into ASDEX Upgrade with 60 keV D^0.

7.5.2 *Real time injected power control*

Ion sources are switched on and off individually by the tokamak discharge controller. In addition, particular sources can be subjected now to variable on/off modulation to produce on the average any neutral power level (Fig. 7.5).

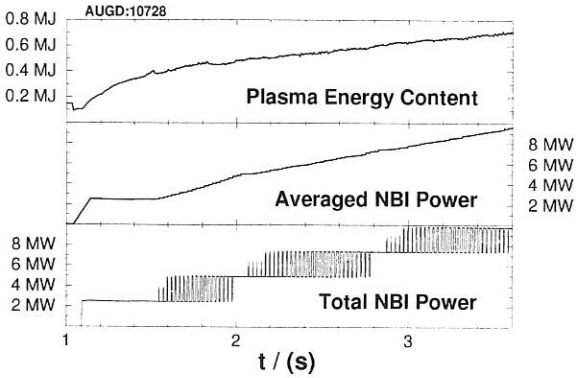

FIG. 7.5: Beam power variation by on/off modulation.

7.5.3 *Tangential NB injection for off-axis current drive*

A proposal to modify the geometry of the second neutral beam injector in order to achieve off-axis current drive was discussed in some detail in the 1997 Annual Report. It involves reorientation of the injector as a whole towards a more tangential injection direction as well as steeper inclination of the two more tangential beams. To this end, the injection port of the tokamak vessel and parts of the support of the PF coils have to be changed. Meanwhile, EURATOM preferential support for this proposal has been granted. Detailed design of the various components to be modified is proceeding. The rearrangement of the injector and the necessary alterations to the ASDEX Upgrade tokamak system are scheduled to start in summer 2000.

7.6 Electron Cyclotron Resonance Heating

The ECRH sytem is still not completed. Its final parameters will be f = 140 GHz, P = 2 MW (4 gyrotrons) and T = 2 sec. Details of the planning can be found in earlier annual reports. Up to now 2 gyrotrons have been installed and used for experiments. Aims of the investigations were mainly heat wave propagation studies, comparison of on-axis and off-axis localized power deposition, and experiments on the stabilization of neoclassical modes. Results are reported in the ASDEX Upgrade experimental sections. For the mode stabilization experiments the gyrotrons were modulated synchronously to the mode signal of the Mirnov coils within a frequency of up to 25 kHz. This fast modulation is only possible via an analog input to the series modulator tetrode. We feed 2 gyrotrons via 1 modulator. The resulting high loading of its anode, limits the pulse duration of 150 m/sec. The transmission lines - partly quasioptical and partly oversized corrugated waveguides - worked reliably. However, the transmission losses were higher than expected. This called for a new determination of the gyrotron

output beam parameters and a new design of beam correction mirrors. Quantitative results of a possible improvement are not yet available. Unfortunately, one of the gyrotrons suffered a cutoff and since that event it is no longer working reliably and needs repair. The remaining two gyrotrons have meanwhile been delivered to IPP. The acceptance tests are in progress. Three gyrotrons are therefore expected to be available in early summer 1999 for the experiments.

8. CORE PLASMA PHYSICS

8.1 Improvement of Plasma Shape Control

Plasma shape control was extensively used to assist experiments with internal transport barriers. The goal was to avoid the H-mode regime during phases with reversed shear and hight edge currents. Shape control was used to place the plasma close to the inner heat shield in order to reduce neutral particle circulation and avoid cooling of the plasma edge. Another approach to shift the H-mode threshold was to establish upper divertor plasma configurations with negative ion ∇B drifts. Even further refinements are required to achieve a stationary transport barrier. These may include medium and highly triangular plasma shapes as well as an alternative start-up scenario where diverted shapes are established before plasma current flat-top. An important improvement to shape control was added with the introduction of redundant actuators. Using more poloidal field coils than controlled variables in the feedback loop provides an opportunity to balance the current load automatically to avoid power supply limitations and thus gain a larger operation window during variations of external heating. A first approach, feedforward $\beta_{pol} - l_i$ compensation, had already been introduced in 1997. A more general and sophisticated method was now developed and implemented. A Riccati state space controller design technique optimizes a coil-load-dependent performance index. The resulant state space controller with state estimator can be be approximated by a matrix PID control law. This is accomplished with a modified version of the frequency collocation method which we have already used for controller design. Thus we still succeeded in preserving the simplicity and robustness of an output feedback structure. Due to its persuasive advantages, the shape controller with redundant coils has meanwhile become our standard control method.

8.2 Protection Reflex Manager

To reduce the risk of damage to the machine when running discharges close to operation limits, a real-time protection reflex mechanism was implemented. It recognises and counteracts a number of instabilities by using the plasma performance controller's heating and refuelling actuators.

1. Locked modes are detected from saddle coils. Disruption mitigation is immediately initiated by impurity injection with pellets or gas puff to radiate the plasma energy and reduce forces on vessel and tiles.
2. Detachment state changes to deeply detached OH or L-mode after transition from H-mode. This is derived from Da in the divertor legs and li. Disruption can be avoided and the plasma be attached again by increasing the neutral beam power with the gas valves closed.
3. Plasma-deposited energy onto divertor tiles is calculated from the ohmic and auxiliary heating powers. When reaching 90% of the limit, the heating power is gradually reduced, and suspended when approaching 100%.
4. Radiation collapse occurs when the radiated power Prad detected by bolometers exceeds the total heating power Pinput. Then the gas valves are closed to reduce the density and radiation, and the auxiliary heating power gradually increases the plasma temperature to drive the power ratio below unity.

Protection reflexes temporarily override all standard discharge control processes to access required actuators immediately. Upon termination, control is passed back to the suspended processes to continue execution of the scheduled discharge. To provide for a context-specific protection strategy the experiment leader may disable individual reflexes for the entire shot or just during certain phases of the discharge.

8.3 Confinement and Transport

8.3.1 Plasma performance at high NBI power

The increase in neutral beam power to 14 MW (H^0) and 20 MW (D^0) by adding a second injector together with the improved power-handling capability of the LYRA divertor (DV-II) allowed us to study the operational windows and the performance of ASDEX Upgrade plasmas over a much larger range of parameters. In pure deuterium plasmas (D_2 gas puff fuelled and heated with D^0 beams), the L-H power threshold for DV-II at low and medium densities is given by $P_{heat} = 2.1\bar{n}_e B_T$, about 20% above the value found for DV-I. This higher threshold is attributed to the higher edge densities in DV-II. For the first time it has been possible to achieve H-mode operation in pure hydrogen plasmas well above the L-H threshold with clear type-I ELMs. Up to densities of around 70% of the Greenwald density (n_{GW}) the power necessary to achieve H-mode is twice the value given above for deuterium discharges. At higher densities the H-mode could not be obtained even with the maximum available heating power.

In high-β experiments the stationary β-values are limited by the occurrence of neo-classical tearing modes (NTM), discussed in detail in a previous section. These modes significantly restrict the performance of high-power-heated plasmas since they are accompanied by a drop of the plasma energy content W_{mhd} by typically 20-30%. Maximum values of W_{mhd}, up to 1.2 MJ, are therefore achieved only transiently. In deuterium, confinement times (τ_{mhd}) normalized to the ITER-89P L-mode scaling with H-mode multipliers, $f_{ITER-89P}$, above 2 are found in many cases. However, there is a clear trend to confinement degradation with increasing density, i.e. with strong gas puffing, $f_{ITER-89P}$ is below 1.8 for $\bar{n}_e/n_{GW} \geq 0.7$. Deuterium discharges not affected by the NTM roughly follow the power dependence $P_{heat}^{-0.5}$ of the scaling law up to the highest

heating power. In hydrogen, H-mode discharges with type-I ELMs have $f_{ITER-89P}$ values of 1.5 - 2.0. The confinement of L-mode (H^+) plasmas is 10-20% higher than predicted by ITER-89P. H-mode plasmas with type-III ELMs as observed close to the L-H threshold or at high densities lie in between L-mode and H-mode with type-I ELMs.

8.3.2 Confinement in ELMy H-mode

Here we compare type-I ELMy H-modes in hydrogen with type-I ELMy H-modes in deuterium and type-III ELMy H-modes in hydrogen to study the effect of isotope mass and ELM type on confinement. Comparison of roughly 20 time slices of type-I ELMy H-modes in hydrogen and much more in deuterium with the ITERH-92P(y,tot) scaling shows no obvious differences. Especially the strong isotope effect, given as $A_{eff}^{0.38}$ in the scaling (A_{eff}: effective ion mass), is evident from the data. Quantitatively, its magnitude is difficult to determine due to the limited number of data which show a large scatter (factor 2 for deuterium). The temperature profiles are higher in deuterium than in hydrogen by a constant factor of 1.66 over the whole radius, in agreement with the ratio of W_{mhd} values. However, $A_{eff}^{0.38}$ yields only 1.33. We noted that the profile similarity seems to be valid for both isotopes. Figure 8.1 shows the result of the global analysis for type-I and type-III ELMy H-modes in hydrogen with moderate densities of up to 60% of the Greenwald limit. The confinement of the different shots is compared by plotting the total energy confinement time τ_E^{tot} versus the ITERH-92P(y,tot) scaling. It can be seen that type-I ELMy H-modes perform about 20% better than type-III ones. Local analysis reveals that the profiles are no longer self-similar in the edge region where the ELMs are different.

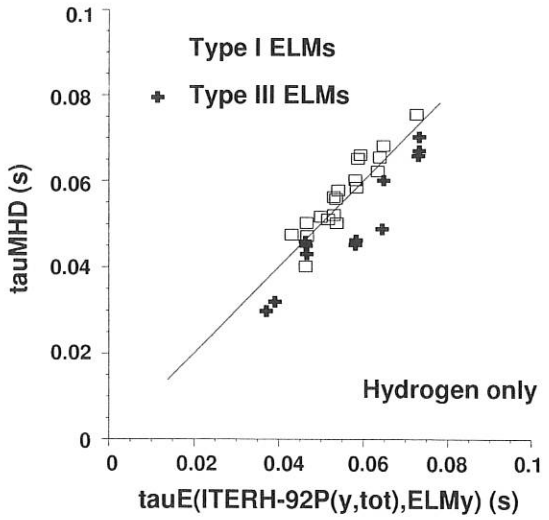

FIG. 8.1: Comparison of type-III and type-I ELMy H-modes in hydrogen with H-mode confinement scaling.

With doubled NBI heating power, the effect of saturation of the stored kinetic energy with increasing power was observed in H and D. The kinetic data are consistent with the magnetic measurement within a few per cent, indicating the reliability of the profiles. For both isotopes the power is ramped up in steps. No neo-classical tearing modes occurred in these cases ($\bar{n}_e \approx 0.65\ \bar{n}_{GW}$). After type-I ELMy H-mode is reached, T_e, T_i, and n_e profiles show strong saturation but do not significantly deviate from their self-similar shape. Describing the saturation by $W_{kin} = P_{heat}^{\alpha}$, we find $\alpha = 0.35$ for deuterium in the range from 7.5 MW to 15 MW. This is in agreement with the thermal ITERH-92P(y,th) scaling whereas similar hydrogen discharges deliver $\alpha \approx 0.19$ for the power range from 8.8 MW to 12.3 MW, which is significantly lower than predicted by the usual confinement scalings. For the ITERH confinement database it was found that the power degradation depends on A_{eff}. Fitted separately, the H and D data show a difference of 0.10 ± 0.04 for α, close to our experimental result. This underlines the importance of including such an interaction in the scaling analyses.

8.3.3 Transport studies with ECRH

ECRH was used to study transport in two types of discharges: ohmic-heated plasmas with off-axis ECRH or NBI-heated L-mode discharges. In the first case up to 600 kW ECRH was deposited in a narrow radial region at about mid-radius in ohmic discharges at a density $\bar{n}_e \approx 4 \times 10^{19}\ m^{-3}$. Clearly, the T_e profile exhibited a strong tendency to keep its shape (profile consistency). Power balance analyses indicate that transport was reduced in the volume between the ECRH deposition and plasma axis, whereas it increased outside this region. In these experiments, a 10% power modulation was added on top of the ECRH pulse to investigate the propagation of temperature perturbations. This allows one to distinguish between diffusive and convective transport, which is not possible in power balance analyses. The results indicate without ambiguity that the tendency of the T_e profile to remain peaked in the presence of off-axis ECRH cannot be explained by an anomalous inward heat pinch. Indeed, the profile of both the amplitude and phase of the temperature modulation are asymmetric, but opposite to the hypothesis of an inward heat pinch. In addition, the phase is expected not to be affected by convection. This behaviour would, however, be in agreement with a transport model based on critical gradient physics. In the second case, the NBI power is dominant and the on/off ECRH modulation makes a negligible contribution to heating. Analysis of the temperature modulation yields a so-called electron perturbative diffusivity χ_e^{pert} which differs, by definition, from the power balance χ_e^{PB}. Comparison of these two transport coefficients yields information on possible transport physics mechanisms. The transport results show that the ratio $\chi_e^{pert}/\chi_e^{PB}$ is around 2 at low heating power (close to ohmic) but quickly increases with auxiliary heating power, reaching 5 to 8, where it seems to saturate. This behaviour implies a strong dependence of χ_e on plasma parameters (e.g. ∇T_e^{α} with $\alpha \approx 5$) or, alternatively, that transport might be governed by physics based on critical gradients.

A second essential result is that χ_e^{pert} is higher in deuterium than in hydrogen. This is in direct contradiction to the well-known isotope effect on global confinement. These two results suggest that transient transport does not reflect time-averaged transport. In addition to the ECRH modulation, the propagation of sawtooth pulses in the same discharges was also analyzed. It appears that χ_e^{pert} for sawteeth is generally somewhat higher

than that of ECRH, but exhibits the same characteristics as the ECRH modulation; in particular, the isotope dependence is the same.

8.3.4 *Transport of H-mode edge plasmas*

A special version of the 1.5–D BALDUR transport code was used to analyze the transport in the steep gradient zone and core of ASDEX Upgrade discharge #7978. Profiles of the electron heat diffusivity χ_e and the ratio of the anomalous inward drift velocity v_{in} and the diffusion coefficient D were determined. It was found that the reduction of χ_e is strongest near the inner boundary of the steep gradient zone (of width 4 cm in the midplane), where it reaches a factor of four. The electron heat diffusivity is still anomalous, i.e. turbulence is reduced but not totally suppressed. The v_{in}/D profile was found to rise significantly at the edge, which causes the steep density decline measured. No degradation of energy transport in the bulk plasma was seen when the density limit was approached.

Fundamental properties of the anomalous inward drift in H-mode plasmas were explored. The strong rise with radius of v_{in}/D in the edge region is explained by a linear dependence on the neutral deuterium density n_0, resulting in a new scaling law $v_{in}(x)/D(x) = F_0 Z_{eff}(x) n_0(x) 2x/(\rho_w x_s^2)$. Applying it in simulations reproduced the empirical fit of the v_{in}/D profile not only in the edge but also in the bulk plasma. Modellings with the scaling yielded the observed flattening of density profiles with rising $\bar{n}_e$. The decreasing penetration of deuterium atoms to the core causes a decline of the inward drift. The new scaling was shown to be compatible with gas oscillation experiments, while n_0 independent scalings are not. It further explains the strong density profile peaking and rise of v_{in}/D during and after pellet injection owing to the increase in neutral density. The width of the steep gradient zone was found to be connected with the penetration of neutrals at the edge and the presence of high inward drift velocities.

8.4 Radiative Cooling Experiments

Owing to the high intrinsic impurity radiation level in ASDEX Upgrade, radiation cooling experiments in 1998 concentrated on trace impurity behaviour and control of the power flux into the divertor. The injection of moderate amounts of impurities in ASDEX Upgrade generally leads to improvement of the energy confinement and peaking of the electron density profile. Density peaking is always correlated with improvement of the global particle confinement. For discharges with the neutral particle flux in the divertor kept constant by feedback control, the improvement of particle confinement causes a pronounced increase of $\bar{n}_e$. If $\bar{n}_e$ is controlled, its rise after impurity injection causes a reduction of the gas valve flux, which may partly explain the observed rise in energy confinement. The rise of Z_{eff} associated with impurity injection is, for a given amount of additional radiation, much higher for conditions with low edge density or low type-I ELM frequency. The beta limit of impurity-seeded discharges seems to be slightly reduced and the MHD activity differs from the behaviour seen in clean discharges, which are typically limited by (3/2) neoclassical tearing modes. In combination with the improvement of energy confinement, the heating power for high-performance radiative discharges is restricted to values below about 10 MW. Impurity seeding has not resulted in increased divertor radiation so far. The divertor radiation in ASDEX Upgrade is dominated by carbon and mainly determined by the power flow into the divertor. The radiative contribution of seeded impurities in the divertor is offset by its inevitable main chamber radiation, which reduces the power flow into the divertor and therefore the intrinsic carbon divertor radiation.

8.5 Core Particle Transport

The particle transport of low to high Z-impurities (neon, argon, krypton and xenon) and of the background ions (deuterium) was investigated in the centre ($\rho_{pol} \leq 0.5$) of H-mode discharges with medium heating power. The impurity densities were extracted from unfolded soft X-ray intensities and the electron densities from deconvoluted interferometric measurements. Diffusion coefficients D and drift velocities v were evaluated by analyzing the temporal evolution of the according density profile between sawtooth crashes. In the case where the density profile reached an equilibrium distribution during the sawtooth period, additional information about v/D was gained from the slope of the static density profile. The measured transport coefficients in the radial range $0.15 \leq \rho_{pol} \leq 0.35$ can be characterized as follows. With increasing atomic charge Z, convective transport dominates more and more over diffusive transport. The drift velocities are always directed inward. For the impurities with $Z = 10$ (neon) to $Z \approx 40$ (xenon) the diffusion coefficient is approximately constant $D \approx 0.05\ m^2/s$, and the drift velocities enhance with Z from $v \approx -0.5\ m/s$ to $v \approx -2.5\ m/s$. The drift velocity decreases with decreasing deuterium density gradient. For the deuterium ions the diffusion coefficient $D \approx 0.2\ m^2/s$ is appreciably higher and the drift velocity is $v \approx -0.3\ m/s$. Neoclassical calculations of impurity and deuterium transport were performed for the investigated discharges. Plasma rotational effects and collisions of puffed impurity with intrinsic impurities were not taken into account. All puffed impurities are in the plateau regime in the plasma centre. Deuterium is in the banana regime. For the impurities the diffusion coefficient decreases with rising Z from $D_{neo} = 0.12\ m^2/s$ to $D_{neo} = 0.02\ m^2/s$, while the drift velocity stays more or less constant at $v_{neo} = -0.5\ m/s$. Thus, the neoclassical values are in the same range, but the dominance of convective transport for high Z is due to a decrease of D_{neo}. For deuterium the neoclassical diffusion coefficient $D_{neo} = 0.01\ m^2/s$ is a factor of ≈ 20 smaller than measured. The drift velocity is dominated by the Ware pinch and is $v_{ware} \approx -0.1\ m/s$. Comparison of measured and neoclassical transport coefficients reveals that the central deuterium transport is dominated by anomalous effects, while for the impurities the transport coefficients are close to neo-classical values. The anomalous transport coefficients found for deuterium do not act on the impurity ions in the investigated Z-range. Thus, deuterium and impurities have different anomalous transport.

8.6 Impurity Pellets for Disruption Mitigation

Several experiments for studying the reduction of the mechanical and thermal loads during disruption by means of impurity pellets were carried out in the period June - August 1998. Earlier experiments in ASDEX Upgrade used frozen neon pellets, prepared in a cryostat and injected with a centrifuge. Since a cryo-system is not quite ideal for stand-by application, typical of a disruption mitigation system, a new pellet gun for injection of solid pellets was developed. The injector was designed, built and put into operation on ASDEX Upgrade by S. Egorov in the framework of the collaboration between the Technical University of St. Petersburg, Russia, and IPP.

The injector installed in sector 5, 210 cm from the plasma, allowed injection of pellets 0.5 - 2.4 mm in diameter with a velocity of 100 - 500 m/s. The pellets used in this experiment were made of silicon (Si) or titanium (Ti) powder mixed with molten polyethylene (PE) and then extruded in the form of a cylinder. Spheres 2 mm in diameter were then obtained by compression and heating. Si and Ti were chosen because of their "good" radiative properties and acceptability in the machine; PE because of its relatively lower sublimation energy.

The pellets were first injected with a timer in order to test the injector and collect data in a variety of plasma conditions. The target plasma did not have pre-disruption characteristics and had energies in the range 100 - 800 kJ, which allowed the penetration depth to be determined as function of the plasma parameters. In all cases the pellet ablation caused disruption within 2 ms from the appearance of the pellet at the plasma edge and reduced the mechanical loads to 20 - 50% of the reference mechanical loads.

In a subsequent experimental campaign several pellets were injected with the locked-mode trigger being used in the presence of a locked mode in plasma and pre-disruption conditions. Due to the relatively long time delay (20 ms) between the trigger and plasma some pellets reached the plasma after disruption. All pellets reaching the plasma before disruption or within a few ms after its onset reduced the mechanical loads to 20 - 50% of the reference mechanical loads. Other measurements also confirm that the Si-PE pellets sufficiently ablated during the immediate post-disruption phase owing to the presence of a large loop voltage and fast electrons. No evidence of run away electrons generated by the pellets was recorded in these experiments.

The injector was recently (end of 1998) installed closer to the plasma in sector 13 in order to reduce to 10 ms the delay time between the trigger and appearance of the pellet in the plasma. A guiding tube is also to be installed in the coming year in order to prevent the propellant gas from streaming a head and aviod premature disruption caused by this gas.

9. SOL AND DIVERTOR PHYSICS

9.1 SOL and Divertor Physics

The main subject in this area in 1998 was a detailed comparison of the two divertor geometries, and the first siliconization of the ASDEX Upgrade vacuum vessel.

9.1.1 *Relation between divertor neutral gas and SOL density*

For the midplane-averaged SOL density ($n_e^{SOL} = 1/L^{SOL} \cdot \int n_e(r)dr; L = 6$ cm) a robust scaling relation $n_e^{SOL} \propto \Gamma_0^{0.5} q_{95}^{0.5}$ (q_{95} being the safety factor at 95% of the flux) is found, which is valid for almost all operational regimes and confinement modes, such as OH, L, and H. For the latter, averaging over ELMs was performed. The parameter n_e^{SOL} is introduced to get a direct measure both of the transparency of the SOL plasma to neutrals and of the SOL width.

For a series of five clean H-mode discharges in DIV-II ($I_p = 0.6 - 1.2$ MA, $B_t = 2.02.5T$, $P_{NBI} = 5$ MW, density ramped up close to the H-L back-transition), a scaling relation similar to that in DIV-I has been found, $n_e^{SOL} \propto \Gamma_0^{0.55} q_{95}^{0.68}$. In Fig. 9.1, this scaling is applied to both, DIV-I and DIV-II data, demonstrating that the midplane n_e^{SOL} is rather well described by one single scaling relation in the two divertor geometries. Very high values of Γ_0 in the more open DIV-I geometry were obtained just by reducing the pumping speed. These discharges, denoted by the symbol x, show a deviation from the scaling because the reduction of the number of active turbomolecular pumps introduces a toroidal asymmetry in the divertor neutral flux density. This variation in the neutral flux density leads to the increased scatter seen in Fig. 9.1.

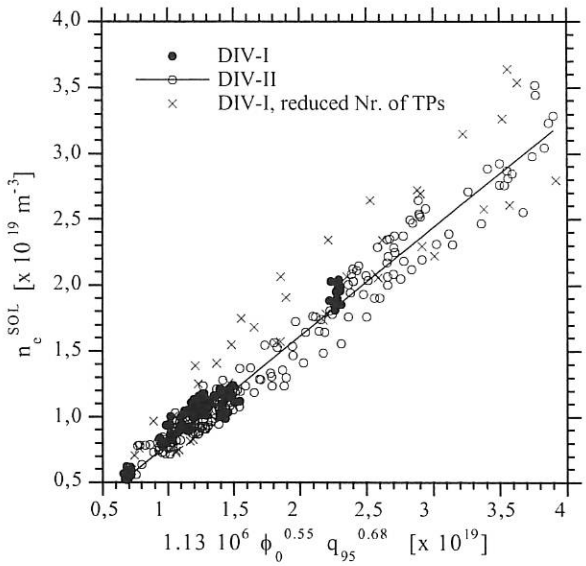

FIG. 9.1: Scaling for the midplane averaged SOL density.

9.1.2 *Neutral gas behaviour and particle exhaust*

The more closed LYRA divertor (DIV-II) resulted in a much higher neutral gas compression as shown in Fig. 9.2. With the same line-averaged density in the two geometries, the midplane neutral flux densities are also the same, but the divertor neutral flux density and hence the deuterium compression $C_D (C_D = \Phi_{o,D}^{divertor} / \Phi_{o,D}^{midplane})$ in DIV-II are a factor of 5 higher. The fact that the tighter baffling in DIV-II does not result in a

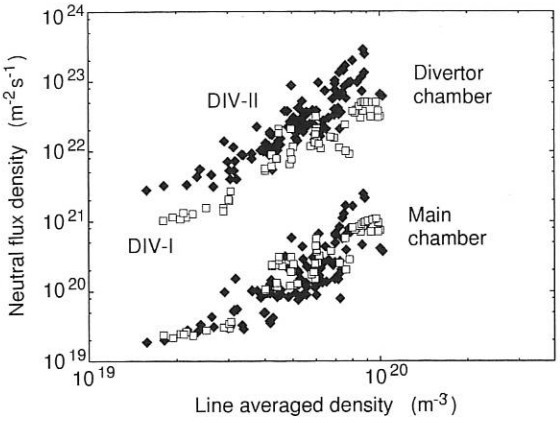

FIG. 9.2: Neutral flux densities in both divertor geometires as a function of $\bar{n}_e$.

lower midplane neutral density for the same plasma density is a clear indication that the midplane neutrals are determined by wall recycling. Small gas puffs of helium and neon were introduced to investigate impurity exhaust. As was predicted by B2–EIRENE, the exhaust rate of helium in DIV-II is higher than in DIV-I, while that of neon decreases. This is a result of the ionization length of helium being larger, therefore allowing better penetration of helium through the divertor plasma into the pump chamber below the dome baffle.

9.1.3 Reciprocating Langmuir probe measurements

The fast reciprocating Langmuir Probe System (LPS), operated by the group from Demokritos, Greece, was equipped with a new "Mach-type" probe head. Apart from the standard T_e and n_e profiles, complex flow patterns were revealed. In the scrape-off layer, the plasma flow is directed towards the divertor plates. Higher Mach numbers are observed at the inner divertor leg. A significant flow is observed between the two divertor legs, in the private flux region. In attached plasmas, the cold plasma flows from the inner to the outer divertor plate. When the inner divertor approaches detachment, the flow reverses direction, from the outer to the inner leg, as seen in Fig. 9.3. These observations are in agreement with data from spectroscopy and B2-EIRENE simulations. The floating potential measurements allow alternative localization of the separatrix position at the

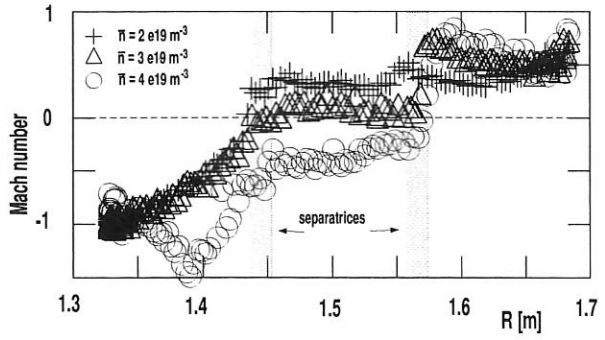

FIG. 9.3: Toroidal flow velocity along the major radius.

height of the LPS trajectory. They suggest an outward shift of the inner separatrix of about 2 cm as compared with the position from the magnetic equilibrium reconstruction (FP without edge currents).

9.1.4 Wall conditioning by siliconization at ASDEX Upgrade

Conditioning by wall coating is performed in fusion devices to reduce the inevitable contamination of plasma discharges due to oxygen after venting of the vessel and to vacuum leaks. The coatings are chosen such as to obtain, to on the one hand, a strong getter effect for oxygen and, on the other, a rather low atomic number (low Z) to prevent strong radiation by contamination of the plasma with particles from the coating itself. Beryllium and boron are the most commonly used coating materials at present. Experiments in the TEXTOR limiter tokamak at Jülich showed that silicon may also be suitable for wall-conditioning purposes, but high silicon concentrations in the plasma had a strong influence on the plasma behaviour. Since plasma-wall interaction in a divertor tokamak strongly differs from that in a limiter tokamak and since there are considerable technical advantages compared with boronization, siliconization was performed in ASDEX Upgrade.

Siliconization procedure

The silicon was deposited in the vessel walls by a DC glow discharge in a He-silane ($Si\ D_4$) mixture. Although silane is highly inflammable, it is much less toxic than diborane, which is used for boronization. This is important not only during the coating procedure itself, but also for subsequent vessel inspections where remnants of the wall conditioning may still be present or will be activated by contact with moist air. Measurement of the discharge current and analysis of deposition probes exposed during the procedure showed a Si-layer thickness of 50 nm. Inspection of the vacuum vessel after venting showed very homogeneous deposition on the walls. Surface analyses of the deposition probes revealed that Si layers are chemically much more stable than boron layers produced in a comparable procedure (more details are presented in section "Surface Physics Division").

Silicon fluxes and concentrations

The silicon fluxes into plasma discharges at the heat shield and in the divertor were strongly density-dependent and decreased for comparable discharges with the temporal distance from the siliconization. The influxes show a smooth variation across the inner heat shield with a broad maximum in the equatorial plane and a strong increase towards the upper divertor region. The Si concentrations in the central plasma also shared a strong decrease with increasing plasma density. The concentration varied from about 2×10^{-3} in low-density H-modes down to $\approx 10^{-4}$ for higher densities. In ohmic discharges the Si concentrations were even lower. During limiter operation the Si concentration was found to be a factor of up to 10 higher than during divertor operation with comparable discharge parameters. This is attributed to the fac, that, due to the siliconization procedure (glow discharge), almost no silicon is deposited in the lower

divertor region. Additionally, the inner heat shield is exposed during limiter operation to a plasma of much higher temperatures than the divertor, which leads to larger erosion yields due to physical sputtering through deuterium. This observation is also in line with the pronounced density dependence found in divertor operation, because higher plasma densities generally lead to lower edge temperatures and therefore to lower sputtering yields. Analyzing the Si content for several days of plasma operation showed that it is reduced to half its value after about 50 discharges after siliconization.

Intrinsic impurities and plasma performance

During the first discharges after siliconization there was a strong, but transient, reduction of the carbon content. It is assumed that the rather fast increase of the C concentrations after siliconization was due to a strong carbon source at the ICRH protection limiters, where obviously high power loads were present and the Si layer was removed very fast. Oxygen is removed very efficiently from the discharges. The effect is somewhat longer lasting than for boronization, especially for ohmic discharges. This also points to higher stability of the Si layers, which was already found in the surface analysis. Analogous behaviour is also found in ohmic density limit discharges, where overall higher densities can be reached, which also lasts for more discharges after boronization. Due to the generally low concentrations of silicon in the discharges there was no negative effect on the overall plasma performance observable. The integral radiated power during divertor operation was found to be very similar to that under boronized conditions.

The above-mentioned properties lead to the conclusion that siliconization is a worthwhile alternative to boronization, having all its advantages and being technically much easier to handle.

10. DIAGNOSTICS

10.1 Motional Stark Effect Diagnostic

The Motional Stark Effect (MSE) diagnostic for determining the ASDEX Upgrade current profile started operation, using 8 spatial channels, covering about half of the plasma cross-section. With observation of one of the 2.5 MW heating beams, the polarization direction of the σ-component of the Doppler-shifted and Stark-split deuterium Balmer-α beam emission is measured with a time resolution of 3 ms. Various calibration techniques were employed to determine the offset of the measured polarization angles due to Faraday rotation (FR) in the optical elements. The FR rotation originates from the parallel component of the toroidal magnetic field along the optical path of each line of sight and therefore differs from channel to channel. For the ASDEX Upgrade MSE diagnostic the FR rotation offset ranges from 0.5 to 1.3 deg/T, which cannot be neglected. The measured MSE polarization angles were included in the equilibrium reconstruction code, CLISTE (CompLete Interpretive Suite for Tokamak Equilibria), which allows the number of free parameters of the inferred current or safety factor (q) profiles to be increased to the extent that even non-monotonic q-profiles can be represented. Figure 10.1 shows the result of such an equilibrium reconstruction for a discharge with 5 MW of neutral beam injection during the current-ramp phase. The rise of the electron temperature due to the additional heating results in reduced current diffusion and hence preservation of the initially negative central magnetic shear ($s = \frac{r}{q}\frac{dq}{dr}$) over a longer period of time.

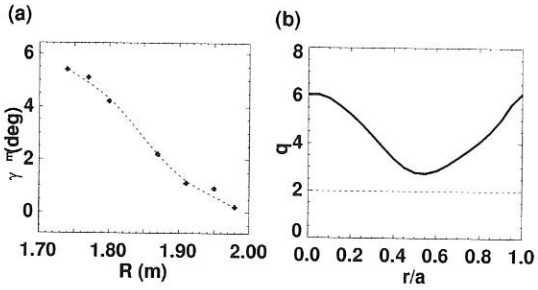

FIG. 10.1: Result of an equilibrium reconstruction using CLISTE for a discharge with negative magnetic shear in the plasma core: (a) Measured MSE polarization angle (crosses) and fit to experimental data (dotted line) . (b) Corresponding q-profile, which clearly shows negative magnetic shear in the plasma core.

10.2 A Sublimation Probe as Impurity Source

In the divertor of ASDEX Upgrade a sublimation probe, as controllable source for high-Z impurities, was installed. With this probe it is possible to inject materials that sublimate at temperatures from about 50° C to 150° C into the plasma through a valve. It consists of a heatable cavity in which the substance to be sublimated can be filled (Fig. 10.2). A coil,

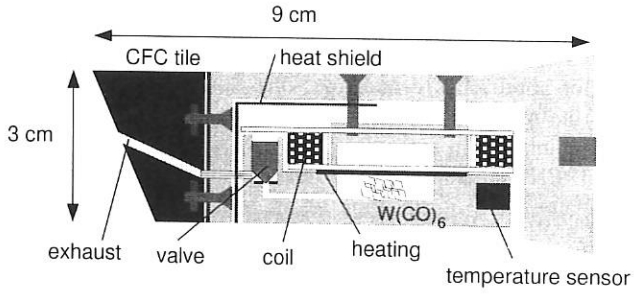

FIG. 10.2: Schematic setup of the sublimation probe.

perpendicular to the toroidal magnetic field, is connected to the valve, which can be opened through the torque acting on the coil's magnetic moment. The valve is then opened in the toroidal when a voltage is applied to the coil. Additionally, an absolutely calibrated array of 5×5 optical fibres was installed which allows spectroscopic observation of the cloud of injected impurities. For investigation of tungsten transport in ASDEX Upgrade the probe was operated with tungsten carbonyl. First applications show that the estimated divertor retention potential for tungsten is consistent with previous investigations.

INTERNATIONAL COOPERATION

The collaboration with other international institutes and universities was considerably extended. Besides the below-mentioned collaborations there was cooperation with the following institutions: Istituto de Fisica del Plasma, CNR (Italy); Ecole Polytechnique Fédérale, Lausanne (Switzerland); University of Strathclyde (Scottland); FOM-Institute voor Plasmafysica, Rijnhuizen (Netherlands); Centre Canadien de Fusion Magnétique, Varennes (Canada); University of Toronto (Canada); Institute of Applied Physics, Nishni Nowgorod (Russia); I.V. Kurchatov Institute of Atomic Energy, Moskau (Russia); IOFFE Institute, St. Petersburg (Russia); Institute for Plasma Research, Bhat, Gandhinagar (India); Southwestern Institute of Physics, Chengdu (China); Institute of Plasma Physics, Academia Sinica, Hefei (China); Korea Basic Science Institute, Yusung (Korea); NIFS, Nagoya (Japan); Kuo University, Yokohama (Japan).

1. DOE – ASDEX Upgrade Activities

Of main emphasis was the investigation of Advanced Tokamak scenarios, i.e. heating during curent ramp-up, confinement improvement and maximization of beta. Therefore, topics of mutual interest in the ASDEX Upgrade and DIII-D research programs were

1. L-H transition physics particularly at low density,
2. the correlation between H-mode pedestal parameters and energy confinement,
3. the scaling of H-mode pedestal parameters.

The primary focus is the analysis and interpretation of data from high resolution spectroscopy of divertor impurities. Of particular interest in addition to impurity dynamics is the determination of the sources of carbon. A common observation on both experiments is that the neutral flux density, following an ELM, always decays with a 10ms time constant, which is much too slow to be related to the ELM re-heat time. Analysis of the data in a similar way showed that this feature is the result of desorption of particles from the wall during the ELM power and heat pulse.

A new field of intensive collaboration arose in tokamak theory. First of all, apparent discrepancies in theoretical descriptions of ballooning instability limits and the onset of type-I ELMs were clarified. Further topics were:

1. building up a common data base for neo-classical tearing-modes (DIII-D, JET, ASDEX Upgrade) and performing a scaling which should allow to predict the stability of ITER against these neo-classical tearing-modes;
2. MHD stability of the plasma edge: computations with the DIII-D code are planned;
3. diagnostics of detached divertor plasmas: computations of the Stark effect broadening with the IPP code are foreseen.

The collaboration in the field of ICRF heating has been intensified between GA, ORNL, and MIT on one side and IPP Garching ont the other side. As already discussed in the previous report, new tetrodes will be necessary in the future for the RF generators in Garching. GA is already testing those. The experience gained there will be beneficial for IPP. Technical tests of a ferrite tuner system (also called hybrid tuner system), developed by AFT (a German company) for D-III-D were successfully performed by the company at IPP. D-III-D has now loaned the system to IPP for tests on plasma at ASDEX Upgrade for the next campaign.

A cooperation with the Oak Ridge National Laboratory on the development of new ICRF antennas for ASDEX Upgrade (adopted for high triangularity) has been initiated.

In collaboration with MIT mode conversion experiments on ASDEX Upgrade were performed and power deposition profiles were measured.

The investigations of new mixed material phases on Be and W surfaces and their plasma-wall interaction properties were continued. They included experimental and calculational investigations of the mixed material system C in W. Preliminary data on the change in surface scattering due to composition changes by the bombardment of W with C were achieved. Calculational work determined deposition and erosion regimes at steady state for the same system.

2. CEA, Cadarache

The six working groups established for collaboration between ASDEX Upgrade, W7X and CEA had a common meeting in July 1998 to discuss special issues.

3. University of Cork, Ireland

The collaboration with the University of Cork concerning MHD equilibrium identification using magnetic measurements was continued. Detailed studies between the different versions of

FP and an interpretative equilibrium package "CLISTE" were performed. The latter includes information from the presently installed MSE diagnostics and from rational q-values from SXR measurements.

4. DEMOKRITOS, Greece

The fast reciprocating Langmuir Probe System (LPS) for the ASDEX Upgrade divertor has been operated mainly, as a "Mach" probe. Apart from the standard ne, Te profiles, complex flow patterns, dependent on the operational regime have been observed. (see section..?.. prepared by Dr. Bosch). The floating potential profiles allow a localisation of the separatrix position at LPS trajectory level. They suggest a 2 cm outward shift of the inner separatrix leg compared to the one predicted by magnetic equilibrium reconstruction (FP - without of edge currents). The work on fluid equations for multispecies plasma including drifts and currents has been completed and implemented in to the tokamak edge simulation code B2.5.

5. Centro de Fusão Nuclear, EURATOM IST Association, Lisbon, Portugal

The cooperation between Centro de Fusao Nuclear and ASDEX Upgrade aims to investigate and exploit microwave reflectometry for profile and fluctuation measurements in ASDEX Upgrade plasmas. A multi-band fast-sweeping frequency modulation (FM) reflectometer is operational for several years and has now been upgraded with heterodyne detection for the higher frequency bands (V-band and W-band, $f = 50 \ldots 110$ GHz). In addition to the sweeping reflectometer, a dedicated fluctuation monitor system has been installed, and the antennas have been adapted to the change of the in-vessel components for more strongly shaped plasmas.

A main focus has been the development of improved density profile evaluation techniques, in particular the use of Fast Fourier Transforms to detect fluctuation-induced signals and discriminate those from the reflection interference pattern. These techniques have been implemented in the form of a data analysis program which facilitates a mostly automatic evaluation procedure. The addition of routinely measured density profiles to the ASDEX Upgrade data base is in progress.

6. UKAEA Culham, United Kingdom

The collaboration continued on the H-mode threshold at low densities, the ideal and resistive MHD stability and the preparation of ECRH/ECCD stabilization experiments of magnetic islands.

7. Institut für Allgemeine Physik, TU Wien and Friedrich Schiedel Foundation

Collaboration with the Austrian Institut für Allgemeine Physik concerns the development and operation of atomic beam diagnostic systems. These activities are made possible by financial support of the Austrian Friedrich Schiedel Foundation für Energietechnik. The current project contributes to the extension of the diagnostic potential by improving necessary atomic data bases for accurate raw data interpretation.

8. TEKES (HUT and VTT), Finland

The Finnish group works on the modeling of kinetic effects in the plasma edge. This includes the confinement of ripple trapped ions by the radial electric field, the ion distribution in the edge of the plasma, and the neoclassical radial electric field driven by orbit losses. The simulations help by the interpretation of diagnostic signals, but also aim at a better understanding of the physics. Of special interest is the question whether the orbit losses play an important role in the L-H transition.

9. Inst. of Electronics, Res. Found. Hellas, Heraklion, Greece

Evolution of Vapour Shields over Divertor Plates during Disruptions. The development of a self-consistent 2-D model for the determination of the current, perturbation magnetic field, and electric field distributions in the poloidal plane has been completed. The results show the onset of a strong $E \times B$ drift in the poloidal plane.

10. KFKI RMKI, Budapest, Hungary

A 1.5-D radiation transport model has been developed for describing radiation emission patterns observed during impurity (carbon) pellet injection in Stellarator W7-AS. First comparisons show good correspondence between measured an calculated results. Further validation by experimental results is needed.

11. Cooperation with Russian Institutes

Numerical Modelling of C Pellet Ablation Scenarios in Stellarator W7-AS. Fourteen randomly selected carbon pellet injection scenarios have been analyzed by the IPP quasi-three-dim. code llpell. In the case of 'tokamak-like' discharges with presumably Maxwellian energy distribution of the background plasma particles, the deviation between the computed and measured penetration lengths was, on the average, less than 6%.

The impurity pellet injector developed by S. Egorov from SPU was installed on ASDEX Upgrade and several successful experiments were carried out with it. The injector performance was quite reliable and the injected impurity pellets reduced the disruption loads as desired.

12. CREATE Group, Napoli, Italy

The collaboration with the CREATE team continued with the prediction of using neural networks.

JET Cooperation Project

(Head of Project: Prof. Dr. Michael Kaufmann)

JET began in 1998 with a month of operations to complete urgent **ITER Physics Studies** in hydrogen and deuterium. The aim was to reduce the uncertainties in extrapolations to ITER by obtaining improved data on confinement, H-mode threshold power, divertor behaviour and stability in ITER-like plasmas in hydrogen and deuterium. The third stage of the JET divertor programme then started early in February 1998 with a four-month shutdown for the exchange, by remote handling without manned intervention in the vessel, of the Mark IIA divertor for the Gas Box divertor (Mark IIGB). This shutdown was highly successful and provided a clear demonstration of remote handling as a method of maintenance, repair and upgrading of fusion devices. The shutdown was completed as planned at the end of May, the first plasma pulse was obtained in early July and, following a planned power outage in August, the experimental campaign with the Mark IIGB divertor commenced in early September. **Task Force A** had the objective of characterising the more closed Mark IIGB divertor and further qualifying the ELMy H-mode for ITER. **Task Force B** had the objective of studying high fusion performance in the optimised shear mode, in which an Internal Transport Barrier (ITB) is maintained in combination with either an L-mode, ELMy H-mode or ELM-free H-mode edge.

Of particular interest in the **ITER Physics Studies** were the identity experiments, in which all dimensionless parameters were kept constant. These experiments were carried out in collaboration with ASDEX Upgrade, DIII-D and ALCATOR C-MOD. The validity of this approach to transport was confirmed and hysteresis in the H-L transition for a fixed normalised power was also demonstrated. Varying the normalised scale size (ρ^*) in JET showed that the same favourable scaling for energy confinement applied to both low and medium β plasmas, that the collisionality (ν^*) scaling was weak, and that even with a low edge safety factor, $q_{95} = 2.76$, confinement remained good. This last result is of particular importance since it should imply good confinement for ITER operating at 24 MA (rather than 21 MA), thus offering a considerable increase in the overall ignition margin. ρ^* scaling studies were also carried out in highly radiating plasmas using neon as the radiator and keeping q, β and the radiated power fraction fixed. While the overall confinement was degraded in comparison with that at lower radiated power fraction, the core plasma appeared to show a favourable (gyro-Bohm) scaling. This result would be consistent with the theoretical picture emerging from JET transport studies that global energy confinement results from contributions from the plasma core (which shows the expected theoretical gyro-Bohm scaling) and a plasma pedestal (which is determined by the edge temperature and density, is affected by edge radiation and edge stability, and has a different scaling to the core). The basic diffusive nature of the core confinement has also been tested in experiments which showed that under many conditions temperature profiles changed in response to the power deposition profile. Finally, neoclassical tearing modes were identified for the first time in JET and can modify temperature profiles and degrade performance of long-pulse ELMy H-modes.

Task Force A demonstrated that the new divertor geometry appears to produce many of the expected results, particularly in L-mode plasmas. Improved deuterium exhaust, more symmetric detachment and a somewhat higher density limit have all been achieved. Access to the H-mode was found to be dependent on divertor geometry. The H-mode threshold power with horizontal targets is found to be lower than with vertical targets and also decreases with increasing divertor closure. Furthermore, magnetic configurations which are limited on the divertor septum have a significantly lower H-mode threshold than conventional vertical target configurations. On the other hand, energy confinement in H-mode discharges with Type I ELMs is largely independent of geometry, although the power needed to produce good confinement with Type I ELMs has a different parametric dependence to the conventional L-H threshold power. More generally, energy confinement does not appear to depend on the method of heating (NB or ICRF) but does appear to depend on the triangularity of the plasma configuration (the character of the ELMs also changes with triangularity). High-current, high-power ELMy H-modes have shown a sudden loss of confinement. This has become more common in Mark IIGB but has been avoided by controlling the plasma current profile and the gas fuelling rate. The fuelling efficiency with pellets injected from a centrifuge injector at 250 ms^{-1} and 500 ms^{-1} into ELMy H-modes appears to be higher than with gas puffing, but the trade-off between density and confinement does not substantially change. Following helium and impurity enrichment studies earlier in 1997/98, helium exhaust studies were completed using argon frosting on the divertor cryopump. This was technically much more successful than with the Mark I divertor and clear pumping of helium has been demonstrated with the ratio of the helium replacement time to the energy confinement time as low as 4 (for infinite pumping speed) in ELMy H-modes, significantly lower than that needed in a reactor ($\approx$10).

Task Force B demonstrated that with the Mark IIGB divertor, transiently high performance has been more difficult to achieve largely due to the earlier onset of an H-mode. On the other hand, steady-state operation has been easier and the ELMs have been more benign. Profile control techniques have been used to engineer high fusion performance and to develop these conditions into steady state. In particular the target current profile was modified so as to increase the volume of the low magnetic shear region, allowing the neutron yield to be increased to $4.5 \times 10^{16} n/s$ with 28 MW of heating power at 3.4 T/3.4 MA. It has also been possible to launch up to 3 MW of LHCD power in the high-power phase, thereby producing significant changes in the current profile and slowing-down of the current diffusion to the plasma core. Finally, the duration of the high-performance phase was extended by preventing excessive edge pressures by injecting krypton, argon or neon impurities to increase the edge radiation. Krypton and argon have allowed discharges with ITBs and L-mode edges, while neon penetrates to the plasma core resulting in too great dilution. In this way, steady-state discharges with double transport barriers have been achieved for 4-5 s using a continuous bleed of argon. The confinement enhancement factor relative to the ITER 89 scaling law is up to 3 and the normalised plasma pressure β_N up to 2.5 for an edge safety factor $q_{95} = 3.3$, which is a reactor-relevant domain.

For many years IPP has been contributing to the exploitation of JET scientific results as well as supporting the development and operation of JET diagnostic systems. A new Task Agreement No. 8 (TA 8) "Study of Advanced Tokamak Scenarios", which deals with experimental as well as theoretical studies of Internal Transport Barriers (ITB) was signed by the end of 1998. Prolongation of JET operation beyond the end of 1999 is presently being discussed and will give all European Associations responsibility for formulation and enforcement of a JET scientific programme in the years 2000 to 2002. IPP intends to contribute to this proposed JET operation phase in fields which are considered as central scientific goals for their own ASDEX Upgrade tokamak. Main points of interests are Advanced Tokamak Scenarios, Operational Limits in the Plasma Edge, Core - Edge Relations and MHD topics relating to these three topics. Enforcement of a similar scientific programme on two tokamaks of different sizes will give the opportunity to verify or reject scientific concepts based on results from a single machine and thus improve credibility for extrapolation of new scenarios to next-step devices.

In the following, present activities in the frame of the Task Agreements are described.

1. TASK AGREEMENT NO. 2

The global mass balance for eroded and redeposited Be, C and Ni+Fe+Cr was performed for the Mark I carbon divertor operational period of JET (April 1994 - March 1995) by MeV ion beam analysis of long-term samples from the walls of the main chamber, a poloidal section of divertor tiles, and tiles from the inner and outer wall limiters. During this period about 70 g Fe+Cr+Ni was eroded from the inner vessel wall. About 25 g Fe+Cr+Ni can be found at deposition-dominated areas at the limiter sides, in the divertor and at the outer vessel wall. About 55 g Be was eroded from the outer wall, of which about 28 g is found in deposition zones. The total amount of eroded carbon could not be measured, but about 370 g was found to be redeposited. All numbers are accurate within a factor of about 2. The vessel walls of the main chamber at JET are sources of Ni+Cr+Fe and Be due to sputtering by energetic charge exchange neutrals. The material eroded at these areas is redeposited at deposition-dominated regions at the sides of the poloidal limiters and in the divertor. Most of the carbon is believed to be eroded from the poloidal limiters, additionally some carbon is eroded at the divertor strike points. The eroded carbon is redeposited in the divertor in areas shadowed by neighbouring tiles or the divertor corners. During the limiter phase of each discharge eroded material is redeposited predominantly at the sides of the inner wall limiters, while during the divertor phase the redeposition occurs in the divertor and at the sides of the outer and, presumably, the inner wall limiters.

2. TASK AGREEMENT NO. 5

A possibility of comparing two tokamaks of different sizes is to perform similarity discharges with equal dimensionless parameters such as ρ^*, ν^* and β^* on both machines. The JET part of this inter-machine comparison was guided by IPP scientists together with the JET team. In the case of low density the expected agreement in energy confinement between comparable discharges is verified by the new results. For higher densities, however, it turned out to be rather uncertain which heating power to choose in order to get identical dimensionless parameters. The energy confinement time τ_e therefore varies in such cases for almost identical values of ρ^*, ν^* and β^* by typically ±25%. This ambiguous situation might be due to missing parameters in the ansatz $\chi = \chi \cdot F(\rho^*, \nu^*, \beta^*, ?)$, or could be an indication of regions of high sensitivity of the function F with respect to small variations in the parameters ρ^*, ν^* and β^* . The required similarity of density and temperature discharges was obtained for the present dataset. However, there are considerable differences in the radial profiles of the deposited heating power as well as in the triangularity of the discharges.

A systematic study of the mass dependence of the L-mode density limit was performed for JET H, D and T divertor plasmas. The density limit is found to scale inversely as the ion mass in vertical target configurations while no isotope effect is found in horizontal target configurations. 2D numerical simulations reproduce the observed mass dependence in vertical target discharges. The experiments indicate coupling between the mass and power dependences of the L-mode density limit, in agreement with predictions by a model that associates the density limit with complete divertor detachment.

ITER COOPERATION PROJECT

(Head of Project: Prof. Dr. Karl Lackner)

ITER was started in 1998 as a joint project involving EURATOM, Japan, Russia and USA. IPP Garching hosted this project during the Conceptual Design Phase (CDA) till 1990 and served as one of the 3 co-centres (Garching Europe, Naka Japan, San Diego USA) during the Engineering Design Phase (EDA). Garching also hosts the NET Team, which supports the ITER design effort, serving as its European Home Team. The EDA effort was completed in July 1998, its results being documented in the Final Design Report. The physics part of it was written by the different Expert Groups with strong participation of IPP scientists.

After completion of the engineering design activity, the ITER partners decided to investigate a reduced-objective, reduced-cost version and carry out its detailed technical design over a three-year period 1998–2001.

Through its scientific work, IPP Garching makes extensive and essential contributions to the ITER design activity. In particular, the programme of ASDEX Upgrade is directly aimed at scientific support of ITER. The stellarator experiments at IPP also make significant contributions to ITER. The results of these efforts are described in the sections dealing with the ASDEX Upgrade and W7-AS projects. The following sections therefore describe only additional, specific design effort projects.

1. PERFORMANCE MODELLING

1.1 H-Mode Confinement Time and Threshold Analysis

O. Kardaun (IPP Garching), in cooperation with the ITER Global Database Working Group.

The ITER Expert Group Meetings, held this year in Princeton (spring) and in Naka (autumn) stimulated the practical and theoretical re-investigation of the ITER confinement and threshold database, which was expanded the previous year. This yielded interesting results. First, with the help of additional data (from ALCATOR C-MOD, COMPASS-D, JT-60U, TCV) in the new version of the dataset (ITERH.DB 3v5, compared with ITERH.DB2), it was found that the relatively high confinement-time residuals of the bean-shaped PBX-M tokamak (with respect to standard power-law scalings) could be converted into approximately 'normal' ones just by redefining the elongation, κ, as the cross-section area divided by πa^2 instead of by the ratio of the vertical and horizontal cross-section axes. This changes the aspect ratio dependence for ELMy confinement from $(a/R)^{0.25}$ to nearly $(a/R)^{2/3}$. The latter is roughly the same dependence as when PBX-M is left out from the analysis. In practice, it tends to predict more favourable confinement than hitherto for small-aspect ratio (e.g. 'spherical') tokamaks. Secondly, by re-analysis of the data, it was found that q_{95}/q_{eng}, which can be especially high for strongly shaped plasmas (such as PBX-M), is empirically also an additional factor relating to confinement, with an 'influence' of up to some 25% when used as a simple multiplicative factor. Both aspects have been included in the ITER Physics Basis Document, as well as in a basic empirical confinement-time analysis paper, both of which are to appear in 1999. The true response surface being somewhat more complicated than a hyperplane (on a logarithmic scale), there are two recommended power-law scalings for ITER prediction, ITERH-98P(y) and ITERH-98P(y,2). In addition to the re-definition of kappa, the second scaling is based on exclusion of the ohmic and ECRH discharges, which stem from the small tokamaks (COMPASS-D, TCV). The point predictions for ITER (FDR) are 6 and 5 seconds respectively. The difference being significant, both values are well within the 95% interval estimate, (3.5, 8) seconds, and both are sufficient for self-sustained, high Q ($\simeq$ 50), burning plasma operation. These analyses have been made possible by the extensions of the database, organised in Garching by F. Ryter. Results of the cooperation in the database group were presented by M. Valovic (intervals for the exponents of scaling laws expressed in physical plasma parameters), Y. Martin (on threshold analysis) and K. Thomsen (on confinement analysis) at Prague and Yokohama, respectively.

1.2 Statistical Fitting of Catastrophe Type Response Functions

O. Kardaun, in cooperation with J. Kardaun (Statistics Netherlands), S.-I. Itoh (Kyushu University, Japan), K. Itoh (NIFS, Japan)

Computational statistical methods have been developed to unify the analysis of plasma confinement, power threshold and operational limits by fitting rather complicated, parametric, classes of ("catastrophe-type") response functions to the basic plasma

performance measurements. A research version of a parallel catastrophe fitting program using PVM and FORTRAN-90 has been constructed, by which new, preliminary, regression fits to the JET and DIII-D data in the ITER DB3v5 database could be obtained. An interim report of the work was presented at the EPS conference in Prague, which points to its possible fruitfulness towards improving ITER performance predictions.

1.3 Application of B2–EIRENE Code to ITER

A. Kukushkin, A. Loarte, H. Pacher (NET-Team Garching), D. Coster, R. Schneider (IPP Garching)

1. FDR ITER: The operation window of the FDR ITER with partially attached divertor plasma, high divertor radiation, low heat load, and acceptable helium pumping, was studied in further detail. Density and Z_{eff} scans were performed for different values of the cross-field transport coefficients, as well as for different divertor shapes. As the operation parameters of the divertor are varied, lower transport coefficients (by a factor 2, $\chi = 0.5m^2/s, D = 0.2m^2/s$) and low n_s are found to lead to heat loads above $10MW/m^2$. These can be rendered manageable (below $10MW/m^2$ for n_s down to $3 \times 10^{19}m^{-3}$ and Z_{eff} below 1.8) if the power incident on the SOL can be reduced by 25% to $150MW$, e.g. by edge radiation with an appropriate impurity. Lower DT throughput at the same n_s can be achieved by reducing pumping, but the margin in He pumping is reduced. A DT throughput a factor of 2 lower than the standard case is found for $n_s = 3 \times 10^{19}m^{-3}$ (only low n_s have been modelled so far) to lead to a helium concentration somewhat above 10%, higher than acceptable, at the core edge interface. Further investigations of DT and He throughput are required. Sensitivity studies and other reasons (improved shielding, possibility of installing a septum) suggest to retain the dome. At the same Z_{eff} and n_s , halving the divertor length leads to an increase of the peak heat load by a factor 1.5 for the configuration investigated (few runs have been carried out so far). Acceptable peak heat loads for this case at $200MW$ are expected at a Z_{eff} of 1.7 - 1.8 and n_s above $3.4 \times 10^{19}m^{-3}$. Helium pumping is affected relatively little. Further optimization of the calculations is required, particularly investigation of the effect of the divertor plate angle (impurities move to the inner divertor in the present runs). In conclusion, the FDR ITER divertor can accommodate low χ and low n_s with a modest SOL power reduction and an acceptable operating window for heat load and He pumping. Modifications desirable for other reasons (shorter divertor, dome removal, reduced DT throughput) reduce this window.

2. RTO/RC ITER: The B2-Eirene code package was used to study the divertor performance in the reduced-size ("Reduced Technical Objectives / Reduced Cost") ITER. In this case, the second X-point moves closer to the primary separatrix due to a higher triangularity, and an asymmetric double-null configuration has to be modelled. The results of these preliminary studies can be summarized as follows. For the reference bottom divertor (1.1 m long) and the reference equilibrium having a distance of 3 cm between the separatrices in the outer mid plane, the peak power loads are 5 to $10MW/m^2$, similar to FDR ITER; the DT neutral pressure in the PFR for the same density is higher than for FDR; and the Z_{eff} is in the acceptable range, 1.3 to 1.65. Variation of DT throughput has a weak effect on the peak power, and there is no strong difference for bottom-divertor operation between top vertical and flat targets; peak power loads on the top targets are low for both configurations. The helium concentration strongly depends on the DT throughput, so that a DT throughput of at least 120 Pam^3/s (200 Pam^3/s with margin) is required to keep the edge helium fraction below 6% for the RTO/RC ITER. When the divertor configuration becomes more up-down symmetric, i.e. the distance between the separatrices decreases, the top divertor starts to receive significant power at D_{sep} between 1 and 2 cm for the transport coefficients assumed.

2. COMPONENT DEVELOPMENT

2.1 Chemical Erosion of Carbon Fibre Composites Deuterium Plasmas

P. Kornejew, W. Bohmeyer, H. Grote, G. Fussmann, H.-D. Reiner (all Berlin Division, IPP Garching)

In 1998, investigation of the interaction of different carbon fibre composites (CFC) with hydrogen or deuterium plasmas was continued in close cooperation with the NET/ITER group at Garching.The PSI-1 plasma generator was shown to be well suited to investigating the mechanism of chemical erosion of carbon and CFCs. In contrast to tokamaks, it is possible to vary the ion flux density ($10^{21}D^+/m^2s...10^{23}D^+/m^2s$), the ion energy (20 eV...300 eV) and the target temperature ($100^oC...700^oC$) independently. Compared with ion beam experiments the PSI-1 can realize considerably higher ion flux densities. For most experiments, diagnostics (mass spectrometry for determination of the CD_4 or CD_4 flux, optical spectroscopy for detecting the CH or CD band at 430 nm and weight loss measurements) have been applied. The first two diagnostics were calibrated directly by injecting a well-defined steady flow of CD_4 or CD_4 molecules for every set of plasma parameters; hence D/XB values relating particle and photon fluxes are not required. Furthermore, the contribution of energetic neutrals to the chemical erosion yield was studied by biasing the target positively in order to reject the ions. The results can be summarized as follows: For a target temperature of about 500^oC the chemical erosion yield decreases with increasing ion flux density reaching values of less than 1% for flux densities of $10^{23}D^+/m^2s$. Under these conditions the erosion yield of NS 31 (SEP) is clearly lower than that of Concept II (Dunlop). For ion bombarding energies between 15 and 30 eV no significant isotope influence was found. There is only a weak dependence of erosion yield on the ion bombarding energy with a weak maximum at 150...200 eV. The contribution of energetic neutrals to the erosion yield was determined too. It is found to depend on the plasma conditions but can reach values of up to 40 %.

2.2 Design of Diagnostics in Reactor-grade environment

G. Haas, H.-J. Hartfuß, A. Herrmann, F. Mast, H. Salzmann (IPP Garching)

During the last few years a number of activities have been performed in the area of ECE, bolometry, neutral gas pressure gauges, Thomson scattering, spectroscopy and thermography for FDR ITER. The corresponding designs are described, in collaboration with the European ITER home team, in "Diagnostic Design Descriptions". Summaries are given in the Proceedings of the Workshop on Diagnostics for Experimental Fusion Reactors, Varenna, Sept. 4–12, 1997. During 1998, activities concerned with access to the ITER machine were discontinued due to the proceeding design changes of ITER. However, irradiation tests for bolometers and pressure gauges were further conducted in collaboration with FZK Karlsruhe and CIEMAT.

STELLARATORS

The work of the W7-X construction project is focused on the design, manufacture and assembly of the stellarator, the in vessel components, the co-ordination of the heating systems and the set-up of the machine control system. The project closely co-operates with the project "diagnostics for W7-X" and the construction branch of the Greifswald branch of the institute to agree on the various interfaces between the machine, the experimental building, the infrastructure and the experiment. Major procurements have been started and the move of the W7-X construction project team from Garching to Greifswald on 1.3.1999 has been fulfilled.

From April to October 1998, the torus of W7-AS was opened to install 10 control coils and to replace the ICRH antenna. The control coils are the first step of the project "Divertor Experiment at W7-AS", which was approved in June by the HGF for support by the strategy fund. The second step, the installation of the divertor modules, titanium getter pumps and additional divertor diagnostics, will occur in the years 1999/2000. The present "broad" ICRH antenna was replaced by a double strap antenna. This is the third antenna version tested in W7-AS. The goal of this programme is to define the „best" first experimental antenna for W7-X.

The control coils allow to control resonant field structures at the edge: "natural" magnetic islands can be enlarged, decreased, fully compensated or even over-compensated. First experiments show a clear dependence of the total energy content on the effective radius of the last closed flux surface. Changes in the "footprints" of 5/9 and 5/10 islands, for example on inboard limiters or at the plasma boundary, can be seen by several diagnostics. The experimental work is accompanied by the development and application of numerical codes.

The research programme with the "broad" ICRH antenna has successfully been completed. Plasma heating and sustainment was proved for a variety of heating schemes.

The ECRH heating power was upgraded late in 1997 by installing a third 140 GHz gyrotron. Thus, very high local power densities were available for heating and current drive. Central electron temperatures could be increased to 5.7 keV. Nonlinear effects are found in the experiments and compared with theoretical predictions.

To further investigate the experimental dependence of the heat transport on high order rational values of the rotational transform and on the magnetic shear a model was developed to enhance the electron heat diffusivity around rational magnetic surfaces. In this way, qualitative agreement with measurements in a wide range could be found.

Theoretical investigations in the Stellarator Theory Division being built up in Greifswald concern four major areas of research: i) further development of the stellarator concept, notably with respect to quasi-isodynamic and quasi-axisymmetric configurations; ii) equilibrium and stability investigations with advanced computational tools, in particular in the areas of Alfven eigenmodes and kinetic MHD; iii) development of a stellarator-specific basis of anomalous-transport theory with investigations of ion-temperature-gradient driven and resistive drift modes; iv) development of 3-D plasma edge theory.

WENDELSTEIN 7-X Construction

(Head of Project: Dr. Manfred Wanner)

Members of the W7-X Construction team and contributors to the project: see section "Division and Groups, WENDELSTEIN 7-X Construction"

1. INTRODUCTION

The W7-X Construction Division is responsible for engineering, design, manufacture and installation of the W7-X device, including the actual stellarator, the heating systems, the specific supply systems and a central control system for operation of the experiment.

The main components of the stellarator are the superconducting magnet system for confinement of the plasma, the cryostat for thermal insulation of the cryogenic parts and the plasma vessel with the plasma-facing components. Plasma heating is based on powerful ECR, ICR and NBI systems. Supply systems for the stellarator comprise the helium refrigeration system for the superconducting coils, the high-voltage power supply for the heating systems as well as the water cooling circuits for the different components.

Augmentation of the project team was continued and relocation from Garching to Greifswald during spring 1999 was prepared.

R & D activities made significant progress. An advanced conductor specified for a higher critical current and increased stability was successfully delivered by industry.

The electromagnetic tests at the temperature of liquid helium confirmed the required operational margin. These tests were a prerequisite for placement of the order for the magnet system.

The DEMO coil, an original-sized superconducting magnet, was manufactured in full conformity with the stringent electrical and mechanical requirements.

The DEMO cryostat, which features all mechanical and cryogenic aspects of a sector of the W7-X cryostat, is approaching completion.

The feasibility of manufacturing the unconventionally shaped plasma vessel and other critical components of the cryostat was demonstrated. The experience gained during manufacture and assembly of this prototype will be considered in the technical specification of the W7-X cryostat.

The lining of the inner wall of the plasma vessel with cooled panels covered with low-Z material calls for sophisticated concepts to reduce the number of wall elements. European industry has indicated interest in developing such elements.

The project schedule is determined by the manufacture and installation of the superconducting coil system and aims at a commissioning date for W7-X by the end of 2005. The planning was detailed and revised to include the advanced integration of the divertor elements into the plasma vessel prior to mapping of the magnetic field.

Cooperation agreements with Forschungszentrum Karlsruhe (FZK) and the Low Temperature Laboratory of Commissariat à L'Énergie Atomique (CEA) at Saclay, were concluded.

FZK is preparing tests of the DEMO coil in the TOSKA test facility and will contribute the complete ECRH system for W7-X. For development of a 140 GHz gyrotron FZK has entered an agreement with Thomson Tube Electronics in France and with EPFL at Lausanne. The design and testing of the microwave transmission line will be performed by IPF at Stuttgart.

CEA will perform the cryogenic acceptance tests of the superconducting coils and has started with the design and set-up of the test facilities.

2. R & D WORK

2.1 Superconductor

Approximately 200 metres of the so-called advanced conductor were manufactured by the Swiss Metal company and wound to a solenoid (STAR IV). This solenoid was tested in the STAR facility at FZK under temperature and magnetic field conditions characteristic of the W7-X magnet system.

Comprehensive tests demonstrated the enhanced properties of the advanced conductor. Quench tests led to critical currents and magnetic inductions significantly beyond the requirements for W7-X and showed that the conductor has sufficient margin with respect to the required operational parameters.

Ramp and cycle tests convincingly demonstrated that the expected AC losses in the cable can be safely handled. During the tests the strands were successfully subjected to high electromagnetic forces exceeding the maximum loads expected in the magnet system of W7-X by 35%. The measured mechanical deflections of the test coil coincided with the predictions.

Separate tests with induced quenches were conducted to study the propagation of the normal zone in the conductor and the pressure evolution of the helium coolant.

In evaluating the quench current of the test coil, emphasis was placed on precise determination of the temperature and magnetic induction at the location where the quench is expected. Evaluation of the STAR IV tests and comparison with the results from former STAR tests showed that the critical current of the coil is identical with the sum of the critical currents of the virgin strands. This means that the conductor is not degraded during the winding, hardening of the aluminium and curing process.

Analysis of the test results from STAR IV clearly confirmed that the concept chosen for the conductor fully meets the requirements of W7-X.

Two methods of jacketing the superconducting cable for W7-X, viz. co-extrusion and CONFORM cladding, were developed.

In order to improve the CONFORM process, a second length of advanced conductor was ordered from Outokumpu/Alstom in 1997. Scrupulous impurity control of the raw material and tools significantly improved the quality of the aluminium jacket.

After additional dimensional problems encountered after winding of the cable were solved, this length of conductor is to be delivered in spring 1999.

2.2 DEMO Coil

The DEMO coil, an original-sized superconducting prototype of a non-planar W7-X coil, is to demonstrate industrial manufacture at the required tolerances.

The winding pack manufactured by ANSALDO was delivered to NOELL for assembly. The winding pack fitted well into the tightly toleranced halves of the steel casing. During welding of the half-shells the winding pack was kept exactly in place by spacers.

Provisions had to be made to keep the winding pack unstressed at cryogenic temperatures. Pre-stressing was therefore applied during embedding of the winding pack which would release during cool-down to cryogenic temperatures owing to the different thermal contractions between the casing and winding. This effect was achieved by heating the casing to approximately 100° C while the winding pack remained at ambient temperature.

The gap of some twenty millimetres between the casing and winding pack was filled with glass sand. Cooling down to ambient temperature resulted in compression of the filler, which was then impregnated with a resin curing at ambient temperature.

Next, the cooling channels for the casing and the sensors for quench detection as well as for temperature and strain measurements were mounted. After thorough dimensional and electrical acceptance tests at NOELL the coil was shipped to FZK by the end of June.

Figure 1 shows the DEMO coil prior to assembly in the TOSKA cryostat.

The functional testing of the DEMO coil is to be performed in the TOSKA test facility of FZK. The forces in the W7-X coil system will be provided by the background field of the European LCT (Large Coil Task) coil, which is already installed in TOSKA. A massive steel frame was built as an interface between the DEMO coil and LCT coil. In addition, a helium distribution system was constructed and tested. Finally, current leads for the DEMO coil had to be re-designed and constructed by FZK to allow horizontal operation.

Preparation of the FZK facility was continued. After completion of the electrical and hydraulic checks cool-down of the DEMO coil is scheduled for May 1999.

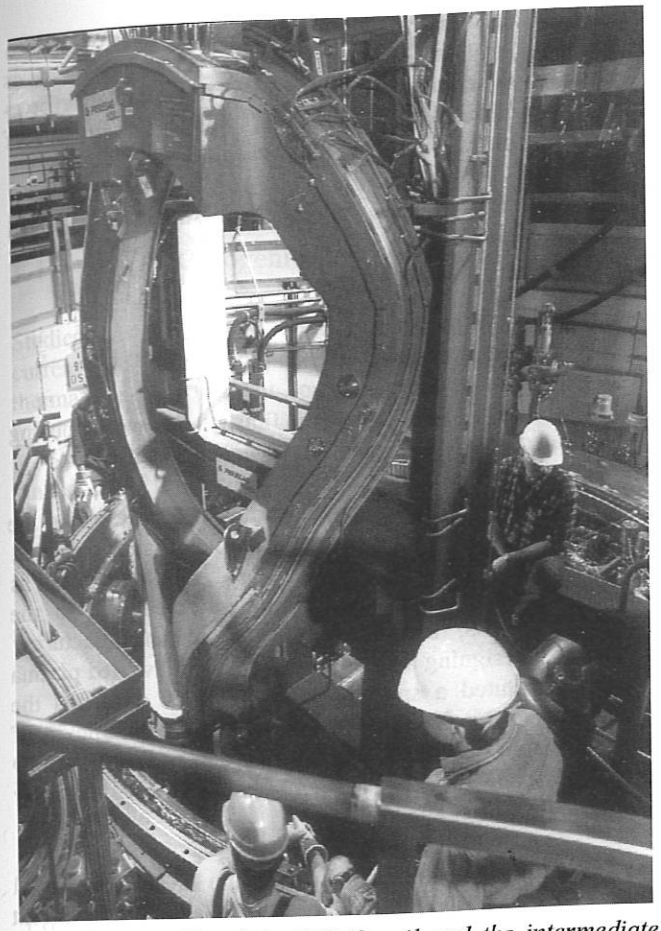

FIG. 1: Assembly of the DEMO coil and the intermediate frame in the TOSKA cryostat.

2.3. DEMO Cryostat

Construction and assembly of the DEMO cryostat was completed at Balcke Dürr AG to the point where road transportation to IPP of basically three components was still possible. These units were shipped to IPP in summer 1998.

The major unit comprises the plasma vessel with the thermal insulation and a heat radiation shield, the coil models with the inter-coil vault structure and the coil support structure. Due to the space constraints each coil, the vault elements and the intermediate thermal insulation had to be aligned and fixed successively around the plasma vessel. The coil system was then attached to a weight support structure, with the plasma vessel being positioned provisionally within the coils. The shapes of the single components and their relative positions were continuously controlled by a precise optical measurement system.

The outer cryostat vessel surrounding the coil system was manufactured and delivered in two halves.

The third delivery comprises the ports connecting the plasma vessel with the outer vacuum vessel. They were pre-assembled with flanges and seals, leak tested and provided with electrical heaters and thermal insulation.

At IPP the shapes and positions of the coils and plasma vessel were re-checked and instrumentation and coolant piping were completed. The plasma vessel was equipped with electrical heaters for thermal control and auxiliary structures were installed for further assembly.

The two halves of the outer vessel were covered with the 80 K copper shield. Packages of multilayer insulation were well prepared in advance and installed in the outer vessel. Fixing of the packages was very time-consuming since many holes and protrusions for ports, coil terminals and legs had to be cut and protected very carefully against heat radiation.

Figure 2 shows the main cryostat and the lower outer vessel-half.

FIG. 2: Lower part of the cryostat vessel (in front) and the basic unit comprising the plasma vessel, the model magnets, the support structure and the insulation.

By the end of 1998 the lower part of the outer vessel is ready to take the coil models and the plasma vessel. After assembly the DEMO cryostat is to be connected to a laboratory helium refrigerator and a distribution box to study its cryogenic performance.

3. W7-X BASIC MACHINE

3.1 Magnet System

Design work on the magnet system proceeded well. For both the non-planar and planar coils technical specifications were produced. After approval by EURATOM calls for European

tenders were issued and invitations to bid were sent to approx. twenty companies.

Two offers were received for the non-planar coils and four for the planar coils. After thorough evaluation of the offers the order for the 50 non-planar coils was given to the NOELL/ANSALDO consortium. This order, which is the largest single order of the project, includes procurement of the superconductor winding, encasing and instrumentation of the coils. Evaluation of the offers for the 20 planar coils is completed and the order will be placed of the beginning of 1999.

The cobalt content of the stainless steel for the coil casings was thoroughly discussed during the contract negotiation phase. A level of 50 ppm was required in the original specification, which was in conformity with the construction licence. However, due to changes in the European steel market "reactor grade steel" of this type is no longer available. The authorities were therefore asked to reduce the requirements to 500 ppm, which can be obtained by careful selection of the raw material. This change of the cobalt content imposes no restrictions during operation and has only a small influence in the handling of the material after shut-down of W7-X.

For the coil support a central, ring-shaped structure was designed. This structure takes the forces from the coils and supports the magnet weight. Assembly studies were conducted. A finite-element model was established for detailed computation of the stresses and strains in all components under non-linear conditions. These calculations have to take into account gliding effects between the winding pack and the casing as well as gliding of the contact surfaces between structural parts. As a result of these calculations local reinforcement of the coils was considered in the design. In order to verify the in-house calculations, parallel structural studies are being performed by industry. Detailed studies of the number and locations of the vault elements between the coils are under way.

For the final acceptance test of the non-planar and the planar coils at cryogenic temperatures an agreement was made with the Low Temperature Institute of CEA at Saclay, France.
The tests will comprise flow tests with liquid helium, operation of each coil at nominal current and a check of the operational margin against quench. Two test cryostats which will house two magnets each for successive testing are being designed. IPP and CEA have agreed on the details of the test requirement specification.

3.2 Magnet Current Supply

The technical concept for the magnet current supply was established. Seven identical modules will supply the five groups of non-planar coils and the two groups of planar coils. An essential requirement for the power supplies is fast and reliable discharge of the magnets in case of a quench in the superconductor. Two options for the breaking switch between the power supplies and magnets were worked out. One is based on an arc chute DC circuit breaker, the other on a force-commuted vacuum circuit breaker. The decision for one of these option will be based on their reliability figures.

The call for tender action for the power supplies is planned for spring of 1999.

3.3 W7-X Cryostat

The basic design of the cryostat is finished and work is being concentrated on preparation of the technical specification.

The plasma vessel was designed in detail. The design of the vessel is determind by the shape of the non-planar coils and has to satisfy a number of boundary conditions such as maximum size of the vessel, minimum clearance to the refrigerated coils, thermal contraction and manufacturing tolerances. Designing a smooth surface of the twisted plasma vessel constituted a special challenge which exceeded the capabilities of the CADDS5 system in use. The complexity of this task could only be solved by a special surface 3D-CAD system. Meanwhile the plasma vessel design is nearly finished.

Mechanical and electromagnetic loads on the plasma vessel are caused by vacuum, fast coil discharges and plasma current variations, etc. These loads were defined and evaluated. In order to validate the IPP estimates, a contract was placed with industry for a detailed mechanical strength analysis.

A support system for horizontal and vertical adjustment of the plasma vessel was provisionally designed and will be finalized when the results of the strength analysis are available. In addition, the temperature of the wall of the plasma vessel is to be controlled by a water cooling and heating system. For that purpose additional cooling loops will be mounted on the outside of the plasma vessel.

Another task was the detailed design of the approx. 300 ports. This work again needed several iterations to meet the requirements imposed by diagnostics, plasma operation, mounting of the supply lines for the in-vessel components and accommodation of the ports within the narrow space between the coils. Additional space had to be considered to allow for the relative movements of the coils against the plasma vessel, mounting of the thermal insulation as well as manufacturing tolerances.

The design of almost all ports could be frozen to allow them to be specified in detail.

Design work on the outer vessel has also started. Here the design has to avoid collisions between the ends of different ports and the domes required for the connections between the coil terminals. In addition, current leads, helium supply lines, vacuum pumping openings, manholes and the support

systems for the outer vessel, the plasma vessel and the coil system have to be accommodated on the vessel surface. A preliminary strength analysis was performed to estimate the required wall thickness and the dimensions of the support elements.

3.4 W7-X Cryogenic Components

Studies on the use of high-temperature superconducting current leads were continued. In order to test the design, a thermal life cycle test with some superconductor samples was initiated.

An automatic test facility was set up to perform the cycle tests on samples from American, Japanese, Russian and German sources.

3.5 W7-X Refrigerator

Evaluation of the refrigerator studies was continued and the major interfaces between the refrigerator and W7-X were defined. The storage vessels for pure helium gas were specified and ordered.

3.6 W7-X Assembly

An essential feature of W7-X is a modular design which could be adopted for designing a later reactor. Basically, assembly of the cryostat consists in joining five prefabricated modules to a torus. Each module comprises two half-modules symmetric to each other. Geometric restrictions of the coils mean that a prefabricated full module can only be moved radially towards its final position at the torus centre.

The detailed concept of the assembly is currently being discussed. The paramount objective of the W7-X coil system is to ensure the required accuracy of the magnetic field. An accuracy in the order of 0.1 mm/m has to be achieved for the positions of the coils. Such precision can be obtained either by machining the coil casings and the support structure on high-precision-milling machines or by using computer controlled theodolites to position the coils and fit the inter-coil support elements during final assembly.

The small clearance between the coils and plasma vessel means that the final positioning of the coils can only be done jointly with the assembly of segments of the plasma vessel. Welding of the sections of the plasma vessel has to be done in parallel with the mounting of the thermal insulation. The coils and plasma vessel of one half-module will then be put into the outer vacuum vessel of the cryostat.

Next, the ports have to be welded to the inner and outer vessel and the electrical and helium connections between the coils have to be made. Finally, the plasma-facing components and other in-vessel components will be installed. Rigidity of the modules will be obtained only when the complete torus is joined together. Therefore, special mounting and support tools for half and full modules have to be prepared in all phases of the assembly, which can be removed after completion of the assembly.

4. HEATING SYSTEMS

4.1 ECRH

FZK has taken the responsibility for developing the complete ECRH and is co-ordinating the various contributions from other laboratories and industry. A new microwave heating project called 'Projekt Mikrowellenheizung für W7-X' (PMW) was established at FZK, which embodies efficient project management, project control and engineering and scientific divisions.

PMW will handle the development and testing a prototype gyrotron jointly with EPFL Lausanne and the french company Thomson Tubes Electroniques (TTE) and manage the manufacture, installation and testing of the ECRH system, including all subsystems. Responsibilities for the various subtasks were agreed between FZK, IPP, IPF Stuttgart, TTE and EPFL Lausanne. Different agreements between the collaborating partners were concluded in 1998.

Conceptual design, engineering and supervision of the construction of the entire transmission system as well as of the ECRH-specific HV system will be done by IPF Stuttgart. IPP contributes to the in-vessel components and the related plasma diagnostics.

The ECRH system for W7-X consists of ten gyrotrons with power of 1 MW per unit at 140 GHz and has steady-state capability. The development of gyrotrons with the required performance and high efficiency (> 45 %) will be performed in close collaboration with industry. Work at TTE started in summer 1998 and significant progress was made on the integrated design of a diode-type gun with an advanced quasi-optical mode converter, a single-stage depressed collector and diamond windows based on a carbon vapour deposition process. First prototype results are expected during 1999.

Contracts for the superconducting magnet, test equipment and water cooling were placed with industry and are well under way. The gyrotron test stand at FZK is presently being upgraded to allow tests of gyrotrons with depressed collector at full power with a pulse length of up to three minutes.

Three diamond windows for the gyrotron and torus port with the required properties for 1 MW CW transmission were delivered on schedule. The ECRH-specific HV supply for depressed collector operation, gyrotron heater supply and a control unit is being developed at IPF. A prototype system is

being manufactured and will be implemented in the test stand at FZK to gain experience for series production.

IPF Stuttgart is also in charge of the design of the quasioptical transmission system and is preparing a prototype transmission line at Stuttgart for optical and thermomechanical tests of the components. First components of this prototype system were manufactured and low-power measurements were performed with separate components. The overall design of the optical transmission system is based on the concept of a multi-beam waveguide, i.e. single mirrors are used for transmission of many individual RF-beams. Provisions were made at the Greifswald site to ensure easy implementation of the system in the ECRH transmission duct. New diagnostic methods for in-situ measurement of the alignment and positioning of the mirrors are being developed and first tests were performed. In particular, development of the required remote control positioning of each mirror is progressing at IPP and a prototype system is presently being tested.

The transmission mirrors require low losses and efficient cooling during CW operations. Technologies with different materials are therefore under investigation and first mirror samples were manufactured. Finite-element calculations on the thermomechanical properties of different possible solutions are under way.

4.2 ICRH

Provisions were made for later installation of the ICRH components. This included, for example, definition of requirements on the high-voltage power supply, the water cooling systems, the cryostat ports as well as the interfaces to the buildings.

As long as the responsibility for ICRH on W7-X is still open, the design of W7-X will leave as much flexibility as possible for later accommodation of the ICRH components. In particular, a flange design was found which allows either additional ICRH antennas in a later stage or application of Negative Ion Beam Injection.

4.3. Neutral Beam Injection

Neutral beam injection is envisaged in W7-X for bulk heating of the plasma in the high-density, high-ß regime. So far only a quarter (stage I heating) of the ultimate neutral beam power (stage II heating, 20 MW, using two injector boxes of the ASDEX Upgrade type) has been approved. In stage I two injector boxes - each capable of housing four PINIs (Plug-In Neutral Injectors) - will be equipped with one PINI, thereby delivering up to a total of 5 MW for pulse lengths of up to 10 seconds. The beamlines will be equipped with RF sources developed for and recently put into operation on the second injector of ASDEX Upgrade. These RF sources offer higher availability and significant cost saving in relation to conventional arc discharge sources.

The main progress in 1998 consisted in detailed design of the near-perpendicular portholes, to be used for both stage I and stage II heating, as well as of the tangential ports, envisaged as potential access in case high-energy, negative-ion-based neutral beams are applied in a future stage of experiments. These tangential portholes were approved by the Scientific Advisory Board of the project.

Manufacture of the PINIs is progressing well. Acceptance tests are planned for summer 1999. In addition, a number of interfaces to the water cooling, experimental building and electrical supply were defined.

5. CONTROL SYSTEM

The experimental device, comprising the machine, diagnostic equipment and data acquisition equipment, will be controlled by one integral control system. Since W7-X permits discharges with a duration of up to 30 min, a large number of scientific experiments will be performed during one discharge. The huge amount of data resulting calls for efficient data management. For that reason the architecture of the control system has to be defined well in advance of the experiments. Most of the components of the device will have their own control system capable of running automatically according to predefined routines and parameters.

Plasma discharges will be subdivided into segments of variable duration. During each of the segments the rules and parameters determining the state of the system will not be changed.

A "segment program" defines an experimental session and allows switching between sets of rules and parameters. Programming can be done before the experiment or, at a later stage, in an intelligent way on the basis of the goals of the experiments and the actual reaction of the system.

Programmable Logic Controllers (PLCs) will be used as far as possible for controlling technical components and diagnostic systems which call for robust controllers and do not require fast response times. In addition, computers running a real-time operating system will be applied. Computers using a general-purpose operating system will be used to provide the man-machine interface for commissioning the sub-systems, for tests, for programming the segments and for supervising and controlling automatic operation and discharges. Hard wiring will be used for interlocks with high safety relevance.

The large number of component controllers will be co-ordinated by one central control system. The central controller will supervise the status of all components of the device. This information will be the data basis for semi- or full-automatic operation of the experiment. Unsafe interactions between the components will be prevented by a

central interlock system. An event-processing system with a central event manager will perform switching between segments and trigger other event-based actions.

Computer networks and field buses will mainly be used to exchange signals between the numerous controllers. This system will allow remote control and maintenance of the system and increase flexibility for future modifications.

Hardware and software components considered as candidates for realization of the concept were selected and tested. A simple prototype system will be set up in order to test and develop the concept and modules.

WENDELSTEIN 7-X

(Head of Project: Prof. Dr. Günter Grieger)

1. W7-X DIVERTOR STUDIES

H. Bitter*, J. Glagla+, H. Greuner, H. Grote+, F.W. Hoffmann, O. Jandl*, J. Kißlinger, B. Mendelevitch*, K. Pfefferle*, H. Renner, R. Rieck+, J. Simon-Weidner*, E. Strumberger,

(+W7-X Construction, * ZTE)

1.1 Physics and Modelling

1.1.1 Definition of divertor components

To test the reliability of the divertor geometry chosen for W7-X [1], corresponding to the HS5V10U magnetic configuration, deposition patterns of fast ions on plasma-facing components were calculated with a system of numerical codes.

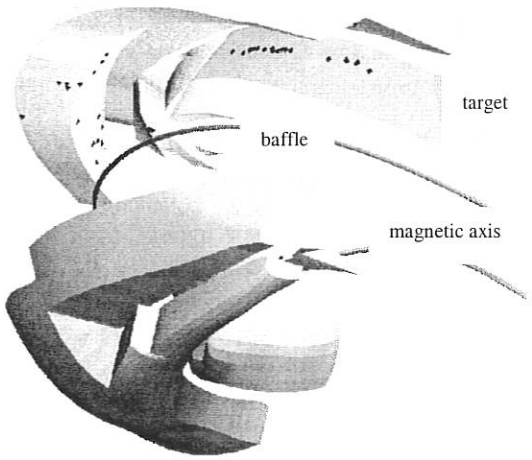

FIG. 1: Evaluated interaction patterns of deuterons (NBI: 65 keV) on the divertor units (indicated by black dots). Assumed plasma parameters: high ι case, B_o=3T, $<\beta>$=2.5 % with $n_{eo}=3\cdot10^{20}$ m^{-3} and $T_{e,i}$=2.85 keV. The two divertor units - combining target and baffle plates - of one W7-X period are shown. The small fraction of lost high energetic particles is hitting the targets.

[1] H. Renner et al., J. Plasma Fus. Res. SERIES, Vol.1(1998), 143

Including finite-ß equilibria for the magnetic field, the guiding centre orbits of 65 keV deuterons without collisions (loss cone) and with slowing-down and pitch-angle scattering and, finally, the intersection points of these particles with the divertor elements and the first wall were evaluated.

The physical studies are concentrated on optimisation of the pumping system. With a view to a more realistic design of the divertor, the geometry of the pumping duct and the positioning of the pumps have to be optimised. In this respect, adaptation of the EMC 3 Monte Carlo code, coupled with the EIRENE code, is envisaged to provide a more appropriate 3D approximation of the neutral-particle balance in W7-X. This is done in co-operation with the W7-AS experts and will provide a supplement to the parameter studies on the basis of the EIRENE code alone.

The TM pumping system was redesigned to take into account the now more realistic geometrical constraints concerning the localisation of the pumps and the conductance of the pumping ducts. The final positioning of the pumps will be dependent on the tolerances of available TMP units and will to be clarified by investigation on a critical test arrangement. A stray-field map for various magnetic parameters was evaluated. It is indicated that the previously intended pump position involves field values of up to 50 mT. The now more detailed specifications of the manufacturer for steady-state operation in magnetic stray fields assumes significantly lower tolerances. The distances and simultaneously the tube diameter must therefore be increased to provide an equivalent pumping efficiency, otherwise the pumps will have to be magnetically screened.

1.1.2 The stochastic edge region of W7-X

The high-ι vacuum and finite-β magnetic fields of W7-X are characterised by 5/4 island remnants embedded in a stochastic region outside the last closed magnetic surface. Mapping of the magnetic fields for $<\beta>$ = 0, 2 and 4% shows reduction of the 5/4 island remnants with increasing β, i.e. the stochasticity is increased in the edge region. In order to quantify the stochasticity, bundles of field lines forming flux tubes are traced in this region taking into account the geometry of the plasma-facing components, i.e. the divertor, target, baffle, side plates and the first wall. Because of the exponential scattering of close field lines in a stochastic field, the circumference of the area enclosed by a flux tube increases exponentially. Calculating this circumference as a function of the length of the flux tube yields the Kolmogorov length L_K, which measures the stochasticity. By comparing

the Kolmogorov lengths of flux tubes with their corresponding connection lengths L_C to the plasma-facing components two transport regimes are distinguished, namely, the stochastic transport region with $L_C > L_K$ and the laminar transport region with $L_C \leq L_K$, where the parallel transport is the dominant feature.

Furthermore, estimates of the field line diffusion coefficient D_{FL} and the corresponding heat diffusion coefficient χ_{erg} are made by determining the radial displacement and the toroidal distance between two flux bundle locations. For the outermost part of the stochastic layer values of $D_{FL} > 1 \cdot 10^{-6}$ m^2/m and $\chi_{erg} > 3.5$ m^2/s are obtained [2].

1.1.3 Deposition patterns of fast ions on plasma-facing components

An extensive code system is used to study the losses of samples of 65 keV deuterons and their deposition patterns on the plasma-facing components of W7-X (FIG. 1). For this purpose, collisionless losses are investigated for various magnetic field configurations (high mirror fields with $\langle\beta\rangle$ = 0, 2.5 and 5%, 5/5 islands in the edge region), and losses influenced by slowing-down and pitch-angle scattering are considered for the so-called high-$n\tau$ scenario, which is assumed for neutral beam injection (NBI). Because of the rather complex 3 D geometry of the plasma-facing components, the AVS 3 D plot software is used to analyse and represent the particle and energy deposition patterns.

1.2 Divertor Engineering

1.2.1 Engineering strategy

As long as the inner cryostat vessel is not yet defined, integration of the divertor components has to be based on a hypothetical surface which is compatible with the contour of the coils and adds some space needed for insulation and temperature control measures (FIG. 2). Concerning the available vessel design studies, corrections in some particular areas may be necessary, but an acceptable compromise for integration of all components seems possible.

The problem of thermal movement and deformation of the vessel, and, in respect of the magnetic configuration, the geometrical displacement of components supported by the vessel may be solved by the proposed thermal control of the cryostat temperature. For that purpose an additional water-cooling circuit with a capacity of 300 kW seems sufficient to decouple the plasma-facing wall - specified for a power exhaust of up to 10 MW with an average power load of 100 kW/m^2 - and the cryostat wall. Stationary plasma operation at first wall temperatures of up to 150° C will be possible for cryostat temperatures of even less than 60° C to provide flexibility in respect of the neutral particle balance.

The time schedule of W7-X construction was revised and now includes the assembling of the complete divertor units before the magnetic surface measurements. The particular properties of the W7-X configuration restrict the danger of overloading in the case of strong misalignment of the target plates: Almost only 1/5 of the input power to the plasma will be loaded on 2 divertor units and then the strong asymmetry will concentrate this on one unit, in the worst case. Therefore, practically no limitations on power and pulse duration in initial plasma operation are expected. Due to the high flexibility in respect of the magnetic parameters a slight increase of the rotational transform leads to an inward shift of the inner separatrix to open the contact between the islands and the targets.

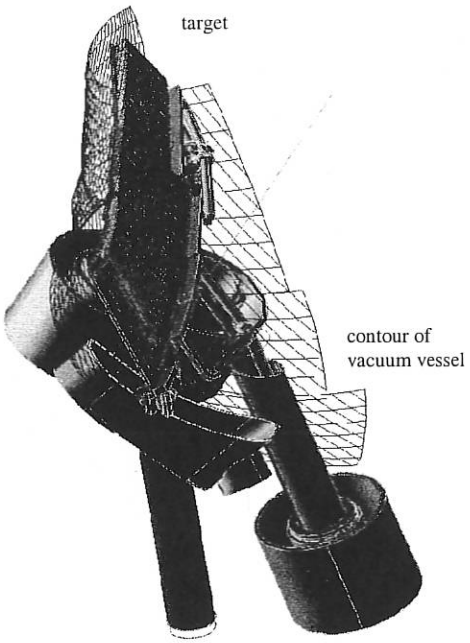

FIG. 2: CAD image of part of the target plates (modules 1 to 6). The vessel contour, water cooling circuits and ports for the supply are added.

Magnetic measurements under these conditions will describe the quality of the magnetic surfaces at the boundary and provide information for magnetic field corrections by means of the control coils. Plasma experiments can be initiated when the magnetic field becomes available under realistic conditions with control by the divertor and adapted diagnostics – without further delay to completion of installation.

1.2.2 Design of divertor components

Integration and optimisation of the divertor is progressing. Particularly, design of the following components has been worked out:

- Target elements, modularisation, support and supply for P/A $\leq$ 10 MW/m^2 [3].

[2] E. Strumberger, J. Nuclear Materials (1999), in print.

[3] H. Greuner et al., Proc. of the 20th SOFT, Marseille (1998), Vol. 1, 249

- Baffle elements for a power load of P/A $\leq$ 0.5 MW/m^2 with integrated cooling circuits
- Wall elements: P/A $\leq$ 0.1 MW/m^2.

  Alternative concepts:

  1. Panels with surface layers of B_4C, SiC, C etc., generated by plasma spray technique (FIG. 3),

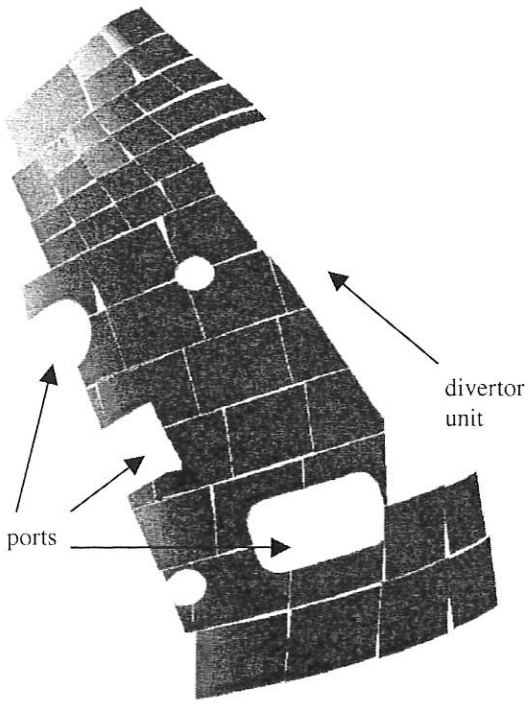

FIG. 3: Design study of the arrangement and geometry of panels for the wall protection. The outer part of the in-vessel installation is shown: The typical size of the 3D elements is 50•50 cm^2. To cover half a period of the W7-X vessel (1/10 of the total surface) 150 elements are needed. The ports and the location of one divertor unit are marked.

  2. 3D-shaped CFC elements with integrated cooling structure, or
  3. clamped C tiles on water cooled supporting structure.

  To satisfy the particular requirements of the heating schemes, ECRF, NBI and ICRF, a combination of the various concepts will be necessary.
- Control coils, including current connectors, cooling circuits and feedthroughs.

Prototypes will be manufactured and tested to optimise the fabrication in respect of cost and reliability.

2. CONTRIBUTIONS OF THE PLASMA DIAGNOSTICS DIVISION (IPP, BERLIN) TO THE W7-X PROJECT

D. Hildebrandt, P. Bachmann, W. Bohmeyer, B. Jüttner[#], M. Laux, D. Naujoks, R. Radtke, J. Sachtleben, D. Sünder, U. Wenzel
([#] Humboldt-Universität, Berlin)

In line with proposals for the development of methods for machine control and of plasma and divertor target diagnostics, activities were focussed on conceptual and experimental studies.

A system of about 20 cameras for thermographic measurements is planned to supervise the surface temperature of the water-cooled divertor target plates. 3D CAD studies were started to examine the possible viewing areas of these cameras with respect to their location and the main divertor components. First results indicate that direct observation of the whole target surface from the intended vessel ports seems possible without light transmission optics. The use of cameras with sensors operating in the µm-wavelength region would allow lower surface temperatures to be measured than with ordinary CCD cameras (Si sensors). Tests and experiments with an uncooled microbolometer array with a high local resolution (320x240 pixels) and sufficient time resolution are under preparation.

First tests of the applicability of active and passive acoustic methods for monitoring signals from divertor targets and baffles have been carried out. Sound wave propagation in carbon-fibre-reinforced carbon (CFC) was studied and the existence of a return side echo at low frequencies (1 MHz) could be demonstrated. The sound bursts accompanied by formation of cracks in CFC were detected and can possibly be used even to localise those events. The potential of supersonic acoustics as a diagnostic for the divertor needs further investigation.

A draft of the experimental arrangement for visible spectroscopy of the plasma in front of the divertor targets was developed. Three different viewing ports, fiber optics and spectrometers equipped with CCD cameras will allow line radiation with a local resolution of a few millimeters to be measured.

As an option for the Z_{eff} diagnostics a highly sensitive, miniature fibre optic UV-VIS-NIR spectrometer with a linear CCD array is being considered as a detector for bremsstrahlung. Calibration of such a spectrometer was performed; estimates of the bremsstrahlung intensity indicate that it is sufficiently sensitive.

Theoretical studies on Marfe formation and bifurcation of the temperature in W7-X were continued by solving 3D heat conduction equation with a conduction matrix depending on temperature and position.

3. STELLARATOR SYSTEMS STUDIES

T. Amano,[1] C.D. Beidler, E. Harmeyer, F. Herrnegger, O. Jandl,[2] J. Junker, A. Kendl, J. Kißlinger, I.N. Sidorenko, E. Strumberger, H. Wobig, A.V. Zolotukhin

3.1 Wendelstein 7–X Studies

In 1998, the Stellarator Systems Study Group investigated special questions of the Wendelstein 7-X configuration and some aspects of the Helias reactor design. Issues relating to the new coil version with 108 turns per coil were considered: the inductance matrix of the coil system was recalculated, the maxima of the magnetic field on the superconductors were evaluated, and the magnetic fields of the coil system were computed in detail. Some work was done on the issues of ferromagnetic material in the machine.

Magnetic field calculations for the different load cases of W 7-X at locations outside the vacuum vessel were made in order to estimate the stray field in this region. The stray fields are important because of their possible impact on diagnostic installations, vacuum pumps, etc.

The manufactured coils of the W 7-X device will be individually tested at the Euratom Association CEA-DAPNIA in Saclay. In each case two coils are to be horizontally installed at a distance of 1.4 m between them in the test arrangement. For this coil arrangement the stray fields at nominal current and the inductance matrix were calculated. The forces on the coils during a fast deloading phase were also considered.

3.2 Helias Reactor Studies

The investigations on a Helias Reactor (HSR) were continued. Particular attention was devoted to the coil system, the α-particle behaviour, the neoclassical transport, the drift waves, the plasma equilibrium, the neutron load on the target plates, and the effect of ferritic structural material on the magnetic field in such a device. The results of the investigations were presented at the EPS Conference in Prague, Czech Republic, at the Conference in Alushta, Ukraine, at the 20^{th} SOFT in Marseille, France, and at the 17^{th} IAEA Fusion Energy Conference in Yokohama, Japan.

The Web site, located at

`http://www.ipp.mpg.de/E2/hsr/hsr.html`

gives an overview and detailed data of the Helias reactor configuration.

3.2.1 Coil system of HSR

The HSR coil system is an upgrade of the magnetic configuration of Wendelstein 7-X. It comprises a single set of 50 modular non-planar coils arranged toroidally in 5 field periods with a major radius of 22 m [545]. In contrast to a previous design, the magnetic field at the coils has been reduced by making the coil cross-section trapezoidal and reducing the average magnetic field by 5%. The winding pack was split into two parts in order to diminish the current density at the location of maximum magnetic field. Because of this modification, a maximum magnetic field at the coils of about 10 T was achieved, which is in the range of NbTi technology at a temperature of 1.8 K.

The ANSYS computer code was used to perform the finite-element computations, which were done over half a field period, taking into account the stellarator symmetry. The boundary conditions were formulated by means of the multipoint constraint technique [101]. The computations were done with a SOLARIS computer in the ZTE Division, consuming about 1 GByte of memory space and about 4,000 seconds for each iteration step.

For the coil arrangement in the assembly the necessary iteration steps will be continued, the geometry of the coil support structure being varied in order to minimize structural material and to homogenize the stress distributions.

3.2.2 Alpha-particle orbits in Helias configurations

In a Helias configuration with $\beta(0) = 3\%$, orbits of the passing α-particles with energies of 3520 keV and 352 keV were studied in the presence of electromagnetic perturbations. Under the influence of magnetic perturbations $\delta B = \nabla \times \alpha B$ with amplitudes $\delta B/B = 10^{-5} - 3 \cdot 10^{-4}$ magnetic island structures were obtained on the surfaces at the periphery ($r \approx 180$ cm) due to 1/1 and 5/5 resonances and inside the plasma ($r \approx 130$ cm) due to the 10/11 resonance. Overlapping of 5/5 and 10/11 resonances and formation of a stochastic layer were observed. The drift rotational transform differs from the magnetic one, and so a drift surface resonance depends on the particle energy, the sign and value of the velocity component parallel to the field, and the electric field in the plasma [696]. The ambipolar electric field changes the shear for the α-particles with energy 352 keV and the radial distance between adjacent resonant values (10/11 and 25/27) becomes smaller. Overlapping of these adjacent resonances and formation of a stochastic layer inside the plasma ($r \approx 70 - 130$ cm) were observed for α-particles with energy 352 keV in the presence of an electrostatic perturbation with an amplitude 1/5 that of the ambipolar electric field. Because of the difference in drift shear the stochasticity did not take place for the α-particles with energy 3520 keV.

The drift losses of highly energetic α-particles and their interaction with the vacuum chamber and divertor plates in Wendelstein 7-X were studied [758]. The launched particles have a normalized Larmor radius of $\rho/a \approx 1/30$ (a is the minor radius of the last closed magnetic surface) to simulate fusion α-particle behaviour in the Helias reactor. It was found that highly energetic α-particles leave the confinement region for two reasons, namely strong outward radial banana drift (for barely and intermediate trapped particles) and trapping in the coil ripple determined by the number of coils (for deeply trapped particles). The confinement time for the majority of lost particles is less than 20 msec. The lost particle footprints on the "first wall" are located on the divertor plates.

---

[1] Guest from NIFS, Toki.

[2] ZTE Division

3.2.3 *Development of interactive transport code*

An interactive helical transport code with graphical interface (GUI using MOTIF) is being developed. The code combines the GUI part of the ITER-Pretor code and the TOTAL helical transport code (in Fortran) of NIFS. It describes neoclassical ripple transport with ambipolar electric field, transport of neutral particles and impurities, and α-particle heating with feedback fuel control. The code is now being used to analyze W 7-AS experiments and make predictions for W 7-X and the Helias reactor.

3.2.4 *Ripple-averaged kinetic theory*

The ripple-averaged kinetic theory of neoclassical transport in stellarators was reformulated so as to avoid a number of simplifying assumptions which limit the validity of the conventional theory. Specifically, averages are truly performed along field lines, the asymmetry of local ripples is treated, and non-localized particles are fully taken into account. Solutions of the appropriate ripple-averaged kinetic equation provide accurate estimates of the $1/\nu$ transport coefficients for advanced stellarators without requiring extensive numerical calculations.

3.2.5 *Drift waves in HSR*

Recent results in linear and nonlinear theory of drift waves in inhomogeneous plasmas show a considerable influence of the geometry on instability and turbulence. Metric effects arise through local and global variation of field line curvature, shear, and field strength. Systematic numerical studies of geometric effects on linear gyrokinetic stability were performed [143]. Furthermore, first results from nonlinear simulations of electrostatic fluid turbulence in the boundary of fusion plasmas with a non-trivial metric were obtained. The three-dimensional flux surface geometry of real stellarators (e.g. W 7-X) was implemented for the first time in turbulence simulations.

3.2.6 *Extension of the MFBE code*

Self-consistent computation of three-dimensional finite-β, free-boundary equilibria is essential for investigating and optimizing Helias configurations. Such computations were made with a package consisting of the NEMEC, MFBE, and GOURDON codes. In order to extend these computations to equilibria with non-vanishing toroidal current, e.g. boostrap current, the MFBE code was improved by using the so-called 'virtual casing' principle (V.D. Shafranov et al., Nucl. Fusion **12** (1972) 599) for calculating the magnetic field outside the plasma boundary. This method not only extends the usage of the code, but also reduces the computing time.

3.2.7 *Interface for the MCNP neutronic code*

Neutronic calculations yield essential information for designing the blanket and shield in a fusion reactor. The MCNP 3D "Monte Carlo" code is an appropriate tool for this task. In this code the modelling of the geometry is done by defining surfaces and their connection into cells. A particle is inside a certain cell if it is on a given side of all surfaces bounding the cell. This condition can only be true for the volume of one cell. The rather complicated shape of the blanket and shield of HSR and the sensitivity of the results to geometrical details made an approximation of the curved surfaces by small planes the best solution.

In the toroidal direction, the device can be segmented into poloidal planes and one obtains strips of poloidally turning shells of the components, beginning radially inside with the first wall and ending at the outside wall of the cryostat vessel. In the poloidal direction, the shells were approximated by small planes which together with the poloidal planes bound, a desired number of cells. In order to reduce the amount of computing time the number of cells should not be too large, so that the cells have to be bounded by many surfaces. The difficulty of this method is finding the rather complicated instructions to connect the surfaces by Boolean operators and brackets into cells. An interface code which calculates these instructions, was written for this purpose.

As an example the first wall was modelled and the wall load due to the 14 MeV neutrons originating in the plasma was calculated. Each toroidal section was defined in this case by one cell enclosing the plasma. The resulting total neutron power was 2.4 GW with an average plasma beta of 4.6% and a magnetic induction of 5 T. The peak neutron wall load was 1.6 MWm^{-2} and the average value 0.8 MWm^{-2}. The maximum value and also the largest variation in the poloidal direction occurs in the neighbourhood of the indented cross-section and reflects the variation of the distance of the plasma centre to the wall.

3.2.8 *Effect of ferritic material on the magnetic field*

In a fusion reactor ferritic/martensitic steel is strongly favoured as structural material, since its low activation after neutron irradiation makes it a very attractive candidate to mitigate the issue of radioactive waste disposal. On the other hand, ferromagnetic material modifies the magnetic field of the current-carrying coils and may have negative effects on the plasma confinement, especially in stellarators since any deviation from symmetry may lead to island formation and destruction of magnetic surfaces. For this reason the general equations governing the magnetic field in stellarators with ferritic structural material were analyzed and the basic effect was investigated in simple straight geometry where analytic solutions are available. A code was established which allows one to compute the modified field in toroidal 3D geometry. Since the ferritic material is saturated under reactor conditions, the effective permeability is in the range of 1.2 to 1.5. This leads to a 2% reduction of the rotational transform under normal conditions where the symmetry of the field generated by the coils is not violated. Symmetry-breaking error fields arise if the properties of the ferritic material differ from period to period. This perturbation can cause islands, but it was found that under moderate assumptions on the inhomogeneity the island formation is tolerable and does not lead to destruction of the divertor action.

WENDELSTEIN 7-X DIAGNOSTICS

(Head of Project: Dr. Hans-Jürgen Hartfuß)

Experimental Division 3: M. Anton, R. Brakel, M. Endler, S. Fiedler, C. Fuchs[1] J. Geiger, L. Giannone, P. Grigull, H. Hartfuß, M. Hirsch, R. Jaenicke, M. Kick, K. Knauer[1], G. Kühner, K. McCormick, A. Weller, C. Wendlandt[1], A. Werner[1], E. Würsching

1) Postdoc

Experimental Division 4: J. Baldzuhn, R. Burhenn, R. König

Plasma Diagnostics Division: D. Hildebrandt, M. Laux, R. Radtke, J. Sachtleben, U. Wenzel

Surface Physics Division: J. Roth

FZ Jülich: W. Biel, G. Bertschinger, P. Mertens, A. Pospieszczyk, R.P. Schorn, U. Samm, B. Schweer

University Heidelberg: B. Wolle

1. OVERVIEW

The project has been founded to develop diagnostics for the W7-X stellarator, to coordinate the contributions from various divisions of IPP and the external partners and to define the needs of data aquisition. The project develops also diagnostics necessary for the control and protection of the W7-X machine. This presentation of the project concentrates on its structure and the main goals. The project is divided into nine subgroups: 1) Fluctuations, (2) Plasma Edge, (3) Microwaves, (4) Charge Exchange, (5) Spectroscopy, (6) Thomson Scattering, (7) Soft-X-Ray and Electromagnetic Diagnostics, (8) Heavy Ion Beam Probe and (9) Neutrons. In addition to these scientific groups a technical group is formed which coordinates the needs in the infrastructure, the design and construction as well as research and development in mechanics and electronics. The work of the project is accompanied by an international advisory board. An electronic documentation system is being built up to store all the relevant information of the project. The documentation system is open to all interested persons and can be reached via the Internet.

2. GENERAL DEMANDS

On the basis of the goals and the scientific program of W7-X the appropriate general diagnostic concept is being defined. In the core plasma, the standard diagnostics, as known from other stellarators, torsatrons and tokamaks, can be used to meet the requirements to measure the basic plasma parameters with sufficient accuracy.

A main goal of W7-X is the experimental verification of the major design elements. These are: (1) selection of iota=1 with moderate shear, (2) improved equilibrium, (3) particle drift optimization, (4) energetic particle confinement, and (5) negligible bootstrap current. In addition the role of the drift optimization on anomalous transport is a major issue. For all this the diagnostics must be capable of providing the necessary information in experiments demonstrating the high performance of the machine in various confinement regimes, making use of stellarator specific properties like long pulse operation and under operation conditions with and without ECCD driven currents for MHD measurements and all studies on the tokamak-stellarator comparison without losing accurate knowledge of the configuration which is expected to be stable close to the vacuum configuration.

In order to provide a set of basic diagnostics at start-up of the machine and to prepare for a later stage of diagnostic needs and developments, possible and desirable diagnostics have been categorized in three levels: Level 1 comprises the basic diagnostics for machine and divertor operation and plasma characterization as given above. Level 2 extends the diagnostic potential of the Level 1 set with respect to additional parameters and/or higher spatial and temporal resolution, redundancy, poloidal/toroidal asymmetries, correlations etc. Level 3 finally includes advanced diagnostics which may be of importance for special investigations in an otherwise already well-diagnosed machine and which may include recent trends and developments towards new diagnostic capabilities and extensive diagnostics for fluctuations in E-field, density and temperature as well as correlations between these quantities.

More than fifty diagnostics of different kind have been proposed and discussed. They are considered in the port design. About twenty diagnostics are categorized to Level 1.

2.1 Design elements flux topology and optimization concerning stability and equilibrium

Extended magnetic and soft x-ray diagnostics are needed to address the optimization of the configuration with respect to equilibrium, stability and pressure driven currents. Soft x-ray tomography will play an important role in this context. It will be complemented by probe arrays and video camera diagnostics which image the edge topology of the plasma including the islands. The verification of the predicted magnetic topology is based on (1) tomographic reconstruction of the x-ray emissivity, (2) deduction of axis and separatrix positions and of Shafranov-shift, (3) the measurement of the dipole field emerging from the Pfirsch-Schlüter currents, (4) verification of low bootstrap current and its parameter dependencies, and (5) the detailed characterization of the edge topology.

Equilibrium and stability indentification require (1) the detection of rational surfaces, stationary islands and the connected MHD activity, (2) the recognition of the operational limits and of enhanced transport due to MHD activity, (3) the verification of predicted instability thresholds and the identification of instability mechanisms and (4) the establishment of unfavorable configurations. The low shear allows stability and turbulence issues as connected with the existence of rational magnetic surfaces to be addressed with local fluctuation and correlation measurements.

2.2 Design elements confinement and transport

Neoclassical transport is a threat to a stellarator reactor since particles trapped in local magnetic mirrors can lead to rapid losses. This is especially true in the collisionless LMFP regime. The key element in these losses is the radial drift of the trapped particles away from magnetic surfaces. This drift is minimized if the particles are localized in regions of small poloidal field variation.

Investigations of neoclassical transport properties will benefit from the configurational flexibility of W7-X, whose mirror ratios can be varied in a wide range and where its influence on trapped particle fractions and neoclassical damping processes can be varied and studied. In order to measure the properties of improved confinement and neoclassical transport, precise measurements of the electron temperature, the ion temperature and the radial E-field profiles are required accompanied by accurate analyses of the power balance. This will be provided by Thomson scattering in both the core plasma and the divertor regions, by radiometry of the electron cyclotron emission, multichannel interferometry and polarimetry measurements, charge exchange neutral particle analysis, charge exchange recombination spectroscopy, reflectometry, fast Li-beam diagnostics and bolometry.

Confinement issues are addressed on the basis of (1) changes of density and temperature profiles, (2) confinement transitions, (3) neoclassical effects connected with trapped particles, (4) changes in the radial electric field, and in addition (5) transport parameters from active perturbation of density and temperature, as well as (6) transient impurity transport studies.

3. STEADY STATE OPERATION

The inherent properties of the stellarator for steady state operation have implications on the diagnostics. Although stationary operation is the ultimate goal, most of the experiments will initially be done with limited pulse duration of the order of 10 s. Different modes of operation will be possibly determined by the various heating scenarios on the basis of ECRH, ICRH and NBI. These scenarios will not require a principally new diagnostic approach, however, intelligent event recognition will be required and especially correlation studies will benefit from the long pulse operation allowing for long integration times. Improved spatial resolution will be possible with diagnostics which can be slowly scanned. Furthermore, temporally separated complex measurements by different diagnostics will be possible in the same volume. The new modes of operation mainly ask for a good feedback control and flexible hardware to safely operate long pulse discharges with sequential operation of different heating systems to run through quite different plasma states and parameters.

Long pulse operation will be a major challenge to the data aquisition system which must be capable of handling tremendous amounts of data. Event recognition and fast response of the centrally controlled diagnostics is demanded and must be developed. The problems connected with the data handling and advanced concepts of the data reduction and aquisition are discussed by a group established at IPP to solve the problems in close collaboration with the diagnostics groups. It is planned that the experiments conducted at W7-X are completely controlled by a central computer which also controls the individual diagnostics. This means that the diagnostics must be remotely controlled and that self-checks and calibrations can be carried out. This measure is a first step to remote participation from a remotely located control room.

4. PORTS AND INFRASTRUCTURE

Despite the complex coil set of W7-X and the 3-dimensional geometry, a large number of ports will be available for plasma diagnostic. Due to the large aspect ratio and the absence of an ohmic transformer, inboard side access to the plasma is also possible. The final design of the diagnostic ports has been done in close collaboration with the diagnostics groups to meet their requirements for optimum access to the plasma and a minimum of restriction to the sightlines by supporting structures. It is planned that altogether about 300 ports in the vacuum vessel will be realized. About 160 ports are designated for the diagnostics. The others are needed for ECRH, ICRH and NBI heating of W7-X and especially for safe divertor operation and control.

After the completion of the design of the vacuum vessel and the diagnostic ports, design of the front end of the basic diagnostics will begin. Search for standardized solutions of the diagnostic electronics and the computer control of individual diagnostic components has already been started.

WENDELSTEIN 7-AS

(Head of Project: Prof. Dr. Friedrich Wagner)

Members of the W7-AS group: see section "Divisions and Groups, Experimental Plasma Physics Division 3".

1. OVERVIEW

From April to October 1998 the torus of W7-AS was opened to install 10 control coils and to replace the ICRH antenna. The control coils are the first step of the project "Divertor Experiment at W7-AS", which was approved in June by the HGF for the strategy fund. The second step, the installation of the divertor modules, titanium getter pumps and additional divertor diagnostics, will occur in the years 1999/2000.

To preserve the symmetry properties of W7-AS, 2 control coils had to be placed on both sides of the 5 triangular flux surface cross sections. Thus, the coils produce 5/m (m = 9, 10, ...) perturbation magnetic field components which, superimposed on the intrinsic 5/*m* components, introduce additional degrees of freedom to control resonant field structures - in particular at the edge. Specifically, depending on the strength and sign of the control coil currents, intrinsic "natural" magnetic islands can be enlarged, decreased, fully compensated or even over-compensated. With the islands compensated, the unperturbed plasma cross-section with closed flux surfaces can be significantly increased in some cases.

First experiments show a clear dependence of the total energy content on the effective radius of the last closed flux surface. Changes in the "footprints" of 5/9 and 5/10 islands, for example on inboard limiters or at the plasma boundary, can be seen by several diagnostics. The experimental work is accompanied by the development and application of numerical codes.

Before replacing the „broad" ICRH antenna by a conventional double strap antenna, the performance of the old antenna was further investigated. Plasma heating and sustainment was proved also for additional heating schemes.

The ECRH heating power was upgraded late in 1997 by installing a third 140 GHz gyrotron. Thus, very high local power densities were available for heating and current drive. Central electron temperatures could be increased to 5.7 keV. Nonlinear effects are found in the experiments and compared with theoretical predictions.

To further investigate the experimental dependence of the heat transport on high order rational values of the rotational transform and on the magnetic shear a model was developed to enhance the electron heat diffusivity around rational magnetic surfaces. In this way qualitative agreement with measurements in a wide range could be found. Other investigations concentrated on particle and impurity transport and on perturbative transport studies.

The periodic multichannel Thomson scattering diagnostic (YAG laser) came into operation in 1998. It measures electron temperature and density profiles every 50 ms. An infrared camera was installed for thermographic measurements on an inboard limiter especially in connection with control coil experiments.

2. EXPERIMENTAL AND THEORETICAL RESULTS

2.1 Boundary Layer Studies

2.1.1 Effects of new control coils

The configurational flexibility of W7-AS was improved by installing five pairs of control coils on the low-field side, each pair placed symmetrically about a plane with triangular plasma cross-section ($\phi = 0°$, for technical details see 4.1). The coils produce 5/m (m = 8, 9, ...) perturbation magnetic field components which, superimposed on the intrinsic 5/*m* components, introduce additional degrees of freedom to control resonant field structures - in particular at the edge. Specifically, depending on the strength and sign of the control coil currents, intrinsic "natural" magnetic islands can be enlarged, decreased, fully compensated or even over-compensated. With the islands compensated, the unperturbed plasma cross-section can be significantly increased. Over-compensation changes the sign of the resulting $B_{5,m}$, and the

islands become phase-shifted. Figure 1 shows respective examples.

Basic aims were to provide a tool to vary resonant structures more independently of other field parameters such as the rotational transform and magnetic shear for confinement and transport studies, and to gain flexibility with respect to island divertor studies planned for next year.

First indications from "footprints" of 5/9 and 5/10 islands (H_α traces on poloidal inboard limiters, ion saturation current distributions from a large poloidal probe array) as well as tangential camera observations in low-ß ECRH discharges with ramped control coil currents suggest that the coils work as expected.

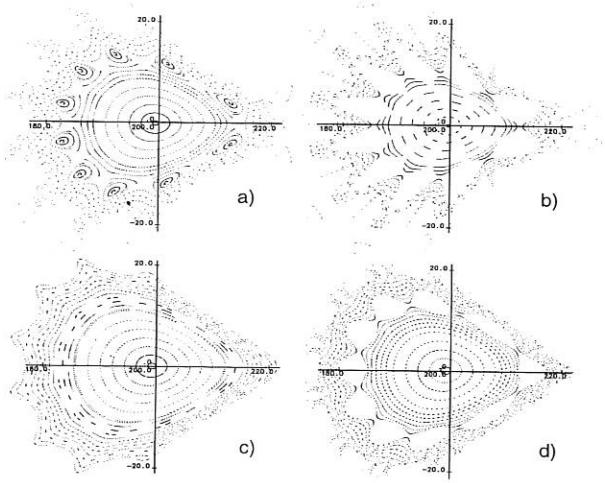

FIG. 1: Effects of control coil currents on edge magnetic islands of the symmetry n/m = 5/10 at B_o = 2.5 T. a) Without control coil current I_{cc} b) with I_{cc} = -2 kA (enlarged islands), c) with I_{cc} = 1.5 kA (compensated islands) and d) with I_{cc} = 3 kA (over-compensated intrinsic perturbation field, islands shifted in phase).

2.1.2 *EMC3 code applications*

Recently the code was applied to high-density "detachment-like" conditions with temperatures down to 1 eV at the targets. Figure 2 shows how the ionisation front shifts from the target towards the separatrix as the upstream density increases, indicating gradual detachment. Compared with that in tokamaks, the small poloidal and radial extent of the divertor region in W7-AS leads to stronger contributions from cross-field transport of particles, momentum and energy. In particular, the EMC3/EIRENE code predicts that cross-field diffusion gives rise to strong momentum losses /435/. These losses strongly smooth the transition from low to high recycling and lead to a parallel pressure drop, even for low recycling, by a factor of 4 - 5 instead of the standard factor of 2.

In the detached case, the toroidal localisation of the recycling zones leads to strong toroidal inhomogeneity of the downstream plasma parameters. This is illustrated in Fig. 3, which shows the distributions of ion sources, energy sinks by neutrals and temperature and density along an island tube cut by the target plates.

FIG. 2: Ion source distribution from an EMC3 code simulation in a divertor half cross-section for three density values, increasing from left to right. The target plate and the two baffles are sketched.

In the recycling regions, an extended cold plasma zone is established over the full radial range of the SOL and the full poloidal angle and toroidally over two field periods. The already mentioned temperature drop and density rise towards the recycling zone are particularly pronounced in the poloidal zones opposite the target positions, where the density and temperature profiles along the island tube are clearly phase-shifted to each other.

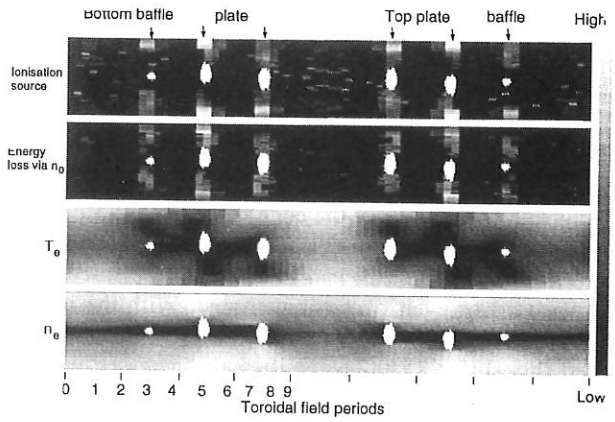

FIG. 3: Distributions of ion sources, energy sinks by neutrals and temperature and density from EMC3 code simulation along an island tube over the full poloidal angle and the full helical periodicity of nine field periods. The island tube is cut by each target plate at two adjacent field periods.

2.2 Transport and Confinement

2.2.1 *The role of rotational transform and magnetic shear*

There is strong experimental evidence that the anomalous electron heat transport is locally enhanced by perturbations

arising in the presence of rational values of the rotational transform, ι, and that these perturbations are suppressed with increasing magnetic shear, ι' = dι/dr. In particular, for ECRH discharges at moderate β optimum confinement is found when, due to low shear, ι (*r*) remains in narrow windows around the low-order rational values 1/2 and 1/3, which are free of higher-order resonances. Moving ι out of these windows degrades confinement by a factor of about 2. This sensitive dependence on ι is gradually lost when magnetic shear is increased by an inductively driven plasma current, finally leading to optimum confinement at any boundary value of the rotational transform, ι (*a*) (Fig. 4).

These findings suggest a simple empirical ansatz for the electron heat conductivity χ_e:

$$\chi_e (r, \iota, \iota') = \chi_0(r) + \Sigma \chi_{nm} (\iota, \iota'),$$
$$\chi_{nm} = \alpha_{nm} \exp (- |\iota - n/m|/\delta - \gamma|\iota'|).$$

χ_0 accounts for the transport in the absence of resonances, i.e. at optimum confinement. It includes both anomalous and neoclassical contributions. χ_{nm} describes an additional enhancement of χ_e near a rational value $\iota = n/m$. The parameters α_{nm}, γ, and δ represent the amplitudes of the perturbations, the damping by the absolute value of magnetic shear, and the width of the perturbed ι range, respectively.

This approach implies close coupling of confinement and magnetic shear. The shear profile results from the pressure-driven bootstrap and Pfirsch-Schlüter (PS) currents and, optionally, externally driven. In turn, the current densities are basically determined by the electron temperature profile, $T_e(r)$, resulting from χ_e.

For explicit calculations a simplified power balance is used to calculate $T_e(r)$, with convective and radiation losses as well as electron-ion coupling being neglected. The bootstrap current density is approximated by $j_{BS} = 0.7\ j_{BS}^{HH}$, with the bootstrap current density j_{BS}^{HH} in a circular tokamak as given by Hinton and Hazeltine. The factor 0.7 adjusts the total bootstrap current to the value obtained with the DKES code for optimum confinement. The inductive current density profile is calculated from the tokamak neoclassical conductivity and normalized such that the bootstrap and inductive currents add up to the given net plasma current I_p. The PS current is neglected due to moderate β. Density, power deposition and Z_{eff} profiles, ι(a) and I_p are input to the calculation. The self-consistent solution is obtained by iteration. Up to m = 20 rational values have been included in χ_{nm}. The values $\alpha_{nm} = 1.1\ g_{nm}^{-1}$ m²/s, $\gamma = 1.1$ m and $\delta = 0.004$ are chosen by reasonable agreement between experimental and simulated confinement data as well as T_e -profiles. g_{nm} is the degeneracy of a n/m value, i.e. every rational number is counted only once.

The model qualitatively reproduces the basic dependencies of confinement on the experimental control parameters, ι(a) and I_p, supporting the hypothesis of the impact of rational ι-values on confinement (Fig. 4).

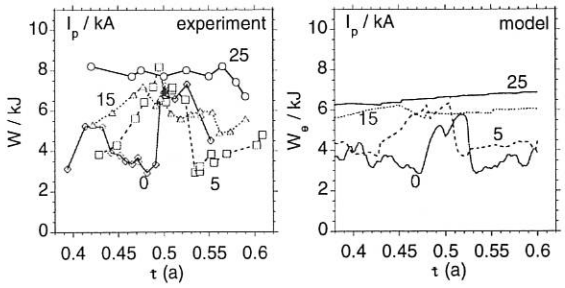

FIG. 4: Plasma energy (experiment) and electron kinetic energy (model) versus ι(a) for various net plasma currents I_p. ($B = 2.5$ T, $P_{ECRH} = 450$ kW, $n_e \approx 4 \times 10^{19}$ m^{-3}, $T_e \leq 2$ keV, $T_i \leq 0.4$ keV).

2.2.2 *Impurity transport*

The measured radiation decay time of the highest ionization states of laser blow-off injected aluminium (Al XII, Al XIII) reveals improved confinement towards higher plasma density. In order to study the density dependence of impurity confinement in more detail, ECRH discharges (P_{ECRH} = 480 kW, ι = 0.34, B = 2.56 T, a = 0.17 m) at two different densities ($n_{e0} = 3.5/7 \cdot 10^{19}$ m^{-3}) are compared (Fig. 5). Local impurity transport coefficients are obtained from analysis of radial and the temporal soft-X camera radiation evolution subsequent to aluminium injection by laser blow-off. As a general feature of ECRH discharges, the transport analysis provides moderate diffusion coefficients D in the central plasma, whereas smaller diffusion coefficients have to be assumed in the outer third of the plasma in order to match the temporal behaviour of the spectral radiation. Here, the transport analysis with soft-X camera data fails due to the drop of intensity as a consequence of low electron density and temperature in this region.

In the case of high electron density ($0.4 \geq D \geq 0.04$ m²/s, 2 cm ≥ r ≥ 17 cm), D (r) is a factor of 2 - 3 lower than in the medium density-discharge (≈ $1 \geq D \geq 0.1$ m²/s, 2 cm ≥ r ≥ 17 cm), the convective velocity u being quite similar. Consequently, the time evolution of the intrinsic impurity radiation and Z_{eff} is appreciably different during the flat-top phase for these two densities. In the medium-density case (Fig. 5 (2)), stationary conditions concerning the intrinsic impurity radiation were usually achieved. In the high-density case (Fig. 5 (1)), impurity radiation and Z_{eff} do not reach steady state within the discharge duration, but show a continuous increase with a tendency to saturate at times longer than the performed pulse length (≈ 1 s). Assuming a constant impurity influx of, for example, intrinsic chlorine from the walls and using just the derived sets of transport parameters, one can achieve a qualitatively good simulation of the difference in the time traces of Cl-XIV radiation: the reduced transport in the high-density case results in longer times to establish steady state concerning the impurity fluxes. This explains the steady increase of chlorine radiation during the pulse and might also be responsible for similar behaviour of SX camera and bolometer radiation as well as Z_{eff}. The helium inventory (introduced by a gas-puff) as measured by

CXRS (He-II at r = 6 cm) shows no temporal increase in the high-density case.

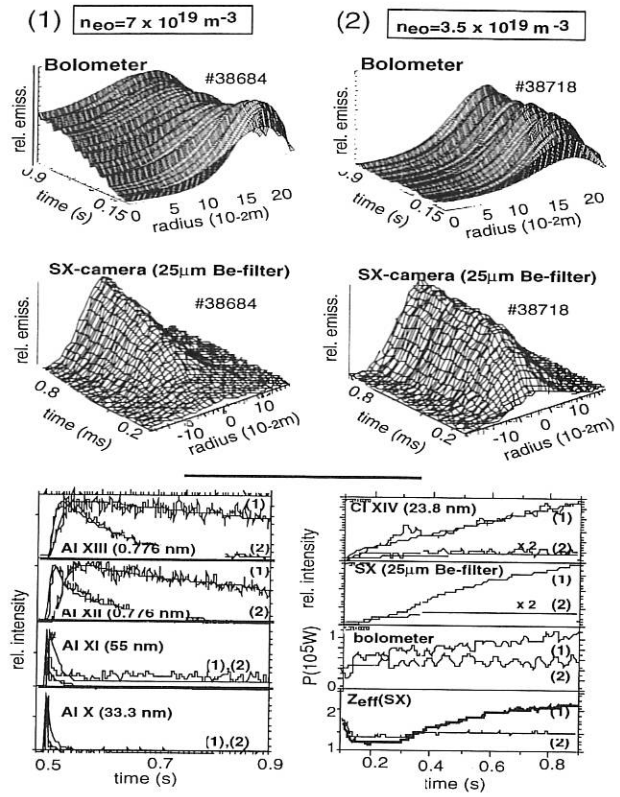

FIG. 5: Comparison of ECRH plasmas with (1) high (n_{eo} = 7 10^{19} m^{-3}) and (2) medium (n_{eo} = 3.5·10^{19} m^{-3}) electron density: bolometer and soft-X camera radiation, time traces and simulations of spectral lines from different ionization states of aluminium after injection by laser blow-off, time evolution of impurity radiation and Z_{eff} (SX), and simulations for Cl-XIV.

2.2.3 *Density limit studies*

Measurements of the time evolution of the density and temperature in front of the limiter were compared with simulations by the ASTRA time-dependent transport code combined with a one-dimensional scrape-off layer model of the plasma edge. A modified two-point model could reproduce the features of a falling temperature and rising density in front of the limiter plates as the line-integrated density was ramped up. The plasma detached when the net power flux at the plasma edge decreased so that power balance in front of the limiter plate could no longer be fulfilled. The plasma collapsed rapidly after the total radiated power was greater than the NBI input power. The simple one-dimensional two-point model therefore describes the physics of the density limit in stellarators and tokamaks.

Density limit discharges with a strong density ramp were compared with a series of discharges with constant line-integrated density approaching the maximum value achieved in the density ramp. The discharges with a strong density ramp were found to have broader density profiles than those discharges with constant line-integrated density. The latter discharges had the electron density profile form found in the improved confinement H-NBI mode in W7-AS.

In discharges at successively higher density plateaus, the rate of diamagnetic energy decrease after the peak in diamagnetic energy was larger at higher densities. Combination of the STRAHL impurity transport code and ASTRA allowed radiation profile measurements of the bolometer and soft X-ray cameras to be simulated. The increase in radiated power during density plateau discharges was shown to be due to central peaking of the radiation power density. Such peaking was previously observed in the W7-A stellarator and accounted for by neoclassical impurity transport of oxygen ions from the vessel walls and tungsten from the NI beams. The radial profiles of the diffusion coefficient, D, and inward pinch velocity, u, used in the simulations were taken from the laser blow-off studies. The experiments also showed that impurity density profiles continuously increased during the discharge. The time constant for attaining equilibrium was therefore greater than the duration of the discharge (up to 1.3 s). These conclusions were confirmed by independent Z_{eff} profile measurements from bremsstrahlung radiation. The consequent increase of the central radiated power and the decrease in net power to the plasma together with the slow central density rise leads to a reduction of the central temperature which reinforces the increase in radiated power. The reduction of impurity fluxes to the discharge by the planned divertor for W7-AS will therefore be critical to achieving steady-state operation at the highest possible density.

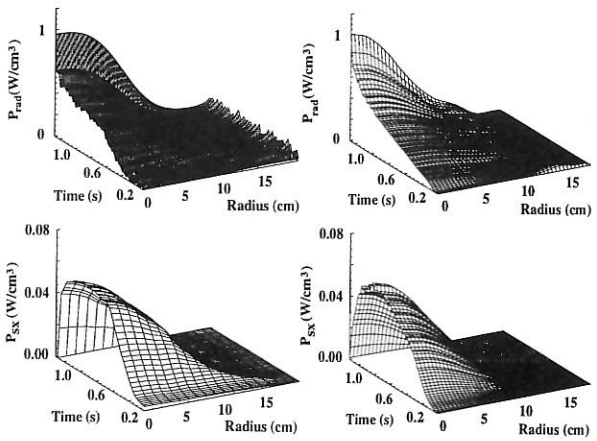

FIG. 6: A comparison of the measured (left column) and simulated (right column) radiation profiles for the density plateau discharge. The radiation profiles deduced from the bolometer and soft x-ray (12.5 mm Be filter) cameras are shown in the first and second rows respectively. The bolometer and soft X-ray profiles were simulated with a diffusion coefficient and inward pinch coefficient profile calculated from Al laser blow-off experiments and time dependent electron temperature and density profiles with the STRAHL impurity transport code and the ASTRA time-dependent transport code. Three impurity flux sources (C, Cl and Cu) at the plasma boundary were assumed.

2.2.4 *Particle transport studies*

Peaking of the density profile was observed when strong off-axis ECRH was used. This observation points to the existence of a particle pinch in W7-AS. Figure 7 shows a time sequence of temperature and density profiles in a discharge where the heating power was switched from on-axis to off-axis and back to combined on/off-axis heating.

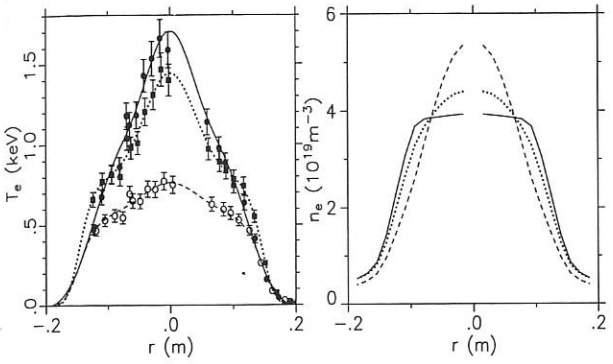

FIG. 7: Electron temperature (from an ECE radiometer) and density profiles (from a 10-chord interferometer) at different time points: on-axis heating (solid line, solid circles), off-axis heating (dashed line, blank circles) and combined on/off-axis heating (dotted line, solid squares).

The transitional phases between the different heating schemes were analyzed by solving the time-dependent transport equation with the ASTRA code. The electron temperature evolution was prescribed by the measurements and the density profile was calculated using for the flux the ansatz

$$\Gamma = n_e (D_{11} \frac{\nabla n_e}{n_e} + D_{12} \frac{\nabla T_e}{T_e} - u).$$

The transient response of the central density to changes in heating power can be best described if $D_{11} \approx 0.2$ m^2/s, a value consistent with the gas-modulation results shown below. Towards the edge, the coefficient was set to increase as $1/n_e$. The D_{12} coefficient was switched between the collisional values determined by the DKES code for the three phases and the convective velocity u was adjusted to fit the measured density evolution. The particle source profile for the three phases, which determines the particle flux Γ, was calculated by the code Monte Carlo EIRENE.

Figure 8 shows the agreement obtained. The evolution in the plasma centre ($r \leq 5$ cm) is obtained with almost constant transport coefficients and can be understood in terms of the ∇T_e -driven transport, which is balanced by a pinch in the phase with on-axis heating. When the heating is moved off-axis, the central temperature gradient vanishes and due to the pinch a density gradient builds up until u is balanced by the D_{11}-driven transport. In an intermediate range r = 5 to 10 cm, the pinch velocity has to become stronger during the off-axis phase. In the edge of the plasma (r > 10 cm) a detailed analysis is not possible since there are three major contributions to transport: the source, the diagonal term, and the pinch. With a D_{11} which rises to an edge value of 0.6 m^2/s, the convective term is inward-directed and of the order of the source term.

A comparison of the data with neoclassical theory was carried out on the basis of DKES calculations. For the discharge shown in Fig. 2.4 at $r \approx 7$ cm, the neoclassical particle fluxes are compared with those calculated from the particle source profiles. Due to the reduced central temperature in the off-axis phase, the neutral particle density and the particle flux increase by a factor of about 2. At the same time, the neoclassical flux is reduced by a factor of 2. In the off-axis phase, the two fluxes agree in magnitude and consequently they differ by a factor of about 4 in the on-axis phase.

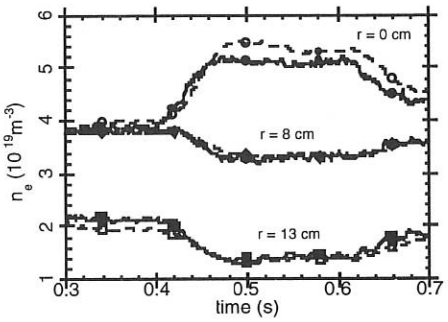

FIG.8: Time traces of measured and calculated (broken lines) local electron density at different radii.

2.2.5 *Perturbative transport studies*

The particle transport coefficients in W7-AS were also determined by an alternative method, by injecting modulated gas feed into the plasma and measuring the propagation of the density perturbation. The results of the experiments carried out at a variety of plasma densities, heating powers, and magnetic field strengths are summarized in the form of a scaling expression for the perturbative diffusion coefficient:

$$D = (0.84 \pm 0.05) n_e^{-1.18 \pm 0.13} T_e^{0.69 \pm 0.22} B^{-0.51 \pm 0.22}$$

The propagation of the density perturbation at the boundary region can only be explained by inward convection. The radial points where the inward pinch comes into action correlate with the radial point where the density gradient region begins. This dependence is illustrated in Fig. 9. It clearly demonstrates that the density gradient is driven also by the inward convection and not only by the particle source. In the core plasma, convection is not needed in normal operations, except with higher resulting in larger ∇T_e power, where clear evidence of outward convection is detected (see 2.2.4).

The results of the transient particle transport studies were compared with the predictions of the neoclassical theory. The measured diffusivities were in most cases higher than the neoclassical ones. The inward pinch is at variance with the neoclassical theory. Making use of three 140 GHz gyrotrons, one more campaign of power modulation experiments was

carried out. More attention than in previous experiments was paid to investigating plasmas under optimum confinement conditions.

At B = 2.55 T, the rotational transform was carefully chosen to avoid confinement degradation due to high-order rational values at $\iota \approx 1/3$. The line-averaged plasma density was varied between 2 and 5 x 10^{19} m^{-3} and the power ranged from 0.2 to 1.3 MW. In 2nd harmonic X-mode, the absorption was close to 100%. The obtained data quality was clearly superior to that in earlier experiments.

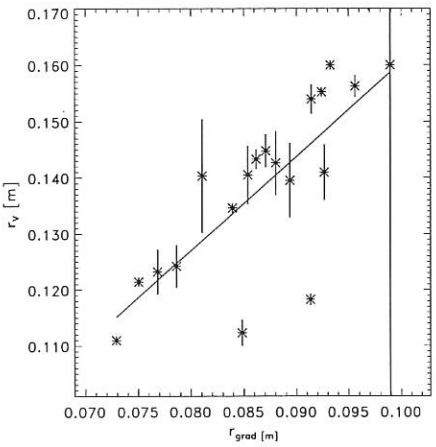

FIG. 9: Radius r_V at which the inward pinch comes into action as a function of r_{grad}, the radial point separating flat-top and gradient regions in the density profile.

The electron thermal diffusivity from the heat pulse experiments, χ^{hp}, was compared with that from a power balance analysis, χ^{pb}. As in previous experiments, the ratio obtained was in the range between 1 and 2. In addition, the new experiments indicate a trend from 2 to 1 when the heating power is increased. This finding is shown in Fig. 10. At higher density, the transition occurs at higher heating power. This might indicate a change in the transport properties when the power density surpasses a critical value.

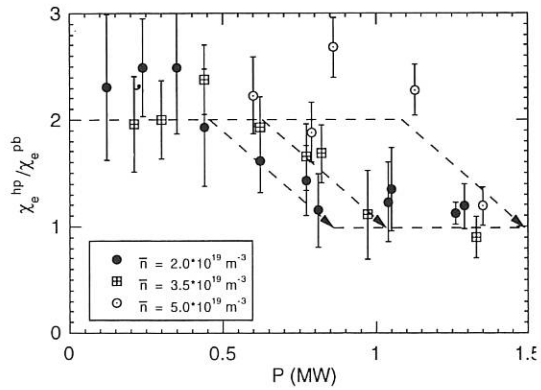

FIG. 10: Ratio of heat pulse to power balance diffusivity as a function of heating power and for three densities.

2.3 Ion Cyclotron Resonance Heating (ICRH)

During the 1998 experimental campaign the performance of the broad antenna was investigated for different heating schemes. In particular, heating of plasmas consisting of a mixture of hydrogen and deuterium - typical for W7-AS - at different hydrogen concentrations was attempted.

In the past it wasshown that the plasma could be heated and sustained as long as the hydrogen concentration was less than about 10 % and the hydrogen resonance and ion-ion hybrid resonance were located inside the plasma. Since fast hydrogen was observed, this heating scheme was identified as minority heating.

It was now shown that at higher hydrogen concentrations plasma heating and sustainment are also possible as long as the ion-ion hybrid resonance is located inside the plasma. For the magnetic field set by the ECRH resonance and the lowest possible generator frequency this necessitates that the hydrogen concentration be in the range of 15 to 40 %. The hydrogen resonance is then located outside the plasma on the low-field side. For hydrogen concentrations in this range direct electron heating, but no increase in the suprathermal hydrogen fluxes, were observed. This heating scheme was therefore identified as mode conversion heating.

The heating efficiency is comparable to minority heating, and so about 80 - 90 % of the radiated power could be accounted for in the plasma. The power deposition was located off-centre in approximate agreement with the estimated location of the ion-ion hybrid resonance. Density control was possible and there was no indication of impurity accumulation on the bolometric signals. A typical shot is shown in Fig. 11.

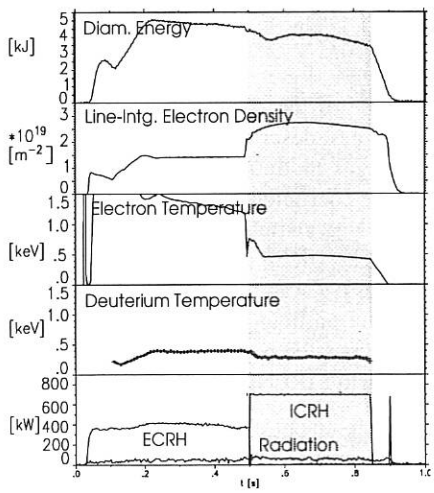

FIG. 11: Sustainment of plasma with D,H mode conversion heating

2.4 Electron Cyclotron Resonance Heating

Investigations on Electron Cyclotron Resonance Heating (ECRH) and Electron Cyclotron Current Drive (ECCD) in W7-AS were continued with an upgraded ECRH heating

power of up to 1.3 MW at 140 GHz, which corresponds to a resonant magnetic field of 2.5 T at 2nd harmonic X-mode (X2). The heating experiments cover the accessible density range up to the cut-off density of 1.25×10^{20} m^{-3}, whereas we restricted the ECCD experiments to densities of around 0.25×10^{20} m^{-3}. The microwaves are absorbed in a narrow region around the resonant magnetic field and thus the power density increases up to 50 MW/ m^{-3} in a flux surface averaged, which is far beyond the limits where linear theory holds and nonlinear phenomena are expected to occur[1].

2.4.1 *Experiments on electron cyclotron resonance heating*

Experiments with strong X2-mode heating were performed in a wide density range at a constant input power of 1.3 MW in low-field-side launch in the equatorial plane. Radial profiles of T_e and n_e are shown in Fig. 12. The central electron temperatures range from 5.7 keV at 1.7×10^{19} m^{-3} to 3 keV at 7.5×10^{19} m^{-3}. Pronounced steepening of the temperature gradients is seen in the centre of the plasma at densities below 4×10^{20} m^{-3}. The stationary transport analysis of these discharges results in a central (r/a < 0.3) electron heat diffusivity which is well below the neoclassical heat diffusivity, once electric fields are neglected. Strong positive radial electric fields of up to 50 kV/m were measured in the plasma centre, which afford good agreement with neoclassical theory including electric fields ("electron root solution"). It is worth noting that the energy balance is dominated by the electrons.

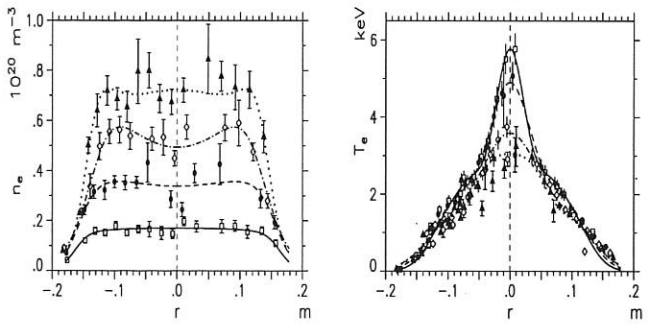

FIG. 12: Radial profiles of the electron density (left) and temperature (right) with 1.2 MW ECRH.

The appearance of the electric field - and the corresponding steep temperature gradients - shows threshold behaviour at a density of around $0.2 - 0.4 \times 10^{20}$ m^{-3}. Similar behaviour was observed during a power scan from an input power of 0.2 MW to 1.3 MW at a constant density of 0.2×10^{20} m^{-3}, where the steepening occurred between 0.2 and 0.4 MW.

The central electron temperature jumps near the threshold between two states of low (say 4 keV) and high (5 keV) temperature during one discharge with some hysteresis between rise and fall time constants. The experiments are explained by a substantial loss of fast trapped particles driven by ECRH itself, which in turn generates a positive electric field with its beneficial effect on the bulk electrons [2,3].

This picture is consistent with the results of switching experiments where the central confinement is lost on a fast time scale (< 0.3 ms), whereas the remaining profile relaxes on the diffusion time scale. These switching experiments also display threshold behaviour while switching from 1.2 to 0.8 to 0.4 MW.

2.4.2 *Experiments on electron cyclotron current drive*

A toroidal launch angle scan was performed at a launched power of 1.2 MW and a density of 2.5×10^{19} m^{-3} with inductive compensation of the EC-driven current to maintain net current free conditions with $I_{ind} + I_{boot} + I_{ECCD} = 0$ (I_{ind} is the inductive component, I_{boot} and I_{ECCD} are the bootstrap and EC-driven components, respectively). The microwaves were injected from the low-field side in X2 mode polarization, Ray-tracing calculations predict a peaked deposition profile with flux-surface-averaged power densities of up to 50 MW/m^3. The required inductive loop voltage for current compensation is shown in Fig. 13 (left) as a function of the launch angle φ_{inj} ($\varphi_{inj} = 0^o$ corresponds to perpendicular injection, $I_{ECCD} = 0$). For quantitative comparison of the measured data with theory, we assume a linear superpositioning of the three current contributions (see 2.6.6).

The bootstrap current is calculated by the DKES code taking into account the ambipolar radial electric field, and the inductive current is calculated on the assumption of neoclassical resistivity (effective charge $Z_{eff} = 3$-6), using the measured profiles of n_e and T_e. The EC driven current from the current balance $I_{ECCD} = -I_{ind} - I_{boot}$ is plotted in Fig. 13 and compared with the linear theoretical ECCD current I_{inj} from ray-tracing.

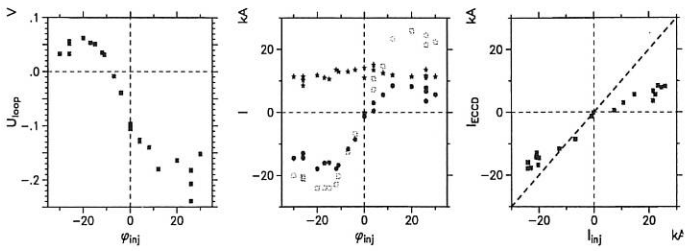

FIG. 13: Left: Loop voltage vs. toroidal angle of injection in net-current-free discharges, $U_{loop} = -(I_{boot} + I_{ECCD}) / R$. Perpendicular injection corresponds to $\varphi_{inj} = 0^o$. Centre: Theoretical (blank squares) and data from current balance of the EC-driven current (dots) together with the bootstrap current (stars) as a function of the launch angle. Right: EC-driven current from current balance versus linear prediction.

[1] M. Romé, Kinetic modelling of the ECRH power deposition in W7-AS, Plasma Phys. Control. Fusion 39 (1997) 117-158

As seen from Fig. 13 (right), where the 'experimental' I_{ECCD} is plotted versus theory, good agreement with linear theory is observed except for launch angles in the co-direction. This may indicate that the assumptions of the linear ECCD approach are violated (see 2.6.6). The quasi-linear theory, which holds in a homogenous magnetic field, must thus be reformulated. In addition, the wave absorption increases the perpendicular energy and pushes electrons into the loss cone. In the bounce-averaged Fokker-Planck calculation the strong heating as formulated by the traditional quasi-linear diffusion term is balanced by the energy loss of mainly suprathermal ripple-trapped electrons. The radial ∇B-drift of suprathermal ripple-trapped electrons broadens the power deposition profile /627/ but has no influence on the ECCD profile. In the electron distribution function, however, positive gradients with respect to $v_{||}$ close to the loss-cone boundary are found, which represent free energy and may drive the distribution function unstable. The fast growth rate of such kinetic instabilities can reduce the CD efficiency.

For co-CD the temperature profiles remain peaked and the ι –profile crosses the ι = 1/3 and ι = 1/2 surfaces with strong shear. The observed MHD modes are the corresponding m = 3 and m = 2 modes. The modes are located around the rational ι values as measured by ECE, soft-X and Mirnov diagnostics. In the opposite case of counter-CD the ι = 0 surface appears in the plasma centre and the temperature profile is flat indicating bad or no confinement within this surface. As a consequence, the EC-driven current within the ι = 0 surface may be distributed over a wider volume than calculated by ray tracing, leading to a reduced power density, a lower deviation from a Maxwellian distribution function and thus to better agreement with linear CD theory.

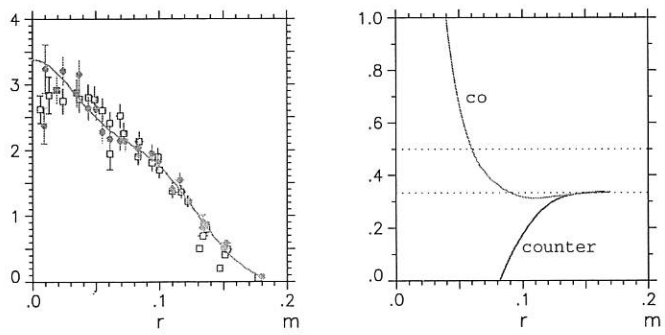

FIG. 14: Radial profiles of the electron temperature T_e (left) and rotational transform ι (right) for co- (dashed line) and counter-CD (solid line) at zero net current, φ_{inj} = + and - 12°, respectively.

2.5 Stability and Fluctuations

2.5.1 *Analysis of MHD activity*

During the experiment shutdown, the "MiniSoX" X-ray tomography system had to be modified due to interference with an internal control coil (only 8 cameras of 10 could be kept). The experimental investigations of MHD modes were continued with emphasis on neutral-beam-driven Alfvén instabilities using X-ray tomography, ECE and magnetic probes. In particular, OH-current drive was used to change shear, including cases with positive and negative shear. Although global plasma parameters, and hence drive and damping effects, depend on the iota profile, the changes of the mode behaviour seem to be in qualitative agreement with expectations on the basis of the modifications of the shear Alfvén continuum. In particular, at higher shear, TAE gaps become accessible as in tokamaks, and the transition from GAE to TAE modes could be observed. The low-frequency coherent Alfvén modes do not cause significantly increased losses. They are typically observed under conditions with $v_A > v_{beam}$, where only sideband excitation is possible. With increasing beam power and density, however, strong bursting mode activity occurs with frequencies of up to 500 kHz, which can induce significant energy and particle losses. Occassionally, strong frequency chirping is observed indicating nonlinear interactions with resonant fast-particles. The onset of these modes coincides in many cases with the decay of the Alfven speed below the maximum fast-particle velocity, and therefore additional modes can be excited. The analysis of the mode structure was experimentally not possible in the high-frequency range, but the observed phenomena seem to be consistent with higher-order global Alfvén modes or kinetic ballooning modes.

In collaboration with D.A. Spong (ORNL), C. Nührenberg (Stellarator Theory) and S.D. Pinches (Tokamak Physics), computational studies with a gyrofluid code, the 3-D MHD code (CAS3D) and the HAGIS guiding center following code, respectively, were made for selected experimental cases.

2.5.2 *Plasma edge fluctuations*

The measurement of electron density fluctuations with beam emission spectroscopy on a fast Li beam, in collaboration with KFKI-RMKI (Budapest), was extended to different discharge conditions. The radial region accessible to this diagnostic ranges from the scrape-off layer (SOL) almost into the plasma core, depending on the density profile. In the SOL, the same kind of density fluctuations is observed as with Langmuir probes or an H_α fluctuation diagnostic. Inside the last closed magnetic surface, fluctuations with different characteristics are found, called "wave-like" fluctuations due to the shape of their autocorrelation function. In contrast to MHD modes, their correlation time is of the order of only 100-500 μs, and their spectrum has a broad peak around 10 - 30 kHz. This fluctuation component is well correlated with Mirnov signals, which indicate an m = 3 structure for $\iota \approx 1/3$ and an m = 2 structure for $\iota \approx 1/2$, as emerging from a data analysis of a poloidal Mirnov coil array. At low plasma density, these wave-like fluctuations can disappear upon introduction of a net toroidal current, whereas the confinement is hardly changed, indicating that this fluctuation component might not be responsible for the anomalous radial transport. The fluctuations in the SOL are uncorrelated with these wave-like fluctuations.

In collaboration with CIEMAT and ORNL, Langmuir probe data from the edge of W7-AS were analysed together with data from other devices by using advanced statistical analysis tools to detect correlations at long time delays and further indications of self-organised criticality (SOC) and of radial transport due to avalanches.

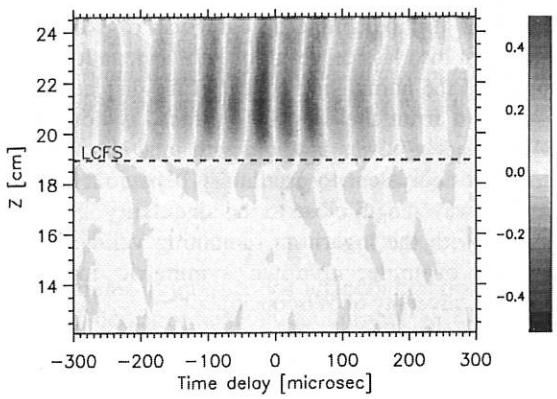

FIG. 15: Normalised correlation of Mirnov coil signal with all Li beam light signals. The horizontal axis gives the time lag, the vertical axis, the distance along the beam.

The statistical properties of the fluctuations in the edge of the magnetic confinement devices analysed were found to be very similar to each other and compatible with the predictions of SOC models.

2.5.3 *Equilibrium and stability with internal net toroidal current densities*

Usually, equilibrium and stability calculations for stellarators neglect internal toroidal net current densities. The main reasons are that ideal stellarator operation is without internal net current densities and that these have to be determined by analysis of the heating deposition profiles and neoclassical transport. Neglect is justified in the cases of low temperatures and high densities. However, there are numerous cases where this assumption is violated. We looked at two cases with respect to equilibrium and local stability to show the importance of the internal net toroidal current densities in certain discharge scenarios.

2.5.3.1 *Equilibrium study of electron root discharges*

Discharges displaying the electron root feature have very high electron temperatures with pronounced peaking at the axis and low densities. Neoclassical transport analysis yields a comparably large electron bootstrap current, which is compensated with the ohmic transformer to achieve a vanishing net toroidal plasma current. The forms of the resulting pressure and toroidal current profiles induce changes in the equilibrium which are usually not resolved in NEMEC equilibrium calculations. The central peaking of the pressure profile leads to a Shafranov shift significantly displacing the axis. However, to resolve this feature in the equilibrium calculation, about 200 radial grid points instead of 55 have to be used. The current density profile derived from the transport analysis shows that the bootstrap current is located at outer radii and the compensating ohmic current closer to the axis. This leads to a significant decrease of iota around the axis resulting in an enhancement of the Shafranov shift (proportional to iota^{-2}) due to the central pressure peaking. The magnetic axis is thus displaced up to 1 cm in the elliptical plane from the position expected by usual calculations or when using the TRANS database. This is of particular importance for interpretating ECE temperature and ECRH deposition profiles.

2.5.3.2 *Local stability analysis of HNBI discharges*

HNBI discharges are also characterised by a large bootstrap current in the gradient region of the profiles and a compensating ohmic current flowing closer to the axis. A local stability analysis of the currentless equilibria shows stability with respect to ideal and resistive interchange modes. Adding the appropriate current profiles to the equilbrium calculations leads to a decrease of the iota profile towards the axis. Scaling the toroidal current profile to higher current densities (but keeping the total plasma current zero) leads to formation of a resistive interchange unstable region where the pressure gradient is strongest. Investigations of the terms in the ideal and resistive interchange criteria reveal that the decrease of the iota values in the gradient region increase the Pfirsch-Schlüter currents, enhancing the destabilising parts of the interchange criterion. On the other hand, the increase in the magnetic well as a stabilising term is not sufficient to keep the resistive interchange stable. The additional effect of the increasing shear, however, keeps the ideal interchange stable.

2.6 Theory

2.6.1 *Fast equilibrium reconstruction*

The fast availability of geometric information on the flux surface structure is important to evaluate experimental data and transform them to a common flux surface label, i.e. the effective minor radius. This was implemented in the TRANS database using the KW code for the 3-D MHD equilibria. To overcome the restrictions in β imposed by the KW code and to utilize statistical methods for the database handling, a new approach was started. Based on calculations with the 3D MHD equilibrium code NEMEC is not restricted in its convergence by the β values, a database was created covering a wide range of parameters but restricted to $\iota < 0.5$. Function parameterization was then used to recover the flux surface geometry very fast. A fast equilibrium reconstruction scheme was possible on the basis of the equilibrium information contained in the asymmetry of the Thomson scattering profiles of electron temperature and density, i.e. the transformation from real space to the flux surface label.

This scheme is valid for discharges where internal net toroidal currents do not strongly alter the equilibrium since these were neglected in the current database (H. Callaghan, University College of Cork, Ireland, UCC, at EPS 1997). In a next step magnetic diagnostics are examined with the existing database to explore the possiblity of obtaining pressure profile information (H. Callaghan, UCC Ireland, at EPS 1998). Ultimately, the database has to include equilibria with toroidal net current densities for full application to magnetic diagnostics in stellarators.

2.6.2 *EMC3 code development*

The Braginski fluid equations for particle, momentum and energy can be written in a common Fokker-Planck form

$$\Delta_{\parallel} [\alpha_{\parallel} f - \Delta_{\parallel} (\beta_{\parallel} f)] + \Delta_{\perp} [\alpha_{\perp} f - \Delta_{\perp} (\beta_{\perp} f)] = S$$

which expresses the basic conservation properties of the fluid equations, with f representing density, parallel Mach number and temperature, and α, β being the transport coefficients for convection and diffusion of f. In the EMC3 code, both the diffusive and convective terms of these equations are solved with the same Monte Carlo algorithm. In order to speed up the computations, both the configuration and the plasma-facing components are represented in magnetic coordinates. Additionally, to avoid memory problems two different meshes are necessary, a fine geometric mesh for accurately tracing Monte Carlo particles in magnetic coordinates and a coarser physical mesh for storing the local plasma parameters. The physical mesh is independent of the particle tracing and can therefore be locally adjusted according to the required physical resolution, e. g. finer cells at the plates (Fig. 16). The temperature equations for ions and electrons are solved simultaneously, which allows the coupling term to be treated in a "natural" way as a simple exchange of T_i and T_e particles. This effectively avoids overshooting problems.

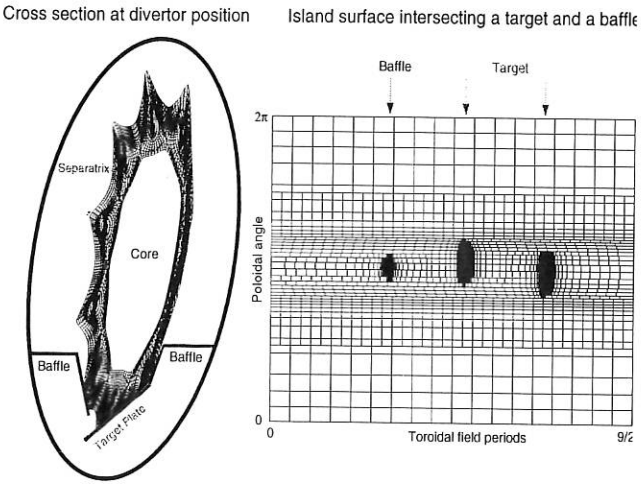

FIG. 16: 3-D grid for a 5/9 island divertor configuration in W7-AS. The grid is adjusted locally according to the required resolution.

2.6.3 *Effect of 3-D geometry on mode structure*

A characteristic feature of modes in the MHD continua ("Alfven" and "slow") is that they become singular at a resonant magnetic surface if the plasma configuration is axisymmetric. In 3-D configurations without this or helical symmetry not much is known about the nature of the singularity. In the course of investigations of asymmetric 3-D configurations the axisymmetric case was re-examined. It was found that the classical result of Pao[2], viz. a logarithmic dependence of the normal component of the displacement on the distance d from the singular surface, is not valid in general. Instead, a power law, d^{σ}, with imaginary value σ, holds. This is equivalent to oscillatory behaviour in d with even shorter wavelength close to the singularity. Exceptions to this law, with the logarithm remaining valid, exist and include, for example, up/down symmetric tori. (With J. Tataronis, University of Wisconsin).

2.6.4 *Plasma currents with momentum conservation*

For solving the kinetic equations, a strongly simplified collision operator is used in most cases. For example, the Lorentz form of the pitch angle collision term violates momentum conservation and leads to inaccurate estimation of parallel currents. The simplest "local" correction corresponds to the Spitzer problem where trapped-particle effects are ignored. On the contrary, trapped particles can be taken into account in the collisionless limit ("non-local" adjoint approach /245/); this approach is implemented in the ray-tracing code for calculating the ECCD for realistic magnetic topology of W7-AS and W7-X. An improved momentum-conserving collision operator[3] is used for the estimation of the bootstrap current as well as for the electron Ohkawa current. The results with this corrected collision operator are in between the two other approaches.

2.6.5 *Non linear ECRH absorption*

For ECRH in W7-AS, the micro wave beam is launched highly focused (width of about 5 cm), leading to a highly peaked power deposition profile (of about 2 cm in the effective radius due to the elongation), as is predicted by ray-tracing calculations with an absorption coefficient from quasi linear theory based on a Maxwellian distribution function. The nonlinear particle dynamics in the electromagnetic field of the 2nd harmonic ECRH (X-mode) in W7-AS is treated numerically. The nonlinearity parameter (i.e. the nonlinear shift of the wave-particle phase during the single pass through the micro wave beam) is not uniform in the whole phase space. Even if it is relatively small for passing particles, it is of order one or bigger for trapped particles, and the "traditional" analytical theory fails.

---

[2] Y. Pao, Nucl. fusion 15 (1975), 631
[3] M. Taguchi, Phys. Fluids B4 (1992) 3638

This nonlinear absorption mechanism has a strong impact on the formulation of the heating term in the Fokker-Planck modelling since the fraction of wave power absorbed by the trapped particles is significantly decreased in comparison with the linear approximation in the "standard" quasi linear diffusion term. (Collaboration with S.V. Kasilov, Kharkov, WTZ, and with TU-Graz, EURATOM).

2.6.6 *Bounce-averaged Fokker-Planck modelling of high power ECCD*

Electron cyclotron current drive (ECCD) experiments in W7-AS with an ECRH input power of up to 1.3 MW at 140 GHz (2^{nd} harmonic X-mode for B = 2.5 T) are analyzed; see 2.4.1.

Driven currents of up to 20 kA are obtained from the current balance of bootstrap and ohmic currents in the net-current free discharges. The linear ECCD prediction based on a Maxwellian distribution with trapped-particle effects included (see 2.6.5) overestimates the ECCD efficiency. This discrepancy is analysed by means of Fokker-Planck modelling.

At higher launching angles (at maximum ECCD efficiency), the non linear degradation of the power absorption is less important; see 2.6.6. In the bounce-averaged Fokker-Planck calculations the strong heating as formulated by the traditional quasi linear diffusion term (with the diffusion coefficient $Q_{\perp\perp}$ obtained from ray-tracing calculations) is balanced by the energy loss of mainly suprathermal ripple-trapped electrons. In this stellarator-specific approach, the radial ∇B-drift of the ripple-trapped electrons broadens the "effective" power deposition profile, but has no influence on the ECCD. The Fokker-Planck calculations show that supra thermal electrons generated by the ECRH have a negligible effect on the electrical conductivity. At high power levels, the formation of a quasi linear "plateau" in the electron distribution function slightly increases the ECCD efficiency. A modelling with an isotropic power sink (simulating "anomalous" transport), however, is related to a strong momentum sink and reduces the ECCD efficiency with increasing power (WTZ collaboration with N. Marushchenko, Kharkov).

2.6.7 *Stability analysis of electron distribution functions*

The bounce-averaged Fokker-Planck simulations (using the convective ∇B-drift loss model) of ECCD at high heating power show strongly positive gradients with respect to $v_{\parallel}$ close to the loss-cone boundary in the electron distribution function. These represent free energy and may drive the electron distribution function unstable. Due to their fast growth, such kinetic instabilities reduce the free energy and degrade the ECCD efficiency. A kinetic stability analysis by finding the roots of the full dispersion relation for these electron distributions was started (WTZ collaboration with S.V. Kasilov and N. Marushchenko, Kharkov).

2.6.8 *Orbit-averaged Monte Carlo code development*

Monte Carlo simulations of the electron distribution function in the 5-D phase space are extremely CPU consuming. "Traditional" bounce-averaging techniques cancel the fast parallel motion, but strong simplification of the magnetic field is necessary to separate the different classes of trapped particles.

In a new approach[4], the electron orbits are integrated numerically and the relevant quantities are stored in Poincaré cuts, allowing a fast "orbit-averaged" Monte Carlo technique. This approach will be tested for realistic configurations of W7-AS and W7-X. The interface to the database with the magnetic configurations (calculated by the NEMEC equilibrium code) is installed (EURATOM collaboration with TU-Graz).

3. DIAGNOSTIC DEVELOPMENT

3.1 Periodic Multichannel Thomson Scattering

In 1998 all calibration measurements necessary for determining electron temperature and density profiles were successfully performed. An automatic system was developed to calibrate and control the relative spectral sensitivities of each channel of the diagnostic. The spectral sensitivities measured with continuous light were found to be slightly different from those measured with 60 ns light pulses. This observation is important for correct determination of electron temperatures. The electron density was absolutely calibrated by Raman scattering using H_2 molecules. The periodic multichannel Thomson scattering diagnostic now allows electron temperature and density profiles to be measured along the entire plasma diameter every 50 ms. Even for most of the discharges of the last experimental campaigns, the T_e and n_e profiles can be subsequently determined (see, for example, Fig. 17).

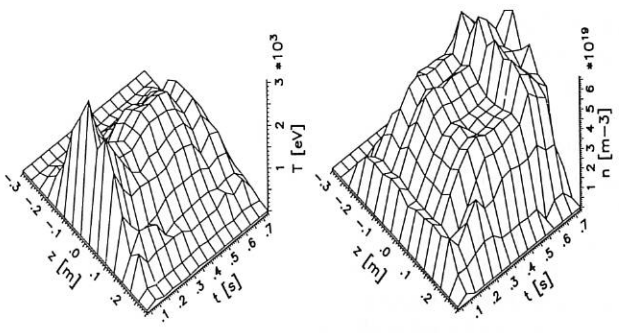

FIG. 17: Profiles of electron temperature and density for the purely ECRH-heated discharge #43856. A C pellet was injected at t = 0.53 s.

[4] S.V. Kasilov, Phys. Plasmas 4 (1997), 2422

3.2 Ruby Thomson Scattering System with High Spatial Resolution

The new Thomson scattering diagnostic with enhanced spatial resolution for plasma edge investigation on the high-field side in the triangular plane was installed. Five interference filter polychromators of the existing 20-channel diagnostic system were replaced by the new polychromator consisting of a Littrow-type spectrometer and an intensified CCD camera.

Five new optical fibre bundles, which transfer the scattered light to the new Littrow polychromator, were installed. The input of these fibre bundles determines the spatial resolution of the new system (4 mm), which is improved by a factor of 5 in relation to the existing polychromator system. At the output, these bundles are formed as the entrance slit of the spectrometer. The spectral resolution is up to 1.8 nm. A total wavelength range of 60 nm can be investigated. By means of a new four-pulse Pockels cell driver, the ruby laser pulse is divided into two single pulses with different energies. The less energetic pulse is suitable for operating of the existing polychromator system. The strong pulse (up to 13 J) is needed for the new system because the improved spatial and spectral resolution leads to a lower signal. The wavelength range of the Littrow system was calibrated by means of a neon spectral lamp. The spectral sensitivity of the detection system and the position of the spatial channels at the CCD chip were measured by means of a calibrated tungsten strip lamp. The absolute intensity calibration will be done at the beginning of 1999 by Raman scattering.

3.3 Collective Thomson Scattering with 140 GHz

See chapter Institut für Plasmaforschung (IPF), University of Stuttgart.

3.4 Turbulence Measurements with Two-Channel $C0_2$ Laser Scattering

A two-channel laser scattering electron density fluctuation diagnostic was installed by scientists of Risø National Laboratory, Roskilde, Denmark, on the W7-AS stellarator. The device uses a 20 W CO_2 CW laser and measures small-angle collective scattering on plasma density waves having a wave number in the 10 - 70 cm^{-1} range and frequencies of up to 10 MHz. In order to analyse the spatial correlation of density fluctuations, the scattering experiment utilises a beam splitter to double both the scattering and the local oscillator beams and detects scattered laser light in two detectors. Due to the small scattering angle, the diagnostic integrates density fluctuations along vertical chords. The two measurement volumes (chords) can be separated either poloidally or toroidally by up to a few cm.

Many plasma discharges were studied under various plasma conditions. Characteristics of the measured frequency spectra of electron density fluctuations were found to be similar to those seen in other plasma experiments. Qualitative changes, both in the shape and amplitude of the frequency spectra were analysed during different changes in plasma confinement. Together with a rich set of fluctuation diagnostics (reflectometry, ECE, microwave scattering, Li-beam BES, Mirnov coils and others) the CO_2 scattering device is expected to deliver valuable information on changes in fluctuations and turbulent transport in the core plasma of the W7-AS stellarator.

3.5 Electron Cyclotron Emission Imaging

A new diagnostic is being prepared which will enable 2-dimensional electron cyclotron emission (ECE) measurements. Applying a poloidal array of ECE detector elements makes it also possible to measure, in addition to the radial characteristics of ECE as in the standard diagnostic, the poloidal one. The miniaturised detector elements can be illuminated by a single set of optical elements for mapping different poloidal sightlines onto the single elements of the array.

A detector array on the basis of heterodyne mixers is under development in collaboration with TU Darmstadt. It consists of individual antennas, the mixer elements, the necessary sideband filters and all matching elements as well as the local oscillator distribution to the numerous mixers. While one mirror is installed inside the vacuum vessel, to ensure an observation sightline along a major radius, the Gaussian beam optics is maintained outside.

3.6 Determination of Z_{eff} from bremsstrahlung in the near IR

The spectral channels of the periodic multichannel Thomson diagnostic (see 3.1.) can also be used for measuring the intensity of bremsstrahlung in the near IR[5]. For the calculation of Z_{eff} -profiles the spectral channels have to be calibrated absolutely. This was performed with a lamp whose emissivity had to be determined using a calibrated Ulbricht sphere. Since the intensity of bremsstrahlung is integrated along the lines of sight, a reconstruction procedure has to be applied to derive a radiation profile. The method described by Zoletnik and Kalvin (Rev. Sci. Instrum. 64, 1208 [1993]) had to be extended to 3-D geometry due to the angle of 38° between the lines of sight and the radial direction of W7-AS. Reconstructed radiation profiles and Z_{eff} profiles could be determined for several discharges. For discharges with pellet injection Z_{eff} profiles can also be derived from bremsstrahlung by the method of Vasin[6]. The advantage of this method is that only the relative changes of T_e , n_e and of the radiation profile are necessary for determining Z_{eff}. A Z_{eff} profile calculated by the method of Vasin et al. is shown in Figure 18.

---

[5] IPP III/157

[6] Sov. J. Plasma Phys. 10 (1984) 650

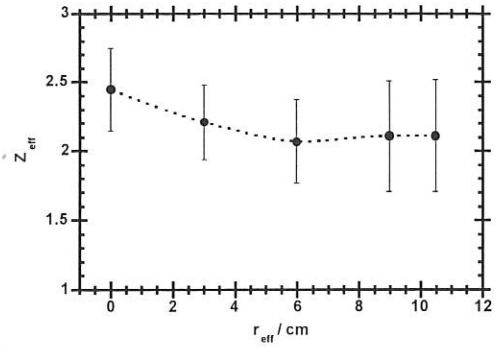

FIG. 18: Z_{eff} profile for #43856 (t = 0.479 s) calculated from bremsstrahlung in the NIR.

3.7 IR Thermography

An infrared camera with an InSb sensor array (120 x 160 pixel) is used for thermographic measurements on surfaces of wall components. The present arrangement with a ZnSe light transmission optics allows inspection of the whole surface of the upper inboard limiter in module 1. A three-dimensional numerical code was developed to evaluate the power flux from the temporal evolution of the measured surface temperature distribution.

3.8 Measurements and Simulations of Bolometer Foil Calibration

A systematic investigation of the calibration of 4 mm thin gold foils mounted on 7.5 mm kapton insulator used in the bolometer sensors was conducted. Tomographic inversion of line-integrated measurements greatly depends on the reliability with which the cooling time constant and heat capacity of the individual foils can be determined. Ohmic heating of the foils with magnitudes of up to 40 mW at various foil temperatures in the range from 20°C to 140°C was carried out.

The time evolution of the foil temperature after application of the heating pulse was measured. A systematic increase of the heat capacity with increasing foil temperature was found. The ANSYS package was used for three-dimensional finite-element simulations of the bolometer foil temperature rise. The tabulated values of the heat capacity and its temperature dependence for gold and the heat capacity for kapton together with a temperature dependence of the heat capacity of kapton chosen, close to that given for similar polymers were used. The measured temperature dependence of the bolometer foil heat capacity with a value of 0.2 mJ/K^2 and a value of the heat capacity at 20°C of 134 mJ/K could be reproduced. The consequences for bolometer measurements in steady-state discharges on W7-X are that the temperature of the bolometer body holding the foil must be actively regulated.

3.9 High Spatial Resolution 2D CCD H_α Imaging System

One of the five upper, inner limiters on W7-AS is imaged in its entirety onto a coherent optical fibre bundle placed deep within port 5' of module 5. The output of the bundle is coupled to a 2D 1/2" CCD camera (480 x 640 pixel, 12 bit) after passing through a 12Å H_a interference filter. The spatial resolution for full-frame 30 Hz operation is 0.5 mm. Up to 200 frames/sec can be achieved via binning. Typically, a time resolution of 17 ms is chosen, thereby generating 30 MB per pulse. The data are stored locally on a PC and transferred to the central database overnight.

The H_α imprint essentially yields a 2D hydrogen flux distribution. Figure 17 gives an example of a 400 kW NBI discharge with a density ramp that leads to an H-mode transition. A temporal comparison of the local H_a intensity with the ion current of a Langmuir probe at the indicated position in another limiter is given in Fig. 19. Corresponding poloidal (vertical) and toroidal H_a profiles are given for 0.542 s, just before the H-mode transition at ~ 0.55 s.

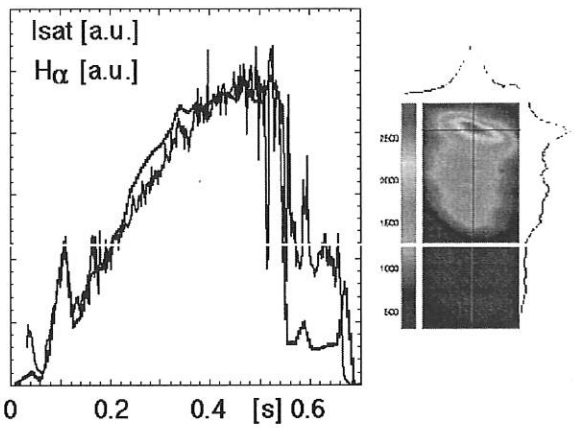

FIG. 19: Temporal traces of I_{sat} and H_a intensity at an equivalent Langmuir probe position - denoted by the cross-hairs - and the corresponding H_a profiles. iota ~ 0.561 "island configuration"), B_t = 2.5 T, 400 kW NBI, #44929.

3.10 Langmuir Probes

The increased configurational flexibility introduced by the additional control coils was adapted to be modifying the movable poloidal Langmuir probe array covering 120° at the high-field side of a triangular cross-section. The number of tips was increased from 16 to 24, each consisting of two half-cylinders, which also allow Mach probe operation. The radial distance between the tips and support structure was increased to avoid limiter-like perturbations of the plasma. In addition to the already fully instrumented top and bottom limiters, one of the five poloidal inboard limiters was equipped with 16 flush-mounted Langmuir probes (poloidal distance 2.8 cm, angles of field line incidence between five and ten degrees).

3.11 Mirnov Diagnostics

Three new Mirnov probes were installed at three different toroidal locations of W7-AS. They are placed between two poloidal arrays of the same type of probes (bandwidth of up to 3MHz) in order to obtain information on the toroidal variation of magnetic fluctuations. All 19 probes of the same kind were also equipped with wideband preamplifiers. The equipment is being tested.

4. MACHINE OPERATION AND TECHNICAL ACTIVITIES OF W7-AS

4.1 Main Activities of W7-AS

In 1998, the W7-AS experiment was operational for about 2,600 pulses in the range of 0.6 T – 2.5 T and at different rotational transforms. During the shut down period from April 1998 until October 1998, a set of ten control coils (two per field period) was installed inside the torus vessel. Each coil consists of 8 turns of a 10 mm x 10 mm copper conductor, with a central cooling duct 5 mm in diameter. The coils are racetrack-wound in two layers and embedded in vacuum-tight stainless-steel casings. After vacuum testing, the gaps inside the casings were filled with epoxy resin. All control coils are connected in series to a 500 V / 6 kA (pulse) regulated power supply. The maximum coil current is 3.4 kA (6 s pulse). The polarity of the series connection of the whole set of coils can be changed as well as the polarity of the upper coil group against the lower coil group.

Two control coils are located very closely to the diamagnetic loop. To reduce interferences, an additional 300 Hz filter unit was installed which reduces the voltage ripple on the control coils.

4.2 Control Systems

The control system of the flywheel generator used for the W7-AS main power supply of W7-AS was redesigned. A new feedback controller with very high resolution (> 16 bit) was installed and tested in combination with a SCADA (Supervision, Control and Data Acquisition) computer. All voltages and currents concerned can be observed and remotely adjusted (TCP/IP) from the W7-AS control room at Garching or via Internet from Greifswald.

4.3 Neutral Injection into W7-AS

4.3.1 Deposition profile

A few shots were devoted to measuring the power and particle deposition of the beams in the plasma. The beams were modulated causing a modulation of T_e (electron temperature) and n_e (electron density). The modulation amplitude of T_e was used to determine the local power density. The measured power deposition profile agreed reasonably well with the results of the FAFNER deposition code when the ion slowing-down time was $t_{sl} < 0.3\ t_{sl}$, t = modulation period. There were systematic deviations of theory and experiment when $t_{sl} > 0.5$ t. The deviations became even stronger when $t_{sl} >$ t. A preliminary conclusion is that the modulation of T_e is not determined by slowing-down beam ions with classical behaviour if the modulation is too fast. Further experiments will have to be done.

4.3.2 Radial injector

The preparation for installing an additional radial injector have been continued. It will direct the ions mainly into lost orbits and should create a radial electric field which should have an impact on confinement. The high-voltage area with an additional modulator is ready for commissioning. The injector box was pre-assembled. At present, the ion sources are being assembled and conditioned. Installation of an additional control area has started. The design for the changes in the torus port is finished.

4.3.3 Additional co-injector

Counter-injection delivers smaller heating efficiencies than co-injection, especially at low magnetic field strengths and higher density. It was therefore decided to reverse the direction of one of the two tangential injectors to allow high-beta investigations with two co-injectors. These changes are being prepared for the next shut-down.

4.5 Installation of New ICRH Antenna

During the 1998 torus opening the "broad" ICRH antenna was replaced by a conventional double-strap antenna. This new antenna is placed closer to the plasma to increase the antenna coupling to the plasma. The new antenna also excites a different spectrum of fast waves in the plasma, in particular, the fraction with high values of k_J is enhanced. The stainless-steel current straps closely match the three-dimensional shape of the plasma. They are shortened outside the vessel so that the current maximum is in the horizontal midplane of the antenna. The antenna is fitted with a Faraday screen that consists of stainless steel rods. The distance between the current straps and the LCFS is reduced by about 2 cm in relation to the previous antenna. Initial results in the beginning of 1999 have shown that this reduced distance increases the coupling of the antenna to the plasma and thus the amount of generator power is radiated into the plasma.

STELLARATOR THEORY

(Prof. Dr. Jürgen Nührenberg)

S. Arndt, M. Borchardt, M. Drevlak, S. Gori, R. Hatzky, Ch. Hennig, R. Kleiber, A. Könies, C. Nührenberg, J. Nührenberg, P. Merkel, J. Riemann, S. Weber, R. Zille.
Guests: K. Appert,[1] G. Jost,[1] R. Dewar,[2] W. Dorland,[3] D. Monticello,[4] N. Nakajima.[5]

1. Introduction

In 1998, the work of the Stellarator Physics Group was concentrated on widening the scope of the theoretical work at the Greifswald Branch Institute and on further development of the stellarator concept[6], notably for quasi-axisymmetric /58,60,85,202,211,314,661/ and quasi-isodynamic configurations.

2. Configuration Studies

2.1. Quasi-Axially Symmetric Stellarators

In collaboration with the NCSX design effort for a quasi-axially symmetric (QA) stellarator in the U.S., coil designs were performed for several configurations of this type.

QA configurations are, in magnetic coordinates, similar to tokamaks and feature considerable toroidal currents, part of which may be supported by bootstrap currents. Therefore, the existing codes used for designing coil systems (NESCOIL, extended NESCOIL, ONSET) had to be upgraded to account for the field from finite-β currents to the total magnetic field of the configuration at the plasma boundary.

Using the upgraded optimization codes, designs for different types of coil systems were pursued.

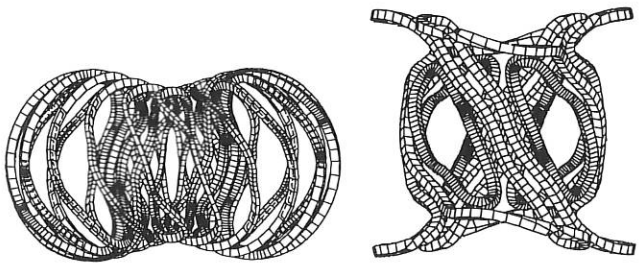

FIG. 1: Left: Side view of modular coils. Right: Side view of saddle coils.

First, a set of modular coils was considered (Fig. 1). These coils are of the same general type as those envisioned for the W7-X experiment. It was shown in free boundary VMEC calculations that these coils reproduce the prescribed plasma configuration with good accuracy. In addition to the primary modular coils, a set of PF coils was designed to produce closed flux surfaces at $\beta = 0$.

As an alternative, the possibility of reusing the existing TF coils of the PBX device and producing only the rotational transform by a set of additional saddle coils was investigated (Fig. 1). Results up to now indicate that, although achieving good values of the field error, saddle coils are less efficient at reproducing the plasma configuration than modular coils /57,59/.

The finite-β NESCOIL /617,194/ code has also been applied to quasi-axisymmetric tokamaks.

Flux surfaces of a free-boundary quasi-axisymmetric equilibrium computed with the NEMEC code is shown in Fig. 2. The case presented here is determined by the shape of the boundary, two field periods, a value of $\langle\beta\rangle \approx .03$ and a toroidal current $I_{\mathrm{tor}} = -.015 I_{\mathrm{pol}}$ (coil current), which results by fixing the ι profile to be $.51(\mathrm{axis}) < \iota < .56(\mathrm{edge})$. The external field is generated by a modular coil set with $N_{\mathrm{c}} = 12$ coils per period.

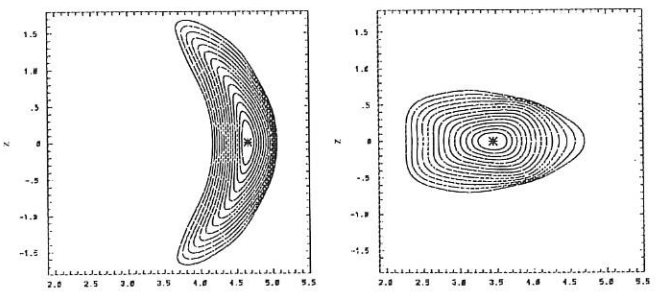

FIG. 2: Free-boundary equilibrium of a quasi-axisymetric tokamak configuration: Aspect ratio $A \approx 4$, $\langle\beta\rangle \approx .03$, external field produced by $N_{\mathrm{c}} = 12$ modular coils per period

2.2. Quasi-isodynamic Stellarators

It was shown that there are qi stellarators (i.e. toroidal stellarator vacuum field configurations with genuinely three-dimensional magnetic field strength and with very good collisionless confinement of the guiding centre orbits of

---

[1] EPFL,CRPP, [2] ANU, [3] U. o. Maryland, [4] PPPL
[5] NIFS, [6] J. Nührenberg, europhysics news **29** (1998) 276

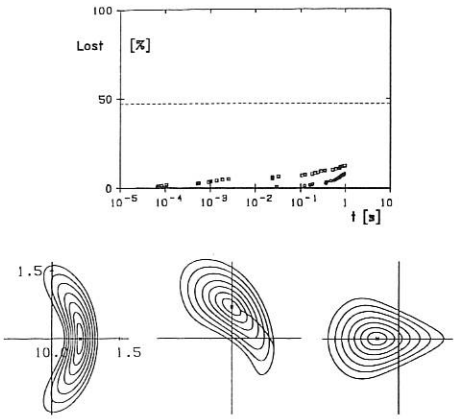

FIG. 3: Top part: Collisionless α-particle losses in the configuration shown in the bottom part at β=0 as a function of the time of flight. Particles are started at $s_{\mathrm{start}} = 0.08$ (○) and $s_{\mathrm{start}} = 0.24$ (□) ($\approx$ 1/4 and 1/2 of the plasma radius); the dashed line shows the fraction of reflected particles. The number of reflected particles followed is 100; each symbol indicates the loss of one particle. Normalizations: $B_0 = 5$ T, average plasma radius $a = 1.6$ m, kinetic energy of α-particles 3.5 MeV. Bottom part: Flux surface cross-sections of this quasi-isodynamic stellarator. Shown are sections at the beginning, quarter of and half a period. The number of periods is five.

high-energy core particles) with a magnetic well and a rotational transform monotonically increasing towards the confinement boundary[1] (compare Fig. 3).

3. Ideal MHD Stability

Owing to the strong interest in Alfvén eigenmodes in experimental work, in the field of ideal MHD stability /440,660,661/, the main focus has been the investigation of stable spectra /302,735,739/. A new version of the CAS3D stability code has been developed.[2] It provides for a physical normalization and the use of a finite adiabatic index γ. With this code the formation of spectral gaps and the existence of gap modes in tokamaks could be recovered; studying W7-X type cases, the computational evidence of gap formation and the existence of global, stable perturbations in truly 3-d configurations could be established. Further, good agreement of measured frequencies and spatial structures of MHD activities in W7-AS and CAS3D3 calculations has been shown /641/.

Figure 4 shows the lower part of the stable spectrum for an ideal MHD stable W7–X-type equilibrium. At the marked crossing points of the cylindrical Alfvén spectra (frame c) spectral gaps form, since in 3-d cases the cylinder symmetry is broken and a degeneracy (crossing) of continuum branches does not occur (e.g. the $n = -6$, $m = 6, 7$ crossing in frame c). The upper part of the figure shows the resulting Alfvén spectrum: frame (a) for $\gamma \approx 0$ and frame

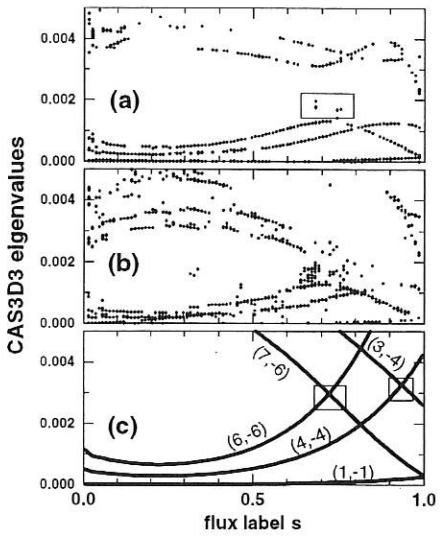

FIG. 4: Ideal MHD spectrum as computed by the CAS3D3 code for a 3-d ideal MHD stable case in the configurational neighbourhood of W7-X (five field periods, $\langle\beta\rangle \approx 0.05$, $\iota \gtrsim 1$): (a) for $\gamma \approx 0$, (b) for $\gamma = 2$, and (c) for the Alfvén continua as obtained from cylinder theory.

(b) for $\gamma = 2$ (the sound branches have been omitted from the plot for more transparency).

In the gap global, smooth perturbations exist (marked in frame a). In this low-shear case ($\iota \gtrsim 1$), global modes exist also below the minima of the Alfvén continuum branches (not visible on the scale chosen here).

4. MHD-Stability with Kinetic Effects

In the last years the generalization of the three dimensional MHD stability code CAS3D towards the inclusion of fast particle effects has been undertaken.

So far an energy principle for zero frequency by Van Dam et al. had been employed and had been implemented in the CAS3D-K code /551/. The influence on the marginal stability limit of a sequence of W7-X like equilibria has been investigated and turned out to be negligible /149/. A zero-frequency theory, however, leads to formal difficulties if the bounce-averaged drift frequencies are close to zero and is not suited to treat a possible destabilization of TAE modes which have successfully been described with CAS3D3.

Therefore a refined theory has been developed. A linearized drift-kinetic equation has been solved in three dimensions for electromagnetic perturbations using a propagator technique developed by Brunner and Vaclavik. Radial drifts are neglected; the integration along the particle trajectory is replaced by an integration along a field line. From the resulting perturbed distribution function an expression for the perturbed pressure has been obtained and finally, when restricting to MHD like (i.e. flux conserving) perturbations a generalized energy principle has been obtained from the force balance equation. The perturbed pressure depends on the mode frequency ω itself and turns

[1] S. Gori, J. Nührenberg, Theory of Fusion Plasmas, Varenna 1998.

[2] C. Nührenberg, Phys. Plasmas **6** (1), 137 (1999)

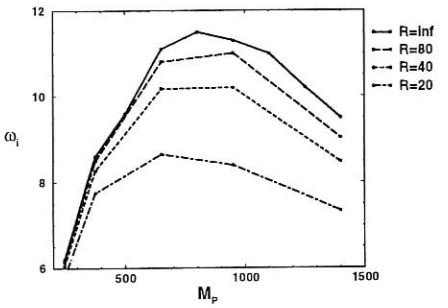

FIG. 5: Normalized growthrate of the resistive drift instability for increasing toroidal curvature R^{-1} in an ℓ=2 stellarator as a function of the poloidal wave number.

the problem to be solved from a real linear eigenvalue problem in ω^2 for the MHD case into a complex nonlinear eigenvalue problem. The relevant matrix elements have to be calculated performing a fivefold integration.

The kinetic energy principle describes both, the hot-particle (fusion α-particles, NBI) component and the thermal component of the plasma.

In the high-frequency limit which is appropriate for thermal plasma particles the well-known Kruskal-Oberman energy principle is obtained.

The zero-frequency case considered by van Dam et al. uses the drift surfaces of the fast particles which rely on the existence of the second adiabatic invariant. Since in the theory developed now drift surfaces do not appear, the zero-frequency principle is not directly a limiting case.

In the two-dimensional and zero-orbit-width limit the results of Porcelli et al. and C.Z. Cheng can be recovered.

The numerical implementation of this theory into the CAS3D-K code is in progress.

5. Drift waves

In order to gain insight into the anomalous transport in stellarators a code allowing the calculation of global linear resistive drift waves in general geometry has been developed /146/. It is based on a two-fluid-description of the plasma and the assumptions of electrostatic perturbations and cold ions. Employing a Fourier decomposition with phase factor transformation (in order to enable the calculation of high wavenumber modes) in the angle-like variables and a finite-difference-discretization in the flux label the resulting generalized complex eigenvalue problem is solved by an implicitly restarted Arnoldi Method.

To investigate the influence of the toroidal curvature on the growth rate a sequence of $\ell = 2$-stellarator equilibria with $P = 5$ field periods, $A/P = 2$ and fixed ι-profile was calculated with VMEC. Starting with a straight stellarator the toroidal curvature increases along this sequence. Using parameters characteristic for the boundary region and a small density scale length unstable eigenmodes with poloidal wave numbers M_P between 20 and 2200 were found in the straigth stellarator. Radially the modes are located near the outer boundary in a region of width approximately the ion inertia length.

In the straigth stellarator relatively few Fourier coefficients for the perturbation have to be taken into account while even a small additional toroidal coupling increases this number considerably. The highest growth rate is attained for $M_P \approx 800$ and is diminished by increasing the toroidal curvature (Fig. 5).

6. Ion-Temperature-Gradient-Driven (ITG) Instabilities

ITG-instabilities are now commonly held responsible for turbulence giving rise to anomalous ion heat transport in the core of tokamaks. It is very likely that ITG-turbulence could become the dominant transport mechanism as collisional transport has been optimized in modern stellarators such as W7-X. Therefore, in a first step, a linear gyrokinetic simulation code for W7-X is being developed.

An intermediate step is to approximate the W7-X equilibrium by a straight so-called bumpy pinch configuration with five periods /107/. This two-dimensional model includes the effects of trapped particles in a field period due to the field mirror, a magnetic well and a rotational transform. Calculations have shown that a variation of the magnetic field along the magnetic axis of 10 % per field period (bumpiness) has only a minor influence on the growth rates. The magnetic well of 10 % has a stabilizing effect and reduces the growth rates for $\eta_i = L_n/L_{T_i} \approx 2.5$ by a factor of $\approx$2. This is expected as the induced ∇B drift is in opposite direction to the diamagnetic drift and has a stabilizing effect on the slab ITG modes. The effect of the rotational transform on the growth rates depends on the relative position of the mode ($\iota = n/m$ value) to the resonant surface. Since slab ITG's are stable at the resonant surface the mode tries to avoid radially the position of the resonant surface. Hence it is radially pushed inside respectively outside and the growth rates can be damped respectively amplified by $\approx$10 %. A marginal point study for the most unstable mode gives a value of $\eta_i \approx 1.6$ and is influenced only little by the effects of bumpiness and magnetic well (Fig. 6). So, with the bumpy pinch model used here, ITG instabilities remain a candidate for the ion heat transport for stellarators like W7-X. Further studies will include the effects of helical and toroidal curvature in a three-dimensional model.

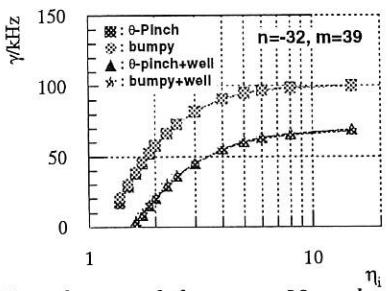

FIG. 6: Growth rate of the $n = -32$ and $m = 39$ mode for different configurations as a function of η_i.

IEA IMPLEMENTING AGREEMENT
for Cooperation in Development of the Stellarator Concept

1. OBJECTIVES OF THE AGREEMENT

The objective of the Implementing Agreement, first concluded in 1985, is to "improve the physics base of the Stellarator concept and to enhance the effectiveness and productivity of research and development efforts related to the Stellarator concept by strengthening co-operation among Agency member countries". To achieve this, it was agreed to exchange information, conduct workshops, exchange scientists, do joint theoretical, design and system studies, coordinate experimental programmes in selected areas, exchange computer codes, and perform joint experiments. In 1995 the Agreement was extended until June 2000. The contracting parties are EURATOM, the U.S. DoE, Japan, and Australia. In September 1994, Russia became an Associate Contracting Party.

2. STATUS OF THE AGREEMENT

In 1997, there were two meetings of the Executive Committee. The 25th meeting was held at Prague, Czech Republic, on June 30, in conjunction with the EPS Conference on Controlled Fusion and Plasma Physics, which took place from June 29 to July 3. The main points were remote participation in experiments, possible association of the Ukraine to the IEA Implementing Agreement, increased collaboration on new devices, the status of the experiments, and meetings and personnel exchanges. The initiative taken by the FPCC to work out and propose ways and means, technologies and standards for remote participation led to the formation of a group of experts.

The 26th meeting was held at Yokohama, Japan, during the IAEA Conference on Fusion Research on October 22. Because of the retirement of G. Grieger in February 1999, A. Iiyoshi, Japan, was elected as the new Chairman of the Executive Committee.

3. REPORT ON 1998 ACTIVITIES

In 1998, nine physicists participated in the exchange of scientists.

M. Yokoyama from Toki visited IPP Greifswald from February 17 to 19, to discuss the stellarator optimization with the theory group. Mr. Yamasaki from Japan used his short stay in February 1998 to exchange information concerning stellarator reactor studies. The short visit of N. Nakajima, National Institute for Fusion Science (NIFS), from June 26 to 28 to Greifswald was devoted to discussions about the continuation of collaboration in the field of MHD stability, in particular ballooning instabilities in LHD-type configurations and Alfvén modes. Staying for four days in Greifswald from July 5 to 9, D. Monticello from PPPL continued the PPPL-IPP collaboration on the PIES 3d-equilibrium code. R. Dewar, also from PPPL, discussed drift waves in stellarators during his visit to Greifswald from July 5 to 7.

P. Merkel from IPP stayed one week at Princeton in spring to continue the cooperation with PPPL on development of the PIES code. From July 4 to October 5, P. Merkel worked at NIFS on quasi-axisymetric devices, in particular realisation with coils of prescribed 3d finite-beta, finite-toroidal-current equilibria. H. Wobig and J. Kisslinger from IPP visited NIFS for 2 weeks in October to prepare collaborative work on stellarator power station studies. G. Cattanei from IPP visited NIFS, Toki, from November 1 to December 15, to participate in the first ICRF experiments on LHD.

Divisions and Groups

THE SCIENTIFIC DIVISIONS OF IPP

Experimental Plasma Physics Division 1
Director: Prof. M. Kaufmann

ASDEX Upgrade (Divertor Tokamak)
- operation of ASDEX Upgrade
- investigation of ITER plasma boundary in a reactor-relevant divertor, especially under high-confinement conditions
- advanced tokamak studies
- investigation of energy transport, MHD stability, beta limit, density limit and disruptions in an ITER-type plasma

JET collaboration
- operation of special discharge scenarios at JET and general collaboration

Experimental Plasma Physics Division 2
Director: Prof. G. Grieger

WENDELSTEIN 7-X
- divertor development
- contributions to stellarator power plant systems studies

Experimental Plasma Physics Division 3
Director: Prof. F. Wagner

WENDELSTEIN 7-AS (Advanced Stellarator)
- stellarator with improved confinement conditions
- toroidal plasma confinement in the stellarator
- net-current-free plasmas, plasma production and heating by neutral injection, and high-frequency waves
- plasma stability and impurity effects
- development of an island divertor

Preparation of the WENDELSTEIN 7-X diagnostics

Experimental Plasma Physics Division 4
Director: Prof. K. Behringer

Experimental and theoretical investigations of plasma boundary and divertor physics, impurity transport, chemical impurity production and plasma radiation in ASDEX Upgrade and WENDELSTEIN 7-AS
- spectroscopic diagnostics on ASDEX Upgrade
- spectroscopic diagnostics on WENDELSTEIN 7-AS
- laboratory experiments at the University of Augsburg, Department of Experimental Plasma Physics

Surface Physics Division
Directors: Prof. V. Dose, Prof. J. Küppers

Surface physics
- atomistic characterization of surfaces

Plasma-wall interactions (analytical)
- interactions of atoms, ions and electrons with solid surfaces
- wall fluxes in the boundary layer of plasma devices
- limiter and wall analyses

Plasma-wall interaction (preparative) (see also Technology Division)
- preparation and characterization of thin-film coatings for plasma devices

Data analysis
- application of Bayesian techniques to experimental data

Stellarator Theory Division
Director: Prof. J. Nührenberg

Further development of the stellarator concept and numerical and analytical methods to investigate equilibrium, stability and transport problems in three-dimensional toroidal configurations.

Technology Division
Director: Prof. R. Wilhelm

Neutral injection
- development and construction of the injection systems for WENDELSTEIN 7-AS, ASDEX Upgrade and WENDELSTEIN 7-X
- implementation of injection experiments

Electron cyclotron resonance heating
- construction and operation of an ECRH system for ASDEX Upgrade

Ion cyclotron resonance heating
- preparation and implementation of ICRH experiments for WENDELSTEIN 7-AS, ASDEX Upgrade and WENDELSTEIN 7-X

Plasma technology (see also Surface Physics Division)
- development, characterization and modelling of low-pressure plasma processes for thin-film formation

Tokamak Physics
Director: Prof. K. Lackner

General tokamak physics
- experiment-oriented theoretical work for the design and interpretation of tokamak experiments

Plasma edge physics
- experimental and theoretical work on plasma edge physics

Nonlinear plasma dynamics
- numerical simulation of turbulent transport and MHD reconnection phenomena

ITER collaboration
Applied mathematics in plasma physics

Computer Science Division
Director: Prof. F. Hertweck

Development of data acquisition systems for experiments at IPP
Studies in parallel computer architectures
Studies in neural networks
Parallelization of programs

Plasma Diagnostics Division
Director: Prof. G. Fussmann

Edge plasma physics
- experimental and theoretical work relating to fusion devices

Plasma generator PSI-1
- basic plasma physics
- plasma interaction with solid surfaces
- development and testing of plasma diagnostics

Electron Beam Ion Trap (EBIT)
- production of highly charged ions
- X-ray spectroscopy and atomic physics measurements

UHV laboratory, arc physics, ITER collaboration

Greifswald Branch of IPP
Director: Prof. G. Grieger

Construction of institute and infrastructure

WENDELSTEIN 7-X Construction
Director: Dr. M. Wanner

WENDELSTEIN 7-X R&D programme
WENDELSTEIN 7-X Construction
- engineering, construction and installation of the WENDELSTEIN 7-X device incl. plasma heating and in-vessel components
- project control and quality management

EXPERIMENTAL PLASMA PHYSICS DIVISION 1

(Prof. Dr. Michael Kaufmann)

The division E1 comprises

1. Four diagnostic groups
   a. pellet injection, electromagnetic measurements, DCN interferometer, plasma control, MSE, halo current measurements, calorimetry
   b. Thomson scattering, bremsstrahlung, bolometer, SXR
   c. He measurements, neutral gas, neutron measurements, HXR, mass spectrometer
   d. ECE, microwave reflectometry, SABA, charge exchange, LENA

   which are responsible for the development of plasma diagnostics as well as for plasma physics exploitation.

2. Three machine groups
   a. operation
   b. mechanical design
   c. assembly,

   which are concerned with the operation and engineering developments of the tokamak experiment ASDEX Upgrade and its peripheral installation.

3. Two computer groups
   a. real-time control of the ASDEX Upgrade plasma,
   b. data acquisition and data evaluation.

These groups are supported by 3 workshops: mechanical, electrical, and electronical.

Divison E1 is also devoted to collaboratin on JET and to continue studies for ITER.

EXPERIMENTAL PLASMA PHYSICS DIVISION 2

(Prof. Dr. Günter Grieger)

The activity of the Experimental Plasma Physics Division 2 is concentrated on the WENDELSTEIN 7-X related work of divertor development and stellarator power plant studies.

The relevant team is:

W 7-X-Team

C.D. Beidler, S. Gori, H. Greuner, G. Grieger, E. Harmeyer, O. Heinrich, F. Herrnegger, F.-W. Hoffmann, J. Junker, A. Kendl, J. Kißlinger, H. Münch, I. Ott, H. Renner, U. Schwenn, I. Sidorenko, E. Strumberger, H. Wobig, A.V. Zolotukhin.

Supporting activities by Plasma Diagnostics Division, Berlin (Prof. Dr. Gerd Fußmann)
D. Hildebrandt, P. Bachmann, W. Bohmeyer, B. Jüttner*, M. Laux, D. Naujoks, R. Radtke, J. Sachtleben, D. Sünder, U. Wenzel.
(* Humboldt University, Berlin)

The W7-X team is supported by contributions from Forschungszentrum Karlsruhe (FZK - Institut für Technische Physik), Forschungszentrum Jülich, by the Tore Supra team of CEA, Cadarache, and by the Central Technical Services of IPP.

EXPERIMENTAL PLASMA PHYSICS DIVISION 3 (W7-AS)

(Prof. Dr. Friedrich Wagner)

The W7-AS group comprises Experimental Plasma Physics Division 3. The work is fully reported in the section "STELLARATOR Project", of which the members are as follows:

Experimental Plasma Physics Division 3

M. Anton, S. Bäumel[21)], T. Baloui[6/21)], J. Bleuel[20)], R. Brakel, H. Callaghan[3/21)], G. Cattanei, J.-H. Chatenet[4)], Ch. Christou[20)], D. Darrow[19)], D. Dorst, O. Dumbrajs[9)], A. Elsner, M. Endler, K. Engelhardt, V. Erckmann, Y. Feng, S. Fiedler, C. Fuchs[20)], U. Gasparino, J. Geiger, T. Geist, L. Giannone, C. Görner[20)], P. Grigull, O. Grulke[7/21)], H. Hacker, H.J. Hartfuß, G. Herre[21)], M. Heyn[1)], M. Hirsch, E. Holzhauer[8)], J.K. Hübner[6)], K. Itoh[11)], S.-I. Itoh[12)], R. Jaenicke, F. Karger, S. Kasilov[16)], M. Keller[22)], M. Kick, A. Kislyakov[13)], T. Klinger[7)], J. Knauer[20)], G. Kocsis[10)], C. Konrad[21)], J.P. Koponen[9/21)], H. Kroiss, G. Kühner, A. Kus, H. Laqua, L. Ledl[21)], H. Maaßberg, N. Marushchenko[16)], K. McCormick, V. Moiseyenko[16)], S. Murakami[11)], I. Nomura[11)], W. Pernreiter[21)], S. Reimbold[6/21)], M. Rodriguez[5/21)], N. Ruhs, J. Saffert, M. Saffman[2)], A. Salat, F. Sardei, S. Schill[6/22)], M. Schubert[22)], V. Sergeev[14)], E. Solano[18)], U. Stroth, W. Svendsen[2)], J. A. Tataronis[18)], G. Theimer, V. Tribaldos[15)], F. Volpe[21)], F. Wagner, H. Walter[20)], A. Weller, Chr. Wendland[20)], A. Werner[20)], E. Würsching, D. Zimmermann, M. Zippe, S. Zoletnik[10)]

1) Guest from Technical University Graz (Austria)
2) Guest from RISø, Roskilde (Denmark)
3) Guest from University of Cork (Eire)
4) Guest from University of Paris-Sud (France)
5) Guest from University Darmstadt (Germany)
6) Guest from IAP/University Heidelberg (Germany)
7) Guest from University of Kiel (Germany)
8) Guest from IPF Stuttgart (Germany)
9) Guest from University of Helsinki, Espoo (Helsinki)
10) Guest from KFKI Research Inst., Budapest (Hungary)
11) Guest from NIFS, Nagoya (Japan)
12) Guest from RIAM, Kyushu (Japan)
13) Guest from IOFFE Institute, St. Petersburg (Rus.)
14) Guest from TUAP, St. Petersburg (Russia)
15) Guest from CIEMAT, Madrid (Spain)
16) Guest from IPT-NSC Kharkov (Ukraine)
17) Guest from Univ. of Wisconsin (USA)
18) Guest from Univ. of Texas (USA)
19) Guest from PPPL (USA)
20) Postdocs
21) Doctoral fellow
22) Undergraduate

Technical Team W7-AS:

G. Abele, S. Bartsch, W. Bendak, M. Bergbauer, P. Böhm, J. Bömerl, K.H. Brumm, H. Czich, S. Eder, A. Eschlwech, M. Fusseder, D. Gonda, H. Greve, G. Grünwald, M. Heckmeier, T. Henningsen, J. Hofner, F.W. Hoffmann, H. Holitzner, F. Hollmann, G. Hussong, H. Ibbach, K. Iraschko, E. Katzmarek, K.H. Knauer, F. Kunkel, D. Lingen, J. Littwin, U. Neumann, R. Neuner, F. Noke, F. Offenbächer, J. Prechtl, F. Purps, S. Ravichandran, T. Richert, M. Richter-Gloetzl, H. Rixner, H. Schmid, L. Schmid, H. Scholz, S. Schraub, R. Semler, H. Speer, J. Stadlbauer, B. Stajminger, M. Steffen, H. Volkenandt, K.H. Wagner, U. Weber, H. Wolf, Chr. Wöstmann, G. Zangl, W.v. Zeppelin, Do. Zimmermann

Experimental Plasma Physics Division 2

K. Kisslinger, J. Sapper, H. Wobig and the workshop of Experimental Division 2.

Experimental Plasma Physics Division 4

J. Baldzuhn, K. Behringer, R. Burhenn, R. König A. Weghorn

ECRH (Electr. Cycl. Resonance Heating):

W. Kasparek, L. Empacher, W. Förster, G. Gantenbein, P.G. Schüller, K. Schwörer (IPF Stuttgart)

S. Filchen'kov, L. Lubyako, E. Suvorov (IAP Nizhny Novgorod)

ICRH (Ion Cycl. Resonance Heating):

W. Becker, F. Braun, H. Faugel, D.A. Hartmann, F. Hofmeister, J.M. Noterdaeme, F. Wesner (Technology Division)

NBI (Neutral Beam Injection):

W. Ott, F.-P. Penningsfeld, F. Probst, E. Speth, R. Süß, (Technology Division),

Plasma Surface Interaction Group:

R. Behrisch, V. Dose, J. Roth, E. Taglauer

Plasmadiagnostics (Berlin)

D. Hildebrandt, D. Naujoks

Computer Centre:

S. Heinzel, H. Lederer, A. Schott

Central Technical Services:

D. Arz, B. Brucker, H. Eixenberger, Th. Franke, E. Grois, F. Gresser, R. Kutzner, W. Melchior, J. Perchermeier, K. Voigt, G. Wenzel

EXPERIMENTAL PLASMA PHYSICS DIVISION 4

(Head of Division: Prof. Dr. Kurt Behringer)

Experimental Plasma Physics Division 4 (E4) consists of the ASDEX Upgrade, W 7-AS and ITER Diagnostics groups. Their work is described in the ASDEX Upgrade and W 7-AS project reports as well as in the ITER Diagnostics contribution. Experimental Plasma Physics at the University of Augsburg is closely linked to E4, allowing physics students to participate in IPP's scientific programme or do basic research at Augsburg. Recent results are given under University Contributions to IPP Programme.

ASDEX Upgrade: I. Altmann, A. Bard, D. Bolshukhin, S. De Peña Hempel, R. Dux, W. Engelhardt, J. Gafert, A. Geier, A. Kallenbach, B. Plaum, R. Neu, H. Meister, D. Schlögl, K. Schmidtmann. W 7-AS: J. Baldzuhn, R. Burhenn, R. König. Augsburg: U. Fantz, B. Heger, A. Kottmair, H. Paulin, B. Schalk. ITER Diagnostics: H. Salzmann.
Technical Staff: G. Daube, M. Hien, J. Fink, G. Schmitt, A. Weghorn. Diplomanden: H. Bucher, T. Madeira, C. Wachter, B. Waldmann.
Co-operation: IPP Berlin, JET, KFA Jülich, TU München, University of Strathclyde (Scotland), Stuttgart University.

The E4 scientific programme deals with plasma boundary and divertor physics, impurity transport and plasma radiation, and low- and high-Z wall materials. Mainly spectroscopic diagnostics and analysis methods are being used in E4. Recent topics in ASDEX Upgrade were divertor plasma parameters, flow reversal, radiative cooling and power deposition in Divertor II, chemical erosion of carbon and neoclassical impurity transport. The interest in W 7-AS is focused on measurements of electric fields, neoclassical impurity transport, impurity pellet injection and magnetic field structures. Spectroscopic diagnostics for W7-X are also being developed.

Spectroscopic measurements of line or continuum intensities as well as molecular band radiation (see Augsburg University contribution) require interpretation on the basis of atomic physics and radiative transfer. To have access to the most up-to-date results, E4 is part of the ADAS international co-operation. Recently, reprocessed ionisation, recombination and radiation data were made available for the elements, hydrogen, helium and carbon ("96" data). Since atomic hydrogen lines become optically thick in high-density divertor plasmas, the existing "Adas Escape" escape factor program was upgraded to include the consequence of opacity on measured line intensities and allow for various spectral line profiles and plasma geometries [1]. It is now available as ADAS214.

Figure 1 shows contributions to the spectral line profile of the hydrogen line L_β, as calculated for ASDEX Upgrade divertor conditions. They consist of Zeeman splitting and Doppler and Stark broadening [1]. Their convolution was used to obtain the n=3 population escape factors. Figure 2 represents the L_β line escape factors for the same conditions. On the basis of these results and measurement of the L_β self-absorption, a typical neutral density of $3 \cdot 10^{19}$ m^{-3} was derived for Divertor I detached conditions in agreement with B2-Eirene code calculations.

[1] K. Behringer, Report IPP 10/11, April 1998

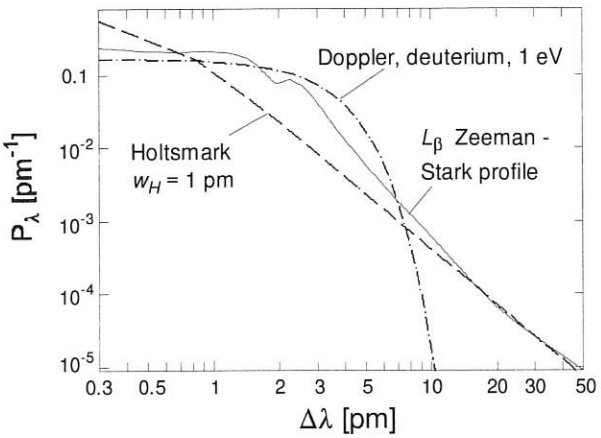

FIG. 1: Calculated L_β line profile for ASDEX Upgrade divertor conditions consisting of Doppler broadening, Stark profile and Zeeman splitting.

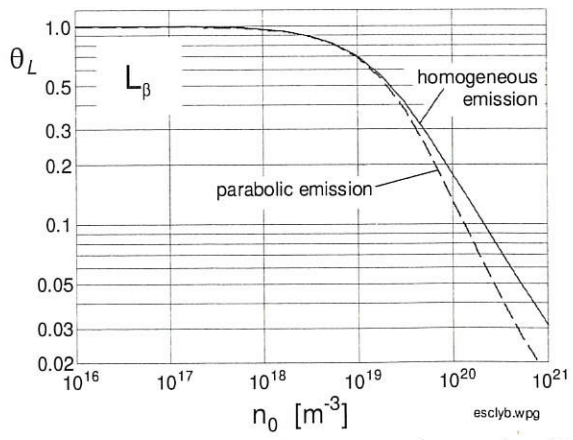

FIG. 2: Calculated L_β line escape factors for ASDEX Upgrade divertor conditions as a function of the neutral hydrogen density.

WENDELSTEIN 7-X Construction

(Dr. Manfred Wanner)

The work of the division is fully reported in section WENDELSTEIN 7-X Construction.

W7-X Construction Division: I. Bojko, R. Bünde, H. Feist, H. Grote, B. Hein, G. Krainz, H. Laqua, H. Niedermeyer, A.Nitsche, M. Pieger-Frey, T. Rummel, J. Sapper, J. Schacht, F. Schauer, F. Schneider, H. Schneider, I. Schoenewolf, A. Schönecker, M. Wanner, L. Wegener, F. Werner

Technology Division (NBI, ICRH): E. Speth, B. Heinemann, S. Obermayer, W. Ott, F.-P. Penningsfeld, R. Riedel, W. Schärich, K. Wittenbecher, D. A. Hartmann, F. Wesner

Experimental Division E3 (ECRH): V. Erckmann, T. Geist, F. Hollmann, H. Laqua

Central Technical Services (ZTE): D. Arz, W. Bitter, H. Eixenberger, R. Holzthüm, N. Jaksic, O. Jandl, F. Kerl, I. Mendelevitch, K. Pfefferle, M. Rehm, J. Simon-Weidner, B. Sombach, J. Tretter, M. Weißgerber

Forschungszentrum Karlsruhe FZK (ITP, PMW): A. Arnold, E. Borie, G. Dammertz, L. Empacher, J. Grimm, P. Grundel, R. Heidinger, T. Höhn, H. Hunger, E. Hütter, S. Illy, K. P. Jüngst, P. Komarek, M. Kuntze, W. Leonhardt, W. Maurer, G. Michel, G. Neffe, B. Piosczyk, M. Schmid, R. Spörl, M. Thumm, A. Ulbricht, A. Weis, G. Zahn

Institut für Plasmaforschung (ITP) Stuttgart: W. Förster, G. Gantenbein, W. Kasparek, G. A. Müller, P. G.Schüller, D. Wagner, W. Xu, H. Zohm

GREIFSWALD BRANCH OF IPP

(Prof. Dr. Günter Grieger)

The Greifswald Branch of IPP is planned to house eventually all the stellarator activities of IPP. At present, the activity is concentrated on the construction of the institute and its infrastructure. Additionally, also the Stellarator Theory Division (see below) under Prof. Dr. J. Nührenberg is located already at Greifswald.

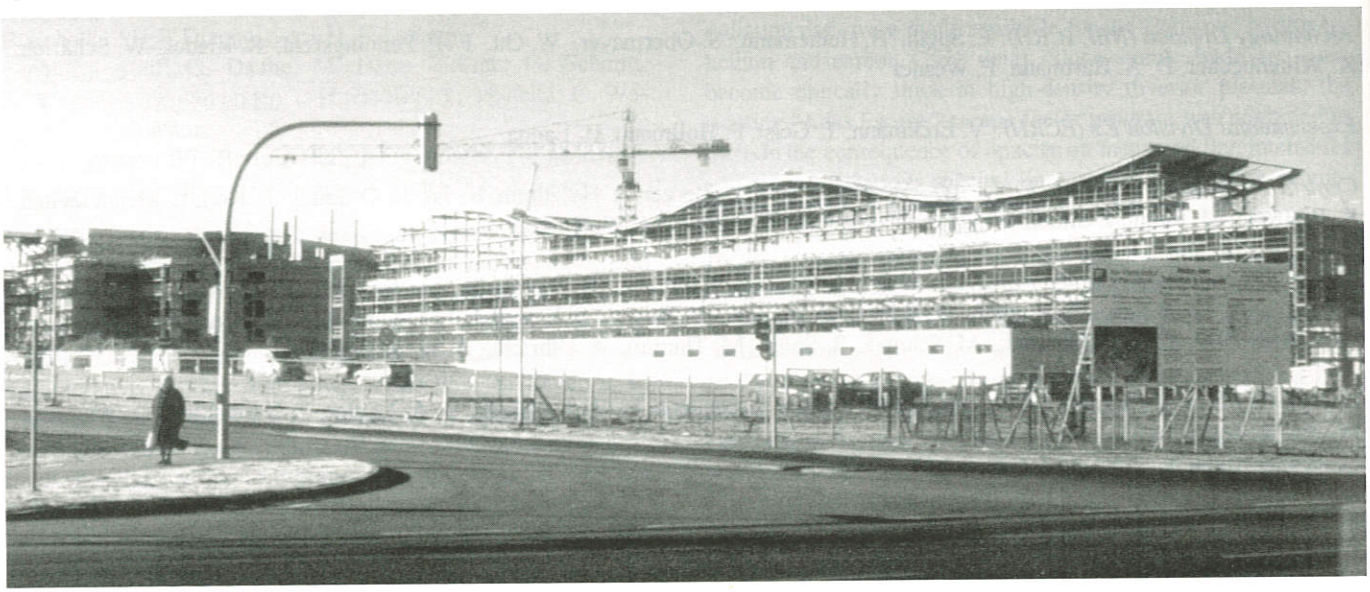

FIG. 100: Institute buildings at the end of 1998.

After the ground-braking ceremony of 19 June 1997, all the concrete shells of the buildings could be finished up to the end of 1998. In fact, the topping-out ceremony could take place already on 24 August 1998. The above photograph shows the institute buildings at the end of 1998. The experimental hall will allow DD-operation of WENDELSTEIN 7-X. The walls, the ceiling and the base-plate of the hall are made of 0.1 % Bor doped concrete with a wall thickness of 1.8 m, and of 1.2 m for the thicknesses of the ceiling and the base plate. In the very neighbourhoud of the experiment, the re-inforcement of the concrete is made of non-ferromagnetic steel. The individual strands of this steel are insulated with respect to each other to avoid eddy currents.

In the mean time, mounting of all the technical equipment belonging to the infrastructure of the institute has begun. It is expected that the institute buildings will be ready for handing them over to IPP at the end of 1999, and for occupation in early spring of 2000. There is full agreement with the time and cost plans.

The relevant team is:
G. Grieger, C. Grohrock, J. Junker, W. König, R. Krampitz, G. Mauser, M. Müller, G. Pfeiffer, M. Winkler, H. Zedler.
The team is supported by the construction division of MPG.

STELLARATOR THEORY DIVISION

(Prof. Dr. Jürgen Nührenberg)

The activity of the Stellarator Theory Division is concentrated on further development of the stellarator concept and numerical and analytical methods to investigate equilibrium, stability and transport problems in three-dimensional toroidal configurations.

The relevant team is:
S. Arndt, M. Drevlak, Ch. Hennig, R. Hatzky, R. Kleiber, A. Könies, P. Merkel, C. Nührenberg, J. Nührenberg, S. Weber.

TOKAMAK PHYSICS

(Head of Project: Prof. Dr. Karl Lackner)

The Tokamak Physics Division conducts basic and applied theory in the area of toroidal plasma confinement, with emphasis on application to existing and planned tokamak experiments. The main areas of research are (1) plasma transport, (2) edge plasma physics, (3) MHD studies, (4) wave physics. The research on MHD instabilities is mainly described in the frame of the ASDEX Upgrade project, as are the major contributions of the edge physics group.

Head: K. Lackner, Deputy: J. Neuhauser
G. Becker, A. Bergmann, D. Biskamp, K. Borrass, M. Brambilla, K. Büchl, A. Carlson, A. Celani, D. Correa-Restrepo, D. Coster, W. Feneberg, S. Günter, K. Hallatschek, B. Janauschek, F. Jenko, O. Kardaun, J. Kim, L. Lengyel, D. Lortz, P. Martin, R. Meyer-Spasche, W.-C. Müller, J. Neuhauser, G. Pautasso, A. Peeters, S. Pinches, W. Sandmann, S. Schade, R. Schneider, W. Schneider, E. Schwarz, J. Schweinzer, B. Scott, G. Spiess, H. Tasso, Ç. Tichmann, A. Teo, M. Weinlich, R. Wunderlich, H.-P. Zehrfeld, A. Zeiler

Guests: C.V. Atanasiu, Institute for Atomic Physics, Romania, I. Bandopadaya, Institute for Plasma Physics, Gandhinagar, India, J. Bowman, University of Alberta, Edmonton, Canada, R. Brandenburg, Technical University of Vienna, H. Bürbaumer, Technical University of Vienna, G. Czapski, IPP, J.F. Drake, University of Maryland, S. Egorov, State Technical University, St. Petersburg, J.H. Han, Korea Basic Science Institute, Korea, U. Holzmüller, University of Innsbruck, Alice Koniges, Lawrence Livermore National Laboratory, Livermore, P. Lalousis, IESL.FORTH, Heraklion, P. McCarthy, University College, Cork, A. Rogister, Institute of Plasma Physics, Jülich, V. Rozhansky, State Technical University, St. Petersburg, Samuli Saarelma, Helsinki University of Technology, G.N. Throumoulopoulos, University of Ioannina, N. Tsois, Demokritos, Athens, A. Ushakov, State Technical University, St. Petersburg, I. Veselova, State Technical University, St. Petersburg, S. Voskoboynikov, State Technical University, St. Petersburg, H. Weitzner, New York University. Q. Yu, Institute of Plasma Physics, Hefei, China

1. TURBULENCE AND TRANSPORT

1.1 Plasma Edge Turbulence

The investigations of plasma edge turbulence are being continued in two subprojects. Electromagnetic effects in η_i mode turbulence are studied with linear and nonlinear simulations performed with the local flux-tube code discussed earlier. A new nonlocal code was established and successfully ported to the massively parallel T3E system. Electromagnetic effects enter the dynamics of small-scale turbulence when magnetic induction delays the parallel currents, and therefore the adiabatic relation $\tilde{n}/n_0 = e\phi/T_e$ cannot be maintained. At the steep gradients typical of the plasma edge the toroidal η_i mode is shifted to longer wavelengths, whereas the growth rate remains relatively unaffected in relation to the electrostatic limit. On the basis of linear theory one would therefore expect a strong increase of the transport rates when electromagnetic effects become important. Nonlinear simulations of the associated turbulence exhibit, however, a strong drop of the transport. This reduction is associated with a fundamental change of the overall character of the underlying turbulence. Highly localized eddies are observed, which result from magnetic reconnection events and lead to strong spikes of the transport. Specific investigations of the secondary instabilities, which terminate the growth of the linear η_i mode and trigger the transition to stationary turbulence, suggest that the double tearing mode becomes the dominant saturation mechanism, taking the role of the Kelvin-Helmholtz, drift-type instabilities, which are characteristic of the electrostatic regime. In contrast to the linear phase of the double tearing mode, which strongly depends on the resistivity, finite-ρ_s effects dominate the nonlinear phase and lead to strong acceleration of the instability. Consequently the saturation level of the turbulence is practically independent of the resistivity. The simulations show that the most important magnetic effects occur in the nonlinear regime and that a purely linear analysis fails to predict the impact of magnetic fluctuations. Consequently, magnetic fluctuations should generally be included in simulations of η_i mode turbulence, at least at the plasma edge.

To relax the assumptions of local turbulence simulations a new code was developed which solves the full nonlinear drift-reduced Braginskii equations. The variation of the plasma parameters with the profile is self-consistently included as well as neoclassical effects in the Pfirsch-Schlüter regime. The current electrostatic version of the code evolves the electrostatic potential ϕ, the density n, and the electron and ion temperature and runs on the T3E system. Currently, it is being used to study the interaction of the η_i mode and resistive ballooning

turbulence, which appear in the same numerical simulation at different radial locations, and the competition of the turbulence with neoclassical transport.

1.2 Computational Drift Turbulence Studies

Several major expansions of our fluid and kinetic computational models for low-frequency plasma turbulence and anomalous transport in tokamaks have been made in the last 12 months. The fluid model has become a gyrofluid model, including finite ion gyroradius effects to arbitrary order as for the Cyclone Group codes in the US. This is the first gyrofluid model to contain the effects of self-consistent, electromagnetic electrons, allowing the resulting drift wave dynamics to tap thermodynamic free energy and drive turbulence. The kinetic model is also electromagnetic, and these two have made the first serious benchmarks between fluid and kinetic codes for electromagnetic drift dynamics; the results agree across parameter space to within 25 per cent for the transport. Both codes have been better parallelized and now operate efficiently on larger numbers of CPUs than before (e.g. a factor of 62 speed-up on 64 CPUs for the gyrofluid code on Garching's Cray-T3E). The fluid model was also extended to include a wider array of boundary conditions, so that it can model bounded as well as closed field lines (hence flux surfaces). It now uses fully realistic ASDEX Upgrade flux surface geometry in the closed flux surface region with no approximation other than axisymmetry. A completely nonlinear/nonlocal companion model was built to compute the self-consistent modifications to the profiles as the transport changes regimes. An early very interesting result is that the imposition of a sheared ExB rotation profile on the turbulence externally can sharply suppress the turbulence — the suppression shows a threshold in agreement with recently updated theoretical criteria. By contrast, the possibility that the turbulence might generate this sheared flow on its own has been largely ruled out for edge turbulence. When this external ExB shear is given physically realistic dependence on the profile parameters, very realistic transition events occur which have the same morphology as and a parameter dependence similar to the L-to-H transition in ASDEX Upgrade. For 1999 efforts are to be made to tighten collaboration with groups working on first-principle neoclassical flow models, in order to improve the self-consistency of both, possibly leading to a quantitatively realistic, and predictive, model for the L-to-H transition in ASDEX Upgrade. We also plan to add gyrokinetic ion dynamics to the kinetic model, and trapped electrons to both, in the preparation of centre-to-edge models for the anomalous transport in ASDEX Upgrade and other tokamaks.

1.3 Scaling Properties of MHD Turbulence

Previous numerical studies of 2D MHD turbulence were resumed with significantly higher resolution, yielding a number of novel results: (a) The energy spectrum exhibits a logarithmic correction $E_k \sim k^{-3/2} \ln k$, which can be interpreted as a nonlocal bottleneck effect, in contrast to the 3D bottleneck effect localized close to the dissipation range. The property is characteristic of 2D motions appearing also in 2D thermal convection and EMHD turbulence. (b) Absolute values of the scaling exponents of the structure functions could be obtained for the first time, which show that 2D MHD turbulence is much more strongly intermittent than predicted in the 3D case (c) The energy decay law is controlled by the conservation of the mean square magnetic potential H and satisfies the relation $-dE/dt = E^2(H/R)^{1/2}(1+R)$, where R is the ratio of kinetic and magnetic energy. A 3D MHD code was developed and high-resolution turbulence simulations with up to 512^3 collocation points are being performed for the first time. Results obtained to date indicate that (a) the decay of the turbulent energy is controlled by the conservation of the magnetic helicity, which gives a decay law $t^{-\alpha}, \alpha \simeq 0.6$ different from the recently published prediction $\alpha \simeq 1$; (b) the ratio of kinetic and magnetic energy decays on the same time scale as the total energy driving the system toward a static state, in contrast to the 2D case, where the ratio is nearly constant; (c) the energy spectrum follows the predicted law $k^{-3/2}$ surpisingly well.

1.4 H-mode Theory

The neoclassical radial electric field due to orbit losses was investigated with a Monte Carlo code. It is found that large negative electric fields develop just inside the separatrix. A bifurcation from a low to a high electric field is, however, never observed and the poloidal Mach number is below 1 over most of the H-mode barrier. Although no bifurcation appears in the neoclassical theory, the shear in the radial electric field can obtain values that are equal to or larger than the shear found to lead to improved confinement in the experiment. A neoclassically driven shear can, therefore, be responsible for the reduction of turbulence and determine the onset of the H-mode. A scaling with plasma parameters that is obtained from this picture compares favourably with the experiments on ASDEX Upgrade. To have more insight into whether the transport in the barrier region is neoclassical, a neoclassical transport code for arbitrary, toroidally symmetric geometry and all collisional regimes was developed. It seems that the transport can in some cases be close to that of neoclassical theory. The code can also be used to study impurity transport. The equations for Stringer spin-up were extended to impure plasma. The impurity-driven particle fluxes can exceed the electron-driven fluxes and drive some rotation.

1.5 Neoclassical Transport

The numerical calculations investigated solutions of an extended kinetic equation including there the effect of large poloidal and toroidal flow on the transport. With the new terms taken into account up to now one obtains a bifurcation for the parallel viscosity in the range where the poloidal Mach number is of order one. A code is in preparation to compute the complete gyro kinetic equation together with the correct collision operator.

2. EDGE PHYSICS STUDIES

2.1 Selected Topics of Edge and Divertor Physics

A semi-empirical model for the ratio n_S/n_C, where n_S and n_C are, respectively, the separatrix and pedestal densities in ASDEX Upgrade H-modes, was proposed. The empirical elements of the model and the detailed comparison with data rely on the extensive edge density database established at ASDEX Upgrade. The model emphasizes the role of scrape-off layer physics. The main result is that the ratio n_S/n_C is essentially determined by the proximity to the Greenwald limit.
The relation between density and temperature fall-off lengths in detached scrape-off layer plasmas was studied. Previous work on analytical models for completely detached gas targets rely on the assumption that $\lambda_n^\star \propto \lambda_T$ holds, where $\lambda_n^\star$ is the density fall-off length at the gas target entrance and λ_T the upstream temperature fall-off length. The validity of this assumption was checked on a set of B2-EIRENE gas target runs covering a wide range of discharge parameters. $\lambda_n^\star/\lambda_T \simeq const$ as well as other predictions made by theory are well reproduced. Analytical considerations were presented which offer the possibility to assess the potential impact of various models for transverse transport.
Geometry effects in the SOL and divertor, which are the main focus of a variety of present tokamaks, were reviewed. Since divertor detachment constitutes a central element in this context, some basic results on divertor detachment were summarized. The discussion of issues that played a role in recent experimental campaigns and their theoretical and numerical analysis form a major part of the review. Emphasis was placed on gas target related effects. An attempt was made to reduce the impact of geometry to a small number of basic mechanisms.

2.2 2-D Particle Simulation of a Classical SOL

A scrape-off layer (SOL) with collisional transport was studied in a slab model with two-dimensional particle simulations in order to determine the influence of classical transport and drift motion on the radial density and temperature profiles. The model with a straight magnetic field includes a bulk plasma with a Maxwellian particle source, a SOL and ''divertors''. Due to symmetry only the plasma between the midplane and wall is modelled. A PIC code with a Fokker-Planck model of Coulomb collisions is used. The results are: The density scale length is basically determined by collisional transport, hence in the midplane it is only a few $\rho_s = \rho_e\sqrt{m_i/m_e}$. Only close to and inside the ''divertor'' does the scale length increase up to values of the order of the poloidal gyro radius $\rho_p = \rho_s B/B_p$. In the divertor, the density profile is shifted away from the separatrix in the direction of the drift, but the electron temperature profile is not. The latter shows less variation of the scale length between the midplane and divertor. The temperature profile is less steep than the density profile even without drift effects. It is characterized by two scale lengths; close to the separatrix 2 to 3 times the density scale lengths; further out a scale length of the order of the poloidal gyro radius.

3. MHD EQUILIBRIUM AND STABILITY

3.1 Dissipative Plasma Equilibria

Various approaches for a consistent description of stationary dissipative equilibrium states of tokamak plasmas with finite current densities near and beyond the separatrix were studied and applied to stability analyses.
In a study with pressure and neoclassical parallel resistivity profiles showing the pedestal-like structure near the separatrix as observed in experiments, the resulting sheared electric field and mass flow were calculated and the expected pressure gradient scales for entering the first and second stability boundaries for ballooning modes determined.
Another concern was resistive equilibrium states at finite Reynolds numbers with compressible, viscous fluid flow. The corresponding stationary MHD equations can be represented as a set of eight coupled partial differential equations for the rate of expansion, for the poloidal fluxes and toroidal circulations of magnetic induction and flow velocity, and for pressure, electric potential and temperature. Central to this set is the free-boundary-value problem for the poloidal magnetic flux and a fourth-order partial differential equation for the poloidal mass flux with no-penetration and no-slip boundary conditions for the poloidal flow at a material surface limiting the region under consideration. The generalization to toroidal geometry of the corresponding coupled vorticity-stream function problem of plane hydrodynamics was formulated and numerically solved for a particular case.

3.2 Analytic Equilibrium and Stability Studies

Previous work on MHD equilibria with incompressible flows was extended to the helical case. A new feature appears for isothermal magnetic surfaces: the governing equations are overdetermined, which suggests that such equilibria do not exist in the stellarator.
A sufficient condition for stability of dissipative systems was derived. It was proved that the Lyapunov stability of mechanical systems persists despite the addition of gyroscopic and circulatory forces if the dissipation dominates inertia, and if the difference between the gyroscopic and circulatory operators is small enough.

3.3 Resistive Instabilities

The classical problem of resistive modes in a plane slab is reconsidered in order to obtain the entire spectrum in the complex frequency plane. The following questions are of interest:
(1) How does the spectrum ranging from ''tearing'' modes for long wavelengths to ''rippling'' modes for short wavelengths change as the resistivity gradient increases (unbounded growth rates occur in the extreme case of a resistivity jump)?
(2) In the case of constant resistivity, are there any overstable modes if there are no purely growing ones because $\Delta' < 0$?

3.4 Resistive Ballooning Modes Near the Edge of Toroidal Configurations

The resistive ballooning mode equations were cast in a new form appropriate to evaluation near the plasma edge of toroidal (axisymmetric as well as three-dimensional) configurations, where resistive ballooning effects outweigh diamagnetic effects. Explicit evaluation was carried out for cylindrically symmetric plasmas and for a tokamak model with circular cross-sections. Owing to the large electrical resistivity of the regions considered, resistive ballooning modes with growth rates comparable to the characteristic growth rate of ideal ballooning modes are possible. A general feature is that modes with large growth rates are localized around the regions of bad curvature and become less unstable with increasing shear, while those with smaller growth rates are extended along the magnetic field lines and are insensitive to shear.

3.5 Application of Neural Networks for Disruption Mitigation

The applicability of an artificial neural network (ANN) to the problem of plasma regime identification started to be investigated this year. The ANN used in this work is a typical multilayer perceptron with one hidden layer of neurons and it is trained by means of the back propagation algorithm. Two different problems were investigated:
Firstly, an ANN was trained to detect the presence of a MARFE using as input two divertor bolometer channels and the plasma internal inductance. The output consisted of 0 (= no MARFE) and 1 (= MARFE present); after the training with a database of 50 shots, the ANN could detect the MARFE reasonably well.
Secondly, an ANN was trained to recognize a forthcoming disruption. The output of the network was chosen to be the time interval up to disruption; the input consisted of time windows of several plasma parameters describing the onset, presence and the evolution of the MARFE, tearing modes and H or L regimes. A sensitivity analysis of the trained ANN allows us to select the most relevant diagnostic signals. The performance of the latter ANN will be checked on discharges of the coming (1999) experimental period.

4. ION CYCLOTRON HEATING

1) Electron Landau damping of ion Bernstein waves excited by mode conversion near ion-ion or first-harmonic cyclotron resonances is important when their wavelength becomes comparable to or shorter than the ion Larmor radius. Quantitative expressions for the absorption rate were obtained and implemented in the TORIC toroidal wave code. This substantially improves the reliability of the power deposition profiles evaluated with this code.
2) The constitutive relation (the HF current as a linear functional of the HF electric field) for plasma waves in tokamak geometry was rederived from the linearized Vlasov equation, with the unperturbed particle orbits described in the drift approximation, but including the gyromotion. This approach extends the gyrokinetic theory to frequencies of the order of or larger than the ion cyclotron frequency; instead of approximating the kinetic equation, however, we approximate its solutions. The wave equations for IC waves solved by the TORIC toroidal wave code are recovered by expanding to second order in the Larmor radius. In addition, integro-differential wave equations for low-frequency drift, shear, and kinetic Alfvén waves are obtained.

5. MATHEMATICAL PHYSICS

5.1 Parameter Dependent Free Boundary Problems

Elliptic equations of type $\Delta^* \psi = f(\psi, \lambda)$ in $D \subset \mathbb{R}^2, \psi|_{\partial D} = g$ were investigated, where D is a bounded domain in the real plane, λ is a real parameter and the nonlinearity f is smooth, except at the free boundary. **a)** Discretization by finite differences (multigrid) was considered. Convergence of the discretization used was proved. The convergence rate depends on the smoothness of f. The fact that f is not differentiable or even jumps at the free boundary slows down convergence. But its order is still at least $h \ln h < \sqrt{h}$. **b)** Convergence of several iteration schemes for treating the nonlinearity f and the dependence on the parameter λ were investigated. The 'recursive projection method' with 'pseudo-arc-length continuations in λ' was found to be most efficient. The theoretical investigations were complemented by computations on examples from plasma physics and gave new insights into solution manifolds.

5.2 Elliptic Operators with Singular Continuous Spectra

Differential operators are considered which occur e.g. in the MHD description of a low pressure plasma in general toroidal geometry (relevant for Alfvén-wave heating) or in the ballooning equation, an equation of Sturm-Liouville type. The spectral properties of such differential operators reflect the properties of the corresponding states: bound states have energies in the point spectrum, scattering states in the absolutely continuous spectrum. These kinds of spectra are common in examples whereas a singular continuous spectrum was considered pathological: the corresponding states are neither bound states nor scattering states, but describe a quantum random walk which is both unbounded and recurrent. Recently it was shown that singular continuous spectra of Schrödinger operators are much more common than was hitherto expected. To get better aquainted with this kind of spectrum, Pearson's analytical method of treating a Schrödinger operator with singular continuous spectrum is transferred to an elliptic system occurring in relativistic quantum mechanics. The study of transfer matrices has proven effective in the Schrödinger case.

SURFACE PHYSICS DIVISION

(Prof. Dr. Dr. h.c. Volker Dose

Prof. Dr. Jürgen Küppers)

The Surface Physics Division is organised in three groups. Contributions to the "Plasma-Facing Components" project constitute the work of the Plasma-Wall Interaction group. This concerns experiments in collaboration with fusion machines as well as more fundamental laboratory studies including work within Sonderforschungsbereich 338. The latter concentrates on adsorption at solid surfaces and integrates work at the Munich Universities and the Max Planck Institutes MPQ and IPP. The second group, working on properties of low-temperature plasmas, their diagnostics and application to thin film deposition, is run as a joint venture with IPP's Technology Division, and its work is being reported in a separate section entitled "Plasma Technology". The third group, Data Analysis, aims at interpreting experimental data from our own work as well as from other divisions employing Bayesian probability theory.

Head: V. Dose, Deputy Head: E. Taglauer

Scientific Staff:

M. Balden[1], R. Behrisch, R. Beikler[2], E. Berger[2], M. Donath, W. Eckstein, K. Ertl, R. Fischer, P. Goldstraß[2], D. Grambole[12], W. Hauffe[13], P. Hayes[4], Ch. Höfner[1], Ch. Hopf[3], A. Horn[2], W. Jacob, M. Jakobi[5], H. Kang[2], A. von Keudell, A. Kohl[2], H. Knözinger[14], K. Krieger, B. Landkammer[2], K. Letourneur[6], W. von der Linden, St. Lindig[3], Ch. Linsmeier, J. Luthin[2], C. Lutterloh[2], K. Maruyama[7], Ch. Math[2], M. Mayer[1], M. Meier[3], N. Memmel[1], V. Milosavljevic[8], N. Naef[9], P. Pecher[1], R. Preuss, G. Rangelov, N. Reinecke[2], J. Reinmuth[2], J. Roth, Th. Schwarz-Selinger[2], V. Shulga[10], G. Staudenmaier, A. Steltenpohl[2], A. Tabasso[1], U. von Toussaint[2], S. Vasquez-Borucki[2], G. Venus, S. Vetter[2], M. Zarrabian[11].

Technical Staff:

S. Bassen, L. Beck, M. Ben Hamdane, Ch. Fritsch, K. Gehringer, R. Hippele, A. Holzer, E. Huber, M. Hunger, P. Matern, J. Mauermair, M. Nagy, W. Ottenberger, B. Plöckl, S. von Polenz, M. Roppelt, J. Schäftner, A. Schlamp, H. Schmidl, I. Zeising.

1 Post Doc
2 Doctoral Candidate
3 Undergraduate Student

Guests:

4 University of Western Australia, Perth, Australia
5 Universität Saarbrücken, Germany
6 Technische Universität Eindhoven, NL
7 Nagaoka University of Technology, Japan
8 University Beograd, Yugoslavia
9 EPF Lausanne, Switzerland
10 Moscow Lomonossov University, Russia
11 Institut des Matériaux de Nantes, France

Collaboration with:

12 Forschungszentrum Rossendorf, Germany
13 Technische Universität Dresden, Germany
14 Ludwig-Maximilians-Universität, Munich, Germany

1. PLASMA-WALL INTERACTION

During the last few years the investigations of plasma-wall interaction have shifted from pure elemental solids to multi-component solids, which may be formed in the interaction of different plasma-facing materials. The main topics are surface erosion and hydrogen retention in the materials. A third section describes the development of new experimental techniques. Investigations of plasma-facing materials in fusion experiments are described in section 1.4.

1.1 Multi-element Wall Materials

1.1.1 Thermal reactions in the ternary system Si-Ti-C

Thin Ti and Si films with thicknesses of about 20 nm were successively evaporated onto substrates of polished pyrolytic graphite. X-ray Photoelectron Spectroscopy (XPS) studies were performed to investigate thermal reactions in the temperature range from room temperature up to 970 K. At elevated temperatures formation of silicides and carbides is observed. Between 570 and 670 K Ti starts to segregate onto the surface. All reactions strongly depend on the oxygen contamination of the samples.

1.1.2 XPS studies on formation of WC by annealing of thin graphite films on tungsten

The carbidisation of thin carbon films evaporated on tungsten substrates under UHV conditions was investigated in the temperature range between room temperature and 970 K by XPS. Investigations of the temperature dependence indicate carbide formation above 870 K, detected by shifts of the binding energies of the W 4f and C 1s electrons. Time-dependent measurements at 970 K and in annealing time of 1200 min. show decreasing C and increasing W surface concentration. After the annealing procedure the C 1s peak shifted to 283 eV, indicating that most of the graphite has reacted with tungsten to form tungsten carbide.

1.1.3 Interaction of oxygen atoms with metal surfaces

Oxygen atoms with thermal energies were produced in a microwave plasma discharge and guided onto several metal surfaces in ultra-high vacuum. Formation of atomic oxygen in this source was proved by adsorption of O_{at} on gold, which is inert to O_2. The reactivities of beryllium and tungsten to O_{at} at room temperature were measured by XPS. Tungsten shows no difference in reactivity and adsorption behaviour between O_{at} and O_2, indicating dissociative adsorption of the oxygen in both cases. Only adsorbed oxygen and a first-layer oxide were formed. Beryllium reacts both with molecular and atomic oxygen species, leading to formation of BeO. However, the reaction rate for O_{at} is several times higher than for O_2, and O_{at} leads to an additional layer of adsorbed oxygen on the surface.

1.1.4 Sputtering of W by carbon and hydrocarbon ions

The use of high-Z materials, such as W, is planned under plasma conditions where the incident D/T ion energy is below the threshold energy for sputtering. The threshold energy for impurity sputtering, however, is much lower (around 10 eV), and therefore impurity sputtering has to be considered.

Pure carbon ion bombardment at room temperature was shown to lead to carbon deposition and formation of protective layers on W. Bombardment at elevated temperatures, however, where carbon can diffuse into the W bulk, results in continuous W erosion. Similarly, simultaneous irradiation of W with C^+ and H^+ ions can lead to erosion by the incident C^+ ions, while H^+ effectively removes the deposited carbon layer at the surface, always leaving W exposed to the ion beam. FIG. 1 shows a comparison of the weight loss of a W target under the erosion of C^+ ions at room temperature and 1070 K and with CH_3^+ ions at 770 K as a function of the C fluence.

While the erosion of W at room temperature is only transient until continuous weight increase occurs due to carbon deposition, it steadily continues at elevated temperatures. Ion beam analysis of the sample after high fluence bombardment shows that W is not protected by a deposited layer under these conditions. For detailed analysis of the conditions where C deposition or W erosion occurs the TRIDYN dynamic code was modified to take into account thermal processes, such as diffusion and surface segregation.

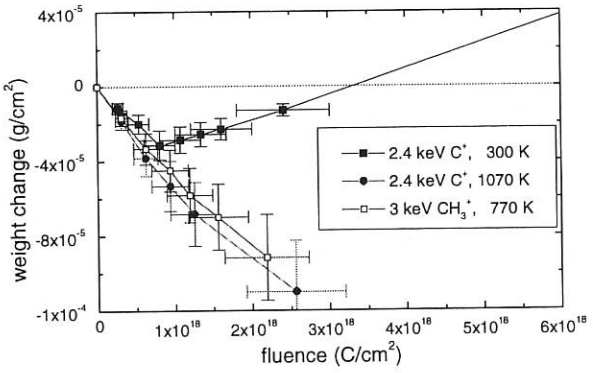

FIG. 1: Deposition/erosion behaviour of tungsten under carbon and CH_3^+ ion bombardment for different substrate temperatures.

1.1.5 Construction and starting of the ARTOSS experiment

Based on the existing BOMBARDON chamber, the new ARTOSS experiment was completed. It is especially well suited to preparation and study of multi-component wall materials. The ion beam analysis methods, Rutherford Backscattering Spectrometry (RBS) and Nuclear Reaction Analysis (NRA), were supplemented by Elastic Recoil Detection (ERD) using a 30° detector. A newly constructed ion

deceleration lens in combination with a 20 keV ion source (magnetic separation) allows ion implantation at energies between 50 eV and 20 keV. Additional chemical state-sensitive photoelectron spectroscopies are provided by using a hemispherical electrostatic analyser and the X-ray (XPS) and ultraviolet (UPS) light sources. An additional ion gun enables Ion Scattering Spectroscopy (ISS). A load lock facilitates quick sample changes without breaking the ultra-high vacuum (10^{-11} hPa). Sample preparation is made possible by using the ion beam sources and a UHV-compatible evaporator. A computer-controlled manipulator allows sample positioning as well as heating and cooling (liquid nitrogen to 1400 K) during analysis and preparation.

1.1.6 Dynamic target behaviour during ion bombardment

To determine effects of ion bombardment at elevated temperatures, the TRIDYN Monte Carlo program, which describes the dynamic behaviour of the target due to ion bombardment, was coupled with the PIDAT diffusion program. Diffusion of implanted atoms during irradiation is simulated by iterative application of both programs, allowing the depth distribution of the target constituents and the implanted species to be determined as a function of fluence and time up to a given maximum fluence. The procedure was applied to bombardment of tungsten with carbon. The calculated results are in qualitative agreement with experimental data for temperatures below 850 K.

1.1.7 Depth of origin of sputtered atoms

The depth of origin of sputtered atoms was investigated with the OKSANA and TRIM.SP computer programs. The results show that the depth of origin of sputtered atoms depends on the atomic target density, the projectile energy, the angle of incidence, and the projectile and target species. Better agreement is found with the analytic theory of Sigmund than with the empirical formula given by Kelly on the basis of a few experimental data.

1.2 Hydrogen Inventory in Plasma-Facing Materials

1.2.1 Deuterium co-deposition

Co-deposition of deuterium with silicon-doped carbon for Si concentrations between 0-100 at% in a temperature range from room temperature to 1000 K was investigated. Material eroded by deuterium ions from targets with different composition in Si and C was collected on probe targets together with reflected D to build up the co-deposited layers. Subsequent analysis was performed by MeV ion beam techniques. The amount of trapped D per re-deposited target atom weakly depends on the Si concentration. The maximum of about 0.7 D/(Si+C) was found at Si/C ~1. For pure C and pure Si the D concentration is about 0.45 and 0.5 D atoms per re-deposited target atom at room temperature, respectively. With increasing deposition target temperature, the D concentration does not significantly decrease until ~600 K. At about 1000 K the D concentration for pure carbon is still 30% of the concentration at room temperature.

Further investigations were carried out for D co-deposition with stainless steel and with titanium-carbon mixtures. With stainless steel the co-deposition of D was below the detection limit. For the titanium-containing layers with Ti/C ~0.4 the ratio of D atoms to re-deposited target atoms is 0.42. In contrast to the Si-containing layers, the Ti mixtures were severely oxidised.

1.2.2 Deep hydrogen isotope depth profiles of divertor tiles of ASDEX Upgrade

(collaboration with FZ Rossendorf)

The hydrogen and deuterium trapped in the inner divertor tiles of ASDEX Upgrade up to depths of several tenths of a mm was measured by ion beam slope cutting and analysis of the slope surface by micro-ion-beam ERDA. At the W-coated divertor tiles a hydrogen concentration of about 30 at% was measured in the approx. 20 µm thick carbon layer deposited above the W, indicating hydrogen trapping by co-deposition.

1.3 Ion Beam Analysis

1.3.1 3 MV tandem accelerator

A new 3 MV tandem accelerator was installed which will replace the 20-year-old 2.5 MV single-ended accelerator, suffering from increasing maintenance problems due to ageing as well as from limited analytic possibilities. The accelerator is equipped with a He gas source and a sputter source for all other elements. The system will cater to new requirements on analysis of surfaces from the plasma experiments: Analysis of the T inventory in the walls of future plasma experiments can be done by accelerator mass spectroscopy, quick and quantitative measurement of a mixture of light elements, such as Be, B, C and O, can be achieved by heavy ion elastic recoil detection (ERD) at sufficient energy.

1.3.2 ERDA station

The elemental composition and depth profiles of all light elements in the near surface-region of a sample can be measured simultaneously and quantitatively by analysing the elastically recoiled atoms (ERDA). Using heavy ions from the new 3 MV tandem accelerator, such as 18 MeV Si ions, the elastically recoiled atoms can be mass and energy-analysed by applying a time-of-flight technique combined with energy analysis in a solid-state detector (TOF-ERDA). Such a spectrometer was elaborated and design studies were performed.

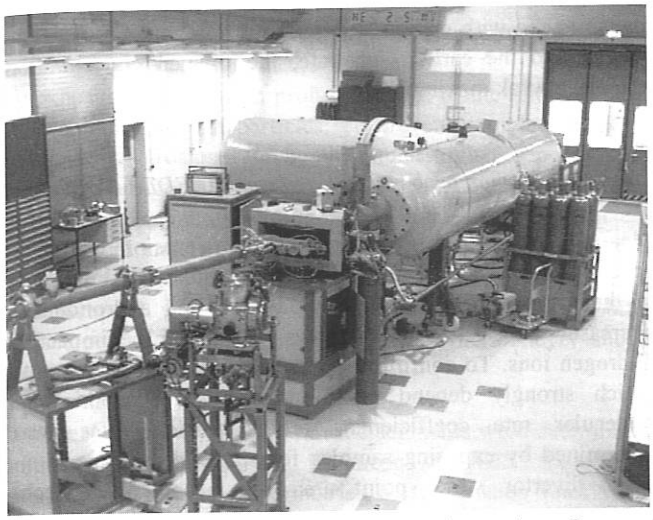

FIG. 2: 3 MV tandem accelerator with test beamline and first backscattering analysis chamber, SAK (SondenAnalyseKammer).

1.3.3 *ERDA detector and stopping power for low-energy hydrogen in a-C:H*

An ERDA detector system with a scattering angle of 30° was installed for $^4He^+$ ion beam analysis of layers containing hydrogen isotopes. The detector can be used with and without a 5.1 µm Ni foil (foil-ERDA) or together with a thin transmission detector (9.3 µm) in telescope arrangement. The two detectors are operated in coincidence and allow simultaneous measurement of depth profiles of different hydrogen isotopes. Depth profiles from implanted deuterium (0.5-8 keV) in hard a-C:H layers (H/C = 0.5) are obtained by using foil-ERDA and the LORI program. The stopping power required to convert the energy distribution into a depth distribution was calculated with Bragg's rule.

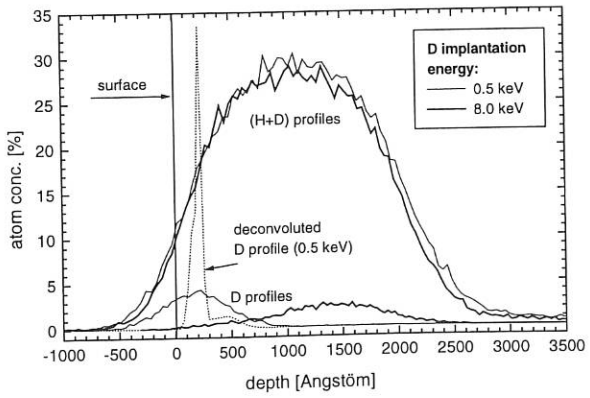

FIG. 3: Deuterium depth profiles for implantation energies of 0.5 and 8 keV. The dotted 0.5 keV D profile is a deconvolution by maximum entropy methods.

It is known that cores and chemical bonds of C and H (CAB model) cause a 1.4-fold increase in the stopping power for 1.5 MeV H recoils compared with Bragg's rule yields. Comparison of precisely measured implantation profiles with computer simulation showed that a 1.5-fold increased electronic stopping power had to be assumed for agreement within the experimental error bars, which result mainly from a 0.5° uncertainty in the scattering angle. This indicates that a similar increase in stopping power is needed for low-energy hydrogen (0.5-8 keV) as for high-energy hydrogen (1.5 MeV) in a-C:H layers. Equivalent results for the implantation depth of H in a-C:D films were obtained by using telescope ERDA.

1.3.4 *Ion beam analysis set-up for large 3-dimensional samples*

To allow direct comparison of virgin and exposed tiles by means of ion beam surface analysis, a manipulator system was developed which is capable of handling whole tokamak tiles in an analysis chamber equipped with detectors for RBS and NRA.

Movement of the manipulator is provided by four independent motors which allow translation of the sample in the x, y and z directions together with rotation around the z-axis. In addition, two intersecting lasers in conjunction with a CCD camera are used to provide a reference for the position where the ion beam hits the target at the correct angle in relation to the detector. These features, together with the four degrees of freedom, allow analysis at different positions for targets of virtually any shape.

The manipulator was employed to analyse the quality and homogeneity of the tungsten coating on ASDEX Upgrade heat shield tiles and will be used for post-mortem analysis of all the tiles at the end of the experimental campaign.

1.4 Wall Erosion and Conditioning Stability at ASDEX Upgrade

1.4.1 *Tungsten erosion at the inner heat shield of ASDEX Upgrade*

As a preliminary test experiment for full-scale tungsten use at the main-chamber inner heat shield, four carbon shield tiles were coated with a tungsten film to study tungsten erosion behaviour under ion and neutral bombardment and to obtain the poloidal distribution of the long-term tungsten erosion rate. A manipulator system for handling large samples was developed (see 1.3.4) to allow direct comparison of virgin and exposed tiles by means of ion beam surface analysis. Analysis of the 10 nm vapour-deposited W on carbon tiles, carried out at several positions, revealed that the average layer thickness is 10^{17} atoms/cm^2 with a uniformity of better than 10%. A relatively high fraction of oxygen (~60%) was detected in the spectra, possibly due to oxygen gettering during evaporation. No other impurity was found.

1.4.2 *Composition and stability of ASDEX Upgrade wall conditioning*

In the 1998 experimental campaign the possibility of replacing boronisation by siliconisation for wall-conditioning purposes was investigated in ASDEX Upgrade. The composition and chemical stability of the boron and silicon-based coatings were analysed by exposing suitable substrate samples inside the ASDEX Upgrade vacuum vessel during wall-conditioning glow discharges. After the conditioning procedure the fresh samples were removed before plasma operation was resumed. The elemental composition of the wall-conditioning films was determined immediately after removal. Subsequently, the samples were stored in air for a total time of 400 hours and repeatedly re-analysed to investigate their chemical stability. Elemental analysis was performed by ion beam techniques. Since the films were created by using fully deuterated gases, they must initially contain only the isotope, deuterium. During storage in air there is no atomic or molecular hydrogen available. A decrease of the D fraction, i.e. of the ratio D/(H+D), with time is therefore a clear indication of chemical reactivity of the films because water is the only source of hydrogen present in air. The respective results are summarised in FIG. 4: Within the boron-based film the deuterium fraction rapidly decreases, while the silicon-based film hardly shows any sign of this exchange reaction. The total amount of hydrogen isotopes remains approximately constant in both samples. For a silicon substrate, these results were confirmed by infrared spectroscopy. While the IR spectra of the silicon-based films remained unchanged, the absorption features of the boron-based films in the spectral vicinity of the B-H and B-D molecular vibrations, respectively, changed strongly with time.

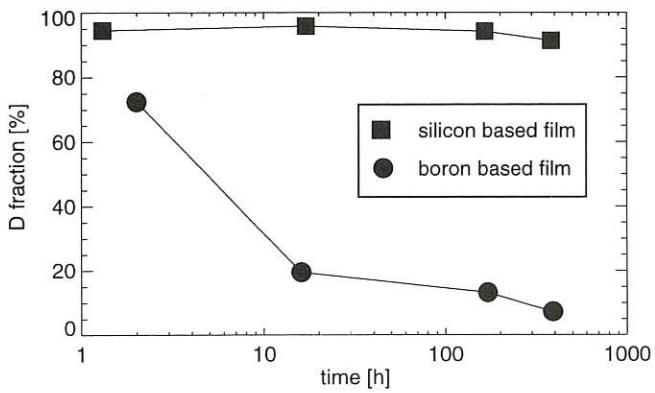

FIG. 4: Time evolution of the chemical composition of surface layers produced by boronisation and siliconisation glow discharges.

It can be concluded that ASDEX Upgrade wall-conditioning films based on silicon are chemically more stable in air than the corresponding boron-based coatings.

The current state of the first wall after multiple boronisation and after siliconisation was determined from a long-term probe which was integrated into the inner heat shield. FIG. 5 shows the depth profiles of the layer composition, measured by XPS and Ar sputtering. The Si layer is very pure and only oxidised at the very surface, presumably due to air contact during transport. The boronisation layer below is heavily contaminated with carbon, oxygen and nitrogen. Close to the interface to the carbon substrate, the oxygen concentration exhibits a weak maximum.

1.4.3 *Erosion probes in the divertor of ASDEX Upgrade*

Measurements of the chemical carbon erosion yield by spectroscopic observation of the CD molecular band emission in the divertor of ASDEX Upgrade revealed a pronounced decrease of the yield with increasing flux of the impacting hydrogen ions. To confirm the results of these measurements, which strongly depend on the accuracy of atomic and molecular rate coefficients, carbon erosion rates were determined by exposing samples for single discharges at the outer divertor strike point area by means of a probe manipulator system.

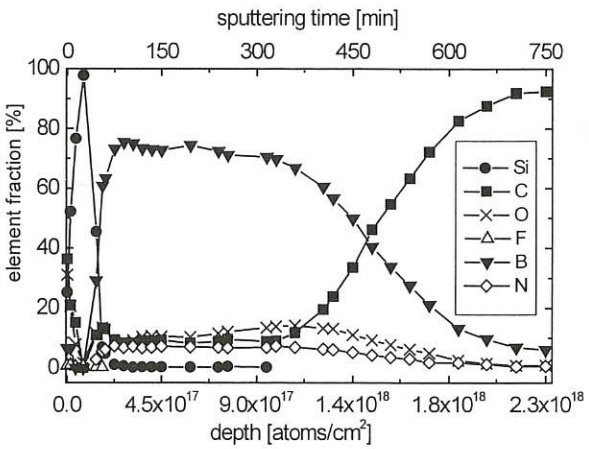

FIG. 5: Depth profile of a long-term probe from the heat shield of ASDEX Upgrade. The surface layer is dominated by Si, whereas the underlying boronisation layer is contaminated by carbon, oxygen and nitrogen.

In addition, an array of optical fibres viewing directly at the probe surface was installed to allow simultaneous spectroscopic flux measurements for direct comparison of the two methods. To allow detection of the small surface erosion by means of RBS analysis without using non-carbon markers, the graphite samples were covered with a 50-200 nm ^{13}C isotope layer. The gross erosion of this layer was determined by measuring the areal density of ^{13}C atoms before and after exposure to the plasma discharge. From the energy spectrum of the backscattered ions the depth distribution of the carbon isotope fractions was derived by means of Maximum Entropy deconvolution. Details of the algorithm are described in the section on data analysis. The ^{13}C areal density and, in addition, the amount of redeposited ^{12}C on top of the ^{13}C layer were obtained by integration over the respective depth profiles. First results confirm the spectroscopically determined carbon erosion yields.

1.4.4 *Long-term erosion probes in the main chamber of ASDEX Upgrade*

Determination of erosion rates due to sputtering by charge-exchange (CX) neutrals in the main chamber is only possible by exposure of long-term probes because of the relatively low flux of impacting CX particles. To prevent complete masking of the small erosion rate by the much higher deposition of material during wall-conditioning glow discharges, a set of probes with magnetic-field-operated shutters was constructed. One toroidal and two poloidal sets of probes were employed during the 1998 experimental campaign of ASDEX Upgrade. The samples were made of polished pyrolytic graphite, surface-coated in two segments with a 2 nm Si layer and a 1 nm W layer segment, respectively.

The areal Si and W densities in the segments were determined before and after exposure by means of RBS. Significant poloidal and toroidal asymmetries of the erosion rates were found. Since the spatial variations of the erosion rate of the two materials are closely correlated, this reflects the corresponding variation of the flux of impacting particles. The poloidal variation of the erosion rates is attributed to the spatial profile of the total CX flux, folded with the mean CX particle energy.

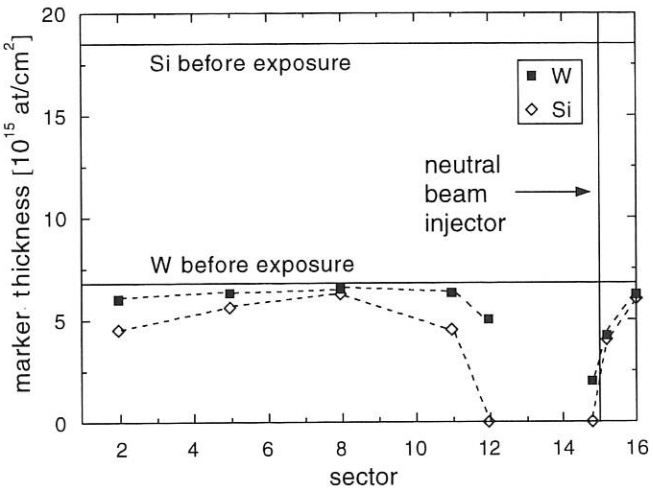

FIG. 6: Toroidal distribution of silicon and tungsten erosion rates along the outer midplane of the ASDEX Upgrade main chamber. The samples were exposed to 251 plasma discharges with approximately 1000 s plasma operation.

The observed toroidal asymmetry, however, is correlated to the entrance port of the neutral beam injector I (see FIG. 6). The much higher erosion rates in the vicinity of the injector port are presumably caused by the impact of fast beam particles.

1.5 Surface Science

The co-operation of the Surface Science group within the Sonderforschungsbereich (SFB 338: Adsorption on Solid Surfaces) is continuing. Recent contributions include the structural and concomitant electronic changes induced by adsorbates on metal surfaces, the role of oxygen as a surfactant influencing thin-film growth and the investigation of model catalysts. Additionally, the magnetic properties of thin-film systems are being studied.

1.5.1 *SFB 338*

Growth of Pd on clean and oxygen-covered Pd(111) was studied for deposition temperatures between 210 K and 420 K by scanning tunnelling microscopy (STM). After determination of the diffusion barriers of adatoms on flat terraces, the diffusion barrier for step-down diffusion was then measured by evaluating the amount of interlayer transport as a function of deposition temperature (an example is shown in FIG. 7). It was found that preadsorption of oxygen enhances interlayer mass transport mainly by increasing the pre-exponential factor ('attempt frequency') and not by changing the height of the additional step edge barrier. This leads to a flatter film morphology with pre-adsorbed oxygen compared with a clean surface, i.e. oxygen operates as a 'surfactant'.

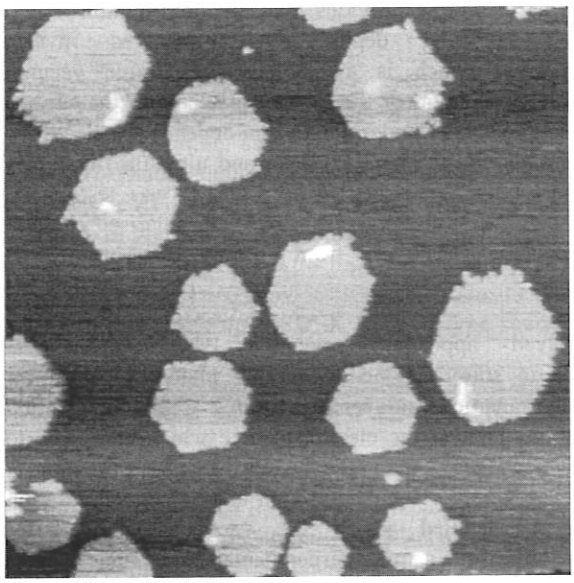

FIG. 7: STM image (3000Å x 3000Å) of 0.04 monolayers of Pd deposited at 270 K on a Pd(111) surface, precovered with 0.3 monolayers of flat, hexagonally shaped Pd islands: on small islands all deposited material moved down the steps, while on large islands some material remained.

Adsorbate-induced reconstruction of Cu surfaces was further investigated. Faceting of the vicinal Cu(115) surface by adsorption of oxygen was studied by scanning tunnelling microscopy. It was found that the facet size increases by increasing the sample temperature (between 410 K and 620 K) during deposition and by decreasing the adsorption rate, i.e. oxygen pressure (between $5.6 \cdot 10^{-9}$ mbar and $2 \cdot 10^{-5}$ mbar). The resulting kinetics can be described by the scheme of 'nucleation and growth'. The required diffusion of copper atoms on the surface is determined by the fluctuation of the kinks at the

double steps. The faceting of the vicinal Cu(119) surface shows different surface structures but similar parameter dependences.

Investigation of supported metal catalysts was continued. Ion scattering (ISS) and X-ray photoelectron spectroscopy (XPS) showed that agglomeration of Rh on the surface of the system $Rh/SiO_2/Mo$ is induced by heating the sample in UHV. The shift in binding energy and the decrease of intensity in the Rh3d signal gave evidence of a cluster size smaller than 2 nm. To investigate the catalytic performance of supported rhodium catalysts a glass reactor experiment was developed. The reaction products derived from a heated gas mixture of H_2 and CO at atmospheric pressure over $Rh/SiO_2/Mo$ and $Rh/VO_x/SiO_2/Mo$ model catalysts will be measured with a mass spectrometer. The Rh cluster size will be determined by atomic force microscopy (AFM) and X-ray photoelectron spectroscopy (XPS).

1.5.2 Surface magnetism

A new experimental set-up for magnetometry using spin-polarised secondary-electron emission (SPSEE) was built and tested. This technique provides magnetic information within the same probing depth as spin-resolved inverse photoemission, which is available in the same vacuum chamber. Combination of the two gives access to the surface magnetisation and underlying spin-dependent electronic structure of in-situ prepared surfaces and ultrathin films. The spin polarisation detector used for SPSEE was tested and calibrated by using electrons from our spin-polarised electron source as well as secondaries from ferromagnetic iron films on W(110).

Spin-resolved appearance potential spectroscopy was employed to study magnetic coupling phenomena and re-orientation transitions in layered structures. A spin polarisation rotator was added to the electron source which allows us to investigate changes of the magnetic anisotropy as a function of film thickness and/or temperature. In addition, magnetisation coils were installed inside the vacuum chamber for magnetisation of the sample perpendicular to the film plane as well as in two directions in the film plane. The work was focused on the magnetisation of ultrathin Fe films on W(110) as a function of the film thickness and as a function of the probing depth for a given thickness. The latter was achieved by varying the angle of incidence of the exciting electrons. The experiments show maximum magnetisation for film thicknesses between 3 and 6 atomic layers and, for thick films, enhanced surface magnetisation. Both observations can be understood as a consequence of the reduced co-ordination number in low-dimensional systems.

2. DATA ANALYSIS

The inference of physical quantities from ill-conditioned data is a ubiquitous and often cumbersome task. Bayesian probability theory provides a general and consistent frame for logical inference. Model selection, parameter estimation and form-free distribution estimation with confidence intervals are prominent problems regularly tackled with this data analysis tool.

Energy confinement in W7-AS has been analysed in terms of dimensionally exact form-free functions employing Bayesian probability theory. On the basis of the International Stellarator database, which contains the energy content for a wide variety of variable settings, predictions for single-variable scans were made and shown to be in quantitative agreement with actual data. Furthermore, the optimal model for description of the global transport in W7-AS was identified as the collisional low-beta kinetic model.

Form-free distribution estimation with confidence intervals is a particular challenge in data analysis. The prior information of the existence of different length scales intrinsic to all natural distributions is exploited by a multi-resolution spatial correlation approach which reduces adaptively the effective degrees of freedom of the form-free distribution. Significant information in the data is supported, while noise fitting is suppressed. Deconvolutions of RBS and ERDA (see 1.3.3) spectra with the measured apparatus transfer functions resulted in resolution enhancements of up to one order of magnitude. The form-free reconstruction of the electron energy distribution curve from only 8 helium emission line intensities of a low-pressure ECRH plasma shows distinct deviations from a Maxwell distribution.

The adaptive kernel method was further applied to Rutherford backscattering spectroscopy (RBS) to obtain least informative depth profiles and the respective reliabilities. The computer code for RBS was considerably extended for multiple constituents and varying layer thicknesses. Erosion and redeposition rates of carbon divertor plates in ASDEX Upgrade are determined from thin-film $^{13}C/^{12}C$ probes after plasma exposition (see 1.4.3).

TECHNOLOGY DIVISION

(Prof. Dr. Rolf Wilhelm)

The Technology Divison of IPP is concerned with the technical development and operation of the three plasma heating systems Neutral Beam Injection (NBI), Ion Cyclotron Heating (ICRH), and Electron Cyclotron Heating (ECRH), for the ASDEX Upgrade tokamak (NBI, ICRH, and ECRH) and W7-AS stellarator (NBI and ICRH) experiments. Another task is to plan and develop the heating systems for the W7-X stellarator (NBI and ICRH) and to study and develop the heating and - specifically - current drive systems for the future tokamak programme at IPP (NBI including high-energy injection based on negative ion technology, ICRH/fast wave current drive, and ECRH/ECCD).

For more detailed information the reader is referred to the respective sections of this report. In the following section you find some additional information on specific technical developments and theoretical work.

1. NEUTRAL INJECTION HEATING

NI Group

1.1 Development of a RF Negative Ion Source

The potential of the large-area RF ion sources developed at IPP for future negative ion-based injection systems is explored in the frame of a collaboration between CEA Cadarache and IPP Garching.

As a first step an ASDEX Upgrade type plasma source (type II) without magnetic electron confinement was combined with a small-size (70 cm^2) negative ion extraction system. Substantial H^--current densities have been extracted from this RF source, but at source pressure levels which are far too high for negative ion beam acceleration systems.

To explore RF source performances at lower pressures, two different types of RF sources with magnetic confinement were constructed and operated in 1998:

One source uses a quartz-insulated antenna immersed in a PINI bucket chamber with checkerboard magnet configuration (type V). From this source positive ion beams were extracted as a diagnostic for plasma production. The results show a significant increase of the source efficiency at low pressures compared with the ASDEX Upgrade type RF source. Langmuir probe measurements demonstrate the effectiveness of a magnetic "tent" filter in reducing the electron temperature within the extraction region. For negative ion extraction experiments the PINI bucket chamber will be replaced by a "long-source" body with modified magnetic confinement on loan from JET. The enlarged distance between the RF coil and extraction grid minimises the undesired heating of the plasma in this region.

A second RF source (type VI) is based on a design which appears particularly suited to extrapolation to larger areas and long-pulse operation, as envisaged in future devices: A quartz or Al_2O_3 cylinder mounted on the rear wall of a bucket chamber supports a RF coil which operates at atmospheric pressure (Fig. 1). In preliminary experiments for extracting H^- ions the source could be operated with high RF power at pressures as low as 0.2 pascal and provides H^--current densities as high as those achieved with the ASDEX Upgrade type source at much higher pressures only (Fig. 2).

To demonstrate the uniformity of the negative ion extraction from a RF source plasma, a large-area extraction system was designed and manufactured. For reasons of economy, an existing triode PINI extraction system for positive ions was modified and only the decel grid is replaced by a new water-cooled extraction grid with integrated magnets for electron suppression (Fig. 3). The design is based on 3D electron and ion trajectory calculations which predict a beamlet divergence of 7.5 mrad at optimum perveance and a low electron leakage of 2%.

Negative ion beam extraction experiments using Cs seeding of the sources to increase the H^--current densities and first experiments with the new large-area grid system are planned for 1999.

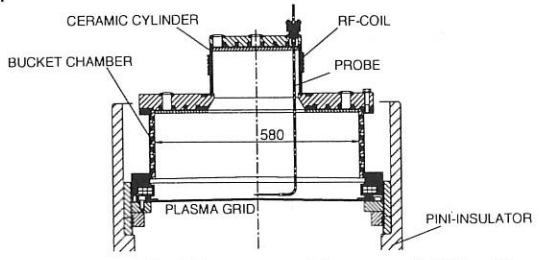

FIG. 1 Type VI RF source with external RF coil.

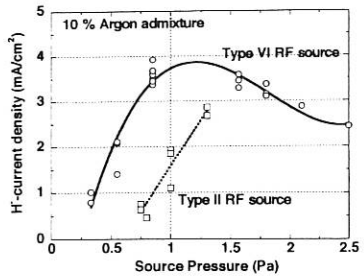

FIG. 2 *Extracted H⁻-current densities for ASDEX Upgrade (type II) and the type VI RF sources.*

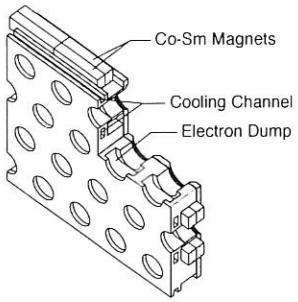

FIG. 3 *Design of the water-cooled extraction grid for the negative ion acceleration system.*

2. ION CYCLOTRON RESONANCE HEATING

ICRH Group

The development of a 3 dB hybrid circuitry proved very successful during the 1998 experiments of ASDEX Upgrade: After the 4 generators and antennas had been combined to two double systems by 3 dB hybrids in 1997 by decoupling the generators from the varying antenna load impedances, the heating power could be appreciably increased to a maximum above 6 MW. Even varying plasmas and ELMy H-modes could routinely be heated with high reliability and powers of 4 to 5 MW.

With a view to the future programmes of ASDEX Upgrade the antennas were modified, now allowing more freedom for triangular plasma shapes, and a circuit modification was developed for current drive utilising the phasing between the hybrid outputs for the required phase between the antenna straps [305]. This system modification is planned in 1999.

At W7-AS a double-strap antenna was installed. A comparison with the broad antenna used hitherto is to show the influence of different antenna types, especially of their wave spectrum, on the heating characteristics in the stellarator.

3. ECRH ON ASDEX UPGRADE

ECRH Group (AUG)
(in cooperation with IPF Stuttgart)

Information about the status of construction of the ECRH system and about experimental results can be found in the ASDEX Upgrade section of this report.

3.1 Nonlinear Effects on Electron Cyclotron Wave Absorption

The gyrotron power for ECRH in ASDEX Upgrade is 500 kW per unit, focused on a few square centimetres. Absorption thus has to be calculated taking nonlinear effects into account.

The main nonlinear effect on the electron trajectory is the dependence of the cyclotron frequency on the relativistic mass. Resonant electrons, which are accelerated or slowed down, depending on their phase when entering the microwave beam, experience a detuning of the microwave and electron cyclotron frequencies. Finally the electrons undergo trapping oscillations in velocity space, not being able to absorb or deliver any power any longer. Best power absorption, averaged over the initial phase, is achieved for electrons having velocities slightly below resonant because they are accelerated into resonance on their way through the beam. On the other hand, electrons with velocities above resonant reveal a phase-averaged energy loss. The result is a strong reduction of the power absorbed by electrons fulfilling exactly the quasilinear resonance condition.

For 500 kW focused on a few square centimetres, the reduction of peak absorption by resonant electrons is more than one order of magnitude. However, the resonance condition in velocity space is broadened and therefore the velocity space integrated local power absorption is only reduced by 25%. Since the optical depth for the X2-mode is large, the power is still fully absorbed, but the place of absorption is shifted by a few millimetres to the high-field side for low-field side launch.

These calculations were made for perpendicular incidence where only electrons with small velocities parallel to the magnetic field are involved. They are most afflicted due to their long stay in the microwave beam. Electrons with high parallel velocities are involved in current drive scenarios where $k_{\parallel} \neq 0$. They have much shorter interaction times, and therefore even higher powers are needed for the nonlinear reduction of absorption. The only exception may be a scenario, where the microwave has a vanishing perpendicular refractive index at the resonance zone. Here, even electrons with a high parallel velocity stay in the beam quite long, possibly giving rise to nonlinear effects.

4. THEORETICAL WORK: ENHANCED IMPURITY AND ALPHA-PARTICLE TRANSPORT VIA KIRCHHOFF RADIATION

S. Puri

Since for the high-frequency Bernstein waves responsible for radiative collisionality, the product of frequency and plasma parameter greatly exceeds the two-particle collision frequency, the expansion procedure in terms of the plasma parameter used in the Balescu-Lenard type of equations is not applicable. Thus, Kirchhoff's law is the only presently available method for determining radiative collisionality. The previous results are now being extended to include multiple ion species with a view to studying the effect of radiation on alpha-particle and impurity transport. Initial study indicates the possibility of efficient ash removal due to anomalously enhanced radiative collisions between alpha-particles and electrons.

PLASMA TECHNOLOGY

(Prof. Dr. Dr. h.c. Volker Dose

Prof. Dr. Rolf Wilhelm)

The Plasma Technology group is concerned with three tasks: Surface coatings are produced by means of plasma chemical vapour deposition (PCVD) for special applications, mainly in fusion plasma devices. New or improved PCVD procedures or devices are being developed for this purpose. As the scientific part of the activity, plasma, plasma edge, and thin-film diagnostics are employed in order to correlate the discharge parameters with the properties of the resulting coatings and improve understanding of the basic mechanisms of plasma deposition. The third goal is modelling of the deposition process which allows the discharge conditions to be adjusted in a predictable way in order to optimise a desired property of the growing film.

In 1998, main activities were in-situ characterisation of the growth and etching of hydrogenated carbon films, modelling of the composition of the ion flux from a methane ECR plasma, and development and characterisation of a neutral beam source for hydrocarbon radicals.

V. Dose (Division Head)[1], C. Hopf[5], W. Jacob[1], G. Kerkloh[3], A. von Keudell[1], B. Landkammer[1], V. Milosavljevic[4], P. Pecher[1], T. Schwarz-Selinger[1], S. Vasquez-Borucki[4], R. Wilhelm (Division Head)[2].

1 Surface Physics Division
2 Technology Division
3 Technical Staff
4 DAAD Scholar
5 Undergraduate Student

1. IN-SITU PLASMA DIAGNOSTICS Charged and Neutral Particle Fluxes from a Methane ECR Plasma

A comprehensive, quantitative study of the particle fluxes impinging on the substrate in an ECR methane plasma has been conducted for the past few years. In collaboration with Ernst-Moritz-Arndt University, Greifswald, the heat flux onto the substrate in methane, hydrogen, and argon electron cyclotron resonance discharges was measured under conditions comparable to those of the preceding mass spectrometric study. First analyses indicate that the measured heat fluxes seem to be dominated by the energy flux due to the impinging ion currents.

Experimental results in the past have shown the outstanding importance of ion-molecule reactions for the composition of the ion flux to the substrate surface. In methane discharges the ion flux above pressures of about 0.5 Pa is dominated by molecular ions which are formed by ion-molecule reactions in the bulk plasma. On the basis of these experimental results, an effort was started to calculate the electron temperature in a methane plasma from mass spectrometric measurements of the composition of the ion flux by applying Bayesian probability theory. Electron temperatures are estimated on the basis of a comparison of experimental results with modelling results for the composition of the ion flux emanating from hydrogen and methane electron cyclotron resonance plasmas. A prerequisite for such a procedure is a sound data base for the electron-impact ionisation cross-sections required for the model calculations. However, published data of such cross-section data differ significantly. A general method was developed to treat different data sets consistently and deduce analytical fit functions with the correct asymptotic behaviour in a mathematically correct manner. It was used to calculate simple and asymptotically correct analytical fit functions for partial ionisation cross-sections and rate coefficients for methane and hydrogen. These fits agree much better with the available data than previously published fits. Fits for dissociative ionisation cross-sections leading to strong fragmentation of methane (e.g. from CH_4 to CH_2^+, CH^+, C^+, and H^+) were determined for the first time.

2. THIN FILM DEPOSITION AND EROSION
Glow Discharge Removal of C:H Films

In-situ investigation of erosion of plasma-deposited hydrogenated carbon (H:C) films by ECR oxygen plasmas was continued. The measurements in 1997 had shown that energetic ions play an important role in the erosion process, but it remained unclear whether it is the chemical nature of the ions or simply the fact that they impinge with substantial kinetic energy that is relevant. To address this question, we measured the erosion in a mixture of oxygen with about 12% of the noble gases helium, argon, and krypton. In addition, we determined the ion energy distributions (IEDs) and the composition of the ion fluxes for these mixtures.

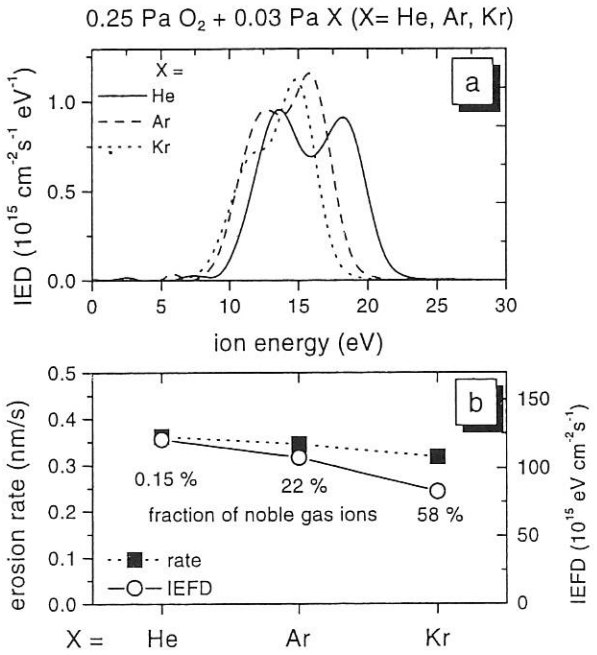

FIG.1: a) Mass-integrated ion energy distributions (IEDs) for ECR oxygen plasmas with a slight admixture of a noble gas (He, Ar, or Kr).
b) Erosion rates (solid squares), fraction of noble gas ions (indicated by the percentage numbers close to the symbols), and deposited ion energy flux density (IEFD) (blank circles).

We found no substantial difference in the IEDs for the three mixtures; only for helium the IED shifts slightly to higher energies due to the higher ionisation potential of helium (see Fig. 1a). While the total ion flux density is very similar in these mixtures, the relative composition of the ion flux differs markedly. In the mixture with helium only 0.15% of the incoming ions are helium ions, the rest being oxygen ions (about 70% O_2^+ and 30% O^+). In the mixture with argon and krypton the fraction of noble gas ions rises to 22% and 58%, respectively (see Fig. 1b). Although the composition of the ion flux varies that much, the erosion rates of hard amorphous hydrogenated carbon films (a-C:H) show no big difference for the three plasma conditions (see Fig. 1b). The erosion rate is correlated rather to the energy deposition due to ions. This is demonstrated in Fig. 1b and is further corroborated by a number of parameter studies. These results indicate that the chemical nature of the ions is of minor importance for the erosion process and that in oxygen-containing plasmas both neutral oxygen atoms and oxygen ions are involved in the erosion of a-C:H films.

3. BASIC STUDIES OF THIN FILM DEPOSITION PROCESSES

Since the foundation of the Plasma Technology group, investigations of basic processes of the deposition of amorphous hydrogenated carbon films have been at the centre of interest. One aspect of this work is the question of the contribution of neutral radicals to film formation. For a future study of the deposition process a particle beam source was developed which is capable of producing thermal beams of neutral hydrocarbon radicals. The radicals are produced in a resistively heated tungsten capillary due to thermal dissociation at the hot walls of the capillary. The maximum temperature of the capillary achievable in our set-up is around 2100 K, which is sufficient to produce also atomic hydrogen from H_2.

First investigations performed with rare gases and hydrogen dealt with the process of dissociation and beam formation in such a hot capillary. As experimental set-up, a rotatable (±20°) quadrupole mass spectrometer in line of sight with the capillary exit was applied which allows one to identify the emitted species and their angular distributions. First experiments with methane as hydrocarbon source gas showed that it is possible to produce thermal neutral-particle beams consisting purely of methyl radicals and methane and hydrogen molecules at a capillary temperature of 1700 K without any contribution of other radicals. The obtained dissociation degree of 5% corresponds to a methyl radical flux density of 10^{16} radicals/(s cm^2) 5 cm from the source exit.

4. GAS PERMEATION THROUGH COATED POLYMERS

In collaboration with the Federal University of Rio de Janeiro (funded by DAAD), we investigated the influence of amorphous hydrogenated carbon (a-C:H) coatings on the permeation of various gases through commercial polymers. The a-C:H layers are deposited in an RF gas discharge using a variety of hydrocarbon source gases under different deposition conditions. So far, most experiments have been carried out with PET (poly-ethylene-therephtalate) foils as substrate and methane and acetylene as precursor gases. a-C:H layers with widely varying density were deposited and in all cases a significant decrease of the permeation coefficient was found. Detailed studies of the dependence of permeation reduction on the structure and density of the a-C:H layers are in progress.

PLASMA DIAGNOSTICS DIVISION

(Head of Division: Prof. Dr. G. Fussmann)

The Plasma Diagnostics Division is part of the Greifswald Branch of IPP; its activities in Berlin are increasingly concentrated on work relating to the WENDELSTEIN 7-X project. Other research activities comprise experimental and theoretical investigations in Berlin (PSI plasma generator, UHV laboratory, electron beam ion trap (EBIT) experiment, analytical and computational studies of edge physics problems) and the ASDEX Upgrade and WENDELSTEIN 7-AS fusion experiments at Garching. Those activities involving close collaboration with the fusion projects at Garching and Greifswald are included in the respective sections of this report.

P. Bachmann, C. Biedermann, W. Bohmeyer, T. Fuchs, D. Hildebrandt, B. Jüttner[1], H. Kastelewicz[1], S. Klose, P. Kornejew, M. Laux, D. Naujoks, R. Radtke, H.D. Reiner, J. Sachtleben, A. Stareprawo, D. Sünder, K. Uludag, U. Wenzel.

1 Humboldt-University, Berlin

1. PSI PLASMA GENERATOR

In 1998, the activities of the PSI group were concentrated on two topics: investigation of carbon fibre composites in contact with hydrogen/deuterium plasmas and study of instabilities and fluctuations in the PSI plasma. In addition, the PSI-1 plasma generator was upgraded (PSI-2) for both better homogeneity of the magnetic field and higher power and particle flux densities. For the work on chemical erosion of carbon fibre composites, the reader is referred to the respective ITER section. Only the results of the analysis of the rotating modes observed in the PSI plasma generator are presented here.

The plasma in the generator is actually a hollow cylinder, with steep radial gradients in the electron/ion pressure profile. At the position where the pressure gradient is at maximum, an extensive spectrum of rotating modes is observed. For discharges in krypton, for example, there is a drift mode exhibiting a pentagonal shape (strong m = 5 mode) and rotating with a frequency of about 12 kHz. This particular mode was analyzed using optical methods and electric probes. The following results were obtained:

(i) The turbulent fluctuations originate from plasma instabilities, and there is a clear correlation between the optical emission pattern and the azimuthal electron-density distribution. The electron-drift wave modulates the optical emission of both neutrals and ions.

(ii) The spectrum of the turbulent fluctuation modes changes if different ions (different masses) are involved in this process. Ions with small masses (e.g. H^+, D^+, and He^+) produce spectra where the fluctuation power is distributed over a wide range of frequency values. In contrast, heavy ions (e.g. Ar^+, Kr^+, and Xe^+) exhibit a substantially smaller power spectrum

(iii) The onset of the drift instability is characterized by a critical value for the speed of the rotating plasma particles. Measurements revealed that this rotation velocity is proportional to the **j** x **B** forces occurring in the anode-cathode region. Further observation showed that the onset of the drift instability takes places under conditions where the product of the magnetic field strength and the anode-cathode current is constant (Fig. 1).

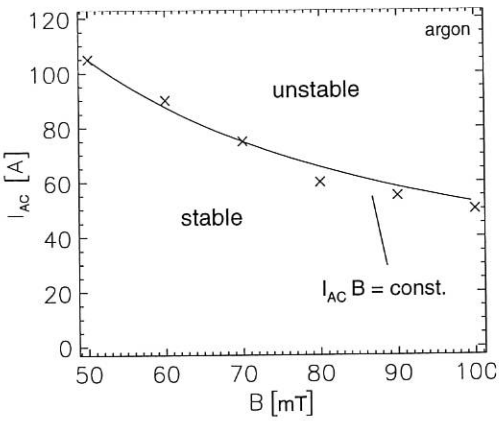

FIG. 1: Dependence of the onset of the drift instability on the magnetic field strength B and anode-cathode current I_{AC} for a discharge in argon.

2. ELECTRON BEAM ION TRAP (EBIT)

One major topic of investigations at EBIT is X-ray spectroscopic measurements of highly charged ions. The radiation produced by highly charged ions is an important issue. For example, it can be used in tokamak plasmas to provide radiative cooling of the edge region and/or is of importance as a diagnostic tool to determine ion temperatures. It is therefore desirable to acquire accurate atomic physics data to establish a quantitative method of measuring high-Z impurities in fusion plasmas and support modelling calculations.

In 1998, investigation of channel-specific dielectronic recombination (DR) of highly charged krypton (in cooperation with the Racah Institute of Physics, Jerusalem) was successfully accomplished. In particular, DR cross-sections were obtained for the KLL, KLM, KLN, and KLO resonances of krypton in helium-, lithium- and beryllium-like charge states. In another experiment, the radiative cooling rates of highly charged krypton ions were measured. The appropriate technique for observing the radiation from the ions in EBIT is to create a particular ion population at one energy and then probe the ions by fast scans of the beam energy. We focused on producing an ion population approaching the ionization balance of a plasma at an electron temperature (T_e) of about 5 keV. The preselected ion population was then sampled by linear sweeps of the beam energy extending from about 1 to 25 keV. The radiative cooling rates were determined by measuring the X-ray emission as a function of both the beam energy and

X-ray energy, normalizing the measurements relative to the intensity of photons from radiative recombination, generating spectra of X-ray intensity versus beam energy for the different radiation processes and taking the Maxwellian average corresponding to the value specified for T_e. Unlike experiments on plasma devices, the EBIT measurement can distinguish between the different radiation channels that contribute to the cooling rates. The measured rates are consistent with calculated values within a factor of two.

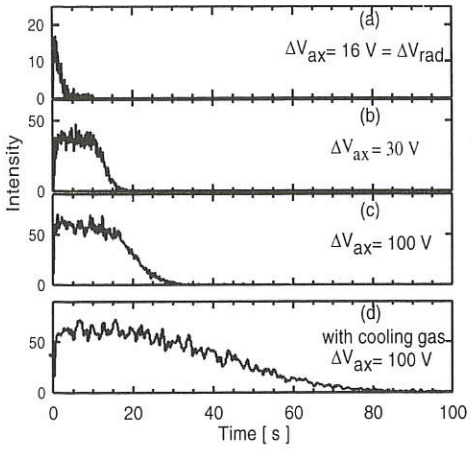

FIG. 2: Evolution of the helium-like Mo^{40+}-ion population in EBIT.

Another topic of investigation is the confinement of ions in EBIT. This information is of special importance for spectroscopy experiments using the ions in EBIT itself, but also for extraction experiments. To look into the confinement of highly charged ions, the characteristic X-ray radiation emitted from trapped Mo^{40+} ions was measured as a function of time after injecting low-charged ions from an external source. Figure 2 shows such a trace of the evolution of helium-like Mo^{40+} for different trapping parameters. The ions are trapped radially by the space charge of the electron beam; axial trapping is provided by the positively biased end-drift tubes of the trap. In (a) a situation is shown where the axial and radial trapping potentials are of equal magnitude. The ions are heated by electron collisions and are lost by axial escape even before the charge-state balance has reached equilibrium. By raising the axial potential (b, c), the intensity of the Mo^{40+} ions increases and levels to a plateau. Nevertheless, the ions are heated and can aquire sufficient energy to surmount the axial trapping potential and escape from the trap. The effect of evaporative cooling, which is essential for producing the highest charge states, is indicated in (d). Here, nitrogen gas is continuously blown into the trap prolonging the storage by a factor of two compared with the case without cooling gas. Modelling of the evolution of the highly charged ions in EBIT has been tried with a variety of computer models. So far, however, only some features within the first few seconds can be correctly predicted. The observed confinement times and sudden vanishing of the ion population could not be explained with the model.

3. UHV LABORATORY

In the UHV laboratory studies were made of fine-grained, isotropic graphite using surface analysis techniques as well as optical surface profilometry. The samples were used as divertor target tiles in ASDEX Upgrade or employed as collector probes and exposed to the plasmas of ASDEX Upgrade, TEXTOR-94, and the PSI-1 facilities. The results of the analyses show that processes such as chemical erosion and particle sputtering leave nonuniform structures on the samples after plasma exposure. It appears that this effect is correlated with the surface morphology of the samples, making preferential erosion possible in regions where the surface constituents have a lower surface-binding energy. The effect is indicated in Fig. 3, showing the surface profile for a sample taken before and after exposure in the PSI plasma generator. Samples with coatings do not exhibit such a high surface roughness after plasma exposure.

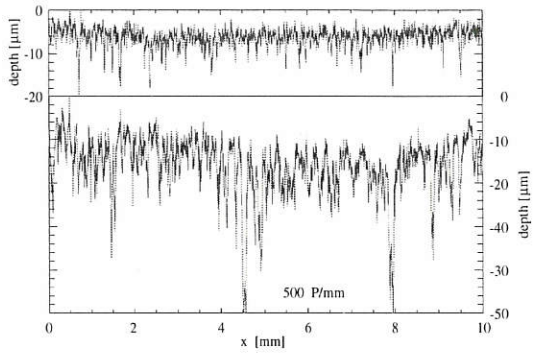

FIG. 3: Surface profile of graphite (EK 98) before (top) and after (bottom) plasma exposure. Plasma fluence: $5 \cdot 10^{25}$ D ions per m^2.

4. THEORY AND MODELLING

The activities of the theory and plasma modelling group comprise the following topics:

(i) Bifurcation of temperature profiles in 3-D plasma equilibria. Starting with the three-dimensional heat conduction equation, Marfe formation and bifurcation of the temperature profiles in stellarators were analyzed. In addition, the one-dimensional problem was treated for special cases (slab and cylinder geometry).

(ii) B2-EIRENE modelling calculations. The modelling calculations include density scans for discharges in ASDEX Upgrade and parameter analyses (temperature and density profiles) for the PSI plasma generator.

(iii) Reaction-diffusion processes in impurity-seeded plasmas. Within the framework of the average ion model, a reaction-diffusion equation was derived for the plasma temperature. The impurities take part in the reaction-diffusion process via heat conduction and radiation. The equations were used to model impurity (carbon, beryllium) -seeded plasmas.

(iv) Modelling of U-I characteristics. On the basis of a model for the energy and particle balance, the U-I characteristic of the PSI plasma generator was calculated. The results for argon and helium can reproduce the main features of measured characteristics. An upper limit for the electron temperature is predicted by the model, depending on the neutral gas density, ionization potential, and ion mass.

COMPUTER SCIENCE DIVISION

(Prof. Dr. Friedrich Hertweck)

F. Hertweck, H. Friedrich, P. Heimann, J. Maier, M.-G. Pacco-Düchs, U. Schneider-Maxon, D. Stolz, Ch. Tichmann, R. Tisma (until June), M. Zilker

Part of the activities of the division closely relate to ASDEX Upgrade: the further development and enhancement of hardware and system software for SoftXray, Mirnov and other diagnostics and maintenance of the AMOS/D data acquisition system. Another important area is parallel processing. It is being pursued along several lines: design of a new generation of parallel computers for data acquisition, development of new and porting of existing algorithms to the Cray T3E, and study of neural algorithms.

1. AMOS/D

Part of the work on AMOS/D is described in the section on ASDEX Upgrade data processing.

1.1 Dependence Data Base

The Dependence Data Base DDB, indicating the interdependence of ASDEX Upgrade shotfile data, is being regularly used and the number of entries is continually growing: there are 67840 entries in the EDTABLE, 180992 entries in the PREDecessor table, and 296960 entries in the SUCCessor table. The new version implemented last year is very stable.

1.2 Design of a new generation of high-speed/ high-volume data acquisition systems

The very long plasma discharges expected in W7-X and also the growing needs of ASDEX Upgrade call for a new generation of data acquisition systems capable of handling high-volume data streams in real-time (typically a few hundred signals in diagnostics like Mirnov or SoftXray, sampled at rates of a few MHz). This also requires high CPU power to do the analysis. Normally, the I/O bandwidth of a processor is limited and it will therefore be necessary to develop parallel systems that are able to cope with the high influx of data.

The hardware will be built from available components, such as ultraSPARC CPUs and interconnection components, such as the SCI (Scalable Coherent Interface). For the latter, a thorough analysis was performed as to its suitablity and performance.

The design, building and testing of the input boards for a PCI computer system was completed. It permits the input of four 4 Mbyte/s data streams per board.

2. PARALLEL COMPUTING ON THE T3E

All the work on parallel programs was done in close cooperation with the owners/users of the programs. A very successful workshop was organized to exchange experience between the users of the T3E.

2.1 The Module MPPenvironment

A Fortran 90 module **`MPPenvionment`** was developed to permit the user an easy access to the functionality of a parallel computer. The program exists in two versions: one Cray T3E specific which uses the shared memory library of

the system, and another which uses the standard MPI (Message Passing Interface) library available on various parallel computers. The code was tested on both the Cray T3E and an IBM SP2, and a timing analysis was done.

2.2 The TRIDYN Monte Carlo Code

The new version of the TRIDYN code (W. Eckstein) which has been parallelized for the Cray T3E was generalized to include both a version for sequential processing on workstations and the parallel version for the Cray T3E. The parallel version was supplied with a special random number generator for program development. It permits TRIDYN to run with identical results independent of the number on processors of the T3E. This random number generator will produce reasonably good random numbers for testing; it is replaced with another generator for production runs where each processor produces ist own disjoint sequence of random numbers.

2.3 Parallelizing codes for the T3E

Two codes existing in sequential or vector versions were parallelized for the Cray T3E (codes EMHD2D, and B5). For both codes the domain decomposition method was successfully applied and in the kernels of the programs the 1d or 2d FFT routines of the Cray library were used.

2.4 Emulation of 128bit Floating Point Numbers on the T3E

Using some existing software for Alpha Workstations as a model, a Fortran 90 module was developed which offers all the standard functions needed for this data type. The performance is as expected.

3. NEURAL NETWORK COMPUTING

After installation of the T3E, this machine became our preferred platform for the development of neural algorithms. A standard backpropagation code (the version of K. Kutzka) was translated into Fortran 90 and parallelized. This permits very efficient training of the neural network. The algorithms were applied to the study of ASDEX Upgrade data with the goal of detecting oncoming disruptions. So far, very promising results were obtained. (For more information, see the chapter on ASDEX Upgrade.)

4. DATA PROCESSING INFRASTRUCTURE

4.1 Conceptual design for an IPP Workstation Environment

In the past few years, a transition from mainframe computing towards powerful UNIX workstations has taken place at IPP. At the same time, more and more personal computers (IBM compatibles and Apple Macintosh) were introduced. Originally mostly intended for word processing, they can be used today for a wide range of applications that used to run on workstations. At the moment there are about equal numbers of workstations and PCs, with the number of PCs growing faster.

In collaboration with the Computing Center RZG, several servers have been installed, interconnecting the workstations and the PCs, to permit centralized management of both hardware and software. A PC service team was established which is responsible for the configuration, the installation and the operation of the NT 4.0 servers.

4.2 Data Processing for Experiments

With the Wendelstein W7X Experiment being built in Greifswald and the continuing demands by ASDEX Upgrade, a new task force was established to look into the future requirements of both experiments in the light of present technological (both, hardware and software) possibilities of data processing.

The first steps were to evaluate present systems of other laboratories (MDS at MIT, also used for a tokamak experiment, and the RD24 project at CERN using an object-oriented data base system), and to study the feasibility of using object-oriented design tools for W7X, including Java and Corba. A first catalog of requirements for W7X was compiled.

GARCHING COMPUTER CENTRE (RZG)

(Head: Stefan Heinzel)

RZG traditionally provides supercomputing power and archival services for IPP and other Max Planck Institutes throughout Germany. Besides operation of the systems, application support is given to Max Planck Institutes with high-end computing needs in fusion research, material science, astrophysics, and other fields. Large experiment data from the fusion experiments of IPP (ASDEX Upgrade, Wendelstein 7-AS, and, later, Wendelstein 7-X), satellite data of MPI of Extraterrestrical Physics (MPE) at the Garching site, and data from supercomputer simulations are administered and stored with high life times. In addition, RZG provides network and standard services for IPP and part of the other MPIs at the Garching site.

A. Altbauer, G. Bacmeister, J. Cox, R. Dohmen, K. Desinger, S. Gross, A. Hackl, M. Heigl (till 9/98), S. Heinzel, K. Lehnberger, H. Lederer, P. Lorrig, G. Mahl, W. Nagel, M. Panea-Doblado, P. Pflüger, Jakob Pichlmeier *, F. Pirker, A. Porter-Sborowski, H. Reuter, H.-G. Schätzko, R. Schmid, J. Schmidt, A. Schott, K. v. Sengbusch, H. Soenke, U. Schwenn, R. Tisma (since 4/98), I. Weidl, V. Weinert

* from SGI Deutschland GmbH

1. MAJOR HARDWARE CHANGES

The Cray T3E massively parallel system was upgraded by 96 processors to 816 processors and a total of 102 GB main memory. The Cray J916 vector system was replaced by a NEC SX-4B vector system with 2 processors and 4 GB main memory. The IBM SP2 general-purpose compute was extended by 2 nodes to 20 nodes and 17 GB main memory. The 8-processor SGI Origin 2000 system at RZG of MPI of Astronomy was upgraded from 2 to 4 GB main memory. The Cray EL archive server was replaced by a SGI Origin system. The number of Redwood tape drives of the attached STK robot system was increased from 4 to 8.

2. DATA MANAGEMENT

2.1 Developments in Multiple-Resident-AFS

Extension of the AFS cell to remote sites such as Greifswald and Berlin required modifications to the AFS database concept. In case the network connection between Garching and the remote sites gets lost, these sites still have access to the data stored on local AFS fileservers by means of a local copy of the databases.

2.2 Pseudo-AFS Client for the T3E System

As no native AFS client is available for the Cray T3E system, a pseudo-AFS client was developed for T3E users which allows files to be copied from and into AFS.

2.3 User-hidden Data Migration to a New HSM System

At the beginning of the year the migration of data from the old archive server (Cray-EL with D2 tapes in the Grau/Emass silo) to the new archive server (SGI Origin 2000 with Redwood tapes in the STK silo) started. First the files belonging to MR-AFS were transferred by a technique which made this transfer invisible to the users. This took 4 months. In a second step files archived with the "arc" command were transferred. The "arc" command had been modified to allow the user to access files in the new or old archive server transparently.

3. PARALLEL COMPUTING

3.1 Code Parallelization and Optimization

General problems and tasks include: use of optimized library routines to improve single-processor performance of some codes and I/O optimization of production jobs with huge restart files. Outstanding projects to support new

developments and code extensions are described in detail below.

3.1.1 *Cosmology: HYDRA*

The HYDRA sequential code for cosmological simulations was parallelized and optimized at RGZ for highly economical memory usage to enable very large-scale simulations, and was brought to production state /183/. The code consists primarily of a particle-particle computation parallelized by domain decomposition over blocks of neighbour-cells, a more regular mesh calculation distributed in planes along one dimension, and several transformations between the two distributions. With the parallel version of the code, the VIRGO consortium under coordination of Simon White (MPI of Astrophysics) undertook the hitherto largest simulations of the development of the mass distribution of the complete observable universe (Science 280 (1998) p. 1522). Data management was a challenge since almost one TB of data was produced per simulation.

3.1.2 *Fusion research*

3.1.2.1 *Turbulence codes*

The KINEM fortran code to study the effect of kinetic drift wave turbulences on anomalous transport phenomena was restructured. The parallelization over two space dimensions was extended to include the 3rd dimension. The exchange of border cells was optimized, and the load balance within the FFT was improved. The new code now allows for efficient use of up to 256 processors and study of problems with 20 GB of memory requirement.

Two further serial turbulence codes, EMH2D and B5, were parallelized by domain decomposition and implementation of a parallel FFT.

3.1.2.2 *Surface physics*

For the two codes, TRIM.sp and TRIDYN improvements and extensions to allow application to a new class of problems were made.

3.1.3 *Material sciences: LAPW*

The LAPW (Linearized Augmented Plane Wave calculations) code plays an important role for electronic structure calculations in material research. Though it is very effective on vector processors, only a serial version of the code is available so far, this being a severe obstacle for applying it to problems that can only be solved with the resources of a massively parallel computer.

The code package consists of 3 different parts: LAPW0 computes the total potential from the total electron density as input. LAPW1 sets up the Hamiltonian and generates eigenvalues and eigenvectors and is the most cpu-consuming part. LAPW2 computes the Fermi energy and the expansions of the electronic charge densities.

In a first step, the cpu-intensive calculation part LAPW1 was parallelized explicitly with message passing. Good scalability and performance were achieved up to 64 T3E processors. By exploiting the embarrassing parallelism over the so-called k-points (typically 8 - 16), 256 T3E PEs can be used with the 4-fold performance of 64 PEs. The ongoing work is now focusing on LAPW0 and LAPW2 and their integration, since efficient parallelism of these parts determines the overall performance.

3.1.4 *Gravitational research: CACTUS*

The CACTUS code of the Albert Einstein Institute in Potsdam is used for production runs on 512 T3E PEs to simulate gravitational waves by solving the complex set of Einstein equations. A severe problem of the highly-efficient parallel code is the large amount of I/O with up to 10 GB of output per hour. The I/O parts of the code were therefore analyzed and modifications suggested to the developers to better benefit from the T3E hardware setup to improve the ratio of calculation times to I/O times.

3.2 PC Cluster Evaluation for Embarrassingly Parallel Applications

The Cray T3E system is heavily loaded, but not all applications that run efficiently there require the fast communication network. Those applications could be shifted to a significantly cheaper cluster of Intel-based personal computers (PCs) with standard network. To test this option, two embarrassingly parallel Fortran 90 codes were ported to a 4-node PC cluster (235-MHz Intel-Pentium II processors with fast Ethernet connection) with LINUX operating system, AFS-client, GNU software, Fortran 90 compilers from NAG and Portland Group, and MPI communication library mpich.

The TRVMC (IPP) and SKYMOS (MPE) codes were first ported from Cray-specific communication calls to MPI, then compared on up to 4 PEs on both systems. For TRVMC, the PC cluster performance was half that of the T3E, independently of the number of nodes. SKYMOS was run on 4 PEs with two data sets, requiring little (0.4%) or high (4%) communication (in fractions of the total execution time). The PC cluster performance degradation relative to T3E was a factor of 2.2 (for 0.4% communication) and 3.6 (for 4% communication). For a broadcast on T3E 163.5 MByte/s were measured, 3.3 MByte/s on the PC cluster. As the T3E communication network is a factor of 50 superior to fast Ethernet (600 MByte/s compared with 100 Mbit/s), the performance degradation on the PC cluster is estimated as

$$\text{T3E perf / pc cluster perf.} = 2 * (1\text{-}c) + 50*c,$$

with c as communication fraction of the execution time. As result, the installation of a production PC cluster did not yet seem to be attractive, due to the performance achieved, the additional maintenance effort, and the lack of quality of the Fortran 90 compilers. But the price-performance ratio and the compiler quality will improve in time.

4. VECTOR COMPUTING

With the replacement of the Cray/SGI J916 system by the NEC SX-4B system, support for code migration especially in the fields of a) library routines and b) data format representation (with the transition from Cray to IEEE format) was given.

5. VISUALIZATION

5.1 Graphical User Interface for W7-AS Diagnostic Routine

A graphical user interface (GUI) was designed and implemented for flexible steering of an existing diagnostic evaluation routine at the W7-AS fusion experiment.

5.2 Interface for Remote Online Visualization

Initial implementations of a TCP/IP-based interface for remote online visualization of parallel alignment of 3D structures of biological macromolecules on the T3E system were done.

6. VIDEO CONFERENCING

Technology evaluations and tests for the various communication needs between IPP-Garching and IPP-Greifswald were carried out. Requirements are as follows: a) joint sessions of the Scientific Directors, b) connection of the two lecture halls in building D2 at Garching and (currently) the Biotechnikum at Greifswald, c) person-to-person connections with personal computers and/or workstations.
The solutions envisaged so far are: a) will be realized using PictureTel Venue2000 Model 50 systems, having proven to be superior to alternative solutions; b) has already been realized with a B-Win network connection, using Powerpoint from MS Office for simultaneous viewgraph presentations and MBone for video/audio transmissions in a symmetric configuration, but allowing multipoint sessions; c) MBone, Netmeeting and SunVideo software packages have been tested. Recommendations depend on the specific requirements and are available on request.

7. DEVELOPMENTS IN NETWORKING

One of the prerequisites for efficient computer-based research is the availability of powerful and reliable data transmission paths. RZG has therefore to provide and keep up to date an appropriate local networking infrastructure (LAN) at the Garching site as well as international connectivity (WAN). With growing needs, the currently installed LAN components based on standard Ethernet, FDDI and fast Ethernet need to be replaced by modern cabling technology (fibre to the desk) and networking techniques (Gigabit Ethernet, ATM). Bottlenecks within the active components have to be identified and eliminated, and therefore planning to replace the majority of the routers by state-of-the-art switches with IP-forwarding capabilities has started and is in progress. With bandwidth improvements of the German Research Network (B-WiN) for national and international connectivity, the necessary adaptations of the local interface infrastructure were configured.

8. PILOT PROJECTS FOR THE NEXT GENERATION GERMAN SCIENCE NETWORK

So-called Gigabit Testbeds funded by the German government were implemented to run pilot projects for the next-generation German science network. In the testbed between Munich, Erlangen, and Berlin RZG contributes to all 4 funded projects in the area of visual supercomputing and metacomputing /586/. For the first project of MPI of Biochemistry in collaboration with Leibniz-Rechenzentrum and RZG, in a first step support was given to port the EM code package to the Cray T3E system, and optimizations were done by replacing user routines by more efficient library routines.

9. EVENTS

The RZG organized and hosted at IPP the 4th European Cray/SGI MPP workshop from Sep 10 to 1, which addressed computer scientists, computer engineers, and end users in application development and optimization on predominantly European Cray T3E and large Origin 2000 systems The application orientation of this event with 26 oral presentations and around 100 participants deserves to be emphasized /49/151/584/. The proceedings were published as IPP Report /IPP/R46/.

CENTRAL TECHNICAL SERVICES

(Dr.-Ing. Harald Rapp)

The Central Technical Services (ZTE) of Max-Planck-Institut für Plasmaphysik support the experimental divisions with the design, construction and operation of experiments and diagnostics. They also run all kinds of utilities for facility operation and employ approximately 160 workers, technicians and engineers. Due to the build-up of another site in Greifswald for the stellarator W7-X the extent of the ZTE in Garching is being matched to the lower needs in future. On the other hand new tasks for planning and co-ordination become part of the ZTE's duty. The working group for site development at Greifswald attended the building construction and started to set up Technical Services. Conditions for energy supply and apprentice training have been agreed upon.

1. MECHANICAL DESIGN AND CALCULATION

(J. Simon-Weidner)

The task of the department is the design and the development of experimental components for the different projects by use of CAD and FE programs. It also cares for the CAD system of IPP at all sites. Half of the crew is involved in the calculation and construction work for W7-X. Manufacturing of the magnet coil system has been given to industry. Now the very detailed construction of the vessel with its more than 250 ports is a next goal. A main difficulty is the full 3-D geometry of the divertor plates including the piping due to the complex stellarator magnet fields and very little space. An Electronic Product Definition (EPD) system for managing all kind of documents has been installed and matched to the specific project needs and is now being commissioned with the project members.

2. ELECTRONICS DEVELOPMENT

(D. Arz)

The department develops electronic measurement and control equipment and fast high voltage switching and control devices for NBI and HF heating. Maintenance is also provided. Again a wide variety of analogue and digital equipment has been delivered to the experiments. Design of modern techniques for sequential control of steady state stellarator plasmas with variable research program modules has been continued. The commissioning of high-voltage modulators has been finished. Much work has been addressed to maintenance and renewal of devices in order to keep operational availability high.

3. MATERIALS TECHNOLOGY

(S. Kötterl, M.Balden)

The department offers technical services for material development, plasma welding, testing of vacuum joints and surface treatment for all kinds of application. Metal coating with electrochemical and PVD methods and production of metal doped killer pellets for controlled plasma formation is part of the service. The chemistry group offers computer based spectroscopic evaluation of optical components. Boronization of experimental plasma chambers has become part of the department's task. For morphological examinations an image analysing system has been installed.

4. ELECTRIC POWER SUPPLY

(W.R. McGlaun)

The department's task is the electric power supply of IPP and the experiments. It operates 4 flywheel generators with a total power of 580 MVA, 20 controlled high current rectifiers (462 MVA in total) and 24 high voltage DC modules up to 140 kVdc.
After renewal of the 1,45 GJ flywheel generator in 1997 unexpected problems with DC regulation due to digital controllers lasted until the end of 1998. In December there happened a severe incident when the oil supply failed and the bearings were damaged.
30 MVAr reactive power compensation of a flywheel generator for poloidal field supply has been successfully commissioned. Design for a 4Q-rectifier with 120 MW has been started. 2 HVDC modules with up to 140 kVdc at 50A for NBI were ordered by industry.

5. FACILITY OPERATION

(H. Rapp)

The department is charged with planning and supervising of all kind of facility installations like heating, cooling and airing systems, elevators, cranes etc. A variety of installations had to be renewed, others had to be constructed or matched to laboratory devices. A major concern is the ground water for experiment cooling which will be largely impaired by future subway construction at the site's borderline.

6. WORKSHOPS

(M. Keiner)

About half of the ZTE personnel work in workshops for mechanical and electric manufacturing of single experimental components. Additional capacity for peak load demand is purchased from industry. Therefore quality assurance, preparatory work and routing becomes more and more important. Co-ordination and work management together with research projects and industry play an increasing role. Apprentice training for electronic craftsmen runs successfully with 6 trainees per year.

ADMINISTRATION

(Dr. Irmtraut Zilker-Kramer, Dr. Hans Jahreiß)

The administration and general services of Max-Planck-Institut für Plasmaphysik are organized in seven departments:

PERSONNEL DEPARTMENT

The personnel department is responsible for administrative matters relating to personnel. The personnel figures of the institute for 1998 were as follows:

Total personnel (including Greifswald and Berlin)	985
Scientists	291
Technicians	427
Directorate and Staff Representative Council	29
General Services	43
Administration	79
Other personnel	116
	01.02.99

CONTRACTS AND PURCHASING DEPARTMENT

The contracts and purchasing department is responsible for placing survey and follow-up of all contracts and orders placed by IPP. In 1998, approximately 9.800 orders were made. They include complex contracts, many of which were signed after European-wide calls for tender. Furthermore, all export and import formalities are handled within this department: about 240 international and European shipments were carried out in 1998.

LEGAL AND PATENT DEPARTMENT

The legal and patent department works out and controls cooperation contracts with german and foreign universities and research institutes.

Concerning patent matters it attends to patent applications and supervision and licensing of patents in cooperation with Garching Innovation GmbH, a subsidiary of the Max Planck Society. In 1998 the division supervised 96 patents and similar rights.

AUDITING DEPARTMENT

The Auditing department is responsible for the auditing of work-flows and proceedings within the administration of IPP with respect to their commercial efficiency and their compliance with regulations. The single tasks are defined in an auditing plan which is drawn up every year according to the directives of the management of IPP.

FINANCE AND ACCOUNTING DEPARTMENT

The finance and accounting department is responsible for the financial planning and all financial transactions and fiscal matters of IPP.

Total expenses in 1998:	255,5 MDM
These expenses were financed as follows:	
Federal Republic of Germany through Federal Ministry of Education, Science, Research and Technology (BMBF)	142,8 MDM
Bavaria	9,6 MDM
Berlin	0,8 MDM
Mecklenburg-Vorpommern	31,3 MDM
EURATOM	42,9 MDM
Other income	28,1 MDM
	25.02.99

SITE AND BUILDINGS DEPARTMENT

The site and buildings department is in charge of planning, construction, structural alteration and reconditioning of buildings and main service facilities. Building maintenance is also provided for the neighbouring Max Planck Institutes of Astrophysics and Extraterrestrial Physics, the European Southern Observatory and the Berlin Division of IPP.

SOCIAL DEPARTMENT

The social department gives assistance to employees seeking housing, provides accommodation for guests in IPP residences, and runs the transport pool, bus and cleaning services.

Publications

Publications and Conference Reports

1. *Annen, A., M. Saß, R. Beckmann, A. von Keudell and W. Jacob:* Structure of Plasma-Deposited Amorphous Hydrogenated Boron-Carbon Thin Films. Thin Solid Films **312**, 147-155 (1998).

2. *Anton, M., T. Klinger*, M. Häse, S. Zoletnik, J. Geiger, C. Görner, H.-J. Hartfuß, R. Jaenicke, A. Weller and W7-AS Team:* Recent Observations of MHD Instabilities on W7-AS. Journal of Plasma and Fusion Research SERIES **1**, 259-262 (1998).

3. *Arndt, S., W. Däppen* and A. Naytonov*:* On Density and Temperature-Dependent Ground-State and Continuum Effects in the Equation of State for Stellar Interiors. The Astrophysical Journal **498**, 349-359 (1998).

4. *Arnold*, W., J.S. de Grassie*, D.B. Remsen*, E. Pivit*, R. Russell* and F. Braun:* Ferrite Hybrid System for Generator Matching in the ICRF. In: Proc. 20th Symp. Fusion Technol., Marseille 1998, (Eds.) B.Beaumont, P.Libeyre, B.de Gentile, G.Tonon. Assoc. Euratom-CEA, Saint-Paul-lez-Durance 1998, 427.

5. *Asmussen, K., K.B. Fournier*, J.M. Laming*, R. Neu, J.F. Seely*, R. Dux, W. Engelhardt, J.C. Fuchs and ASDEX Upgrade Team:* Spectroscopic Investigations of Tungsten in the EUV Region and the Determination of its Concentration in Tokamaks. Nuclear Fusion **38**, 967-986 (1998).

6. *Bachmann, P. and D. Sünder:* Multi-Fluid Description of Reaction-Diffusion Processes. Contributions to Plasma Physics **38**, 290-295 (1998).

7. *Bachmann, P. and D. Sünder:* Reaction-Diffusion Processes in Impurity Seeded Radiative Plasmas. In: Proc. Int. Congress Plasma Phys. and 25th EPS Conf. Control. Fusion and Plasma Phys., Prague 1998, (Ed.) P.Pavlo. ECA 22C. Europ. Phys. Soc., Geneva 1998, 2010-2013.

8. *Bachmann, P., D. Sünder and H. Wobig:* On Bifurcations of Temperature Profiles. Contributions to Plasma Physics **38**, 379-384 (1998).

9. *Balden, M., J. Roth and C.H. Wu*:* Thermal Stability and Chemical Erosion of the Silicon Doped CFC Material NS31. Journal of Nuclear Matererials **258-263**, 740-744 (1998).

10. *Baldzuhn, J., M. Kick, H. Maaßberg and W7-AS Team:* Measurement and Calculation of the Radial Electric Field in the Stellarator W7-AS. Plasma Physics and Controlled Fusion **40,** 967-986 (1998).

11. *Baldzuhn, J., M. Kick, H. Maaßberg, W. Ohlendorf and W7-AS Team:* Overview on the Radial Electric Field, Plasma Rotation and Transport in the Stellarator W7-AS. Journal of Plasma and Fusion Research SERIES **1**, 226-229 (1998).

12. *Baldzuhn, J. and W7-AS Team:* Spectroscopic Measurement of the Non-Thermal Electron-Root Feature in W7-AS. In: Proc. Int. Congress Plasma Phys. and 25th EPS Conf. Control. Fusion and Plasma Phys., Prague 1998, (Ed.) P.Pavlo. ECA 22C. Europ. Phys. Soc., Geneva 1998, 403-406.

13. *Bard, A., J. Stober, D.P. Coster, A. Kallenbach and ASDEX Upgrade Team:* Measurement of Radial H_α and H Density Profiles near the Separatrix and Implications on Ion Temperature Determination. In: Proc. Int. Congress Plasma Phys. and 25th EPS Conf. Control. Fusion and Plasma Phys., Prague 1998, (Ed.) P.Pavlo. ECA 22C. Europ. Phys. Soc., Geneva 1998, 1518-1521.

14. *Barnes*, C.W., H.-S. Bosch, H.W. Hendel*, A.G.A. Huibers*, D.L. Jassby*, R.W. Motley*, E.B. Nieschmidt*, T. Saito*, J. Strachan*, M. Bitter*, R. Budny*, K.W. Hill*, D.K. Mansfield*, D.C. McCune*, R. Nazikian*, H.K. Park*, A.T. Ramsey*, S.D. Scott*, G. Taylor* and M.C. Zarnstorff*:* Triton Burnup Measurements and Calculations on TFTR. Nuclear Fusion **38**, 597-618 (1998).

15. *Becker, G.:* Transport Simulations of ITER with Empirical Heat Diffusivity Scaling. Nuclear Fusion **38**, 293-312 (1998).

16. *Becker, G., O. Gehre and ASDEX Upgrade Team:* Simulation of Gas Oscillation Experiments on ASDEX Upgrade. In: Proc. Int. Congress Plasma Phys. and 25th EPS Conf. Control. Fusion and Plasma Phys., Prague 1998, (Ed.) P.Pavlo. ECA 22C. Europ. Phys. Soc., Geneva 1998, 1848-1851.

17. *Behrisch, R., S. Grigull, U. Kreissig* and R. Grötzschel*:* Influence of Surface Roughness on Measuring Depth Profiles and the Total Amount of Implanted Ions by RBS and ERDA. Nuclear Instruments and Methods in Physics Research **B 136-138**, 628-632 (1998).

18. *Behrisch, R., V. Khripunov*, R.T. Santoro* and J.M. Yesil*:* Transmutation of Plasma Facing Materials by the Neutron Flux in a DT Fusion Reactor. Journal of Nuclear Materials **258-263**, 686-693 (1998).

19. *Behrisch, R. and K. Wittmaak* (Eds.):* Raspilinie pod deistviem bombardirovki chastzami, Charakteristiki raspiliennikh chastizami, Primennia v technike. MIR Verlag, Moskau, 1998. 470 p.

20. *Beidler, C.D., G. Grieger, E. Harmeyer, F. Herrnegger, J. Kisslinger, E. Strumberger, H. Wobig, A.V. Zolotukhin and N. Karulin*:* Physics and Engineering Studies of a Helias Reactor. Journal of Plasma and Fusion Research SERIES **1**, 176-179 (1998).

21. *Bergmann, A.:* Parallelized PIC Code for Kinetic Modelling of a "Classical" Scrape-off Layer. Contributions to Plasma Physics **38**, 231-235 (1998).

22. *Bertel, E. and J. Lehmann:* Electronic Structure of Self-Organized Lateral Superlattices on a Metal Surface: O/Cu(110). Physical Review Letters **80**, 1497-1500 (1998).

23. *Biederer*, Th., Th. Kammler* and J. Küppers:* A Structural Effect in Direct Reactions: Kinetics of D Abstraction from Pt(110) 1 x 2 Surfaces with Gaseous H Atoms. Chemical Physics Letters **286**, 15-20 (1998).

24. *Biskamp, D., E. Schwarz and A. Celani*:* Nonlocal Bottleneck Effect in Two-Dimensional Turbulence. Physical Review Letters **81**, 4855-4858 (1998).

25. *Biskamp, D., E. Schwarz and A. Zeiler:* Instability of a Magnetized Plasma Jet. Physics of Plasmas **5**, 2485-2488 (1998).

26. *Bleuel, J., B.D. Scott, M. Endler, H. Niedermeyer, U. Pfeiffer, G. Theimer and W7-AS Team:* Plasma Edge Turbulence: Comparison between Theory and Experiment. In: Proc. Int. Congress Plasma Phys. and 25th EPS Conf. Control. Fusion and Plasma Phys., Prague 1998, (Ed.) P.Pavlo. ECA 22C. Europ. Phys. Soc., Geneva 1998, 2330-2333.

27. *Bohmeyer, W., P. Kornejew, H.-D. Reiner and C.H. Wu*:* Fluence and Energy Dependence of Chemical Erosion of Carbon Fibre Components (CFC). In: Proc. Int. Congress Plasma Phys. and 25th EPS Conf. Control. Fusion and Plasma Phys., Prague 1998, (Ed.) P.Pavlo. ECA 22C. Europ. Phys. Soc., Geneva 1998, 2797-2800.

28. *Borrass, K., J. Lingertat* and R. Schneider:* A Scrape-off Layer Based Density Limit for ELMy H-Modes. Contributions to Plasma Physics **38**, 130-135 (1998).

29. *Brakel, R., M. Anton, J. Chatenet, J. Geiger, T. Geist, H.-J. Hartfuß, M. Hirsch, G. Kühner, H. Maaßberg, U. Stroth, A. Weller, W7-AS Team and ECRH Group (W7-AS):* On the Influence of Rotational Transform and Magnetic Shear on Confinement in the W7-AS Stellarator. In: Proc. Int. Congress Plasma Phys. and 25th EPS Conf. Control. Fusion and Plasma Phys., Prague 1998, (Ed.) P.Pavlo. ECA 22C. Europ. Phys. Soc., Geneva 1998, 423-426.

30. *Brakel, R., M. Anton, V. Erckmann, S. Fiedler, J. Geiger, H.-J. Hartfuß, M. Hirsch, R. Jaenicke, G. Kühner, H. Maaßberg, U. Stroth, F. Wagner, A. Weller, W7-AS Team and ECRH Group (W7-AS):* The Role of Magnetic Shear in the Confinement of W7-AS Plasmas. Journal of Plasma and Fusion Research SERIES **1**, 80-83 (1998).

31. *Brambilla, M.:* Electron Landau Damping of Ion Bernstein Waves in Tokamak Plasmas. Nuclear Fusion **38**, 1805-1817 (1998).

32. *Brambilla, M.:* Fundamentals of Plasma Physics and Controlled Fusion. Nuclear Fusion **38**, 641-642 (1998).

33. *Brambilla, M.:* Kinetic Theory of Plasma Waves (Homogeneous Plasmas). Cambridge Univ. Press, Cambridge 1998, 644 p.

34. *Brambilla, M. and J.-M. Noterdaeme:* Variational Evaluation of the Scattering Matrix of Array Antennas for Ion Cyclotron Heating and Current Drive in Tokamaks. In: Proc. 2nd Europhys. Top. Conf. Radio Frequency Heating and Current Drive of Fusion Devices, Brussels 1998, (Eds.) J.Jacquinot, G.Van Oost, R.R.Weynants. ECA 22A. Europ. Phys. Soc., Geneva 1998, 33-36.

35. *Brandenburg*, R., S. Fiedler, J. Schweinzer, G. Petravich*, F. Aumayr*, H.P. Winter*, W7-AS Team and ASDEX Upgrade Team:* Impurity Ions in ASDEX Upgrade and Wendelstein 7-AS Studied by Lithium Beam Charge-Exchange Spectroscopy. In: Proc. Int. Congress Plasma Phys. and 25th EPS Conf. Control. Fusion and Plasma Phys., Prague 1998, (Ed.) P.Pavlo. ECA 22C. Europ. Phys. Soc., Geneva 1998, 1518-1521.

36. *Brandenburg*, R., J. Schweinzer, F. Aumayr* and H.P. Winter*:* Li (2p ← 2s) Excitation by Impact of Slow Ions. Journal of Physics **B 31**, 2585-2599 (1998).

37. *Breger*, P., C. Flewin*, K.-D. Zastrow*, S.J. Davies*, N.C. Hawkes*, R.W.T. König, Z.A. Pietrzyk*, L. Porte*, D.D.R. Summers* and M.G. von Hellermann*:* Plasma-Edge Gradients in L- and Elm-Free H-Mode JET Plasmas. Plasma Physics and Controlled Fusion **40**, 347-359 (1998).

38. *Brenner*, A., H.-G. Grobelny*, M. Podhorsky*, F. Schauer and B. Sombach:* Design and Manufacture of the Demonstration Cryostat for the Fusion Experiment WENDELSTEIN 7-X. In: Proc. 20th. Symp. on Fusion Technol., Marseille 1998, (Eds.) B.Beaumont, P.Libeyre, B.de Gentile, G.Tonon. Assoc. Euratom-CEA, Saint-Paul-lez-Durance 1998, 1725-1728.

39. *Brongersma*, H.H., M. Carrere-Fontaine*, R. Cortenraad*, A.W. Denier van der Gon*, P.J. Scanlon*, I. Spolveri*, B. Cortigiani*, U. Bardi*, E. Taglauer, S. Reiter, S. Labich, P. Bertrand*, L. Houssiau*, S. Speller*, S. Parascandola*, H. Ünlü-Lachnitt* and W. Heiland*:* A Round Robin Experiment of Elemental Sensitivity Factors in Low-Energy Ion Scattering. Nuclear Instruments and Methods in Physics Research **B 142**, 377-386 (1998).

40. *Burhenn, R., M. Anton, J. Baldzuhn, R. Brakel, L. Giannone, H. Hacker, M. Hirsch, L. Ledl, H. Maaßberg, E. Unger, A. Weller, W7-AS Team, ECRH Group (W7-AS) and NI Group:* Impurity Transport Investigations at W7-AS. Journal Plasma Fusion Research SERIES **1**, 255-258 (1998).

41. *Callaghan*, H.P., P. McCarthy* and J. Geiger:* Rapid Equilibrium Reconstruction on W7-AS Using Function Parametrization. In: Proc. Int. Congress Plasma Phys. and 25th EPS Conf. Control. Fusion and Plasma Phys., Prague 1998, (Ed.) P.Pavlo. ECA 22C. Europ. Phys. Soc., Geneva 1998, 1470-1473.

42. *Carlson, A. and M. Weinlich:* MHD Theory of Langmuir Probes with Dimensions between the Gyroradius and the Fluctuation. Contributions to Plasma Physics **38**, Special Issue, 38-46 (1998).

43. *Carreras*, B.A., B.Ph. van Milligen*, M.A. Pedrosa*, R. Balbín*, C. Hidalgo*, D.E. Newman*, E. Sánchez*, M. Frances*, I. García-Cortés*, J. Bleuel, M. Endler, S.J. Davies* and G.F. Matthews*:* Long-Range Time Correlations in Plasma Edge Turbulence. Physical Review Letters **80**, 4438-4441 (1998).

44. *Carreras*, B.A., B.Ph. van Milligen*, M.A. Pedrosa*, R. Balbín*, C. Hidalgo*, D.E. Newman*, E. Sánchez*, M. Frances*, I. García-Cortés*, J. Bleuel, M. Endler, C. Ricardi*, S.J. Davies*, G.F. Matthews*, E. Martines*, V. Antoni*, A. Latten* and T. Klinger*:* Self-Similarity of the Plasma Edge Fluctuations. Physics of Plasmas **5**, 3632-3643 (1998).

45. *Chernysh*, V.S., W. Eckstein, A.A. Haidearov*, V.S. Kulikauskas*, V.A. Kurnaev*, E.S. Mashkova* and V.A. Molchanov*:* Angular Distributions of Particles Sputtered from Polycrystalline Platinum. Nuclear Instruments and Methods in Physics Research **B 135**, 285-288 (1998).

46. *Christou, C., J. Baldzuhn, M. Hirsch, H. Maaßberg, M. Anton and W7-AS Team:* Analysis of E-Field Profile Effects and Fluctuations in the W7-AS Plasma. In: Proc. Int. Congress Plasma Phys. and 25th EPS Conf. Control. Fusion and Plasma Phys., Prague 1998, (Ed.) P.Pavlo. ECA 22C. Europ. Phys. Soc., Geneva 1998, 1466-1469.

47. *Davies*, S.J., M. Endler, S.K. Erents*, I. García-Cortés*, H. Guo*, C. Hidalgo*, A. Loarte*, J.R. Martin-Solis*, G.F. Matthews*, K. McCormick, R.D. Monk* and P.C. Stangeby*:* Overview of Probe Measurements at JET. Contributions to Plasma Physics **38**, Special Issue, 61-67 (1998).

48. *De Peña Hempel, S., A. Kallenbach, H. Meister and ASDEX Upgrade Team:* Measurements of the Radial Electric Field at ASDEX Upgrade. In: Proc. Int. Congress Plasma Phys. and 25th EPS Conf. Control. Fusion and Plasma Phys., Prague 1998, (Ed.) P.Pavlo. ECA 22C. Europ. Phys. Soc., Geneva 1998, 484-487.

49. *Dohmen, R., F. Hertweck and M.-G. Pacco-Düchs:* A Portable an Easy-to-use Fortran90 MPP Environment. In: Proc. 4th Europ. Cray/SGI MPP Workshop, Garching 1998, (Eds.) H.Lederer, F.Hertweck. IPP, Garching 1998, 209-224.

50. *Dohmen, R. and U. Schwenn:* Performance and Load Balancing of Diverse Parallel Implementations of the Plasma Code HINT. In: Proc. Parallel Computing: Fundamentals Applications and New Directions, Bonn 1997, (Eds.) E.H.D.Hollander, G.R.Joubert, F.J.Peters, U.Trottenberg. Elsevier, Amsterdam 1998, 137-143.

51. *Donath, M., P.A. Dowben* and W. Nolting* (Eds.):* Magnetism and Electronic Correlations in Local-Moment Systems: Rare-Earth Elements and Compounds. World Scientific Publ., Singapore 1998, 454 p.

52. *Donath, M. and B. Gubanka*:* Spin-Dependent Unoccupied Electronic States of Thin Gd Films on W(110). In: Magnetism and Electronic Correlations of Local-Moment Systems: Rare-Earth Elements and Compounds, (Eds.) M.Donath, P.A.Dowben, W.Nolting. World Scientific Publ., Singapore 1998, 217-233.

53. *Dorst, D., P. Grigull, J. Kisslinger, K. McCormick, H. Niedermeyer, F. Sardei and F. Wagner:* Divertor Experiment in the W7-AS Stellarator. In: Proc. 20th Symp. on Fusion Technol., Marseille 1998, (Eds.) B.Beaumont, P.Libeyre, B.de Gentile, G.Tonon. Assoc. Euratom-CEA, Saint-Paul-lez Durance 1998, 55-58.

54. *Dose, V., R. Fischer and W. von der Linden:* Deconvolution Based on Experimentally Determined Apparatus Functions. In: Maximum Entropy and Bayesian Methods, (Ed.) G.Erickson. Kluwer, Dordrecht 1998, 147-152.

55. *Dose, V., R. Preuss and W. von der Linden:* Dimensionally Constrained Energy Confinement Analysis of W7-AS Data. Nuclear Fusion **38**, 571-583 (1998).

56. *Dose, V., R. Preuss and W. von der Linden:* Dimensionally Exact Energy Confinement Scaling in W7-AS. Physical Review Letters **81**, 3407-3410 (1998).

57. *Drevlak, M.:* Automated Optimization of Stellarator Coils. Fusion Technology **40**, 106-117 (1998).

58. *Drevlak, M.:* Coil Design and Equilibrium Studies for a Quasi-Axially Symmetric Tokamak. Journal of Plasma and Fusion Research SERIES **1**, 426-428 (1998).

59. *Drevlak, M.:* Coil Designs for a Quasi-Axially Symmetric Stellarator. In: Proc. 20th Symp. on Fusion Technol., Marseille 1998, (Eds.) B.Beaumont, P.Libeyre, B.de Gentile, G.Tonon. Assoc. Euratom-CEA, Saint-Paul-lez-Durance 1998, 883-884.

60. *Drevlak, M.:* Modular Coils and Finite β Operation of a Quasi-Axially Symmetric Tokamak. Nuclear Fusion **38**, 1409-1420 (1998).

61. *Düchs, D.F. and G.C. Vlases* (Eds.):* Proc. 6th Int. Workshop on Plasma Edge Theory in Fusion Devices, Oxford 1997. Contributions to Plasma Physics **38**, 1998, 384 p.

62. *Dumbrajs*, O., R. Meyer-Spasche and A. Reinfelds*:* Analysis of Electron Trajectories in a Gyrotron Resonator. IEEE Transactions on Plasma Science **26**, 846-853 (1998).

63. *Dux, R., C. Fuchs, A. Gude, A. Kallenbach, R. Neu and ASDEX Upgrade Team:* Central Impurity Transport. In: Proc. Int. Congress Plasma Phys. and 25th EPS Conf. Control. Fusion and Plasma Phys., Prague 1998, (Ed.) P.Pavlo. ECA 22C. Europ. Phys. Soc., Geneva 1998, 508-511.

64. *Eckstein, W., K. Krieger and J. Roth:* Erosion of W and Deposition of C due to Bombardment with D and CH_3. Journal of Nuclear Materials **258-263**, 912-916 (1998).

65. *Erckmann, V., U. Gasparino, H.P. Laqua, H. Maaßberg, W7-AS Team, ECRH Group (W7-AS), K.S. Kasilov*, N. Marushchenko*, V. Irkhin* and S. Malygin*:* ECRH and ECCD Experiments in an Extended Power Range at the W7-AS Stellarator. In: Stellarator News, Issue 60, 9-10 (1998), http://www.ornl.gov/fed/stelnews/sn60.html.

66. *Erckmann, V., T. Geist, H.P. Laqua, M. Weißgerber, L. Empacher*, W. Förster*, G. Gantenbein*, W. Kasparek*, G.A. Müller*, P.G. Schüller* and K. Schwörer*:* ECRH System for the W7-X Stellarator. In: Proc. 20th Symp. on Fusion Technol., Marseille 1998, (Eds.) B.Beaumont, P.Libeyre, B.de Gentile, G.Tonon. Assoc. Euratom-CEA, Saint-Paul-lez Durance 1998, 299-302.

67. *Erckmann, V., H.-J. Hartfuß, M. Kick, H. Renner, J. Sapper, F. Schauer, E. Speth, F. Wesner, F. Wagner, M. Wanner, A. Weller, H. Wobig, W7-AS Team and W7-X Team:* The W7-X Project. Scientifc Basis and Technical Realization. In: Proc. 17th Symp. on Fusion Engineering, San Diego,CA 1997. (Ed.) IEEE, Piscataway,NJ 1998, 40-48.

68. *Feng, Y., G. Herre, P. Grigull, F. Sardei and W7-AS Team:* The Effects of Field Reversal on the W7-AS Island Divertor at Low Densities. Plasma Physics and Controlled Fusion **40**, 371-380 (1998).

69. *Feng, Y., F. Sardei, P. Grigull and W7-AS Team:* Modelling Drift Effects on the Limiter SOL of Low Density Plasmas in W7-AS. Contributions to Plasma Physics **38**, 195-200 (1998).

70. *Fiedler, S., R. Brandenburg*, J. Baldzuhn, K. McCormick, F. Aumayr*, J. Schweinzer, H.P. Winter* and W7-AS Team:* Impurity Investigation by Means of Li-Beam Induced Charge Exchange Spectroscopy on W7-AS. Journal of Plasma and Fusion Research SERIES **1**, 314-317 (1998).

71. *Fischer R., M. Mayer, W. von der Linden and V. Dose:* Energy Resolution Enhancement in Ion Beam Experiments with Bayesian Probability Theory. Nuclear Instruments and Methods in Physics Research **B 136-138**, 1140-1145 (1998).

72. *Frank, P., J. Bucalossi*, B. Heinemann, W. Kraus, F. Probst, E. Speth, R. Trainham* and O. Vollmer:* Progress on the "Batman", RF Source for Negative Hydrogen Ions. In: Proc. 20th Symp. Fusion Technol., Marseille 1998, (Eds.) B.Beaumont, P.Libeyre, B.de Gentile, G.Tonon. Assoc. Euratom-CEA, Saint-Paul-lez-Durance 1998, 429-431.

73. *Franzen, P., M. Kaufmann, V. Mertens, G. Neu, G. Raupp, T. Zehetbauer, ASDEX Upgrade Team and NI Team:* On-Line Confinement Regime Identification for the Discharge Control System at ASDEX Upgrade. Fusion Technology **33**, 84-96 (1998).

74. *Fuchs, C. and H.-J. Hartfuß:* Cotton-Mouton Effect Measurement in a Plasma at the W7-AS Stellarator. Physical Review Letters **81**, 1626-1629 (1998).

75. *Fuchs, C. and H.-J. Hartfuß:* Polarimetric Line Density Measurements at W7-AS Using the Cotton-Mouton Effect. In: Proc. Int. Congress Plasma Phys. and 25th EPS Conf. Control. Fusion and Plasma Phys., Prague 1998, (Ed.) P.Pavlo. ECA 22C. Europ. Phys. Soc., Geneva 1998, 1458-1461.

76. *Fuchs, J.C., K.-F. Mast, D.P. Coster, A. Herrmann, M. Münch, R. Schneider and ASDEX Upgrade Team:* Radiation Distribution and Power Balance. In: Proc. Int. Congress Plasma Phys. and 25th EPS Conf. Control. Fusion and Plasma Phys., Prague 1998, (Ed.) P.Pavlo. ECA 22C. Europ. Phys. Soc., Geneva 1998, 1510-1513.

77. *Fuchs, T., C. Biedermann, R. Radtke, E. Behar* and R. Doron*:* Channel-Specific Dielectronic Recombination of Highly Charged Krypton. Physical Review **A 58**, 4518-4525 (1998).

78. *Gafert, J., K. Behringer, D.P. Coster, C. Dorn, A. Kallenbach, R. Schneider, U. Schumacher* and ASDEX Upgrade Team:* Spectroscopic Evidence for Flow Reversal at High Density in ASDEX Upgrade Divertor II. In: Proc. Int. Congress Plasma Phys. and 25th EPS Conf. Control. Fusion and Plasma Phys., Prague 1998, (Ed.) P.Pavlo. ECA 22C. Europ. Phys. Soc., Geneva 1998, 516-519.

79. *Gantenbein*, G., L. Empacher*, V. Erckmann and M. Weißgerber:* Simulations and Experiments on a Multi-Beam Waveguide ECRH Transmission System. In: Proc. 20th Symp. on Fusion Technol., Marseille 1998, (Eds.) B.Beaumont, P.Libeyre, B.de Gentile, G.Tonon. Assoc. Euroatom-CEA, Saint-Paul-lez Durance 1998, 423-426.

80. *Gasparino, U., V. Erckmann, H.-J. Hartfuß, H. Maaßberg and M. Romé*:* Transport Analysis through Heat Waves Driven at Different Radial Positions. Plasma Physics and Controlled Fusion **40**, 233-244 (1998).

81. *Gasparino, U., H. Idei*, S. Kubo*, N. Marushchenko* and M. Romé*:* High Harmonic Electron Cyclotron Resonance Heating in the Large Helical Device. Nuclear Fusion **38**, 223-235 (1998).

82. *Geier, H. and H. Niedermeyer:* Transient Behaviour of Langmuir Probes in a Magnetized Plasma. Contributions to Plasma Physics **38**, Special Issue, 86-92 (1998).

83. *Geist, T.:* Simple Millimeterwave Dielectric Disc Filters with very Flat Passband Characteristic. International Journal of Infrared and Millimeter Waves **19**, 887-893 (1998).

84. *Geist, T. and U. Siart*:* Diplexing Millimeter Waves. International Journal of Infrared and Millimeter Waves **19**, 957-962 (1998).

85. *Gori*, S., C. Nührenberg, J. Nührenberg and R. Zille*:* Beta Studies in Quasi-Symmetric Configurations. Journal of Plasma and Fusion Research SERIES **1**, 62-65 (1998).

86. *Greuner, H., A. Herrmann, H. Renner, P. Chappuis* and R. Mitteau*:* Development of Divertor Targets for Wendelstein 7-X. In: Proc. 20th Symp. on Fusion Technol., Marseille 1998, (Eds.) B.Beaumont, P.Libeyre, B.de Gentile, G.Tonon. Assoc. Euratom-CEA, Saint-Paul-lez-Durance 1998, 249-252.

87. *Grigull, P., L. Giannone, U. Stroth, K. Borrass, R. Brakel, R. Burhenn, A. Elsner, S. Fiedler, H. Hacker, H.-J. Hartfuß, A. Herrmann, D. Hildebrandt, G. Kühner, R. Schneider, F. Wagner, A. Weller, X.D. Zhang* and W7-AS Team:* Density Limit Study on the W7-AS Stellarator. Journal of Plasma and Fusion Research SERIES **1**, 291-294 (1998).

88. *Grigull*, S., W. Jacob, D. Henke*, Ch. Spaeth*, L. Sümmchen* and W. Sigle*:* Transport and Structural Modification during Nitrogen Implantation of Hard Amorphous Carbon Films. Journal of Applied Physics **83**, 5185-5194 (1998).

89. *Grote*, K. and R. Meyer-Spasche:* Euler-Like Discrete Models of the Logistic Differential Equation. Computers and Mathematics with Applications **36**, 211-225 (1998).

90. *Gude, A., K. Hallatschek, S. Günter, A. Kallenbach, S.D. Pinches, S. Sesnic and ASDEX Upgrade Team:* Radially Propagating High-n/High-m Mode Cascades during Flattening or Inversion of Central q Profile in ASDEX Upgrade. Plasma Physics and Controlled Fusion **40**, 1057-1069 (1998).

91. *Gude, A., M. Maraschek, S. Günter, S. Sesnic and ASDEX Upgrade Team:* Neoclassical Tearing Modes and their Interaction with Fishbones at ASDEX Upgrade. In: Proc. Int. Congress Plasma Phys. and 25th EPS Conf. Control. Fusion and Plasma Phys., Prague 1998, (Ed.) P.Pavlo. ECA 22C. Europ. Phys. Soc., Geneva 1998, 528-531.

92. *Günter, S., A. Gude, M. Maraschek, S. Sesnic, H. Zohm* and ASDEX Upgrade Team: β* Scaling for the Onset of Neoclassical Modes at ASDEX Upgrade. Nuclear Fusion **38**, 1431-1434 (1998).

93. *Günter, S., S.D. Pinches, A. Gude, K. Hallatschek, K. Lackner and ASDEX Upgrade Team:* Pressure Driven High-*n*/High-*m* Tearing Modes in Low Shear Regions with High Pressure Gradients and High Resistivity. Nuclear Fusion **38**, 325-329 (1998).

94. *Günter, S., Q. Yu*, A. Gude, H.R. Koslowski*, M. Maraschek, S.D. Pinches, S. Schade and ASDEX Upgrade Team:* MHD Phenomena in Low and Reversed Shear Plasmas. In: Proc. Int. Congress Plasma Phys. and 25th EPS Conf. Control. Fusion and Plasma Phys., Prague 1998, (Ed.) P.Pavlo. ECA 22C. Europ. Phys. Soc., Geneva 1998, 1840-1843.

95. *Haas, G. and H.-S. Bosch:* In Vessel Pressure Measurement in Nuclear Fusion Experiments with ASDEX Gauges. Vacuum **51**, 39-46 (1998).

96. *Haas, G., H.-S. Bosch, D.P. Coster, L. de Kock*, R. Maingi*, J. Neuhauser and R. Schneider:* Pressure Gauges and Neutral Pressure Measurement in ITER. In: Diagnostics for Experimental Thermonuclear Fusion Reactors 2, (Eds.) P.E.Stott, G.Gorini, P.Prandoni, E.Sindoni. Plenum Press, New York 1998, 559-568.

97. *Hallatschek, K.:* Neuartige Algorithmen für die Ereigniserkennung und Datenreduktion in Echtzeit an der Röntgendiagnostik des Fusionsexperiments ASDEX Upgrade. In: Forschung und wissenschaftliches Rechnen, (Eds.) T.Plesser, P.Wittenburg. GWDG, Göttingen 1998, 111-126.

98. *Hallatschek, K., A. Gude, D. Biskamp, S. Günter and ASDEX Upgrade Team:* High Frequency Mode Cascades in the ASDEX Upgrade Tokamak. Physical Review Letters **80**, 293-296 (1998).

99. *Hallatschek, K., A. Zeiler, D. Biskamp, J.F. Drake* and B.N. Rogers*:* Nonlocal Three-Dimensional Simulations of Plasma Edge Turbulence. In: Proc. Int. Congress Plasma Phys. and 25th EPS Conf. Control. Fusion and Plasma Phys., Prague 1998, (Ed.) P.Pavlo. ECA 22C. Europ. Phys. Soc., Geneva 1998, 1915-1918.

100. *Hallatschek, K. and M. Zilker:* Real Time Data Acquisition with Transputers and PowerPCs Using the Wavelet Transform for Event Detection. IEEE Transactions on Nuclear Science **45**, 1872-1876 (1998).

101. *Harmeyer, E., O. Jandl and H. Wobig:* The Coil System of a Helias Reactor. In: Proc. 20th Symp. on Fusion Technol., Marseille 1998, (Eds.) B.Beaumont, P.Libeyre, B.de Gentile, G.Tonon. Assoc. Euratom-CEA, Saint-Paul-lez-Durance 1998, 719-722.

102. *Hartfuß, H.-J.:* RF Techniques in Plasma Diagnostics. Plasma Physics and Controlled Fusion **40**, A231-A250 (1998).

103. *Hartfuß H-J., M. Häse and M. Hirsch:* Parameter Dependencies of Temperature Fluctuations and their Correlation with Density Fluctuations. In: Proc. Int. Congress Plasma Phys. and 25th EPS Conf. Control. Fusion and Plasma Phys., Prague 1998, (Ed.) P.Pavlo. ECA 22C. Europ. Phys. Soc., Geneva 1998, 399-402.

104. *Hartmann, D.A., G. Cattanei, ICRH Group and W7-AS Team:* CD1/5: Plasma Heating and Sustainment in the Ion Cyclotron Range of Frequencies on the Stellarator W7-AS. Stellarator News **60**, 10 (1998), http://www.ornl.gov/fed/stelnews/sn60.html.

105. *Hartmann, D.A., G. Cattanei, W7-AS Team and ICRF Group:* Second Harmonic Hydrogen Heating on the W7-AS Stellarator. In: Proc. Int. Congress Plasma Phys. and 25th EPS Conf. Control. Fusion and Plasma Phys., Prague 1998, (Ed.) P.Pavlo. ECA 22C. Europ. Phys. Soc., Geneva 1998, 1206-1209.

106. *Häse, M., W. Pernreiter and H.-J. Hartfuß:* Core Fluctuations and Non-Thermal Electron Distribution at W7-AS. Journal of Plasma and Fusion Research SERIES **1**, 99-102 (1998).

107. *Hatzky, R. and M. Fivaz*:* Simulation of Ion-Temperature-Gradient-Driven (ITG) Modes for the Bumpy Pinch. In: Proc. Int. Congress Plasma Phys. and 25th EPS Conf. Control. Fusion and Plasma Phys., Prague 1998, (Ed.) P.Pavlo. ECA 22C. Europ. Phys. Soc., Geneva 1998, 1804-1807.

108. *Heikkinen*, J.A., W. Herrmann and T.K. Kurki-Suonio*:* Fast Response in the Ripple Trapped Ion Distribution to Abrupt Changes in a Radial Electric Field in Tokamaks. Nuclear Fusion **38**, 419-424 (1998).

109. *Heikkinen*, J.A., T.P. Kiviniemi*, A.G. Peeters, T.K. Kurki-Suonio*, S.K. Sipilä*, W. Herrmann, W. Suttrop and H. Zohm*:* Ion Orbit Loss Current in ASDEX Upgrade. Plasma Physics and Controlled Fusion **40**, 693-696 (1998).

110. *Heikkinen*, J.A., T.K. Kurki-Suonio* and W. Herrmann:* Ripple-Trapped Beam Ions in the Presence of a Radial Electric Field. Plasma Physics and Controlled Fusion **40**, 679-682 (1998).

111. *Heinemann, B., J. Bucalossi*, P. Frank, R. Riedl, A. Simonin*, E. Speth, R. Trainham* and O. Vollmer:* Large Area, High-Transparency Extraction System for Negative Ions. In: Proc. 20th Symp. Fusion Technol., Marseille 1998, (Eds.) B.Beaumont, P.Libeyre, B.de Gentile, G.Tonon. Assoc. Euratom-CEA, Saint-Paul-lez-Durance 1998, 433-436.

112. *Herrmann, A., J.C. Fuchs, V. Rohde, M. Weinlich, ASDEX Upgrade Team, NI Team and ICRH Team:* Heat Flux Distribution in ASDEX Upgrade - Comparison of Divertor I and II. In: Proc. Int. Congress Plasma Phys. and 25th EPS Conf. Control. Fusion and Plasma Phys., Prague 1998, (Ed.) P.Pavlo. ECA 22C. Europ. Phys. Soc., Geneva 1998, 488-491.

113. *Herrmann, A. and H. Salzmann:* High Resolution IR Temperature Monitoring System for the ITER Target Plates. In: Diagnostics for Experimental Thermonuclear Fusion Reactors 2, (Eds.) P.E.Stott, G.Gorini, P.Prandoni, E.Sindoni. Plenum Press, New York 1998, 569-572.

114. *Herrmann, W. and ASDEX Upgrade Team:* Diagnostic Method for Radial Electric Fields in Tokamaks by the Observation of Ripple-Trapped Ions. Review of Scientific Instruments **69**, 3165-3175 (1998).

115. *Herrmann, W., J.A. Heikkinen*, T.K. Kurki-Suonio* and ASDEX Upgrade Team:* The Time Behaviour of Radial Electric Fields at the L-H Transition from the Observation of Ripple-Trapped Ions. Plasma Physics and Controlled Fusion **40**, 683-687 (1998).

116. *Hildebrandt, D., M. Akbi, B. Jüttner, V. Rohde and W. Schneider:* Deuterium and Impurity Contamination of Divertor Tiles and Collector Probes of ASDEX-Upgrade. In: Proc. Int. Congress Plasma Phys. and 25th EPS Conf. Control. Fusion and Plasma Phys., Prague 1998, (Ed.) P.Pavlo. ECA 22C. Europ. Phys. Soc., Geneva 1998, 536-539.

117. *Hildebrandt, D., R. Brakel, A. Elsner, S. Fiedler, C. Görner, P. Grigull, H. Hacker, H.-J. Hartfuß, G. Herre, D. Naujoks and W7-AS Team:* Plasma Radiation with Impurity Injection into the Edge Plasma of the Stellarator W7-AS. Journal of Plasma and Fusion Research SERIES **1**, 283-286 (1998).

118. *Hirsch, M., P. Amadeo*, M. Anton, J. Baldzuhn, R. Brakel, J. Bleuel, S. Fiedler, T. Geist, P. Grigull, H.-J. Hartfuß, E. Holzhauer*, R. Jaenicke, M. Kick, J. Kisslinger, J.P.T. Koponen, F. Wagner, H. Wobig, S. Zoletnik and W7-AS Team:* Operational Range and Transport Barrier of the H-Mode in the Stellarator W7-AS. Plasma Physics and Controlled Fusion **40**, 631-634, (1998).

119. *Hirsch, M., M. Anton, J. Baldzuhn, J.H. Chatenet, C. Christou, M. Endler, J. Geiger, T. Geist, H.-J. Hartfuß, E. Holzhauer*, G. Kühner, U. Stroth, S. Zoletnik and W7-AS Team:* ELM-Like Transport Events and their Impact on Confinement in W7-AS. In: Proc. Int. Congress Plasma Phys. and 25th EPS Conf. Control. Fusion and Plasma Phys., Prague 1998, (Ed.) P.Pavlo. ECA 22C. Europ. Phys. Soc., Geneva 1998, 2322-2325.

120. *Hofmeister, F., F. Braun, H. Faugel, D.A. Hartmann and J.-M. Noterdaeme:* Matching Considerations in an ICRH-System with Hybrid Couplers. In: Proc. 20th Symp. Fusion Technol., Marseille 1998, (Eds.) B.Beaumont, P.Libeyre, B.de Gentile, G.Tonon. Assoc. Euratom-CEA, Saint-Paul-lez-Durance 1998, 437-440.

121. *Holzhauer*, E., M. Hirsch, T. Grossmann*, B. Branas* and F. Serra*:* Theoretical and Experimental Investigation of the Phase-Runaway in Microwave Reflectometry. Plasma Physics and Controlled Fusion **40**, 1869-1886 (1998).

122. *Horn*, A., J. Biener* and J. Küppers:* A Dimerization Reaction Induced by Hydrogen Atoms: from $B(CH_3)_3$ Adsorbed on C/Pt(100) to $B_2H_2(CH_3)_4$. Surface Science **414**, 290-297 (1998).

123. *Igitkhanov*, Yu., G. Janeschitz*, G.W. Pacher*, M. Sugihara*, H.D. Pacher*, D. Post*, E. Solano, J. Lingertat*, A. Loarte*, T. Osborne*, O.P. Pogutse*, M. Shimada* and W. Suttrop:* Edge Parameter Operational Space and Trajectories for ITER. Plasma Physics and Controlled Fusion **40**, 837-844 (1998).

124. *Ingesson*, L.C., B. Alper*, H. Chen*, A. Edwards*, G.C. Fehmers*, J.C. Fuchs, R. Giannella*, R.D. Gill*, L. Lauro-Taroni* and M. Romanelli*:* Soft X-Ray Tomography during ELMs and Impurity Injection in JET. Nuclear Fusion **38**, 1675-1694.

125. *Ishi*, S.-I. and J. Küppers:* Numerical Analysis of TDS of H2 from Hydrogenated Diamond Surfaces. Hyomen kagaku. Journal of the Surface Science Society Japan **19**, 37-38 (1998).

126. *Jacob, W.:* Surface Reactions during Growth and Erosion of Hydrocarbon Films (Invited Review). Thin Solid Films **326**, 1-42 (1998).

127. *Jaksic, N., J. Simon-Weidner and J. Sapper:* Support System for the W7-X Coil Assembly. In: Proc. 20th Symp. Fusion Technol., Marseille 1998, (Eds.) B.Beaumont, P.Libeyre, B.de Gentile, G.Tonon. Assoc. Euratom-CEA, Saint-Paul-lez-Durance 1998, 819-822.

128. *Jandl, O. and G. Krainz:* Wirbelströme im Kälteschild eines Durchführungsstutzen. In: Proc. 14th Int. Conf. on Computational Mechanics, Pernink 1998, (Ed.) J.Kren. Univ. Pilsen 1998, 85-92.

129. *Jenko, F. and B.D. Scott:* Effect of Nonlinear Electron Landau Damping in Collisionless Drift-Wave Turbulence. Physical Review Letters **80**, 4883-4886 (1998).

130. *Jenko, F. and B.D. Scott:* Kinetic and Fluid Models of Drift Wave Turbulence. In: Proc. Workshop Nonlinear MHD and Extended MHD, Atlanta,GA 1998. Wisconsin Univ., Madison,WI 1998, 1-4.

131. *Jones*, T.T.C., P. Andrew*, B. Alper*, B. Balet*, A. Cherubini*, J.P. Christiansen*, F. Crisanti*, R. de Angelis*, H.P.L. de Esch*, N. Deliyanakis*, F. de Luca*, M. Erba*, A. Edwards*, L.G. Eriksson*, C. Frewin*, P. Galli*, C. Gowers*, G. Gorini*. K. Günther*, H. Guo*, N.C. Hawkes*, T.C. Hender*, G. Huysmans*, R.W.T. König, K.D. Lawson*, H. Lingertat*, M. Mantsinen*, K. McCormick, A.C. Maas*, F.B. Marcus*, F. Nave*, V. Parail*, L. Porte*, F.G. Rimini*, B. Schunke*, P. Smeulders*, A. Taroni*, P.R. Thomas*, G. Saibene* and K.-D. Zastrow*:* DT Mixture Control with Neutral Beam Fuelling and Importance of Particle Recycling and Isotope Exchange in the JET ELM-Free-H-Mode. In: Proc. Int. Congress Plasma Phys. and 25th EPS Conf. Control. Fusion and Plasma Phys., Prague 1998, (Ed.) P.Pavlo. ECA 22C. Europ. Phys. Soc., Geneva 1998, 369-372.

132. *Jüttner, B.:* Displacement Times of Arc Cathode Spots in Vacuum. In: Proc. 18th Int. Symp. on Discharges and Electrical Insulation in Vacuum, Eindhoven 1998, (Ed.) J.Wetzer. IEEE Service Center, Piscataway,NJ 1998, 194-197.

133. *Jüttner, B.:* The Dynamics of Arc Cathode Spots in Vacuum. Part III: Measurements with Improved Resolution and UV Radiation. Journal of Physics **D 31**, 1728-1736 (1998).

134. *Jüttner, B.:* Surface Migration as a Possible Cause for Late Breakdowns. In: Proc. 18th Int. Symp. on Discharges and Electrical Insulation in Vacuum, Eindhoven 1998, (Ed.) J.Wetzer. IEEE Service Center, Piscataway,NJ 1998, 488-491.

135. *Jüttner B. and H. Pursch:* Substructure of Arc Spots at Thermionic Cathodes. In: Proc. 8th Int. Symp. on the Science and Technol. of Light Sources, Greifswald 1998, (Ed.) G.Babucke. Inst. for Low-Temperature Plasma Phys., Greifswald 1998, 324-325.

136. *Kallenbach, A. and G.M. Stäbler*:* Issues and Status of "Basic Divertor and SOL Physics" from Papers and Discussions. Czechoslovak Journal of Physics **48**, 147-150 (1998).

137. *Kallenbach, A., A. Thoma, A. Bard, K. Behringer, K. Schmidtmann, M. Weinlich and ASDEX Upgrade Team:* Evidence for Hydrogen Flux Dependence of the Apparent Chemical Erosion Yield of Graphite under High Flux Conditions. Nuclear Fusion **38**, 1097-1103 (1998).

138. *Kammler*, Th., S. Wehner* and J. Küppers:* The Role of Sticking and Reaction Probabilities in Hot-Atom Mediated Abstraction Reactions of D on Metal Surfaces by Gaseous H Atoms. Journal of Chemical Physics **109**, 4071-4077 (1998).

139. *Kardaun, O., J.W.P.F. Kardaun*, S.-I. Itoh and K. Itoh:* Catastrophe-Type Models to Fit Non-Linear Plasma Response Functions. In: Proc. Int. Congress Plasma Phys. and 25th EPS Conf. Control. Fusion and Plasma Phys., Prague 1998, (Ed.) P.Pavlo. ECA 22C. Europ. Phys. Soc., Geneva 1998, 1975-1978.

140. *Kass, T., H.-S. Bosch, F. Hoenen*, K. Lackner, M. Maraschek, H. Zohm* and ASDEX Upgrade Team:* The Fishbone Instability in ASDEX Upgrade. Nuclear Fusion **38**, 807-819 (1998).

141. *Kass, T., S. Günter, M. Maraschek, W. Suttrop, H. Zohm* and ASDEX Upgrade Team:* Characteristics of Type I and Type III ELM Precursors in ASDEX Upgrade. Nuclear Fusion **38**, 111-116 (1998).

142. *Kastelewicz, H., R. Schneider, D.P. Coster, U. Wenzel, M. Laux and J. Neuhauser:* B2-Eirene Density and Energy Scans for ASDEX Upgrade Shots. In: Proc. Int. Congress Plasma Phys. and 25th EPS Conf. Control. Fusion and Plasma Phys., Prague 1998, (Ed.) P.Pavlo. ECA 22C. Europ. Phys. Soc., Geneva 1998, 1852-1855.

143. *Kendl, A. and H. Wobig:* Linear Drift Waves in Advanced Stellarators. In: Proc. Int. Congress Plasma Phys. and 25th EPS Conf. Control. Fusion and Plasma Phys., Prague 1998, (Ed.) P.Pavlo. ECA 22C. Europ. Phys. Soc., Geneva 1998, 1730-1733.

144. *Keudell, A. von and J.R. Abelson*:* The Interaction of Atomic Hydrogen with Very Thin Amorphous Hydrogenated Silicon Films Analyzed Using in situ Real Time Infrared Spectroscopy: Reaction Rates and the Formation of Hydrogen Platelets. Journal of Applied Physics **84**, 489-495 (1998).

145. *Kick, M., F. Wagner and W7-AS Team:* W7-AS; Programme and Recent Results. Journal of Plasma and Fusion Research SERIES **1**, 19-26 (1998).

146. *Kleiber, R.:* Resistive Drift Waves in Stellarators. In: Proc. Int. Congress Plasma Phys. and 25th EPS Conf. Control. Fusion and Plasma Phys., Prague 1998, (Ed.) P.Pavlo. ECA 22C. Europ. Phys. Soc., Geneva 1998, 1753-1756.

147. *Klose, S. and M. Laux:* Fluctuations and the Shape of a Rotating Magnetized Plasma Column. In: Proc. Int. Congress Plasma Phys. and 25th EPS Conf. Control. Fusion and Plasma Phys., Prague 1998, (Ed.) P.Pavlo. ECA 22C. Europ. Phys. Soc., Geneva 1998, 1550-1553.

148. *Klose, S., H. Meyer and M. Laux:* Asymmetries of Double Probe Characteristics Observed in the PSI-1. Contributions to Plasma Physics **38**, Special Issue, 80-85 (1998).

149. *Könies, A.:* Numerical Analysis of Low Frequency Stability in a 3D Plasma Equilibrium with Energetic Particles. In: Proc. Int. Congress Plasma Phys. and 25th EPS Conf. Control. Fusion and Plasma Phys., Prague 1998, (Ed.) P.Pavlo. ECA 22C. Europ. Phys. Soc., Geneva 1998, 1749-1752.

150. *König, R.W.T., H. Anderson*, W.G.F. Core*, N. Hawkes*, M.G. von Hellermann*, A. Howman*, A.C. Maas*, P. Morgan*, M.F. Stamp*, H.P. Summers*, J. Svensson*, M. Tunklev*, P.R. Thomas* and K.-D. Zastrow*:* Active Spectroscopy on JET and ITER. In: Diagnostics for Experimental Thermonuclear Fusion Reactors 2, (Eds.) P.E.Stott, G.Gorini, P.Prandoni, E.Sindoni. Plenum Pr., New York 1998, 371-380.

151. *Koniges, A., R. Dohmen, G. Czapski and B.D. Scott:* Migration of Production Plasma Codes to the T3E. In: Proc. 4th Europ. Cray/SGI MPP Workshop, Garching 1998, (Eds.) H.Lederer, F.Hertweck. IPP, Garching 1998, 124-132.

152. *Koponen, J.P.T., T. Geist, U. Stroth, O. Dumbrajs*, S. Fiedler, H.-J. Hartfuß, O. Heinrich and W7-AS Team:* Measurement of Transient Particle Transport Coefficients in W7-AS. In: Proc. Int. Congress Plasma Phys. and 25th EPS Conf. Control. Fusion and Plasma Phys., Prague 1998, (Ed.) P.Pavlo. ECA 22C. Europ. Phys. Soc., Geneva 1998, 415-418.

153. *Köppendörfer, W.:* Der Tokamak als Fusionskraftwerk. Stand der Forschung. Atomwirtschaft Atomtechnik (atw) **43**, 14-19 (1998).

154. *Kraus, W., P. Frank, B. Heinemann, R. Riedl, E. Speth and O. Vollmer:* An RF Source Optimized for Low Pressure Operation. In: Proc. 20th Symp. Fusion Technol., Marseille 1998, (Eds.) B.Beaumont, P.Libeyre, B.de Gentile, G.Tonon. Assoc. Euratom-CEA, Saint-Paul-lez-Durance 1998, 441-444.

155. *Kraus, W., E. Speth, J.-H. Feist, B. Heinemann, R. Riedl, R. Trainham* and C. Jacquot*:* Large-Area Radio Frequency Plasma Sources for Fusion Applications. Review of Scientific Instruments **69**, 956-958 (1998).

156. *Kristof, G. and L.L. Lengyel:* Two-Fluid Magnetohydrodynamics Simulation of Confinement of Pellet-Produced Hydrogen Clouds in Hot Magnetized Plasmas. Physics of Plasmas **5**, 315-318 (1998).

157. *Kronhardt*, H., O. Dormicchi* and J. Sapper:* Design and Manufacturing of a WENDELSTEIN 7-X Demonstration Coil. In: Proc. 20th. Symp. on Fusion Technol., Marseille 1998, (Eds.) B.Beaumont, P.Libeyre, B.de Gentile, G.Tonon. Assoc. Euratom-CEA, Saint-Paul-lez-Durance 1998, 735-738.

158. *Kukushkin*, A.S., H.D. Pacher*, D.P. Coster, G. Janeschitz*, D. Reiter* and R. Schneider:* 2D Modelling of the Edge Plasma in ITER. Contributions to Plasma Physics **38**, 20-25 (1998).

159. *Kurzan, B., M. Maraschek, W. Schneider, J. Schweinzer, B.D. Scott, F. Serra*, W. Suttrop, A. Zeiler, ASDEX Upgrade Team, ICRH Team and NI Team:* Measurement of Correlation Lengths by Reflectometry in the Edge Plasma of ASDEX Upgrade. In: Proc. Int. Congress Plasma Phys. and 25th EPS Conf. Control. Fusion and Plasma Phys., Prague 1998, (Ed.) P.Pavlo. ECA 22C. Europ. Phys. Soc., Geneva 1998, 540-543.

160. *Küstner, M., W. Eckstein, V. Dose and J. Roth:* The Influence of Surface Roughness on the Angular Dependence of the Sputter Yield. Nuclear Instruments and Methods in Physics Research **B 145**, 320-331 (1998).

161. *Labich, S., A. Kohl, E. Taglauer and H. Knözinger*:* Silicide Formation by High-Temperature Reaction of Rh with Model SiO_2 Films. Journal of Chemical Physics **109**, 2052-2055 (1998).

162. *Lackner, K.:* Compatibility of Improved Confinement Regimes with Reactor Requirements. Plasma Physics and Controlled Fusion **40**, 557-568 (1998).

163. *Lang, P.T., K. Büchl, M. Kaufmann, R.S. Lang, A. Lorenz, V. Mertens, M. Maraschek, H.W. Müller, J. Neuhauser, H. Salzmann and ASDEX Upgrade Team:* Controlled High Density Operation beyond the Greenwald Limit on ASDEX Upgrade by Inboard Pellet Injection. In: Proc. Int. Congress Plasma Phys. and 25th EPS Conf. Control. Fusion and Plasma Phys., Prague 1998, (Ed.) P.Pavlo. ECA 22C. Europ. Phys. Soc., Geneva 1998, 293-296.

164. *Lang, P.T. and P. Cierpka:* High Repetition Inboard Launch of Hydrogen Pellets. Review of Scientific Instruments **69**, 2806-2807 (1998).

165. *Lang, P.T., P. Cierpka, R.S. Lang, A. Lorenz, C. Sihler and ASDEX Upgrade Team:* Plasma Refueling by Inboard Pellet Launch. In: Proc. 20th Symp. on Fusion Technol., Marseille 1998, (Eds.) B.Beaumont, P.Libeyre, B.de Gentile, G.Tonon. Assoc. Euratom-CEA, Saint-Paul-lez-Durance 1998, 1025-1028.

166. *Laqua, H.P., V. Erckmann, W7-AS Team and ECRH Group (W7-AS):* Electron Cyclotron Heating beyond the Cutoff Density by O-X-B Mode Conversion in W7-AS. Journal of Plasma and Fusion Research SERIES **1**, 314-317 (1998).

167. *Laqua, H.P., V. Erckmann, W7-AS Team and ECRH Group (W7-AS):* Recent ECRH and ECCD Experiments at W7-AS. In: Proc. 10th Joint Workshop on Electron Cyclotron Emission and Electron Cyclotron Resonance Heating, Ameland 1997, (Eds.) T.Donné, T.Verhoeven. World Scientific Publ., Singapore 1998, 317-328.

168. *Laqua, H.P., H.-J. Hartfuß and W7-AS Team:* Electron Bernstein Wave Emission from an Overdense Plasma at the W7-AS Stellarator. Physical Review Letters **81**, 2060-2063 (1998).

169. *Lederer, H.:* Grand Challenge Applications of the Max Planck Society on the Garching T3E. In: Proc. Supercomputer 98, Anwendungen, Architekturen, Trends, Mannheim 1998, (Ed.) H.W. Meuer. Saur-Verl., München 1998, 68-81.

170. *Lengyel, L.L., K. Lackner, P.J. Lalousis*, P.N. Spathis*, V.A. Rozhanskij*, I.Yu. Veselova* and P.B. Parks*:* Divertor Plate Erosion and Radiating Vapour Shield Formation during Hard Disruptions: Theory and Numerical Modelling. Nuclear Fusion **38**, 1435-1459 (1998).

171. *Leonard*, A.W., A. Herrmann, K. Itami*, J. Lingertat*, A. Loarte*, T. Osborne*, W. Suttrop, ITER Divertor Modeling and Database Expert Group and ITER Divertor Physics Expert Group:* ELM Heat Flux in the ITER Divertor. In: Proc. Int. Congress Plasma Phys. and 25th EPS Conf. Control. Fusion and Plasma Phys., Prague 1998, (Ed.) P.Pavlo. ECA 22C. Europ. Phys. Soc., Geneva 1998, 679-682.

172. *Leuterer, F., A.G. Peeters, G. Pereverzev, F. Ryter, ECRH Group (AUG) and ASDEX Upgrade Team:* ECRH Deposition Studies in ASDEX Upgrade. In: Proc. 10th Joint Workshop on Electron Cyclotron Emission and Electron Cyclotron Heating, Ameland 1997, (Eds.) T.D.Donné, T.Verhoeven. World Scientific Publ., Singapore 1998, 349-356.

173. *Leuterer, F., F. Ryter, M. Beckmann, H. Brinkschulte, A.G. Peeters, M. Münich, G. Pereverzev, W. Suttrop, ASDEX Upgrade Team and ECRH Group (AUG):* ECRH Experiments in ASDEX Upgrade. In: Proc. 2nd Europ. Top. Conf. RF Frequency Heating and Current Drive of Fusion Devices, Brussels 1998, (Eds.) J.Jacquinot, G.VanOost, R.R.Weynants. ECA 22A. Europ. Phys. Soc., Geneva 1998, 233-236.

174. *Linden, W. von der, V. Dose, N. Memmel and R. Fischer:* Probabilistic Evaluation of Growth Models Based on Time-Dependent Auger Signals. Surface Science **409**, 290-301 (1998).

175. *Linden, W. von der, V. Dose and A. Ramaswami*:* Bayesian Group Analysis. In: Maximum Entropy and Bayesian Methods, (Eds.) J.Rychert, G.Erickson, R.Smith. Kluwer, Dordrecht 1998, 87-99.

176. *Loarte*, A., N. Asakura*, H.-S. Bosch, S.J. Davies*, T. Hatae*, A. Herrmann, A. Hubbard*, K. Itami*, G. Janeschitz**, A.W. Leonard*, J. Lingertat*, B. Lipschultz*, G.F. Matthews*, K. McCormick, R. Mohanti*, R.D. Monk*, T. Osborne*, H.D. Pacher*, S. Pitcher*, G. Porter*, D. Post*, G. Saibene*, J. Schweinzer, M. Shimada*, E. Solano, M. Sugihara* and W. Suttrop:* Experimental Edge Results and Multimachine Comparisons. Contributions to Plasma Physics **38**, 11-19 (1998).

177. *Loarte*, A., R.D. Monk*, J.R. Martin-Solis*, D.J. Campbell*, A.V. Chankin*, S. Clement*, S.J. Davies*, J. Ehrenberg*, S.K. Erents*, H. Guo*, P.J. Harbour*, L.D. Horton*, L.C. Ingesson*, H. Jäckel*, J. Lingertat*, C. Lowry*, C.F. Maggi*, G.F. Matthews*, K. McCormick, D.P. O'Brien*, R. Reichle*, G. Saibene*, R.J. Smith*, M.F. Stamp*, D. Stork* and G.C. Vlases*:* Plasma Detachment in JET Mark I Divertor Experiments. Nuclear Fusion **38**, 331-371 (1998).

178. *Logatchev*, A.A., V.P. Afanas'ev*, S.M. Shkol'nik*, H. Pursch and B. Jüttner:* The Behaviour of Vacuum Arc Discharges at Hydrogen Impregnated Electrodes. In: Proc. 18th Int. Symp. on Discharges and Electrical Insulation in Vacuum, Eindhoven 1998, (Ed.) J.Wetzer. IEEE Service Center, Piscataway,NJ 1998, 288-291.

179. *Lortz, D. and G.O. Spies:* Extended Theory of Interface Localized Modes. Physics of Plasmas **5**, 1255-1258 (1998).

180. *Luthin, J., K.P. Lieb*, M. Neubauer*, M. Uhrmacher* and B. Lidgren*:* Electric-Quadrupole Interactions at ^{111}Cd in HfO_2 and ZrO_2: A Perturbed Angular Correlation Study. Physical Review **B 57**, 15272-15281 (1998).

181. *Maas, A.C.*, P. Andrew*, P. Coad*, A. Edwards*, J. Ehrenberg*, A. Gibson*, K. Günther*, M.G. von Hellermann*, D. Hillis*, A. Howman*, O.N. Jarvis*, J.F. Jünger*, R.W.T. König, J. Lingertat*, M.J. Loughlin*, P.D. Morgan*, J. Orchard*, G. Sadler*, M.F. Stamp* and C.H. Wilson*:* Diagnostic Experience during Deuterium-Tritium Experiments in JET, Techniques and Measurements. In: Proc. 20th Symp. on Fusion Technol., Marseille 1998, (Eds.) B.Beaumont, P.Libeyre, B.de Gentile, G.Tonon. Assoc. Euratom-CEA, Saint-Paul-lez-Durance 1998, 693-696.

182. *Maaßberg, H., C.D. Beidler, U. Gasparino, S. Murakami*, M. Romé*, U. Stroth and W7-AS Team:* Transport Analysis in Low-Collisionality W7-AS Plasmas. Journal of Plasma and Fusion Research SERIES **1**, 103-107 (1998).

183. *MacFarland, T., H.M.P. Couchman*, F.R. Pearce* and J. Pichlmeier*:* A New Parallel P^3M Code for Very Large-Scale Cosmological Simulations. New Astronomy **3**, 671-685, 1998.

184. *Maier, H., S. Kötterl, K. Krieger, R. Neu, M. Balden and ASDEX Upgrade Team:* Performance of Tungsten Coatings as Plasma Facing Components in ASDEX Upgrade. Journal of Nuclear Materials **258-263**, 921-926 (1998).

185. *Manso*, M., F. Serra*, B. Kurzan, I. Nunes*, J. Santos*, A. Silva*, W. Suttrop, P. Varela* and S. Vergamota*:* H-Mode Studies with Microwave Reflectometry on ASDEX Upgrade. Plasma Physics and Controlled Fusion **40**, 747-752 (1998).

186. *Manso*, M., F. Serra*, I. Nunes*, S. Vergamota*, J. Santos*, A. Silva*, P. Varela*, M. Maraschek, B. Kurzan, W. Suttrop and ASDEX Upgrade Team:* Local Measurement with Microwave Reflectometry of Density Profile Perturbations due to MHD Activity on ASDEX Upgrade. In: Proc. Int. Congress Plasma Phys. and 25th EPS Conf. Control. Fusion and Plasma Phys., Prague 1998, (Ed.) P.Pavlo. ECA 22C. Europ. Phys. Soc., Geneva 1998, 544-547.

187. *Maraschek, M., J.C. Fuchs, K.-F. Mast and V. Mertens:* Real-Time Determination of Total Radiated Power by Bolometric Cameras with Statistical Methods. Review of Scientific Instruments **69**, 109-115 (1998).

188. *Maraschek, M., S. Günter, T. Kass, S. Saarelma*, H.-P. Zehrfeld, H. Zohm* and ASDEX Upgrade Team:* MHD Characteristics of ELMs and their Precursors. In: Proc. Int. Congress Plasma Phys. and 25th EPS Conf. Control. Fusion and Plasma Phys., Prague 1998, (Ed.) P.Pavlo. ECA 22C. Europ. Phys. Soc., Geneva 1998, 492-495.

189. *Martin, Y. and ITER Confinement and Threshold Database Working Group:* Prediction of ITER H-Mode Power Threshold by Means of Various Statistical Techniques. In: Proc. Int. Congress Plasma Phys. and 25th EPS Conf. Control. Fusion and Plasma Phys., Prague 1998, (Ed.) P.Pavlo. ECA 22C. Europ. Phys. Soc., Geneva 1998, 675-678.

190. *Mayer, M., A. Annen, W. Jacob and S. Grigull:* The $^{11}B(p,\alpha_0)^8Be$ Nuclear Reaction and $^{11}B(p,p)^{11}B$ Backscattering Cross Sections for Analytical Purposes. Nuclear Instruments and Methods in Physics Research **B 143**, 244-252 (1998).

191. *Mayer, M., M. Balden and R. Behrisch:* Deuterium Retention in Carbides and Doped Graphites. Journal of Nuclear Materials **252**, 55-62 (1998).

192. *Mayer, M., R. Behrisch, C. Gowers*, P. Andrew* and A.T. Peacock*:* Change of the Optical Reflectivity of Mirror Surfaces Exposed to JET Plasmas. In: Diagnostics for Experimental Thermonuclear Fusion Reactors 2, (Eds.) P.Stott, G.Gorini, P.Prandoni, E.Sindoni. Plenum Press, New York 1998, 279-286.

193. *Memmel, N.:* Monitoring and Modifying Properties of Metal Surfaces by Electronic Surface States. Surface Science Reports **32**, 91-164 (1998).

194. *Merkel, P. and M. Drevlak:* Coils for 3D MHD Equilibria. In: Proc. Int. Congress Plasma Phys. and 25th EPS Conf. Control. Fusion and Plasma Phys., Prague 1998, (Ed.) P.Pavlo. ECA 22C. Europ. Phys. Soc., Geneva 1998, 1745-1747.

195. *Mertens, V., M. Kaufmann, P.T. Lang, R.S. Lang, H. Murmann, J. Neuhauser, H. Salzmann, J. Schweinzer and ASDEX Upgrade Team:* Edge Density Characterization Close to the Greenwald Density Limit with the New Closed Divertor in ASDEX Upgrade. In: Proc. Int. Congress Plasma Phys. and 25th EPS Conf. Control. Fusion and Plasma Phys., Prague 1998, (Ed.) P.Pavlo. ECA 22C. Europ. Phys. Soc., Geneva 1998, 523-527.

196. *Meyer-Spasche, R.:* Difference Schemes of Optimum Degree of Implicitness for a Family of Simple ODEs with Blow-up Solutions. Journal of Computational and Applied Mathematics **97**, 137-152 (1998).

197. *Milch, I.:* Ein Divertor für ITER. HGF Jahresheft, 18-19 (1998).

198. *Milch, I.:* Kernfusion - Weltrekorde ohne Schlagzeilen. Die Leitung. Mitarbeitermagazin der OBAG, Heft 1, 16-17 (1998).

199. *Milch, I. and M. Endler:* Topping-out Ceremony of the New Buildings of the IPP Greifswald Branch. Stellarator News **59**, 1-2 (1998), http://www.ornl.gov/fed/stelnews/sn59.html.

200. *Milligen*, B.Ph. van, B.A. Carreras*, M.A. Pedrosa*, R. Balbín*, C. Hidalgo*, D.E. Newman*, E. Sánchez*, I. García-Cortés*, J. Bleuel, M. Endler, C. Riccardi*, S.J. Davies*, G.F. Matthews*, E. Martines*, V. Antoni*, A. Latten* and T. Klinger*:* Long-Range Correlations and Universality in Plasma Edge Turbulence. In: Proc. Int. Congress Plasma Phys. and 25th EPS Conf. Control Fusion and Plasma Phys., Prague 1998, (Ed.) P.Pavlo. ECA 22C. Europ. Phys. Soc., Geneva 1998, 2302-2305.

201. *Miri*, A.M., N.A. Riegel*, C. Meinecke*, C. Sihler and F. Schauer:* Investigation of the Transient Electromagnetic Processes and Forces in Metallic Environments of Large Superconducting Magnets by an Optimized Finite Element Approach. In: Proc. 6th Int. Conf. on Optimization of Electrical and Electronic Equipments, Brasov 1998. Transilvania Univ. of Brasov, Brasov 1998, 71-76.

202. *Monticello*, D., G.Y. Fu*, R.J. Goldston*, L.-P. Ku*, H. Mynick*, R. Nazikian*, G.H. Neilson*, N. Pomphrey*, A.H. Reiman*, M. Redi*, M.C. Zarnstorff*, I. Zatz*, W. Cooper*, S.P. Hirshman*, M. Drevlak, P. Merkel, C. Nührenberg, J. Nührenberg, A. Boozer* and B. Blackwell*:* Physics Considerations for the Design of NCSX. In: Proc. Int. Congress Plasma Phys. and 25th EPS Conf. Control. Fusion and Plasma Phys., Prague 1998, (Ed.) P.Pavlo. ECA 22C. Europ. Phys. Soc., Geneva 1998, 1742-1744.

203. *Müller*, G.A., W. Förster*, V. Erckmann and H.P. Laqua:* Voltage Regulate for Power Modulation of a Gyrotron with Voltage Depressed Collector. In: Proc. 20th Symp. on Fusion Technol., Marseille 1998, (Eds.) B.Beaumont, P.Libeyre, B.de Gentile, G.Tonon. Assoc. Euroatom-CEA, Saint-Paul-lez Durance 1998, 877.

204. *Naujoks, D., G. Fußmann and H. Meyer:* I(U)-Characteristics of the Plasma Generator PSI-1: Experiment and Theory. Contributions to Plasma Physics **38**, Special Issue, 127-133 (1998).

205. *Neubauer*, M., N. Reinecke, A. Kulinska*, K.P. Lieb*, M. Uhrmacher*, P. Wodniecki*, M. Störmer* and H.U. Krebs*:* PAC Measurements in Laser Deposited Ag/Fe and In/Fe Alloys. Journal of Magnetism and Magnetic Materials **189**, 8-18 (1998).

206. *Neubauer*, M., N. Reinecke, M. Uhrmacher*, K.P. Lieb*, M. Münzenberg* and W. Felsch*:* Ion-Beam Induced Magnetic Anisotropies in Iron Films. Nuclear Instruments and Methods in Physics Research **B 139**, 332-337 (1998).

207. *Niemann, C., A. Bard , H.-U. Fahrbach, G. Haas, W. Herrmann, J. Stober, W. Treutterer, T. Zehetbauer, ASDEX Upgrade Team and NI Team:* H/D Ratio Control Experiments at ASDEX Upgrade. In: Proc. Int. Congress Plasma Phys. and 25th EPS Conf. Control. Fusion and Plasma Phys., Prague 1998, (Ed.) P.Pavlo. ECA 22C. Europ. Phys. Soc., Geneva 1998, 532-535.

208. *Nitsche, A. and J. Sapper:* Power Supply and Quench Protection for the WENDELSTEIN 7-X Magnet. In: Proc. 20th Symp. on Fusion Technol., Marseille 1998, (Eds.) B.Beaumont, P.Libeyre, B.de Gentile, G.Tonon. Assoc. Euratom-CEA, Saint-Paul-lez-Durance 1998, 755-762.

209. *Noterdaeme, J.-M., M. Brambilla, B. Brüsehaber, J. Gafert, A. Gude, W. Suttrop, H.-P. Zehrfeld, ICRH Group and ASDEX Upgrade Team:* Variation of the Sawtooth Activity with ICRF in ASDEX Upgrade. In: Proc. 2nd Europ. Top. Conf. RF Frequency Heating and Current Drive of Fusion Devices, Brussels 1998, (Eds.) J.Jacquinot, G.VanOost, R.R.Weynants. ECA 22A. Europ. Phys. Soc., Geneva 1998, 9-12.

210. *Ohyabu*, N. and H. Renner:* Advanced Divertor Concepts for Helical Devices. Contributions to Plasma Physics **38**, 94-105 (1998).

211. *Okamura*, S., K. Matsuoka*, M. Fujiwara*, M. Drevlak, P. Merkel and J. Nührenberg:* Conceptual Design of a Quasi-Axisymmetric Stellarator. Journal of Plasma and Fusion Research SERIES **1**, 164-167 (1998).

212. *Ott, W., J.P.T. Koponen, F.-P. Penningsfeld, E. Speth and H. Walter:* Neutral Beam Modulation for Profile Measurements of Power and Particle Deposition in the W7-Stellarator. In: Proc. Int. Congress Plasma Phys. and 25th EPS Conf. Control. Fusion and Plasma Phys., Prague 1998, (Ed.) P.Pavlo. ECA 22C. Europ. Phys. Soc., Geneva 1998, 1202-1205.

213. *Pautasso, G., P. Franzen, J.C. Fuchs, J. Gernhardt, O. Gruber, A. Kallenbach, K. Lackner, M. Maraschek, V. Mertens, H. Pfeiffer*, W. Schneider, C. Tichmann, ASDEX Upgrade Team, NBI Group, ICRH Group and ECRH Group (AUG):* Causes, Presursors and Mechanisms of Disruptions in ASDEX Upgrade. In: Proc. Int. Congress Plasma Phys. and 25th EPS Conf. Control. Fusion and Plasma Phys., Prague 1998, (Ed.) P.Pavlo. ECA 22C. Europ. Phys. Soc., Geneva 1998, 520-523.

214. *Pecher, P. and W. Jacob:* Determination of the Absolute CH_3 Radical Flux Emanating from a Methane Electron Cyclotron Resonance Plasma. Applied Physics Letters **73**, 31-33 (1998).

215. *Peeters, A.G.:* Equations for the Evolution of the Radial Electric Field and Poloidal Rotation in Toroidally Symmetric Geometry. Physics of Plasmas **5**, 763-767 (1998).

216. *Peeters, A.G.:* Stringer Spin Up Due to Anomalous Transport. Physics of Plasmas **5**, 2399-2404 (1998).

217. *Peeters, A.G., J. Stober, D.P. Coster, R. Schneider and ASDEX Upgrade Team:* The Influence of Neutral Friction and Neoclassical Viscosity in the Edge of ASDEX Upgrade. Plasma Physics and Controlled Fusion **40**, 703-706 (1998).

218. *Pereverzev, G.:* Beam Tracing in Inhomogeneous Anisotropic Plasmas. Physics of Plasmas **5**, 3529-3541 (1998).

219. *Pereverzev, G., A.G. Peeters and E. Poli:* Propagation of Paraxial Gaussian Beams in Anisotropic Plasmas. In: Proc. 2nd Europ. Top. Conf. RF Frequency Heating and Current Drive of Fusion Devices, Brussels 1998, (Eds.) J.Jacquinot, G.VanOost, R.R.Weynants. ECA 22A. Europ. Phys. Soc., Brussels 1998, 265-268.

220. *Pereverzev, G., R. Wolf, O. Gruber, A. Kallenbach, H. Meister, K. Lackner, S. de Peña Hempel, F. Ryter, S. Sesnic, J. Stober and ASDEX Upgrade Team:* Advanced Tokamak Operation in ASDEX Upgrade: First Experiments and Feasibility Study for Stationary Operation. In: Proc. Int. Congress Plasma Phys. and 25th EPS Conf. Control. Fusion and Plasma Phys., Prague 1998, (Ed.) P.Pavlo. ECA 22C. Europ. Phys. Soc., Geneva 1998, 496-499.

221. *Pfeiffer, U., M. Endler, J. Bleuel, H. Niedermeyer, G. Theimer and W7-AS Team:* Density, Temperature and Potential Fluctuation Measurements with Multiple Fast Swept Langmuir Probes on W7-AS. Contributions to Plasma Physics **38**, Special Issue, 134-144 (1998).

222. *Pinches, S.D., R.J. Akers*, L.C. Appel*, S. Günter, M. Maraschek and ASDEX Upgrade Team:* Fast Particle Driven MHD Activity. In: Proc. Int. Congress Plasma Phys. and 25th EPS Conf. Control. Fusion and Plasma Phys., Prague 1998, (Ed.) P.Pavlo. ECA 22C. Europ. Phys. Soc., Geneva 1998, 1844-1847.

223. *Pinches, S.D., L.C. Appel*, J. Candy*, S.E. Sharapov*, H.L. Berk*, D. Borba*, B.N. Breizman*, T.C. Hender*, K.I. Hopcraft*, G. Huysmans* and W. Kerner*:* The HAGIS Self-Consistent Nonlinear Wave-Particle Interaction Model. Computer Physics Communications **111**, 133-149 (1998).

224. *Pinkau, K.:* Freiheit der Forschung bei den Zukunftstechnologien. In: Globalisierung und informationelle Rechtskultur in Europa, (Eds.) S.Lamnek, M.-T.Tinnefeld. Nomos Verl.-Ges., Baden-Baden 1998, 51-58.

225. *Pinkau, K.:* Silhouettes: Rhetoric and Science. European Review **6**, 327-332 (1998).

226. *Pinkau, K. and O. Renn* (Eds.):* Environmental Standards. Kluwer, Dordrecht 1998, 432 p.

227. *Poli, E., A.G. Peeters and G. Pereverzev:* Beam Tracing Description of EC Wave Beams in Tokamak Plasmas. In: Proc. Int. Congress Plasma Phys. and 25th EPS Conf. Control. Fusion and Plasma Phys., Prague 1998, (Ed.) P.Pavlo. ECA 22C. Europ. Phys. Soc.,Geneva 1998, 1352-1355.

228. *Popp*, V., R. Kladny*, Th. Schimmel* and J. Küppers:* Structuring of Mica Surfaces with a Vibrating AFM Tip. Surface Science **401**, 105-111 (1998).

229. *Porkolab*, M., A. Bécoulet*, P.T. Bonoli*, C. Gormezano*, R. Koch*, R.J. Majeski*, A. Messiaen*, J.-M. Noterdaeme, C. Petty*, R. Pinsker*, D. Start* and R. Wilson*:* Recent Progress in ICRF Physics. Plasma Physics and Controlled Fusion **40**, A35-A52 (1998).

230. *Preuss, R., V. Dose and W. von der Linden:* Model Comparison with Energy Confinement Data from Large Fusion Experiments. In: Maximum Entropy and Bayesian Methods, (Eds.) G.Erickson, J.Rychert, R.Smith. Kluwer, Dordrecht 1998, 137-145.

231. *Prozesky*, V.M., J. Padayachee*, R. Fischer, W. von der Linden, V. Dose and A. Weller:* Bayesian Techniques and the Principle of Maximum Entropy in Ion-Beam Analysis Applications. Nuclear Instruments and Methods in Physics Research **B 136-138**, 1146-1151 (1998).

232. *Puri, S.:* Anomalous Transport via Kirchhoff Radiation. In: Proc. Int. Congress Plasma Phys. and 25th EPS Conf. Control. Fusion and Plasma Phys., Prague 1998, (Ed.) P.Pavlo. ECA 22C. Europ. Phys. Soc., Geneva 1998, 1682-1685.

233. *Puri, S.:* Enhanced Transport via Kirchhoff Radiation. Physics of Plasmas **5**, 2932-2935 (1998).

234. *Quian*, J.P., J. Roth, J.R. Song*, F. Zhang*, L. Yang* and G.T. Zhai*:* Development of Multi-Element Doped Graphite and its Modification of Chemical Erosion. Journal of Nuclear Materials **258-263**, 706-712 (1998).

235. *Rangelov, G. and V. Dose:* Appearance Potential Spectroscopy Study of Diamond Films. Surface Science **395**, 1-9 (1998).

236. *Rangelov, G., K. Ertl, F. Passek, M. Vonbank, S. Bassen, J. Reinmuth, M. Donath and V. Dose:* High-Performance X-Ray Detector for Appearance Potential Spectroscopy. Journal of Vacuum Science and Technology **A 16**, 2738-2741 (1998).

237. *Raupp, G., R. Cole*, K. Lüddecke*, V. Mertens, G. Neu, W. Treutterer, D. Zasche, T. Zehetbauer and ASDEX Upgrade Team:* Next Generation Discharge Control System for ASDEX Upgrade. In: Proc. 20th Symp. on Fusion Technol., Marseille 1998, (Eds.) B.Beaumont, P.Libeyre, B.de Gentile, G.Tonon. Assoc. Euratom-CEA, Saint-Paul-lez-Durance 1998, 29.

238. *Reimerdes*, H., A. Pochelon* and W. Suttrop:* Toroidally Asymmetric ELM Precursors in TCV. Nuclear Fusion **38**, 319-323 (1998).

239. *Reinmüller, K.:* Determination of the Plasma Potential Using Emissive Probes - Implications from PIC Simulations. Contributions to Plasma Physics **38**, Special Issue, 7-12 (1998).

240. *Reinmuth, J., M. Donath, F. Passek and V.N. Petrov*:* Temperature-Dependent Surface Magnetization of $FeNi_3$(111) Studied by Spin-Resolved Appearance Potential Spectroscopy. Journal of Physics. Condensed Matter **10**, 4027-4034 (1998).

241. *Rensink*, M.E., L. Lodestro*, G. Porter*, T.D. Rognlien* and D.P. Coster:* A Comparison of Neutral Gas Models for Divertor Plasmas. Contributions to Plasma Physics **38**, 325-330 (1998).

242. *Riedl, R., A. Stäbler, B. Heinemann, J. Sielanko* and E. Speth:* An Injection System for Off-Axis NBCD on ASDEX Upgrade. In: Proc. 20th Symp. Fusion Technol., Marseille 1998, (Eds.) B.Beaumont, P.Libeyre, B.de Gentile, G.Tonon. Assoc. Euratom-CEA, Saint-Paul-lez-Durance 1998, 445-448.

243. *Rimini, F.G.*, P. Andrew*, B. Balet*, R. Budny*, J. Bull*, N. Deliyanakis*, H.P.L. de Esch*, L.-G. Eriksson*, R. Giannella*, C. Gowers*, H. Guo*, T. Hender*, G. Huysmans*, T.T.C. Jones*, M. Keilhacker*, R.W.T. König, M. Lennholm*, P. Lomas*, M. Loughlin*, A. Maas*, M. Mantsinen*, F.B. Marcus*, F. Nave*, V. Parail*, J. Strachan*, A. Taroni*, P.R. Thomas* and K.- D. Zastrow*:* High DT Fusion Performance in ELM-Free H-Modes in JET. In: Proc. Int. Congress Plasma Phys. and 25th EPS Conf. Control. Fusion and Plasma Phys., Prague 1998, (Ed.) P.Pavlo. ECA 22C. Europ. Phys. Soc., Geneva 1998, 329-332.

244. *Rogers*, B.N., J.F. Drake* and A. Zeiler:* Phase Space of Tokamak Edge Turbulence, the L-H Transition, and the Formation of the Edge Pedestal. Physical Review Letters **81**, 4396-4399 (1998).

245. *Romé*, M., V. Erckmann, U. Gasparino and N. Karulin*:* Electron Cyclotron Resonance Heating and Current Drive in the W7-X Stellarator. Plasma Physics and Controlled Fusion **40**, 511-530 (1998).

246. *Roth, J., D. Walsh*, W.R. Wampler* and M. Mayer:* Ion Beam Analysis of Oxidised a-C:D Layers on Be - A Comparison of ^{4}He RBS and ^{28}Si ERD Analysis. Nuclear Instruments and Methods in Physics Research **B 136-138**, 689-694 (1998).

247. *Rozhanskij*, V.A., I.Yu. Veselova*, L.L. Lengyel and P.J. Lalousis*:* Drifts in the Scrape-off Layer during Hard Disruptions. Contributions to Plasma Physics **38**, 124-129 (1998).

248. *Ryter, F., F. Leuterer, M. Beckmann, H. Brinkschulte, M. Münich, G. Pereverzev and W. Suttrop:* Transport with On-Axis and Off-Axis ECRH in ASDEX Upgrade. In: Proc. Int. Congress Plasma Phys. and 25th EPS Conf. Control. Fusion and Plasma Phys., Prague 1998, (Ed.) P.Pavlo. ECA 22C. Europ. Phys. Soc., Geneva 1998, 500-503.

249. *Ryter, F., W. Suttrop. B. Brüsehaber, M. Kaufmann, V. Mertens, H. Murmann, A.G. Peeters, J. Stober, J. Schweinzer, H. Zohm* and ASDEX Upgrade Team:* H-Mode Power Threshold and Transition in ASDEX Upgrade. Plasma Physics and Controlled Fusion **40**, 725-729 (1998).

250. *Schauer, F.:* W7-X Demonstration Cryostat Close to Completion. Stellarator News **59**, 2-3 (1998), http://www.ornl.gov/fed/stelnews/sn59.html.

251. *Schlögl, D., R. Neu, R. Dux and ASDEX Upgrade Team:* Concentrations of Spurious Impurities in ASDEX Upgrade. In: Proc. Int. Congress Plasma Phys. and 25th EPS Conf. Control. Fusion and Plasma Phys., Prague 1998, (Ed.) P.Pavlo. ECA 22C. Europ. Phys. Soc., Geneva 1998, 512-515.

252. *Scott, B.D.:* Computation of Warm-Ion Drift Alfvén Turbulence. Contributions to Plasma Physics **38**, 171-176 (1998).

253. *Scott, B.D.:* Global Consistency for Thin Flux Tube Treatments of Toroidal Geometry. Physics of Plasmas **5**, 2334-2339 (1998).

254. *Scott, B.D.:* Warm-Ion Drift Alfvén Turbulence and the L-H Transition. Plasma Physics and Controlled Fusion **40**, 823-826 (1998).

255. *Scott, B.D. and F. Jenko:* Fluid and Kinetic Computation of Drift Alfvén Turbulence. In: Proc. Int. Congress Plasma Phys. and 25th EPS Conf. Control. Fusion and Plasma Phys., Prague 1998, (Ed.) P.Pavlo. ECA 22C. Europ. Phys. Soc., Geneva 1998, 2149-2152.

256. *Sesnic, S., S. Günter, S.D. Pinches, R. Kaita*, S.H. Batha*, R.E. Bell*, S. Bernabei*, M.S. Chance*, E. de la Luna*, J.L. Dunlap*, A.C. England*, R.C. Isler*, S. Jones*, S.M. Kaye*, J. Kesner*, H. Kugel*, B. LeBlanc*, F.M. Levinton*, S.C. Luckhardt*, J. Manickam*, M. Okabayashi*, M. Ono*, F. Paoletti*, S.F. Paul*, A.P. Post-Zwicker*, J. Sanchez Sanz*, N.R. Sauthoff*, T. Seki*, H. Takahashi*, W. Tighe*, S. von Goeler*, P. Woskov* and A. Zolfaghari*:* Magnetohydrodynamic Behaviour during Core Transport Barrier Experiments with Ion Bernstein Wave Heating in PBX-M: II -- $n = m - 1$ and $n = m$ Modes. Nuclear Fusion **38**, 861-884 (1998).

257. *Sesnic, S., R. Kaita*, S.H. Batha*, R.E. Bell*, S. Bernabei*, M.S. Chance*, E. de la Luna*, J.L. Dunlap*, A.C. England*, R.C. Isler*, S. Jones*, S.M. Kaye*, J. Kesner*, H. Kugel*, B. LeBlanc*, F.M. Levinton*, S.C. Luckhardt*, J. Manickam*, M. Okabayashi*, M. Ono*, F. Paoletti*, S.F. Paul*, A.P. Post-Zwicker*, J. Sanchez Sanz*, N.R. Sauthoff*, T. Seki*, H. Takahashi*, W. Tighe*, S. von Goeler*, P. Woskov* and A. Zolfaghari*:* Magnetohydrodynamic Behaviour during Core Transport Barrier Experiments with Ion Bernstein Wave Heating in PBX-M: I ELMs, Fluctuations and Crash Events. Nuclear Fusion **38**, 835-859 (1998).

258. *Shay*, M.A., J.F. Drake*, R.E. Denton* and D. Biskamp:* Structure of the Dissipation Region during Collisionless Magnetic Reconnection. Journal of Geophysical Research **103**, 9165-9176 (1998).

259. *Shishkin*, A.A., I.N. Sidorenko and H. Wobig:* Magnetic Islands and Drift Resonances in Helias Configurations. Journal of Plasma and Fusion Research SERIES **1**, 480-483 (1998).

260. *Shulga*, V.I. and W. Eckstein:* Depth of Origin of Sputtered Atoms for Elemental Targets. Nuclear Instruments and Methods in Physics Research **B 145**, 492-502 (1998).

261. *Sidorenko, I.N. and H. Wobig:* Trapped Alpha-Particle Orbits under the Effect of Drift Waves. In: Proc. Int. Congress Plasma Phys. and 25th EPS Conf. Control. Fusion and Plasma Phys., Prague 1998, (Ed.) P.Pavlo. ECA 22C. Europ. Phys. Soc., Geneva 1998, 1836-1839.

262. *Sihler, C., B. Streibl, R. Klein*, W. Schlüter* and M. Krohn*:* Reactive Power Compensation for the Pulsed Power Supply of ASDEX Upgrade. In: Proc. 20th Symp. on Fusion Technol., Marseille 1998, (Eds.) B.Beaumont, P.Libeyre, B.de Gentile, G.Tonon. Assoc. Euratom-CEA, Saint-Paul-lez-Durance 1998, 887-890.

263. *Silva*, A., L. Cupido*, C. Loureiro*, S. Vergamota*, P. Varela*, J. Santos*, M. Manso*, F. Serra*, L. Meneses*, M. Tavares*, I. Nunes*, B. Kurzan, W. Suttrop and V. Grossmann*:* Next Generation Discharge Control System for ASDEX Ugprade. In: Proc. 20th Symp. on Fusion Technol., Marseille 1998, (Eds.) B.Beaumont, P.Libeyre, B.de Gentile, G.Tonon. Assoc. Euratom-CEA, Saint-Paul-lez-Durance 1998, 28.

264. *Simon-Weidner, J. and N. Jaksic:* Fast Evaluation of W7-X Components with Aspects of Safety Based on FE-Calculations. In: Proc. 20th Symp. Fusion Technol., Marseille 1998, (Eds.) B.Beaumont, P.Libeyre, B.de Gentile, G.Tonon. Assoc. Euratom-CEA, Saint-Paul-lez-Durance 1998, 823-826.

265. *Solano, E., M. Taguchi, H. Maaßberg, F.-P. Penningsfeld and W7-AS Team:* Momentum Conservation and Friction Effects on Neoclassical Flows in Stellarators. In: Proc. Int. Congress Plasma Phys. and 25th EPS Conf. Control. Fusion and Plasma Phys., Prague 1998, (Ed.) P.Pavlo. ECA 22C. Europ. Phys. Soc., Geneva 1998, 1718-1725.

266. *Sombach, B., J.-H. Feist, H. Schneider and J. Simon-Weidner:* Acceptable Manufacturing Accuracy of Components Used to Built up the Stellarator W7-X. In: Proc. 20th Symp. on Fusion Technol., Marseille 1998, (Eds.) B.Beaumont, P.Libeyre, B.de Gentile, G.Tonon. Assoc. Euratom-CEA, Saint-Paul-lez-Durance 1998, 683.

267. *Speth, E., P. Frank, B. Heinemann, W. Kraus, R. Riedl, R. Trainham*, O. Vollmer and R. Wilhelm:* RF Sources for Fusion Applications: Design, Development and Performance. In: Proc. 20th Symp. Fusion Technol., Marseille 1998, (Eds.) B.Beaumont, P.Libeyre, B.de Gentile, G.Tonon. Assoc. Euratom-CEA, Saint-Paul-lez-Durance 1998, 27.

268. *Stäbler, A., M. Alexander*, B. Heinemann, R. Riedl, E. Speth and ASDEX Upgrade Team:* A Proposal for Off-Axis Heating and Current Drive with NBI on ASDEX Upgrade. In: Proc. Int. Congress Plasma Phys. and 25th EPS Conf. Control. Fusion and Plasma Phys., Prague 1998, (Ed.) P.Pavlo. ECA 22C. Europ. Phys. Soc., Geneva 1998, 1312-1315.

269. *Stäbler, A., F. Ryter, P. Franzen, O. Gruber, S. Günter, M. Maraschek, V. Mertens, O. Vollmer and ASDEX Upgrade Team:* Operational Window and Performance at High Heating Power in the ASDEX Upgrade Tokamak. In: Proc. Int. Congress Plasma Phys. and 25th EPS Conf. Control. Fusion and Plasma Phys., Prague 1998, (Ed.) P.Pavlo. ECA 22C. Europ. Phys. Soc., Geneva 1998, 472-475.

270. *Starke*, U., J. Schardt*, W. Weiß*, G. Rangelov, Th. Fauster* and K. Heinz*:* Structure of Epitaxial $CoSi_2$ Films on Si(111) Studied with Low-Energy Electron Diffraction (LEED). Surface Review and Letters **5**, 139-144 (1998).

271. *Steltenpohl, A. and N. Memmel:* Homoepitaxial Growth of Pd on Pd(111) - a Search for the Contribution of Electronic Surface States to the Ehrlich-Schwoebel Barrier. Surface Science **402-404**, 277-280 (1998).

272. *Stobbe*, M., A. Könies, S. Günter and J. Halenka*:* Shift and Width of HeII Lines. Journal of Quantum Spectroscopy and Radiation Transfer **60**, 531-542 (1998).

273. *Stober, J., O. Kardaun, F. Ryter, A. Stäbler, W. Suttrop, O. Gruber and ASDEX Upgrade Team:* Confinement and Transport Studies at High Power in ASDEX Upgrade. In: Proc. Int. Congress Plasma Phys. and 25th EPS Conf. Control. Fusion and Plasma Phys., Prague 1998, (Ed.) P.Pavlo. ECA 22C. Europ. Phys. Soc., Geneva 1998, 476-479.

274. *Streibl, B., M. Balden, H. Greuner, A. Herrmann, S. Kötterl, S. Mukherjee, S. Schweizer, J. Simon-Weidner, H. Euringer*, J. Linke*, M. Sauer*, M. Scheerer*, R. Uhlemann*, P. Chappuis*, M. Lipa* and R. Mitteau*:* Non-Brazed Plasma Facing Component for High Steady State Heat Flux. In: Proc. 20th Symp. on Fusion Technol., Marseille 1998, (Eds.) B.Beaumont, P.Libeyre, B.de Gentile, G.Tonon. Assoc. Euratom-CEA, Saint-Paul-lez-Durance 1998, 263-266.

275. *Stroth, U.:* A Comparative Study of Transport in Stellarators and Tokamaks. Plasma Physics and Controlled Fusion **40**, 9-74 (1998).

276. *Stroth, U., J. Baldzuhn, J. Geiger, T. Geist, L. Giannone, H.-J. Hartfuß, M. Hirsch, R. Jaenicke, M. Kick, J.P.T. Koponen, G. Kühner, F.-P. Penningsfeld, F. Wagner and W7-AS Team:* High-Confinement NBI Discharges in W7-AS Stellarator. Plasma Physics and Controlled Fusion **40**, 1551-1565 (1998).

277. *Strumberger, E.:* Stochastic Magnetic Field Structure in the Edge Region of W7-X. Contributions to Plasma Physics **38**, 106-111 (1998).

278. *Suttrop, W., O. Gehre, J.C. Fuchs, H. Reimerdes*, W. Schneider, J. Schweinzer and ASDEX Upgrade Team:* Effects of Type-I Edge-Localized Modes on Transport in ASDEX Upgrade. Plasma Physics and Controlled Fusion **40**, 771-774 (1998).

279. *Suttrop, W., C. Lowry*, F. Ryter, P. Lomas*, J. Stober, B. Schunke*, J.G. Cordey*, H. Murmann, G. Conway*, B. Brüsehaber and D.V. Bartlett*:* H-Mode Threshold Edge Parameter Similarity Discharges in JET and ASDEX Upgrade. In: Proc. Int. Congress Plasma Phys. and 25th EPS Conf. Control. Fusion and Plasma Phys., Prague 1998, (Ed.) P.Pavlo. ECA 22C. Europ. Phys. Soc., Geneva 1998, 317-320.

280. *Suvorov*, E.V., E. Holzhauer*, W. Kasparek*, A.B. Burov*, Y.A. Dryagin*, S.E. Fil'chenkov*, A.A. Fraiman*, L.V. Lubyako*, D.A. Ryndik*, N.K. Skalyga*, O.B. Smolyakova*, V. Erckmann, T. Geist, M. Kick, N. Rust, W7-AS Team and ECRH Group (W7-AS):* Lower Hybrid Turbulence Exited by a Fast Transverse Ion Beam in a Magnetized Plasma. Nuclear Fusion **38**, 661-671 (1998).

281. *Tasso, H. and G.N. Throumoulopoulos*:* Axisymmetric Ideal Magnetohydrodynamic Equilibria with Incompressible Flows. Physics of Plasmas **5**, 2378-2383 (1998).

282. *Tataronis*, J.A., R. Torass* and A. Salat:* The Ideal Magneto-hydrodynamic Continuous Spectra of a Cylindrical Plasma, Solution of the Initial Value Problem. Physics of Plasmas **5**, 3789-3792 (1998).

283. *Teo, A.C.-Y., A. Weller, C. Konrad, W7-AS Team and NI Team:* Further Observations of Neutral Beam Driven Global Alfvén Eigenmodes in Wendelstein W7-AS. Nuclear Fusion **38**, 409-417 (1998).

284. *Thomas, P.R*, P. Andrew*, B. Balet*, D. Bartlett*, J. Bull*, H.P.L. de Esch*, A. Gibson*, C. Gowers*, H. Guo*, G. Huysmans*, T. Jones*, M. Keilhacker*, R.W.T. König, M. Lennholm*, P. Lomas*, A. Maas*, F. Marcus*, F. Nave*, V. Parail*, F. Rimini*, J. Strachan*, K.-D. Zastrow* and N. Zornig*:* Observation of Alpha Heating in JET DT Plasmas. Physical Review Letters **80**, 5548-5551 (1998).

285. *Treutterer, W., O. Gruber, P. McCarthy*, G. Raupp and ASDEX Upgrade Team:* Progress in Shape Control at ASDEX Upgrade. In: Proc. 20th Symp. on Fusion Technol., Marseille 1998, (Eds.) B.Beaumont, P.Libeyre, B.de Gentile, G.Tonon. Assoc. Euratom-CEA, Saint-Paul-lez-Durance 1998, 521-524.

286. *Tunklev, M.*, H. Chen*, M.G. von Hellermann*, A. Howman*, R.W.T. König and M. Romanelli*:* Transport of Light Impurities in the JET Tokamak. In: Proc. Int. Congress Plasma Phys. and 25th EPS Conf. Control. Fusion and Plasma Phys., Prague 1998, (Ed.) P.Pavlo. ECA 22C. Europ. Phys. Soc., Geneva 1998, 392-394.

287. *Unverzagt, M.:* Energy Related Conservation Law for Fluids and Multi-Fluid Plasmas with Equilibrium Flow. Physics of Plasmas **5**, 556-563 (1998).

288. *Valovic, M. and ITER Confinement and Threshold Database Working Group:* An Analysis of the H-Mode Confinement Database. In: Proc. Int. Congress Plasma Phys. and 25th EPS Conf. Control. Fusion and Plasma Phys., Prague 1998, (Ed.) P.Pavlo. ECA 22C. Europ. Phys. Soc., Geneva 1998, 675-678.

289. *Verbeek, H., J. Stober, D.P. Coster, W. Eckstein and R. Schneider:* Interaction of Charge Exchange Neutrals with the Main Chamber Walls of Plasma Machines. Nuclear Fusion **38**, 1789-1803 (1998).

290. *Vollmer, O., A. Stäbler, E. Speth, M. Ciric, P. Franzen, B. Heinemann, W. Kraus, W. Melkus, R. Riedl and W. Schärich:* Commissioning and Performance of the New ASDEX Upgrade Neutral Beam Injector. In: Proc. 20th Symp. Fusion Technol., Marseille 1998, (Eds.) B.Beaumont, P.Libeyre, B.de Gentile, G.Tonon. Assoc. Euratom-CEA, Saint-Paul-lez-Durance 1998, 449-452.

291. *Wagner, F., R. Jaenicke, M. Anton, L. Giannone, U. Stroth and W7-AS Team:* Operational Experience in W7-AS Discharges with Rotational Transform from Bootstrap Current. In: Proc. Int. Congress Plasma Phys. and 25th EPS Conf. Control. Fusion and Plasma Phys. Prague 1998, (Ed.) P.Pavlo. ECA 22C. Europ. Phys. Soc., Geneva 1998, 395-398.

292. *Wagner, F. and M. Wanner:* The Wendelstein 7-X Stellarator Project. Physics and High Technology **7**, 24-27 (1998).

293. *Walter, H., U. Stroth, J. Bleuel, R. Burhenn, T. Geist, L. Giannone, H.-J. Hartfuß, J.P.T. Koponen, L. Ledl and G. Pereverzev:* Transient Transport Phenomena Induced by Cold Pulses in W7-AS. Plasma Physics and Controlled Fusion **40**, 1661-1672 (1998).

294. *Walter, H., U. Stroth, J. Bleuel, R. Burhenn, T. Geist, L. Giannone, H.-J. Hartfuß, J.P.T. Koponen, L. Ledl, G. Pereverzev and W7-AS Team:* Local and Global Transport in Perturbative Experiments in W7-AS. In: Proc. Int. Congress Plasma Phys. and 25th EPS Conf. Control. Fusion and Plasma Phys., Prague 1998, (Ed.) P.Pavlo. ECA 22C. Europ. Phys. Soc., Geneva 1998, 411-414.

295. *Wanner, M., V. Erckmann, J.-H. Feist, J. Sapper, F. Schauer and W7-X Team:* Technical Challenges of the Wendelstein 7-X Stellarator. Journal of Plasma and Fusion Research SERIES **1**, 139-142 (1998).

296. *Weber, S.:* Aiming at 3-Dimensional Plasma Fluid Modelling of the W7-X Divertor. Contributions to Plasma Physics **38**, 43-48 (1998).

297. *Wehner*, S. and J. Küppers:* Abstraction of D Adsorbed on Pt(111) Surfaces with Gaseous H Atoms. Journal of Chemical Physics **108**, 3353-3359 (1998).

298. *Wehner*, S. and J. Küppers:* Abstraction of H Adsorbed on Pt(111) Surfaces with Gaseous D Atoms: Isotope and Flux Effects. Surface Science **411**, 46-53 (1998).

299. *Wehner*, S. and J. Küppers:* Interaction of Gaseous D Atoms with CH_3I Adsorbed on Pt(111), H/Pt(111), and C/Pt(111) Surfaces: From Hot-Atom to Eley-Rideal Phenomenology. Journal of Chemical Physics **109**, 294-300 (1998).

300. *Wehner*, S. and J. Küppers:* Two Consecutive Eley-Rideal Reaction Steps in D Atom/Adsorbate Interaction: from Methylene Iodide via Methyl Iodide to Methane. Chemical Physics Letters **288**, 873-878 (1998).

301. *Weinlich, M., A. Carlson, V. Rohde, K. Reinmüller, ASDEX Upgrade Team and NI Team:* Return Currents from a Single Probe in a Magnetized Plasma. Contributions to Plasma Physics **38**, Special Issue, 13-18 (1998).

302. *Weller A., M. Anton, R. Brakel, J. Geiger, C. Görner, H.-J. Hartfuß, M. Hirsch, C. Nührenberg, S.D. Pinches, D.A. Spong*, S. Zoletnik, W7-AS Team, NBI Group and ECRH Group (W7-AS):* Investigation of Equilibrium, Global Modes and Microinstabilities in the Stellarator W7-AS. Stellarator News **60**, 10-11 (1998), http://www.ornl.gov/fed/stelnews/sn60.html.

303. *Weller, A., C. Görner, A.C.-Y. Teo, M. Anton, J. Geiger, R. Jaenicke, C. Konrad, F.-P. Penningsfeld, D.A. Spong*, W7-AS Team and NBI Group:* Alfvén Instabilities in Wendelstein 7-AS. Journal of Plasma and Fusion Research SERIES **1**, 263-266 (1998).

304. *Wenzel, U., K. Behringer, A. Carlson, K. Schmidtmann and ASDEX Upgrade Team:* Volume Recombination in the ASDEX Upgrade Divertor. In: Proc. Int. Congress Plasma Phys. and 25th EPS Conf. Control. Fusion and Plasma Phys., Prague 1998, (Ed.) P.Pavlo. ECA 22C. Europ. Phys. Soc., Geneva 1998, 504-507.

305. *Wesner, F., W. Becker, M. Brambilla, F. Braun, H. Faugel, D.A. Hartmann, F. Hofmeister, J.-M. Noterdaeme and T. Sperger:* Status and Planning for ICRF at ASDEX Upgrade. In. Proc. 2nd. Europ. Topical Conf. RF Frequency Heating and Current Drive of Fusion Devices, Brussels 1998, (Eds.) J.Jacquinot, G.VanOost, R.R.Weynants. ECA 22A. Europ. Phys. Soc., Brussels 1998, 13-16.

306. *Wilhelm, R.:* The Strength, Needs and Possible Drawbacks of Different Heating and Current Drive Systems in Relation to ITER. In: Proc. 2nd Europ. Topical Conf. RF Frequency Heating and Current Drive of Fusion Devices, Brussels 1998, (Eds.) J.Jacquinot, G.VanOost, R.R.Weynants. ECA 22A. Europ. Phys. Soc., Brussels 1998, 9-12.

307. *Wilhelm, R.:* The Strengths, Needs and Possible Drawbacks of Different Heating and Current Drive Systems in Relation to ITER. Plasma Physics and Controlled Fusion **40**, A1-A12 (1998).

308. *Wu*, C.H., C. Alessandrini*, P. Bonal*, H. Grote, R. Moormann*, M. Rodig*, J. Roth, H. Werle* and G. Vieider*:* Overview of EU CFCs Development for Plasma Facing Materials. Journal of Nuclear Materials **258-263**, 833-838 (1998).

309. *Wu*, C.H., A.A. Haasz*, W. Jacob, R. Moormann*, V. Philipps* and J. Roth:* Recent Results of EU R & D on Removal of C-Deposited Layers and Tritium. In: Proc. 20th Symp. on Fusion Technol., Marseille 1998, (Eds.) B.Beaumont, P.Libeyre, B.de Gentile, G.Tonon. Assoc. Euratom-CEA, Saint-Paul-lez-Durance 1998, 185-188.

310. *Yu*, Q. and S. Günter:* Modeling of the Nonlinear Growth of Neoclassical Tearing Modes. Physics of Plasmas **5**, 3924-3928.

311. *Yu*, Q. and S. Günter:* Modelling of the Neo-Classical Tearing Mode and its Stabilisation by ECCD/ECRH. In: Proc. Int. Congress Plasma Phys. and 25th EPS Conf. Control. Fusion and Plasma Phys., Prague 1998, (Ed.) P.Pavlo. ECA 22C. Europ. Phys. Soc., Geneva 1998, 1899-1902.

312. *Yu*, Q. and S. Günter:* Nonlinear Growth and Motion of Magnetic Islands in Regimes with a High Fraction of Bootstrap Current Density. Plasma Physics and Controlled Fusion **40**, 1989-1998 (1998).

313. *Yu*, Q. and S. Günter:* On the Stabilization of Neoclassical Tearing Modes by Phased Electron Cyclotron Waves. Plasma Physics and Controlled Fusion **40**, 1977-1987 (1998).

314. *Zarnstorff*, M.C., B. Blackwell*, A. Boozer*, A. Brooks*, M. Drevlak, G.Y. Fu*, R.J. Goldston*, L. Grisham*, S.P. Hirshman*, M. Hughes*, H. Kugel*, D. Monticello*, H. Mynick*, L.-P. Ku*, P. Merkel, W. Miner*, G.H. Neilson*, N. Pomphrey*, A.H. Reiman*, M. Redi*, W. Reiersen* and P. Valanju*:* Objectives and Design of a Quasi-Axisymmetric Stellarator Experiment. In: Proc. Int. Congress Plasma Phys. and 25th EPS Conf. Control. Fusion and Plasma Phys., Prague 1998, (Ed.) P.Pavlo. ECA 22C. Europ. Phys. Soc., Geneva 1998, 431-434.

315. *Zastrow, K.-D.*, P. Andrew*, N.P. Basse*. P. Breger*, R. Budny*, W.G.F. Core*, J. Ehrenberg*, M.G. von Hellermann*, O.N. Jarvis*, R.W.T. König, L. Lauro-Taroni*, M.J. Loughlin*, F.B. Marcus*, G.F. Matthews*, M.G. O'Mullane*, G. Sadler*, J. Strachan* and N. Watkins*:* Particle Transport in Steady-State ELMy H-Modes Studied by Trace Tritium Injection during JET DTE-1. In: Proc. Int. Congress Plasma Phys. and 25th EPS Conf. Control. Fusion and Plasma Phys., Prague 1998, (Ed.) P.Pavlo. ECA 22C. Europ. Phys. Soc., Geneva 1998, 385-388.

316. *Zastrow, K.-D.*, W.G.F. Core*, L.G. Eriksson*, M.G. von Hellermann*, A. Howman* and R.W.T. König:* Transfer Rates of Toroidal Angular Momentum during Neutral Beam Injection. Nuclear Fusion **38**, 257-263 (1998).

317. *Zecho*, Th., B. Brandner* and J. Küppers:* Abstraction of D Adsorbed on Pt(100) Surfaces by Gaseous H Atoms: Effect of Surface Heterogeneity. Surface Science **418**, L26-L30 (1998).

318. *Zecho*, Th., A. Horn*, J. Biener* and J. Küppers:* Hydrogen Atom Reactions with Monolayer Graphite Edges on Pt(100) Surfaces: Hydrogenation and H Abstraction. Surface Science **397**, 108-115 (1998).

319. *Zehetbauer, T., G. Neu, M. Maraschek, V. Mertens, G. Raupp, W. Treutterer, D. Zasche and ASDEX Upgrade Team:* Automatic Real-Time Protection Reflexes to Counteract Instabilities. In: Proc. 20th Symp. on Fusion Technol., Marseille 1998, (Eds.) B.Beaumont, P.Libeyre, B.de Gentile, G.Tonon. Assoc. Euratom-CEA, Saint-Paul-lez-Durance 1998, 537-540.

320. *Zehrfeld, H.-P.:* Equilibrium and Ballooning Stability of Resistive Tokamak Plasma near the Separatrix. In: Proc. Int. Congress Plasma Phys. and 25th EPS Conf. Control. Fusion and Plasma Phys., Prague 1998, (Ed.) P.Pavlo. ECA 22C. Europ. Phys. Soc., Geneva 1998, 1927-1930.

321. *Zeiler, A., D. Biskamp, A. Celani*, K. Hallatschek, W.C. Müller, E. Schwarz and R. Tisma:* Production Codes in Nonlinear Plasma Dynamics. In: Proc. of the 4th SGI-Cray MPP Workshop, Garching 1998, (Eds.) H.Lederer, F.Hertweck. IPP, Garching 1998, 109-114.

322. *Zeiler, A., D. Biskamp, J.F. Drake* and B.N. Rogers*:* Three-Dimensional Simulations of Tokamak Edge Turbulence. In: Proc. 7th Europ. Fus. Theory Conf., Jülich 1998, (Ed.) A.Rogister. Forschungszentrum Jülich 1998, 21-28.

323. *Zeiler, A., D. Biskamp, J.F. Drake* and B.N. Rogers*:* Transition from Resistive Ballooning to η_i Driven Turbulence in Tokamaks. Physics of Plasmas **5**, 2654-2664 (1998).

324. *Zohm*, H., G. Gantenbein*, S. Günter, F. Leuterer, M. Maraschek, J. Meskat, A.G. Peeters, W. Suttrop, D. Wagner, ASDEX Upgrade Team and ECRH Group (AUG):* Experiments on MHD Mode Stabilisation by ECCD in ASDEX Upgrade. In: Proc. Int. Congress Plasma Phys. and 25th EPS Conf. Control. Fusion and Plasma Phys., Prague 1998, (Ed.) P.Pavlo. ECA 22C. Europ. Phys. Soc., Geneva 1998, 480-483.

325. *Zoletnik, S., M. Anton, J. Bleuel, M. Endler, S. Fiedler, M. Hirsch, K. McCormick, J. Schweinzer and W7-AS Team:* Properties of Density and Magnetic Field Fluctuations in the SOL and the Edge Regions of the W7-AS Stellarators. In: Proc. Int. Congress Plasma Phys. and 25th EPS Conf. Control. Fusion and Plasma Phys., Prague 1998, (Ed.) P.Pavlo. ECA 22C. Europ. Phys. Soc., Geneva 1998, 407-410.

326. *Zoletnik, S., S. Fiedler, G. Kocsis*, K. McCormick, J. Schweinzer and H.P. Winter*:* Determination of Electron Density Fluctuation Correlation Functions via Beam Emission Spectroscopy. Plasma Physics and Controlled Fusion **40**, 1399-1416 (1998).

Diploma Theses

327. *Bäumel, S.:* Entwicklung eines schnell abstimmbaren Heterodynempfängers zur Messung von Dichteprofilen und Dichtefluktuationen an W7-AS mit Reflektometrie. Univ. Regensburg, 1998.

328. *Bucher, H.:* Analyse des transienten Elektronenenergietransports im Tokamak ASDEX Upgrade. Univ. Regensburg 1998.

329. *Liebisch, P.:* Untersuchungen zum Einschluß und zur Entwicklung der Ladungsverteilung in einer Elektronenstrahl-Ionenfalle. Humboldt-Univ. Berlin 1998.

330. *Niemann, C.:* Zum Isotopenverhältnis H/D in ASDEX Upgrade. Univ. Erlangen-Nürnberg 1998.

331. *Wachter, C.:* Characterization of the Tore Supra Neutral Hydrogen Beam by Means of Active Balmer-α-Spectroscopy. Univ. Augsburg 1998.

Doctoral Theses

332. *Bleuel, J.:* Elektrostatische Turbulenz am Plasmarand des Stellarators Wendelstein 7-AS. Techn. Univ München 1998.

333. *Fuchs, C.:* Messung des Cotton-Mouton-Effekts am Stellarator W7-AS. Univ. Regensburg 1998.

334. *Görner, C.:* Tomographische Untersuchung von globalen Alfvén-Eigenmoden am Stellarator Wendelstein 7-AS. Techn. Univ. München 1998.

335. *Häse, M.:* Untersuchung von Temperaturfluktuationen und deren Korrelation mit Dichtefluktuationen an W7-AS. Techn. Univ. München 1998.

336. *Hallatschek, K.:* Beobachtung hochfrequenter kaskadierender Röntgenoszillationen mit Hilfe von Zeit-/Frequenztransformationen zur Erkennung von Ereignissen und Identifikation der Oszillationen als Tearing-Moden. Techn. Univ. München 1998.

337. *Meyer, H.:* Analyse der Plasmarotation in einer linearen Magnetfeldkonfiguration = Analysis of the Plasma Rotation in a Linear Magnetic Configuration. Humboldt-Univ. Berlin 1998.

338. *Nitsche, A.:* Technische Applikationen von Verfahren zur dreidimensionalen Feldberechnung beim Entwurf elektrischer Maschinen. Techn. Univ. München 1998.

339. *Pecher, P.:* Quantitative Bestimmung der Teilchenflüsse aus Methan-ECR-Plasmen = Quantitative Determination of the Particle Fluxes Emanating from Methane ECR Plasmas. Univ. Bayreuth 1998.

340. *Pinches, S.D.:* Nonlinear Interaction of Fast Particles with Alfvén Waves in Tokamaks. Nottingham Univ. 1998

341. *Reinmüller, K.:* Emittierende Sonden und Entstehung von Hot Spots - Untersuchung des Kontakts zwischen Plasma und Elektronen emittierender Wand durch Teilchensimulation mit Modell für Stossprozesse. Techn. Univ. München 1998.

342. *Vetter, S.:* Struktur und Dynamik von reinen und sauerstoffbedeckten gestuften Kupferoberflächen. Univ. Bayreuth 1998.

Habilitation

343. *Meyer-Spasche, R.:* Stationäre Taylor-Wirbel-Strömungen = Stationary Taylor Vortex Flows. Techn. Univ. München 1998.

Patents

344. *Carlson, A.:* Vorrichtung und Verfahren zur Trennung von Substanzen mit unterschiedlichem atomaren Gewicht. Freigabe: 1.12.1998.

345. *Geist, T.:* Filter für Millimeterwellen bestehend aus dielektrischen Scheiben. Freigabe: 17.3.1998.

346. *Haas, G.:* Heißkathoden-Ionisationsmanometer. Frankreich 2.685.126. Ablauf des Gebrauchsmusters: April 1998.

347. *Kraus, W.:* Isolierte Antenne für Hochfrequenz-Plasmagenerator en. US-Patent 5,434,353. Freigabe: 3.11.1998.

348. *Mast, K.-F., G. Schramm and M. Münch:* Folienmanometer. PCT-Anmeldung Europa, USA, Japan: 19.3.1998.

349. *Schäftner, J.:* Dichtringabziehvorrichtung NW 35 CF. Deutschland Gbm 296 01 651.9. Freigabe: 3.11.1998.

350. *Schneider, F.:* Hybrider Regler. Europa-Patent (CH, FR, NL, GB) 901 17 958.0. Freigabe: 18.8.1998.

351. *Wittenbecher, K.:* Verfahren und Vorrichtung zur Frequenzmultiplikation oder -division. Deutschland 198 10 576.2. Patentanmeldung 11.3.1998.

352. *Wittenbecher, K., P. Turba and K. Klaster:* Lichtschranke mit hoher Störsicherheit. Gebrauchsmusteranmeldung 298 17 357.1: 28.9.1998.

Lectures

353. *Allain*, M.M.C., D. Alman*, D.N. Ruzic* and R. Behrisch:* Modeling of Beam-Target Fusion due to Charge Exchange Neutrals Incident on the ITER First Wall. 4th Annual Meeting of the Div. of Plasma Phys. of the APS, New Orleans,LA 1998.

354. *Balden, M.:* Doped Carbons. EU HT / JCT Progress Review Meeting on Carbon Chemical Erosion and Tritium Inventory and Control in ITER PFC's, Garching 1998.

355. *Balden, M.:* Erosion of Doped Carbons. 8th Int. Workshop on Carbon Materials, Jülich 1998.

356. *Balden, M. and R. Behrisch:* Hydrogen Trapping and Recycling in Fusion Devices such as ASDEX Upgrade and JET. Int. Workshop on Hydrogen Recycle at Plasma Facing Materials, Tokyo 1998.

357. *Balden, M., M. Mayer and J. Roth:* Codeposition of Deuterium with Silicon Doped Carbon. 13th Int. Conf. on Plasma Surface Interactions in Control. Fusion Devices, San Diego,CA 1998.

358. *Baloui, T., B. Wolle*, R. Bätzner*, G. Gonda, H. Klein*, B. Wiegel* and J. Wittstock*:* Sandman - A New Detector System for Flux Measurements of Collimated 2.5 MeV Neutrons. Verhandl. DPG (VI) **33**, 347, P29.35 (1998).

359. *Bard, A., J. Stober, D.P. Coster, K. Büchl and ASDEX Upgrade Team:* Messung von radialen Neutralteilchenflüssen und -dichteverteilungen in der Nähe der Separatrix von ASDEX-Upgrade. Verhandlg. DPG (VI) **33**, 345, P29.19 (1998).

360. *Bäumel, S., M. Hirsch and H.-J. Hartfuß:* Entwicklung eines schnell abstimmbaren Heterodynempfängers zur Messung von Dichteprofilen und Dichtefluktuationen an W7-AS mit Reflektometrie. Verhandl. DPG (VI) **33**, 347, P29.34 (1998).

361. *Behringer, K.:* Einführung in die Plasmaspektroskopie. Vorlesung, Univ. Augsburg, WS 1998/99.

362. *Behringer, K.:* Seminar über aktuelle Fragen der Plasmaphysik. Univ. Augsburg, SS 1998, WS 1998/99.

363. *Behringer, K.:* Spektroskopie von Nichtgleichgewichtsplasmen. Vorlesung, Univ. Augsburg, SS 1998.

364. *Behringer, K. and U. Fantz*:* Physik III (Atom- und Molekülphysik). Vorlesung, Univ. Augsburg, WS 1998/99.

365. *Behringer, K. and U. Fantz*:* Physikalisches Praktikum für Fortgeschrittene. Univ. Augsburg, SS 1998.

366. *Behringer, K., U. Fantz* and Th. Hamacher:* Probleme der zukünftigen Energieversorgung. Seminar, Univ. Augsburg, SS 1998, WS 1998/99.

367. *Behringer, K., B. Stritzker*, U. Fantz* and M. Schreck*:* Seminar über Anwendungen und Diagnostik von Niederdruckplasmen. Universität Augsburg, SS 1998, WS 1998/99.

368. *Behrisch, R.:* Demands for Materials Facing the Hot Plasma in Control. Thermonuclear Fusion. CEIT, Univ. of Navarra, San Sebastian 1998.

369. *Behrisch, R.:* Fast and Quantitative Analysis of the Composition and Depth Profiles of Surface Layers of Solids by Elastic Recoil Detection Analysis (ERDA). Geel 1998.

370. *Behrisch, R.:* Materials Demands for the Plasma Facing Areas in Fusion Devices. Jahrestagung Kerntechnik des Deutschen Atomforums e.V., München 1998.

371. *Behrisch, R.:* Materials for the Plasma Facing Areas of Fusion Devices. Materials Science Div., Los Alamos Nat. Lab., Los Alamos, NM 1998.

372. *Behrisch, R.:* Physics of Plasma Solid Interaction Processes. Workshop on Plasma Wall Interaction and Cold Plasma Physics, Univ. of Marseille 1998.

373. *Behrisch, R., S. Grigull and S. Parascandola*:* Nitrogen Implantation into Carbon: Retention, Release, and Target-Erosion Processes. 13th Int. Conf. on Plasma Surface Interactions in Control. Fusion Devices, San Diego,CA 1998.

374. *Behrisch, R., V. Khripunov* and R.T. Santoro*:* Neutron Bombardment Induced Hydrogen and Helium Isotope Production in Low Z Materials at the Vessel Walls of Fusion Reactors. Carbon Workshop, Jülich 1998.

375. *Beidler, C.D., G. Grieger, E. Harmeyer, F. Herrnegger, J. Kisslinger, W. Maurer*, J. Sapper, I.N. Sidorenko, E. Strumberger, H. Wobig and A.V. Zolotukhin:* Physics and Engineering Studies of a Helias Reactor. 6th IAEA Techn. Comm. Meeting on Fusion Power Plant Design, Culham 1998.

376. *Beidler, C.D., F. Herrnegger, J. Kisslinger, H. Wobig and A.V. Zolotukhin:* Guiding Center Studies of Collisionless Alpha-Particles in a Helias Configuration. VI Ukrainian Conf. and School on Plasma Phys. and Control. Fusion, Alushta, Crimea 1998.

377. *Bergmann, A.:* Kinetic Effects on the Temperature Measured by Probes. 13th Int. Conf. on Plasma Surface Interactions in Control. Fusion Devices, San Diego,CA 1998.

378. *Bergmann, A.:* Particle Simulation of a Scrape-off Layer with Collisional Transport and Drift Motion. Edge-Plasma Theory and Simulation Workshop, Innsbruck 1998.

379. *Bergmann, A.:* PIC Simulation of a Strongly Magnetized Plasmas Boundary Layer. Kolloquiumsvortrag, Univ. Innsbruck 1998.

380. *Bessenrodt-Weberpals, M.:* Astrophysikalische Plasmen. Vorlesung, Univ. Düsseldorf, SS 1998.

381. *Bessenrodt-Weberpals, M.:* Basic Plasma Physics. Summer Univ. Plasma Phys., Garching 1998.

382. *Bessenrodt-Weberpals, M.:* Plasmadynamik in Fusionsexperimenten: Messungen, Modelle, Meilensteine. 2. Deutsche Physikerinnentagung, Hamburg 1998.

383. *Bessenrodt-Weberpals, M.:* Plasmaphysik in technischen Anwendungen. Vorlesung, Univ. Düsseldorf, WS 1998/99.

384. *Biederer*, Th., Th. Kammler* and J. Küppers:* Struktureinfluß bei der Deuteriumabstraktion durch thermische H Atome auf Pt(111) Flächen. Verhandl. DPG (VI) **33**, 900, O32.7 (1998).

385. *Biedermann, C., T. Fuchs, P. Liebisch, R. Radtke, E. Behar* and R. Doron*:* X-Ray Spectroscopic Measurements of Dielectronic Recombination of Highly Charged Krypton Ions. 9th Int. Conf. Physics on Highly Charged Ions, Bensheim 1998.

386. *Biskamp, D.:* Magnetic Reconnection and Turbulence. VII. Int. Plasma Physics Conf., Lindau 1998.

387. *Bleuel, J., B.D. Scott, M. Endler, H. Niedermeyer and G. Theimer:* Turbulenz am Plasmarand: Vergleich zwischen Theorie und Experiment. Verhandl. DPG (VI) **33**, 316, P2.1 (1998).

388. *Bohmeyer, W., P. Kornejew, H.-D. Reiner, H. Grote and C.H. Wu*:* Untersuchungsergebnisse zur chemischen Erosion von Graphiten im Plasmagenerator PSI-1. Symp. zur chemischen Erosion, Garching 1998.

389. *Bohmeyer, W., P. Kornejew, H.-D. Reiner, H. Grote, C.H. Wu*, R. Schlögl* and G. Weinberg*:* Chemical Erosion of Graphites. EU/JCT Meeting, Garching 1998.

390. *Borrass, K.:* Geometry Effects in the SOL and Divertor. Edge-Plasma Theory and Simulation Workshop, Innsbruck 1998.

391. *Bosch, H.-S.:* Basic Nuclear Fusion. Summer Univ. Plasma Phys., Garching 1998.

392. *Bosch, H.-S.:* Comparison of Divertor I und Divertor II (LYRA). JET-IPP Workshop on Plasma Edge and Divertor Physics, Garching 1998.

393. *Bosch, H.-S.:* Energiegewinnung im 21. Jahrhundert - Forschung zur Kernfusion im IPP. Starnberger Kunstkreis BUZENTAUR, Starnberg 1998.

394. *Bosch, H.-S.:* Magneto-Hydrodynamik. Vorlesung, Humboldt-Univ. Berlin, WS 1998/99.

395. *Bosch, H.-S.:* Die Physik "brennender" Fusionsplasmen. Physikalisches Kolloquium, Humboldt-Univ. Berlin 1998.

396. *Bosch, H.-S., D.P. Coster, G. Haas, A. Kallenbach, R. Schneider, W. Ullrich and ASDEX Upgrade Team:* Divertortransport von He und Ne im ASDEX Upgrade Divertor. Verhandl. DPG (VI) **33**, 331, P21.3 (1998).

397. *Bosch, H.-S., J.C. Fuchs, J. Gafert, G. Haas, A. Herrmann, A. Kallenbach, M. Kaufmann, J. Neuhauser, F. Ryter, R. Schneider, J. Schweinzer, W. Ullrich, U. Wenzel, G.C. Vlases*, L.D. Horton*, G.F. Matthews*, ASDEX Upgrade Team and JET Divertor Physics Topic Group:* Effect of Divertor Geometry on Boundary and Core Plasma Performance in ASDEX Upgrade and JET. Invited Talk, Int. Congress Plasma Phys. and 25th EPS Conf. Control. Fusion Plasma Phys., Prague 1998.

398. *Bosch, H.-S., W. Ullrich, A. Bard, D.P. Coster, G. Haas, A. Kallenbach, J. Neuhauser, R. Schneider and ASDEX Upgrade Team:* Noble Gas Exhaust with a Strongly Baffled Divertor in ASDEX Upgrade. 13th Int. Conf. on Plasma Surface Interactions in Control. Fusion Devices, San Diego,CA 1998.

399. *Burhenn, R. and A. Weller:* Derivation of Local Impurity Transport Quantities from Soft-X Radiation Evolution During Tracer Injection at W7-AS. Proc. 12th Topical Conf. High-Temperature Plasma Diagnostics, Princeton,NJ 1998.

400. *Carlson, A. and A. Bergmann:* Effects of *T(x)* and *T(V)* on Probe Measurements. 13th Int. Conf. on Plasma Surface Interactions in Control. Fusion Devices, San Diego,CA 1998.

401. *Coster, D.P., K. Borrass, R. Schneider and ASDEX Upgrade Team:* B2-EIRENE Modelling of the Density Limit on ASDEX Upgrade. 13th Int. Conf. on Plasma Surface Interactions in Control. Fusion Devices, San Diego,CA 1998.

402. *Coster, D.P., R. Schneider, ASDEX Upgrade Team and NI Team:* A Comparison of B2-Eirene Code Results and ASDEX Upgrade Divertor II. Edge-Plasma Theory and Simulation Workshop, Innsbruck 1998.

403. *De Peña Hempel, S., A. Kallenbach, H. Meister and ASDEX Upgrade Team:* Spektroskopische Bestimmung der poloidalen Plasmarotation an ASDEX Upgrade. Verhandlg. DPG (VI) **33**, 338, P25.8 (1998).

404. *Donath, M.:* Elektronische Oberflächenzustände in magnetischen Systemen. Univ. Ulm 1998.

405. *Donath, M.:* Ferromagnetismus und spinabhängige elektronische Struktur: Auf dem Weg zu einem mikroskopischen Verständnis magnetischer Phänomene in niedrigdimensionalen Strukturen. Seminar über Atom-, Kern- und Elementarteilchenphysik, Univ. Heidelberg 1998.

406. *Donath, M.:* Magnetische Oberflächenzustände: Untersuchungen mit spinaufgelöster Inverser Photoemission. Univ. Hamburg 1998.

407. *Donath, M.:* Magnetische Ordnung und elektronische Struktur: Untersuchungen mit spinaufgelösten Elektronenspektroskopien, EKM (Elektronische Korrelationen und Magnetismus). Univ. Augsburg 1998.

408. *Donath, M.:* Magnetische Ordnung und elektronische Struktur: Untersuchungen mit spinpolarisierten Elektronen. Univ. Tübingen 1998.

409. *Donath, M.:* Magnetische Ordnung und elektronische Struktur in Dünnschichtsystemen. DFG-Rundgespräch "Herstellung und Eigenschaften von Clustern und atomaren Schichten", Bad Honnef 1998.

410. *Donath, M.:* Spin-Dependent Empty Electronic States of Thin Gd Films on W(110). 190. WE-Heraeus-Seminar "Magnetism and Electronic Correlations in Local-Moment Systems: Rare-Earth Elements and Compounds", Berlin 1998.

411. *Donath, M.:* Spin-Polarized Electron Studies of Low-Dimensional Magnetic Systems. Seminar, IBM Almaden Res. Center, San Jose,CA 1998.

412. *Donath, M.:* Spin-Polarized Electron Studies of Low-Dimensional Magnetic Systems. Australian-German Workshop on Electron Correlations in Association with the 13th Nat. Congress of the Australian Inst. of Physics, Fremantle, Western Australia 1998.

413. *Donath, M.:* Spin-Resolved Inverse Photoemission from Low-Dimensional Magnetic Systems. 12th Int. Conf. on Vacuum Ultraviolet Radiation Physics, San Francisco,CA 1998.

414. *Donath, M.:* Technische Physik II: Kern- und Energiephysik. Vorlesung, Univ. Bayreuth, SS 1998.

415. *Donath, M., J. Reinmuth, H. Kang and G. Rangelov:* Spin-Resolved Appearance Potential Spectroscopy of Magnetic Surfaces and Layered Structures (Poster). 12th Int. Conf. on Vacuum Ultraviolet Radiation Physics, San Francisco,CA 1998.

416. *Düchs, D.F.:* Makroskopische und kinetische Plasmainstabilitäten. Vorlesung, Univ. Bochum, SS 1998.

417. *Düchs, D.F.:* Theorie von Stoßwechselwirkungen in heißen Plasmen. Vorlesung, Univ. Bochum, WS 1997/98.

418. *Düchs, D.F.:* Wozu Energie aus kontrollierter Kernfusion? Vorlesung, Univ. Bochum, WS 1998/99.

419. *Dux, R.:* Plasmaphysik und Fusionsforschung II. Vorlesung, Univ. Augsburg, SS 1998.

420. *Dux, R., K. Asmussen, A. Gude, A. Kallenbach, R. Neu and ASDEX Upgrade Team:* Untersuchungen zum Transport von Verunreinigungen im Zentrum von ASDEX Upgrade. Verhandl. DPG (VI) **33**, 319, P6.1 (1998).

421. *Eckstein, W.:* Dynamic Behavior of Carbon Implantation into Beryllium and Tungsten. Sandia Nat. Labs., Livermore 1998.

422. *Eckstein, W.:* Ion Bombardment of Beryllium and Tungsten with Carbon. Osaka Univ. 1998.

423. *Eckstein, W.:* Ionenbeschuß von Oberflächen. Univ. Magdeburg 1998.

424. *Eckstein, W.:* Rutherford Backscattering beyond the Binary Collision Model. Electro-Communication Univ., Osaka 1998.

425. *Eckstein, W.:* Zerstäubung - Status von Simulation und Experiment. Kolloquium, Univ. Essen 1998.

426. *Empacher*, L., G. Gantenbein*, F. Hollmann, W. Kasparek*, H. Zohm*, V. Erckmann and M. Weißgerber:* Present Developments for the 140 GHz Transmission System for ECRH on the Stellarator W7-X. 23rd Int. Conf. on Infrared and Millimeter Waves, Colchester 1998.

427. *Endler, M.:* Fluctuations and Turbulent Transport in the SOL and Edge Plasma Region. 6th Europ. Fusion Physics Workshop, Cadarache 1998.

428. *Endler, M.:* Turbulent SOL Transport in Stellarators and Tokamaks. 13th Int. Conf. on Plasma Surface Interactions in Control. Fusion Devices, San Diego,CA 1998.

429. *Erckmann, V.:* Recent Results on ECRH and ECCD at W7-AS. 10th Joint Russian-German Meeting, Nizhny Novgorod 1998.

430. *Erckmann, V.:* Status of the W7-X Project. 10th Joint Russian-German Meeting, Nizhny Novgorod 1998.

431. *Erckmann, V., U. Gasparino, H.P. Laqua, H. Maaßberg, W7-AS Team, ECRH Group (AUG), K.S. Kasilov*, N. Marushchenko*, V. Irkhin* and S. Malygin*:* ECRH and ECCD Experiments in an Extended Power Range at the W7-AS Stellarator. 17th IAEA Fusion Energy Conf., Yokohama 1998.

432. *Erckmann, V., W7-X Team and W7-AS Team:* ECRH and ECCD with High Power Gyrotrons and the Stellarators W7-AS and W7-X. Research Workshop of the Israel Science Foundation-Cycl. Res., Tel Aviv 1998.

433. *Fantz*, U., K. Behringer, J. Gafert, D.P. Coster and ASDEX Upgrade Team:* Optical Emission Measurements of H_2 and D_2 Molecules in the Divertor Region of ASDEX Upgrade. 13th Int. Conf. on Plasma Surface Interactions in Control. Fusion Devices, San Diego,CA 1998.

434. *Feng, Y., F. Sardei, P. Grigull and G. Herre:* Drift Effects in W7-AS Limiter- und Divertorkonfigurationen. Jülich-Garching-Arbeitstreffen, Forschungszentrum Jülich 1998.

435. *Feng, Y., F. Sardei, P. Grigull and G. Herre:* Drift Effects in W7-AS Limiter and Island Divertor Configurations. 13th Int. Conf. on Plasma Surface Interactions in Control. Fusion Devices, San Diego,CA 1998.

436. *Feng, Y., F. Sardei and J. Kisslinger:* 3D Fluid Modelling of the Edge Plasma by Means of a Monte Carlo Technique. 13th Int. Conf. on Plasma Surface Interactions in Control. Fusion Devices, San Diego,CA 1998.

437. *Fiedler, S., R. Brandenburg*, K. McCormick, G. Petravich*, J. Schweinzer, F. Aumayr*, H.P. Winter*, W7-AS Team and ASDEX Upgrade Team:* Impurity Investigations by Means of Lithium Beam Induced Charge Exchange Spectroscopy on W7-AS and ASDEX Upgrade. 13th Int. Conf. on Plasma Surface Interactions in Control. Fusion Devices, San Diego,CA 1998.

438. *Fischer, R., W. Jacob, W. von der Linden and V. Dose:* Bayesian Reconstruction of Electron Energy Distributions in Helium Plasmas from Emission Line Intensities. 18th Int. Workshop on Maximum Entropy and Bayesian Methods, Garching 1998.

439. *Franzen, P., H. Maier, R. Behrisch, D. Schleußner, G.Y. Sun* and C. Garcia-Rosales*:* Hydrogen Isotope Rentention in the First Wall of ASDEX Upgrade. Workshop on Tritium Experiences in Large Tokamaks; Application to ITER, Princeton,NJ 1998.

440. *Fu*,G.Y., L.-P. Ku*, N. Pomphrey*, M.H. Redi*, C. Kessel*, D. Monticello*, A. Reiman*, M. Hughes*, W. Cooper* and C. Nührenberg:* MHD Stability Calculations of High-beta Quasi-Axisymmetric Stellarators. 17th IAEA Fusion Energy Conf., Yokohama 1998.

441. *Fuchs, C. and H.-J. Hartfuß:* Line Integrated Density Measurements Based on Cotton-Mouton Polarimetry. 12th Topical Conf. on High-Temperature Plasma Diagnostics, Princeton,NJ 1998.

442. *Fuchs, C. and H.-J. Hartfuß:* Messung der Liniendichte am W7-AS über den Cotton-Mouton-Effekt. Verhandl. DPG (VI) **33**, 317, P3.4 (1998).

443. *Fuchs, J.C., K.-F. Mast, A. Herrmann and ASDEX Upgrade Team:* Radiation Distribution and Power Balance in the ASDEX Upgrade LYRA Divertor. JET-AUG Workshop on Plasma Edge and Divertor Physics, Garching 1998.

444. *Fuchs, T., C. Biedermann, P. Liebisch, R. Radtke, E. Behar* and R. Doron*:* Dielektronische Rekombination heliumartiger Krypton-Ionen. Verhandl. DPG (VI) **33**, 111, A5.6 (1998).

445. *Fußmann, G.:* Als Physiker in einem Max-Planck-Institut. Berufsinformationstag der DPG, Magnushaus, Berlin 1998.

446. *Fußmann, G.:* Einführung in die Plasmaphysik. Vorlesung, Humboldt-Univ. Berlin, SS 1998.

447. *Fußmann, G.:* Einstein in Berlin. Rotary-Club, Berlin 1998.

448. *Fußmann, G.:* Fusionsreaktor: Heutiger Stand, physikalische und technische Probleme. Techn. Univ. Berlin 1998.

449. *Fußmann, G.:* Plasmaphysikalische Experimente im IPP-Berlin. Kolloquiumsvortrag, Univ. Düsseldorf 1998.

450. *Fußmann, G., C. Biedermann and R. Radtke:* EBIT: An Electron Beam Source for the Production and Confinement of Highly Ionized Atoms. NATO ASI - Advanced Technologies Based on Wave and Beam Generated Plasmas. Sozopol 1998.

451. *Gafert, J., K. Behringer, D.P. Coster, C. Dorn, A. Kallenbach, R. Schneider, U. Schumacher* and ASDEX Upgrade Team:* Spectroscopic Investigation of the Dynamics of Ions and Neutrals in the ASDEX Upgrade Divertor II. 13th PSI Conf., San Diego,CA 1998.

452. *Gafert, J., K. Behringer, D.P. Coster, U. Schumacher* and ASDEX Upgrade Team:* Dynamik von Neutralen und Ionen im ASDEX Upgrade Divertor II. Verhandl. DPG (VI) **33**, 317, P3.2 (1998).

453. *Giannone, L.:* Edge Modelling Workshop. W7-X Joint Workshop, Jülich 1998.

454. *Giannone, L., R. Burhenn, P. Grigull, U. Stroth, R. Brakel, R. Dux, A. Elsner, S. Fiedler, G. Kühner, F. Penningsfeld, G. Pereverzev, F. Wagner, A. Weller, C. Wendland, NI Team and W7-AS Team:* Radiation Measurements and Modelling of the Density Limit on the W7-AS Stellarator. 13th Int. Conf. on Plasma Surface Interaction, San Diego,CA 1998.

455. *Geier, A., K. Asmussen, R. Dux, R. Neu and ASDEX Upgrade Team:* Transport von Hoch-Z Verunreinigungen. Verhandlg. DPG (VI), **33**, 338, P25.11 (1998).

456. *Goldstraß, P., W. Eckstein and C. Linsmeier:* Erosion of Be and Deposition of Carbon and Oxygen due to Bombardment with C^+ and CO^+ Ions. 13th Int. Conf. on Plasma Surface Interactions in Control. Fusion Devices, San Diego,CA 1998.

457. *Goldstraß, P., W. Eckstein and C. Linsmeier:* Schichtaufbau auf Beryllium durch Beschuß mit C- und CO-Ionen. Verhandl. DPG (VI) **33**, 880, O15.7 (1998).

458. *Gottschall*, R., G. Mestl*, M. Dieterle*, U. Wild*, N. Pfänder*, G. Weinberg*, C. Linsmeier and R. Schlögl*:* Einfluß der Struktur auf die katalytische Aktivität eines $MoVO_x$ Katalysators. Dechema Jahrestagung, Wiesbaden 1998.

459. *Grambole*, D., F. Herrmann*, R. Behrisch and W. Hauffe*:* Hydrogen and Deuterium Depth Profiling in Divertor Tiles of a Fusion Experiment by Micro ERDA. 8th Int. Conf. on Nuclear Microprobe Technology, Spiers 1998.

460. *Grieger, G.:* Fusion - Option für verträgliche und nachhaltige Zukunftsenergie. Heinrich-Böll-Stiftung, Greifswald 1998.

461. *Grieger, G.:* Fusionsmaschinen - Optionen für verträgliche und nachhaltige Zukunftsenergie. Fachhochschule Stralsund 1998.

462. *Grieger, G.:* Grundlagen der Fusion - Warum W7-X in Greifswald - Was ist mit ITER. Besuch des CDU-Umweltausschusses des Landes MVP, IPP Greifswald 1998.

463. *Grieger, G.:* Report of the IEA Fusion Power Coordinating Committee (FPCC) to the IEA Committee on Energy Research and Technology (CERT). IEA Paris 1998.

464. *Grieger, G.:* Status and Future Prospects of Power Generation by Magnetic Fusion. LHD Inauguration Ceremony, Nat. Inst. of Fusion Science, Toki 1998.

465. *Grieger, G.:* Stellarator Activities of IPP. Nat. Inst. of Fusion Science, Toki 1998.

466. *Grigull, P.:* Status of Edge Diagnostics Concepts for W7-X. W7-X Joint Workshop, Jülich 1998.

467. *Grigull, P., Y. Feng, J. Kisslinger and F. Sardei:* Island Divertor Studies in Stellarators. 6th Europ. Fusion Physics Workshop, Cadarache 1998.

468. *Grigull, P., S. Fiedler and G. Kühner:* General Status of W7-X. W7-X Joint Workshop, Jülich 1998.

469. *Grigull, P. and D. Hildebrandt:* Status of Edge Diagnostics for W7-X. Jülich-Greifswald Workshop on Plasma Edge Phys. and Plasma Surface Interaction, Jülich 1998.

470. *Grote, H., W. Bohmeyer, P. Kornejew, H.-D. Reiner, G. Fußmann, R. Schlögl*, G. Weinberg* and C.H. Wu*:* Chemical Sputtering Yields of Carbon Based Materials at High Ion Flux Densities. 4th Int. Workshop on Tritium Effects in Plasma Facing Components, Santa Fé,NM 1998.

471. *Gruber, O.:* Investigation of Advanced Tokamak Scenarios in ASDEX Upgrade. Kolloquium, General Atomics, San Diego,CA 1998.

472. *Gruber, O.:* Untersuchungen am Tokamak ASDEX Upgrade: Zwischen ITER und Verbesserung des Tokamakkonzepts. Kolloquium, IPF Stuttgart 1998.

473. *Gruber, O. and ASDEX Upgrade Team:* Advanced Tokamak Operation on ASDEX Upgrade. Workshop on Research Programme on Advanced Mode of Operations on the Existing European Facilities, ENEA Frascati Centre, Frascati 1998.

474. *Gruber, O. and ASDEX Upgrade Team:* Advanced Tokamak Results on ASDEX Upgrade. 8th ITER Physics R&D Expert Group Meeting on Disruption, Plasma Control and MHD, San Diego,CA 1998.

475. *Gruber, O. and ASDEX Upgrade Team:* System Enhancements for AT Operation in ASDEX Upgrade. Workshop on Research Programme on Advanced Mode of Operations on the Existing European Facilities, ENEA Frascati Centre, Frascati 1998.

476. *Gruber, O., H.-S. Bosch, S. Günter, A. Herrmann, A. Kallenbach, M. Kaufmann, K. Krieger, K. Lackner, V. Mertens, R. Neu, F. Ryter, J. Schweinzer, A. Stäbler, W. Suttrop, R. Wolf, K. Asmussen, A. Bard, G. Becker, K. Behler, K. Behringer, A. Bergmann, M. Bessenrodt-Weberpals, K. Borrass, B. Braams*, M. Brambilla, R. Brandenburg*, F. Braun, H. Brinkschulte, R. Brückner, B. Brüsehaber, K. Büchl, A. Buhler, A. Carlson, H.P. Callaghan*, D.P. Coster, L. Cupido*, S. De Peña Hempel, C. Dorn, R. Drube, R. Dux, S.M. Egorov*, W. Engelhardt, H.-U. Fahrbach, U. Fantz*, J.-H. Feist, P. Franzen, J.C. Fuchs, G. Fußmann, J. Gafert, G. Gantenbein*, O. Gehre, A. Geier, J. Gernhardt, E. Gubanka, A. Gude, G. Haas, K. Hallatschek, D.A. Hartmann, B. Heinemann, G. Herppich, W. Herrmann, F. Hofmeister, E. Holzhauer*, D. Jacobi, M. Kakoulidis*, N. Karakatsanis*, O. Kardaun, A. Khutoretski*, H. Kollotzek, S. Kötterl, W. Kraus, B. Kurzan, G. Kyriakakis*, P.T. Lang, R.S. Lang, M. Laux, L.L. Lengyel, F. Leuterer, A. Lorenz, H. Maier, M. Manso*, M. Maraschek, M. Markoulaki*, K.-F. Mast, P. McCarthy*, D. Meisel, H. Meister, R. Merkel, J. Meskat, H.W. Müller, M. Münich, H. Murmann, B. Napiontek, G. Neu, J. Neuhauser, M. Niethammer, J.-M. Noterdaeme, G. Pautasso, A.G. Peeters, G. Pereverzev, G. Raupp, , K. Reinmüller, R. Riedl, V. Rohde, H. Röhr, J. Roth, H. Salzmann, W. Sandmann, H.-B. Schilling, D. Schlögl, K. Schmidtmann, H. Schneider, R. Schneider, W. Schneider, G. Schramm, J. Schweinzer, S. Schweizer, R.R. Schwörer, B.D. Scott, U. Seidel, F. Serra*, S. Sesnic, C. Sihler, A. Silva*, E. Speth, K.-H. Steuer, J. Stober, B. Streibl, A. Thoma, W. Treutterer, M. Troppmann, N. Tsois*, W. Ullrich, M. Ulrich, P. Varela*, H. Verbeek, O. Vollmer, H. Wedler, M. Weinlich, U. Wenzel, F. Wesner, R. Wunderlich, N. Xantopoulos*, Q. Yu*, D. Zasche, T. Zehetbauer, H.-P. Zehrfeld, H. Zohm* and M. Zouhar:* Overview on ASDEX Upgrade Results. 17th IAEA Fusion Energy Conf., Yokohama 1998.

477. *Gruber, O., A. Gude, S. Günter, M. Maraschek and ASDEX Upgrade Team:* Neoclassical Mode Studies on ASDEX Upgrade. 8th ITER Physics R&D Expert Group Meeting on Disruption, Plasma Control and MHD, San Diego,CA 1998.

478. *Gruber, O., S. Günter, M. Maraschek, H. Zohm* and ASDEX Upgrade Team:* Feedback Control of Neoclassical Tearings on ASDEX Upgrade. Workshop on Research Programme on Advanced Mode of Operations on the Existing Europ. Facilities, ENEA Frascati 1998.

479. *Gruber, O., G. Pautasso, U. Seidel and ASDEX Upgrade Team:* Halo Currents and Thermal Loads in Div II. 8th ITER Physics R&D Expert Group Meeting on Disruption, Plasma Control and MHD, San Diego,CA 1998.

480. *Gruber, O., G. Pautasso, C. Tichmann, V. Mertens, G. Raupp, T. Zehetbauer and ASDEX Upgrade Team:* Disruption Avoidance and Mitigation on ASDEX Upgrade. 8th ITER Physics R&D Expert Group Meeting on Disruption, Plasma Control and MHD, San Diego,CA 1998.

481. *Grulke, O.:* Experimental Investigation of Coherent Structures in Drift Wave Turbulence. Seminar, Risoe Nat. Lab., Risoe 1998.

482. *Grulke, O.:* Fluktuationen in toroidalen Plasmen. Seminar, Univ. Kiel 1998.

483. *Gubanka, E., H.-S. Bosch, W. Ullrich, M. Hoek* and ASDEX Upgrade Team:* Tritonen Burnup an ASDEX Upgrade. Verhandl. DPG (VI) **33**, 338, P25.7 (1998).

484. *Gude, A., S. Sesnic and ASDEX Upgrade Team:* Beobachtung von mehrfachen Frequenzen beim (1,1) Sägezahn Precursor an ASDEX Upgrade. Verhandl. DPG (VI) **33**, 316, P2.5 (1998).

485. *Günter, S.:* Confinement limitierende MHD Instabilitäten an ASDEX Upgrade. Kolloquium, IPF Stuttgart 1998.

486. *Günter, S.:* Confinement Limiting MHD Instabilities. Seminarvortrag Graduiertenkolleg, Univ. Düsseldorf 1998.

487. *Günter, S.:* Confinement Limiting MHD Instabilities. Seminarvortrag, CRPP Lausanne 1998.

488. *Günter, S.:* MHD an ASDEX Upgrade. Kolloquium, Jülich 1998.

489. *Günter, S.:* MHD Phenomena at ASDEX Upgrade. Seminarvortag, Princeton Univ., Princeton,NJ 1998.

490. *Günter, S.:* Neoclassical Tearing Modes in ASDEX Upgrade. Seminarvortrag, General Atomics, San Diego,CA 1998.

491. *Günter, S.:* Optical Properties in Dense Plasmas. Seminarvortrag Graduiertenkolleg, Univ. Düsseldorf 1998.

492. *Günter, S.:* Phänomene in dichten und sehr stoßfreien Plasmen. Kolloquium, Univ. Bochum 1998.

493. *Günter, S.:* Plasmaspektroskopie. Vorlesung, Univ. Rostock, SS 1998.

494. *Günter, S., A. Gude, K. Hallatschek, T. Kass, M. Maraschek, S. Sesnic, Q. Yu*, H. Zohm* and ASDEX Upgrade Team:* Neue MHD-Phänomene am Tokamak. Verhandl. DPG (VI) **33**, 313, P I (1998).

495. *Günter, S., A. Gude, M. Maraschek, S.D. Pinches, S. Sesnic, Q. Yu*, H. Zohm* and ASDEX Upgrade Team:* MHD Phenomena at ASDEX Upgrade. 17th IAEA Fusion Energy Conf., Yokohama 1998.

496. *Günter, S., A. Könies, J. Gafert, A. Kallenbach, K. Schmidtmann and ASDEX Upgrade Team:* Dichtebestimmung aus Wasserstoff-Linienprofilen in Divertorplasmen. Verhandl. DPG (VI) **33**, 343, P29.5 (1998).

497. *Haas, G., R. Maingi*, J. Neuhauser, ASDEX Upgrade Team and DIII-D Team:* Dynamic Hydrogen Retention in the Walls of the Tokamaks ASDEX Upgrade and DIII-D. 13th Int. Conf. on Plasma Surface Interactions in Control. Fusion Devices, San Diego,CA 1998.

498. *Hallatschek, K., A. Zeiler, D. Biskamp, J.F. Drake* and B.N. Rogers*:* Nonlocal Three-Dimensional Simulations of Plasma Edge Turbulence. EU-US Transport Task Force Workshop, Gothenburg 1998.

499. *Hartfuß, H.-J.:* Correlation Radiometry for Temperature Fluctuation Measurements in Fusion Plasma. 23rd Int. Conf. on Infrared and Millimeter Waves, Colchester 1998.

500. *Hartfuß, H.-J.:* Detektion von mm- und submm-Wellen. Vorlesung, Univ. Regensburg, WS 1997/1998.

501. *Hartfuß, H.-J.:* Mikrowellenspektroskopie. Vorlesung, Univ. Regensburg, SS 1998.

502. *Hartfuß, H.-J.:* Plasmadiagnostik I. Vorlesung, Univ. Greifswald, WS 1998/1999.

503. *Hartmann, D.A.:* Plasmaheizung. Summer Univ. for Plasma Physics, Garching 1998.

504. *Hartmann, D.A., G. Cattanei, ICRH Group and W7-AS Team:* Plasma Heating and Sustainment in the Ion Cyclotron Range of Frequencies on the Stellarator W7-AS. 17th IAEA Fusion Energy Conf., Yokohama 1998.

505. *Häse, M., H.-J. Hartfuß and M. Hirsch:* Temperature Fluctuations and its Correlations with Density Fluctuations in W7-AS. 12th Topical Conf. on High-Temperature Plasma Diagnostics, Princeton,NJ 1998.

506. *Heger*, B., U. Fantz* and K. Behringer:* Spektroskopische Untersuchung der Vibrationsbesetzung von H_2 und D_2 in mikrowellenangeregten ECR-Plasmen. Verhandlg. DPG (VI) **33**, 331, P22.2 (1998).

507. *Herre, G., P. Grigull and R. Schneider:* B2-Eirene Code Modelling of an Island Divertor. 13th Int. Conf. on Plasma Surface Interactions in Control. Fusion Devices, San Diego,CA 1998.

508. *Herrmann, A., J.C. Fuchs, V. Rohde, M. Weinlich, ASDEX Upgrade Team, NI Team and ICRH Team:* Heat Flux Distribution in the Divertor-II of ASDEX Upgrade. 13th Int. Conf. on Plasma Surface Interactions in Control. Fusion Devices, San Diego,CA 1998.

509. *Heumann*, M., F. Goschenhofer*, C. Becker*, J. Geurts*, V. Wagner*, C. Siry*, A. Annen and W. Jacob:* Thermische Stabilität der Bindungsstruktur von amorphen BC-Schichten. Verhandl. DPG (VI) **33**, 624, DS24.24 (1998).

510. *Hildebrandt, D.:* Influence of Surface Roughness on the Deuterium Inventory of ASDEX-Upgrade Divertor Tiles. 4th Int. Workshop on Tritium Effects in Plasma Facing Components, Santa Fé,NM 1998.

511. *Hildebrandt, D., M. Akbi, H. Grote, B. Jüttner, V. Rohde and W. Schneider:* Deuterium Trapping in Divertor Tiles of ASDEX Upgrade. 13th Int. Conf. on Plasma Surface Interactions in Control. Fusion Devices, San Diego,CA 1998.

512. *Hildebrandt, D., H. Grote, W. Schneider, P. Wienhold* and J. von Seggern*:* Observation of Non-Uniform Erosion and Deposition Phenomena on Graphite after Plasma Exposure. 8th Int. Workshop on Carbon Materials, Jülich 1998.

513. *Höfner, C., S. Wolf and E. Taglauer:* Entwicklung der Größenverteilung bei der Facettierung vizinaler Cu-Oberflächen. Verhandl. DPG (VI) **33**, 897, O29.6 (1998).

514. *Horn*, A. and J. Küppers:* Wechselwirkung von Neopentan mit thermischen Wasserstoffatomen. Verhandl. DPG (VI) **33**, 871, O11.67 (1998).

515. *Jacob, W.:* Basic Mechanisms of the Deposition of Codeposited Layers. 4th Int. Workshop on Tritium Effects in Plasma Facing Components, Santa Fe,NM 1998.

516. *Jacob, W.:* Deposition Mechanisms, a-C:H Deposition. Summer School: Course on Low Temperature Plasma Physics and Applications, Techn. Univ. Eindhoven 1998.

517. *Jacob, W.:* Elektronische Zustände in 3, 2 und 1 Dimensionen. Habilitationskolloquium, Univ. Greifswald 1998.

518. *Jacob, W.:* Experimentelle Physik: Leitungsphänomene. Probevorlesung, Univ. Greifswald 1998.

519. *Jacob, W.:* Plasma Technology. Summer Univ. of Plasma Physics, Garching 1998.

520. *Jacob, W.:* Technische Anwendungen von Plasmen: Plasmatechnologie / Plasmatechnik. Techn. Univ. München, Garching 1998.

521. *Jacob, W. and B. Landkammer:* Removal of Codeposited Layers by ECR Discharge Cleaning. 4th Int. Workshop on Tritium Effects in Plasma Facing Components, Santa Fe,NM 1998.

522. *Jacob, W., B. Landkammer and A. von Keudell:* Low-Pressure Glow Discharge Removal of Codeposited Hydrogenated Carbon Layers. ITER EU/JCT Meeting on Plasma-Wall Interaction, Garching 1998.

523. *Jacob, W., B. Landkammer and C.H. Wu*:* Removal of Codeposited Layers by ECR Discharge Cleaning. 13th Int. Conf. on Plasma Surface Interactions in Control. Fusion Devices, San Diego,CA 1998.

524. *Janauschek, B.:* Erzeugung singulärstetiger Maße. 2 Vorträge, Univ. München 1998.

525. *Janauschek, B.:* Die Spektralfunktion eines Dicrasystems mit Buckelpotential. 2 Vorträge, Univ. München 1998.

526. *Jüttner, B.:* Blitze und schnelle Entladungen. Vorlesung, Humboldt-Univ. Berlin 1998.

527. *Kallenbach, A.:* Chemical Erosion of Carbon in the Divertor of ASDEX Upgrade. 8th Int. Workshop on Carbon Materials, Forschungszentrum Jülich 1998.

528. *Kallenbach, A.:* Plasmaphysik. Univ. Hannover, WS 1998/99.

529. *Kallenbach, A.:* Recent Results on Chemical Erosion and the Carbon Content in ASDEX Upgrade. EU/JCT Meeting on Plasma-Wall Interaction, ITER Garching 1998.

530. *Kallenbach, A., A. Bard, D.P. Coster, R. Dux, C. Fuchs, J. Gafert, A. Herrmann, R. Schneider and ASDEX Upgrade Team:* New Results on Carbon Release and Transport in ASDEX Upgrade. 13th Int. Conf. on Plasma Surface Interactions in Control. Fusion Devices, San Diego,CA 1998.

531. *Kallenbach, A., A. Bard, K. Krieger, J. Roth, U. Wenzel and ASDEX Upgrade Team:* Flux Dependence and Isotope Effect of the Chemical Erosion of Carbon under Tokamak Conditions. 17th IAEA Fusion Energy.Conf., Yokohama 1998.

532. *Kallenbach, A. and A. Stäbler:* Summary and Status of Basic Divertor and SOL Physics. EPTS Workshop, Univ. Innsbruck 1998.

533. *Kammler*, Th. and J. Küppers:* Adsorption, Absorption and Abstraction of Hydrogen on Cu(111) Surfaces. 45th AVS Symp., Baltimore,MD 1998.

534. *Kappel*, M., J. Biener* and J. Küppers:* Ionenstrahl-induzierte Gitterschädigung von Graphit. Verhandl. DPG (VI) **33**, 861, O10.4 (1998).

535. *Kardaun, O.:* Des Lois D'Echelle Simples pour le Temps de Confinement á ITER. Séminaire du Tokamak de Varennes, Varennes 1998.

536. *Kardaun, O.:* Random Coefficients and Hidden Variables in Confinement Time Scalings. ITER Confinement Database and Transport Modelling Workshop, Naka 1998.

537. *Kardaun, O.:* Simple Power Laws for Energy Confinement Prediction. ITER Confinement Database and Transport Modelling Workshop, Princeton,NJ 1998.

538. *Kass, T., J. Gernhardt, M. Maraschek, G. Pautasso, D. Zasche and ASDEX Upgrade Team:* Online-Erkennung von "Locked Modes" an ASDEX Upgrade. Verhandl. DPG (VI) **33**, 316, P2.3 (1998).

539. *Kastelewicz, H., S. Klose and H. Meyer:* Parameteruntersuchungen zum Plasmatransport im linearen Plasmasimulator PSI-1. Verhandl. DPG (VI) **33**, 339, P25.12 (1998).

540. *Kaufmann, M.:* Edge Operational Regimes in Tokamaks. Edge-Plasma Theory and Simulation Workshop, Innsbruck 1998.

541. *Kaufmann, M.:* Effect of Divertor Geometry on Power Loading and the Importance of Carbon Radiation. 6th Europ. Fusion Phys. Workshop, Cadarache 1998.

542. *Kaufmann, M.:* Einführung in die Plasmaphysik und Fusionsforschung I. Univ. Bayreuth, WS 1998/99.

543. *Kaufmann, M., H.-S. Bosch, A. Herrmann, A. Kallenbach, K. Borrass, A. Carlson, D.P. Coster, J.C. Fuchs, J. Gafert, K. Lackner, J. Neuhauser, R. Schneider, J. Schweinzer, W. Suttrop, W. Ullrich, U. Wenzel and ASDEX Upgrade Team:* Energy and Particle Control Characteristics of the ASDEX Upgrade "LYRA" Divertor. 17th IAEA Fusion Energy Conf., Yokohama 1998.

544. *Kaufmann, M., V. Mertens, J. Neuhauser, F. Ryter and W. Suttrop:* Edge Operational Regimes in Tokamaks. Edge-Plasma Theory and Simulation Workshop, Innsbruck 1998.

545. *Kisslinger, J., C.D. Beidler, E. Harmeyer, F. Herrnegger, H. Wobig and W. Maurer*:* Coil System of a Helias Reactor. 17th IAEA Fusion Energy Conf., Yokohama 1998.

546. *Kleiber, R.:* Development of a Code for Linear Drift Waves in Stellarators. Verhandl. DPG (VI) **33**, 339, P25.13 (1998).

547. *Klinger*, T., J. Bleuel, M. Endler and G. Theimer:* Experimentelle Untersuchung der symbolischen Dynamik turbulenter Randschichtfluktuationen. Verhandl. DPG (IV) **33**, 342, P28.9 (1998).

548. *Klose, S., H. Meyer and M. Laux:* Asymmetrische Strom-Spannungs-Kennlinien elektrischer Doppelsonden. Verhandl. DPG (VI) **33**, 347, P29.33 (1998).

549. *Kohl, A., S. Labich, H. Knözinger* and E. Taglauer:* Rhodium als Reduktionskatalysator auf Oxidoberflächen. Verhandl. DPG (VI) **33**, 873, O11.79 (1998).

550. *Kohl, A., E. Taglauer and H. Knözinger*:* Surface Analytical Investigations of $Rh/VO_x/SiO_2$ Model Catalysts. 2nd German-Brazilian Workshop on Applied Surface Science, Templin 1998.

551. *Könies, A.:* Stability Analysis of a 3D Plasma Equilibrium with Energetic Particles. Verhandl. DPG (VI) **33**, 316, P2.4 (1998).

552. *Koponen, J.P.T., O. Dumbrajs*, T. Geist, U. Stroth, and W7-AS Team:* New Particle Transport Results at W7-AS. Transport in Fusion Plasma US-Europ. Transport Task Force Workshop, Göteborg 1998.

553. *Koponen, J.P.T., T. Geist, O. Dumbrajs* and U. Stroth:* Recent Results of Particle Transport Studies at W7-AS Stellarator. Verhandl. DPG (VI) **33**, 320, P6.5 (1998).

554. *Kornejew, P., W. Bohmeyer and H.-D. Reiner:* Measurements of Chemical Erosion at PSI-1. 8th Int. Workshop on Carbon Materials, Jülich 1998.

555. *Krieger, K.:* Erosion of the ASDEX Upgrade Divertor. EU/JCT Meeting on Plasma Wall Interaction, Garching 1998.

556. *Krieger, K.:* Plasma Wall Interaction in Nuclear Fusion Devices. Summer Univ. for Plasma Physics, Garching 1998.

557. *Krieger, K. and ASDEX Upgrade Team:* Wolframtransport in Divertor und Randschicht von ASDEX Upgrade. Verhandl. DPG (VI) **33**, 330, P21.1 (1998).

558. *Krieger, K., R. Dux, A. Kallenbach, H. Maier, R. Neu, V. Rohde, J. Roth and ASDEX Upgrade Team:* Comparison of Low-Z and High-Z Wall Materials. 6th Europ. Fusion Physics Workshop, Cadarache 1998.

559. *Krieger, K., H. Maier, R. Neu and ASDEX Upgrade Team:* Conclusions about the Use of Tungsten in the Divertor of ASDEX Upgrade. 13th Int. Conf. on Plasma Surface Interactions in Control. Fusion Devices, San Diego,CA 1998.

560. *Küppers, J.:* Atom-Adsorbate Reactions: Eley-Rideal and Hot-Atom Processes. Univ. of Massachusetts, Amherst,MA 1998.

561. *Küppers, J.:* Atom-Adsorbate Reactions: Eley-Rideal and Hot-Atom Processes. Purdue Univ. 1998.

562. *Küppers, J.:* Atom-Adsorbate Reactions: Eley-Rideal and Hot-Atom Processes. Univ. of Washington, Seattle,WA 1998.

563. *Kurzan, B., M. Maraschek, A. Silva*, W. Schneider and ASDEX Upgrade Team:* Korrelationslängenmessung durch Mikrowellenreflektrometrie an ASDEX Upgrade. Verhandl. DPG (VI) **33**, 338, P25.5 (1998).

564. *Lackner, K.:* Die Vorbereitung der physikalischen Grundlagen für den Plasmareaktor ITER. Verhandl. DPG (VI) **33**, 273, PV III (1998).

565. *Lackner, K., R. Schneider, D.P. Coster, K. Borrass and ASDEX Upgrade Team:* Consequences of Core and Edge Similarity for Experiments. Edge-Plasma Theory and Simulation Workshop, Innsbruck 1998.

566. *Landkammer, B. and W. Jacob:* Correlation of Ion Fluxes and Carbon Erosion Rates. 8th Int. Workshop on Carbon Materials, Jülich 1998.

567. *Landkammer, B. and W. Jacob:* Erosion von a-C:H-Schichten in einem O_2-ECR-Plasma: Korrelation von Erosionsraten und Teilchenflüssen. Verhandl. DPG (VI) **33**, 327, P17.2 (1998).

568. *Landkammer, B., W. Jacob and J. Roth:* Removal of Codeposited Layers by ECR Discharge Cleaning. IEA Workshop on Tritium Experience in Large Tokamaks and Application to ITER, PPPL, Princeton,NJ 1998.

569. *Lang, P.T.:* Energie aus Kernfusion. Schulvortrag, Europäische Schulwochen, München 1998.

570. *Lang, P.T.:* Feuer und Eis: Einsatz höchster und tiefster Temperaturen im Fusionsreaktor. 2 Schulvorträge, MPG Hauptversammlung, Weimar 1998.

571. *Lang, P.T., J. Neuhauser, K. Büchl, R.S. Lang, V. Mertens, H.W. Müller and ASDEX Upgrade Team:* Flexiblere Entladungsführung durch effiziente Pelletinjektion. Verhandl. DPG (VI) **33**, 324, P13.1 (1998).

572. *Lang, R.S., L. Hu*, P.T. Lang, A. Lorenz, G. Weber and ASDEX Upgrade Team:* Guiding of D2 Pellets in a Funnel. Verhandl. DPG (VI) **33**, 342, P28.8 (1998).

573. *Laqua, H.P.:* Electron Bernstein Wave Heating and Emission via the OXB Process at W7-AS. Topical Lecture, Int. Congress Plasma Phys. and 25th EPS Conf. Control. Fusion Plasma Phys., Prague 1998.

574. *Laqua, H.P.:* Elektron-Bernstein-Wellen in Überdichten Plasmen. Verhandl. DPG (VI) **33**, 314, PV II (1998).

575. *Laqua, H.P.:* Fusionsplasmen.Vorlesung, Fachhochschule Stralsund, WS 1998/1999.

576. *Laqua, H.P.:* Heating and Diagnostic with Electron Bernstein Waves. 10th Joint Russian-German Meeting on ECRH, Nizhny Novgorod 1998.

577. *Laqua, H.P.:* Other Schemes of ECRH above the Cutoff. 10th Joint Russian-German Meeting on ECRH, Nizhny Novgorod 1998.

578. *Laqua, H.P.:* Plans on High Field Launch Experiments on W7-AS. 10th Joint Russian-German Meeting on ECRH, Nizhny Novgorod 1998.

579. *Laqua, H.P.:* Plasma Waves. Summer Univ. of Plasma Physics, Garching 1998.

580. *Laqua, H.P. and W7-AS Team:* Über die Geometrie von Korkenziehern und den magnetischen Einschluß von Fusionsplasmen in Stellaratoren. Verhandl. DPG (VI) **33**, 1058, AKE15.1 (1998).

581. *Lederer, H.:* Grand Challenge Applications of the Max Planck Society on the Garching T3E System. Supercomputer Seminar, Mannheim 1998.

582. *Lederer, H.:* Neues vom RZG. Frühjahrstreffen Arbeitskreis Supercomputing des ZKI, München 1998.

583. *Lederer, H.:* Neues vom RZG. Herbsttreffen Arbeitskreis Supercomputing des ZKI, Berlin 1998.

584. *Lederer, H.:* Overview of MPP Production Applications at the Computer Center Garching. 4th Europ. SGI/Cray MPP Workshop, Garching 1998.

585. *Lederer, H.:* RZG Status Report, Cray T3E-System, Vektorrechner NEC Sx4/5, Gigabitprojekte des DFN-Vereins mit MPG-Beteiligung. 15. DV-Tagung, Göttingen 1998.

586. *Lederer, H.:* Visual Supercomputing and Metacomputing – Gigabit Testbed Projects with Contributions of the Max Planck Society. Workshop on Distributed High Performance Computing and Gigabit Wide Area Networks, Univ. Essen 1998.

587. *Leonard*, A.W., A. Herrmann, K. Itami*, J. Lingertat*, A. Loarte*, W. Suttrop and ITER Divertor Modelling and Database Expert Group and ITER Divertor Physics Expert Group:* The Impact of ELMs on the ITER Divertor. 13th Int. Conf. on Plasma Surface Interactions in Control. Fusion Devices, San Diego,CA 1998.

588. *Leuterer, F.:* Calibration of Detectors and Power Balance for the Zodiak 2 and 3 Transmission Lines. 10th Joint Russian-German Workshop on ECRH and Gyrotrons, Nizhny Novgorod 1998.

589. *Leuterer, F.:* Power Deposition in the Plasma Depending on Polarization and Launching Angle. 10th Joint Russian-German Workshop on ECRH and Gyrotrons, Nizhny Novgorod 1998.

590. *Liebisch, P., C. Biedermann, T. Fuchs, G. Fußmann and R. Radtke:* Untersuchungen zum Einschluß und zur Entwicklung der Ladungszustände in einer Elektronenstrahl-Ionenfalle. Verhandl. DPG (VI) **33**, 127, A16.6 (1998).

591. *Linsmeier, C., G. Jung* and J. Wanner*:* Wechselwirkung von Sauerstoffatomen mit Metalloberflächen. Verhandl. DPG (VI) **33**, 873, O11.80 (1998).

592. *Linsmeier, C. and J. Wanner*:* Interaction of Oxygen Atoms with Metal Surfaces. 2nd German-Brazilian Workshop on Applied Surface Science, Döllnsee 1998.

593. *Linsmeier, C., J. Wanner*, M. Scheuer* and X. Li*:* Reaktion von Sauerstoffatomen mit Oberflächen. SFB-Tag SFB 338, Garching 1998.

594. *Loarte*, A., H.-S. Bosch, A.V. Chankin*, S. Clement*, A. Herrmann, D. Hill*, K. Itami*, J. Lingertat*, B. Lipschultz*, K. McCormick, R.D. Monk*, G. Porter*, M. Shimada* and M. Sugihara*:* Multimachine Scaling of the Divertor Peak Heat Flux and Width for L-mode and H-mode Discharges. 13th Int. Conf. Plasma Surface Interactions in Control. Fusion Devices, San Diego,CA 1998.

595. *Lortz, D.:* Hydrodynamik. Vorlesung und Übungen, Univ. München, WS 1998/99.

596. *Mahl, G.:* DMF unter IRIX. Arbeitskreis Unicos, Berlin1998.

597. *Mahl, G.:* Portierung einer DMF DATABASE von J90 auf Origin2000. Arbeitskreis Unicos, Berlin 1998.

598. *Maier, H., K. Krieger, M. Balden, J. Roth and ASDEX Upgrade Team:* Deposition und Erosion im ASDEX Upgrade Wolfram Divertor Experiment. Verhandl. DPG (VI) **33**, 339, P26.2 (1998).

599. *Maier, H., K. Krieger, M. Balden, J. Roth and ASDEX Upgrade Team:* Erosion and Deposition in the ASDEX Upgrade Tungsten Divertor Experiment. 13th Int. Conf. on Plasma Surface Interactions in Control. Fusion Devices, San Diego,CA 1998.

600. *Maraschek, M., S. Günter, T. Kass, H. Zohm* and ASDEX Upgrade Team:* Die Stabilitätseigenschaften resistiver neoklassischer Tearing-Moden an ASDEX Upgrade. Verhandl. DPG (VI) **33**, 320, P6.2 (1998).

601. *Marmar*, E.S., P. Acedo*, O. Batishchev*, R. Bengtson*, R. Boivin*, F. Bombarda*, X. Bonnin*, P.T. Bonoli*, C. Boswell*, R. Bravenec*, N. Bretz*, C. Christensen*, G. Cima*, W. Dorland*, J.F. Drake*, E. Eisner*, H.G. Esser*, M. Finkenthal*, C. Fiore*, K.B. Fournier*, T. Fredian*, R. Gandy*, S. Gangadhara*, K. Gentle*, J. Goetz*, R. Granetz*, M. Greenwald*, H. Griem*, G. Hallock*, J. Heard*, J. Hosea*, A. Hubbard*, I. Hutchinson*, J. Irby*, D. Johnson*, J. Ke*,, J. Kesner*, S. Krasheninnikov*, B. LaBombard*, H. Lamela*, B. LeBlanc*, Y. Lin*, B. Lipschultz*, S. Lisgo*, R. Maqueda*, M. May*, A. Mazurenko*, S. Migliuolo*, E. Nelson-Melby*, G. Miller, D. Mosessian*, R. Nachtrieb*, R. Nazikian*, R. Neu, H. Ohkawa*, P. O'Shea*, T.S. Pedersen*, D. Pappas*, C.K. Phillips*, A. Pigarov*, C. Pitcher*, M. Porkolab*, J. Ramos*, J. Readon*, J. Rice*, B.N. Rogers*, J.C. Rost*, W. Rowan*, J. Schachter*, G. Schilling*, H. Scott*, C. Skinner*, J. Snipes*, V. Soukhanovskii*, P.C. Stangeby*, P. Stek*, J. Stillermann*, Y. Takase*, G. Taylor*, J. Terry*, T. Tutt*, M. Umansky*, W.R. Wampler*, A. Wan*, C. Watts*, L. Weather*, J. Weaver*, B. Welch*, J.R. Wilson*, S. Wolfe*, K.-L. Wong*, A. Woottou*, S. Wukitch*, G. Wurden*, Y. In*, H. Yuh*, S. Zweben and MIT Plasma Science and Fusion Center, Cambridge,MA:* Overview of Recent Results from the Alcator C-Mod Tokamak. 17th IAEA Fusion Energy Conf., Yokohama 1998.

602. *Marushchenko*, N., V. Erckmann, U. Gasparino, K.S. Kasilov*, H. Maaßberg, S. Murakami* and W7-AS Team:* W7-AS - Suprathermal Effects Driven by High-Power ECRH. 6th Ukrainian Conf. and School on Plasma Physics and Control. Fusion, Alushta 1998.

603. *Maruyama*, K., W. Wang*, W. Jacob and J. Roth:* Comparison of the Erosion Behavior of Soft and Hard a-C:D Films by Heat Treatment in Air. IEA Workshop on Tritium Experience in Large Tokamaks and Application to ITER, PPPL, Princeton,NJ 1998.

604. *Massmann*, P.*, P. Bayetti*, J. Bucalossi*, C. Desgranges*, E. di Pietro*, P. Frank, M. Fumelli*, M. Fujiwara*, M. Hanada*, B. Heinemann, R.S. Hemsworth*, T. Inoue*, C. Jacquot*, W. Kraus, Y. Okumura*, F. Probst, A. Simonin*, E. Speth, R. Trainham* and O. Vollmer:* European Contributions to the Beam Source Design and R&D of the ITER Neutral Beam Injectors. 17th IAEA Fusion Energy Conf., Yokohama 1998.

605. *Mayer, M.:* Codeposition of Deuterium with Various Doped Graphites and Removal of Deuterium from Codeposited Doped Layers. IEA Workshop on Tritium Experience in Large Tokamaks and Applications to ITER, PPPL, Princeton,NJ 1998.

606. *Mayer, M.:* Erosion und Redeponierung in JET. Forschungszentrum Jülich 1998.

607. Mayer, M.: SIMNRA, a Simulation Program for the Analysis of NRA, RBS and ERDA. 15th Int. Conf. on the Application of Accelerators in Research and Industry, Denton 1998.

608. *Mayer, M., M. Balden, R. Behrisch and J. Roth:* Codeposition of Deuterium with Beryllium Doped Graphites. EU HT / JCT Progress Review Meeting on Carbon Chemical Erosion and Tritium Inventory and Control in ITER PFC's, Garching 1998.

609. *Mayer, M., M. Balden, R. Behrisch and J. Roth:* Das Wasserstoffinventar in den Wänden von Fusionsexperimenten. Verhandl. DPG (VI) **33**, 327, P17.1 (1998).

610. *Mayer, M., R. Behrisch, P. Andrew*, P. Coad* and A.T. Peacock*:* Transport and Redeposition of Eroded Material in JET. 8th Int. Workshop on Carbon Materials, Jülich 1998.

611. *Mayer, M., R. Behrisch, P. Andrew* and A.T. Peacock*:* Erosion and Deposition Dominated Areas in JET. ITER EU/JCT Meeting on Plasma Wall Interaction, Garching 1998.

612. *Mayer, M., R. Behrisch, K. Plamann*, P. Andrew*, A.T. Peacock* and P. Coad*:* Wall Erosion and Material Transport to the MARK I Carbon Divertor of JET. 13th Int. Conf. on Plasma Surface Interactions in Control. Fusion Devices, San Diego,CA 1998.

613. *McCormick, K.:* Final Evaluation of the ITER SOL-Edge Database. 8th Joint ITER Divertor Physics and Divertor Modeling and Database Expert Group Workshop, San Diego,CA 1998.

614. *McCormick, K., N. Asakura*, H.-S. Bosch, S.J. Davies*, S. Fielding*, K. Itami*, H. Kawashima*, B. LaBombard*, B. Lipschultz*, A. Loarte*, R.D. Monk*, G. Porter*, J. Schweinzer, M. Shimada* and M.Sugihara*:* ITER Edge Database Investigations of the SOL Width. 13th Int. Conf. Plasma Surface Interactions in Control. Fusion Devices, San Diego,CA 1998.

615. *Meier, M.:* Spektroskopie mit spinpolarisierten Elektronen. Univ. Regensburg 1998.

616. *Meister, H., S. de Peña Hempel, A. Kallenbach and ASDEX Upgrade Team:* Erste Messungen des radialen elektrischen Feldes an ASDEX Upgrade. Verhandl. DPG (VI) **33**, 325, P14.3 (1998).

617. *Merkel, P.:* Coils for Prescribed 3D Finte-beta Equilibria. Int. Sherwood Fusion Theory Conf., Atlanta,GA 1998.

618. *Mertens, V., K. Borrass, M. Kaufmann, P.T. Lang, R.S. Lang, H.W. Müller, J. Neuhauser, R. Schneider, J. Schweinzer, W. Suttrop and ASDEX Upgrade Team:* Operational Limits of High Density H-Modes in ASDEX Upgrade. 17th IAEA Fusion Energy Conf., Yokohama 1998.

619. *Meyer-Spasche, R.:* Das Maximumprinzip bei elliptischen Gleichungen. Akad. Vortrag, Techn. Univ. München 1998.

620. *Meyer-Spasche, R.:* Mathematische Probleme aus der Plasmaphysik. Vorlesung, Techn. Univ. München, SS 1998.

621. *Meyer-Spasche, R.:* Nichtlineare Dynamik, numerisch betrachtet. Vorlesung, Techn. Univ. München, WS 1997/98.

622. *Milch, I.:* Energie aus dem Sonnenfeuer - Kernfusionsforschung. Vortragsreihe Frauen führen Frauen. Dt. Museum München 1998.

623. *Monticello*, D., A.H. Reiman*, S. Arndt and P. Merkel:* Free-Boundary PIES Calculations. 40th APS Plasma Physics Meeting, New Orleans,LA 1998.

624. *Müller, H.W., A. Bard, K. Büchl, R. Dux, S. Günter, M. Kaufmann, P.T. Lang, R.S. Lang, V. Mertens, J. Neuhauser and ASDEX Upgrade Team:* Aufheizung des Pellet Hoch-β-Plasmoids. Verhandl. DPG (VI) **33**, 338, P25.9 (1998).

625. *Münich, M.:* Experience with the Operation of Gyrotrons Zodiak 2 and 3. 10th Joint Russian-German Workshop on ECRH and Gyrotrons, Nizhny Novgorod 1998.

626. *Münther*, C. and P.T. Lang:* Flexibler Li-Injektor für die Fusionsforschung. Verhandl. DPG (VI) **33**, 348, P29.38 (1998).

627. *Murakami, S.*, U. Gasparino, H. Idei*, S. Kubo*, H. Maaßberg, N. Marushchenko*, N. Nakajima*, M. Romé* and M. Okamoto*:* 5D Simulation Study of Suprathermal Electron Transport in Non-Axisymmetric Plasmas. 17th IAEA Fusion Energy Conference, Yokohama 1998.

628. *Naujoks, D.:* Ein Aspekt der Kernfusion: die chemische Erosion von Kohlenstoff. Humboldt-Univ. Berlin 1998.

629. *Naujoks, D., D.P. Coster, H. Kastelewicz and R. Schneider:* Transport of Hydrocarbon Molecules in the Edge Plasma of Fusion Experiments. 13th Int. Conf. Plasma Surface Interactions in Control. Fusion Devices, San Diego,CA 1998.

630. *Naujoks, D., G. Fußmann und H. Meyer:* I(U)-Kennlinien des Plasmagenerators PSI-1: Experiment und Theorie. Verhandl. DPG (VI) **33**, 317, P4.1 (1998).

631. *Neu, R.:* Diagnostics for Fusion Plasmas. Summer Univ. Plasma Phys., Garching 1998.

632. *Neu, R.:* Einführung in die Plasmaphysik, Univ. Tübingen, SS 1998, WS 1998/99.

633. *Neu, R.:* Energie aus Kernfusion. Schulvortrag, Gymnasium Oberhaching, 1998.

634. *Neu, R., K. Asmussen, D. Schlögl, K.B. Fournier*, A. Geier and ASDEX Upgrade Team:* Spektrallinien von hochinionisiertem Wolfram. Verhandlg. DPG (VI) **33**, 348, P29.41 (1998).

635. *Noterdaeme, J.-M.:* Experiments with ICRF on ASDEX Upgrade. Seminar. Univ. Kharkov 1998.

636. *Noterdaeme, J.-M.:* ICRF on ASDEX Upgrade and Voltage Limits in RF Systems. Coord. Comm. on Fast Wave Heating and Current Drive, Garching 1998.

637. *Noterdaeme, J.-M.:* Status of ICRF Experiments on AUG and W7-AS. Coord. Comm. on Fast Wave Heating and Current Drive, Oak Ridge 1998.

638. *Noterdaeme, J.-M., ASDEX Upgrade Team, ICRF Group and NI Group:* Ion Cyclotron Resonance Frequency Heating on ASDEX Upgrade: An Overview. Invited Talk, 6th Ukrainian Conf. and School on Plasma Physics and Control. Fusion, Alushta 1998.

639. *Noterdaeme, J.-M., D.A. Hartmann, A. Stäbler, M. Brambilla, B. Brüsehaber, J.C. Fuchs, J. Gafert, A. Gude, B. Kurzan, R. Neu, W. Suttrop, S. Vergamota*, F. Serra*, H.-P. Zehrfeld, ASDEX Upgrade Team, ICRF Group and NI Group:* Comparing High Power Ion Cyclotron Resonance Frequency Heating with Neutral Injection in ASDEX Upgrade: Differences, Similarities and Synergies. 17th IAEA Fusion Energy Conf., Yokohama 1998.

640. *Nührenberg, C.:* Ion-Temperature Gradient Driven Instability in a Theta-Pinch, Drift-Kinetic Plasma-Equilibrium. Verhandl. DPG (VI) **33**, 337, P25.2 (1998).

641. *Nührenberg, C., J. Geiger, C. Görner and A. Weller:* Computational Study of Alfvén Eigenmodes in W7-AS. Theory of Fusion Plasmas, Varenna 1998.

642. *Ott, W.:* Measurement of the NBI Deposition Profile in the Plasma by Beam Modulation. JDC Meeting, Garching 1998.

643. *Paulin*, H., U. Fantz* and K. Behringer:* Chemische Erosion von Kohlenstoff in H_2- und D_2-Plasmen. Verhandlg. DPG (VI) **33**, 339, P26.1 (1998).

644. *Pecher, P. and W. Jacob:* Die Zusammensetzung der Ionenflüsse aus ECR-Methan-Plasmen. Vergleich von quantitativen Messungen mit plasmachemischer Modellierung. Oberflächentechnologie mit Plasmaprozessen, Mühlleithen 1998.

645. *Pecher, P. and W. Jacob:* Die Zusammensetzung des Ionenflusses aus ECR-Methan-Plasmen: Messung und Modellierung. Verhandl. DPG (VI) **33**, 328, P18.3 (1998).

646. *Peeters, A.G.:* Kinetic Theory. Proc. Summer Univ. Plasma Phys., Garching 1998.

647. *Peeters, A.G.:* Physics of the L-H Mode Transition. 6th Europ. Fusion Phys. Workshop, Cadarache 1998.

648. *Penningsfeld, F.-P.:* Attempts for Higher Beta in W7-AS. JDC Meeting, Garching 1998.

649. *Pernreiter, W. and H.-J. Hartfuß:* Untersuchungen zu nichtthermischen Elektronen-Energieverteilungen aus ECE-Messungen am Stellarator W7-AS. Verhandl. DPG (VI) **33**, 317, P3.5 (1998).

650. *Pfeiffer, U., M. Endler, J. Bleuel, H. Niedermeyer, G. Theimer and W7-AS Team:* Density, Temperature and Potential Fluctuation Measurements with Multiple Fast Swept Langmuir Probes on W7-AS. Réunion Physique, Cadarache 1998.

651. *Pinkau, K.:* The ESA Science Programm - A View from Germany. ESA History Symp., London 1998.

652. *Pinkau, K.:* Forschung im freien Staat. Festveranst. der Karl-Heinz-Beckurts-Stiftung, Bad Godesberg 1998.

653. *Pinkau, K.:* Forschungsfreiheit und Forschungspflicht. Workshop: Neue Nukleartechnologien, IANUS, Techn. Univ. Darmstadt 1998.

654. *Pinkau, K.:* Fusion Research between Science and Politics. IIASA SERF-Workshop, Laxenburg 1998.

655. *Pinkau, K.:* Fusionsforschung zwischen Wissenschaft und Politik. Verleihung der Ehrendoktorwürde, Univ. Greifswald 1998.

656. *Porter*, G., A. Loarte*, K. McCormick, M. Shimada* and M. Sugihara*:* Analysis of Separatrix Plasma Parameters Using Local and Multi-Machine Databases. 13th Int. Conf. Plasma Surface Interactions in Control. Fusion Devices, San Diego,CA 1998.

657. *Puri, S.:* Kirchhoff Thermal Radiation - Cause behind Anomalous Plasma Transport. Transport Task Force Workshop, Göteborg 1998.

658. *Rangelov, G., K. Ertl, F. Passek, M. Vonbank, S. Bassen, J. Reinmuth, M. Donath and V. Dose:* Effizienter Röntgenstrahlungs-Detektor für Auftrittspotential-Spektroskopie. Verhandl. DPG (VI) **33**, 887, O21.9 (1998).

659. *Raupp, G. and ASDEX Upgrade Team:* New Plans for Tokamak Control. EPCS General Assembly, Sincrotrone Trieste, Trieste 1998.

660. *Redi*, M., D. Monticello*, G.Y. Fu*, M.C. Zarnstorff*, C. Nührenberg and W. Cooper*:* Calculations with the CAS3D MHD Stability Code for a Quasi-Axial Stellarator. ICC98, Princeton,NJ 1998.

661. *Reiman*, A.H., L.-P. Ku*, D. Monticello*, H. Mynick*, A. Brooks*, G.Y. Fu*, R. Goldston*, L. Grisham*, T.S. Hahm*, Z. Lin*, R. Nakazian*, G. Neilson*, N. Pomphrey*, M. Redi*, W. Reiersen*, J. Schmitt*, R. White*, M.C. Zarnstorff*, I. Zatz*, W. Cooper*, M. Drevlak, P. Merkel, C. Nührenberg, D. Batchelor*, S. Hirshman*, J. Lyon*, R. Sanches*, D.A. Spong*, M. Hughes*, A. Boozer*, W. Miner*, P. Valanju*, K.Y. Watanabe*, N. Nakajima*, M. Okamoto*, B. Blackwell* and J. Harris*:* Physics Issues in the Design of a High ß Quasi-Axisymmetric Stellarator. 17th IAEA Fusion Energy Conf., Yokohama 1998.

662. *Reimbold, S., B. Wolle*, M. Kick, K. Hübner* and N. Rust:* Experimentelle und numerische Untersuchung von Slowing-Down-Spektren an W7-AS. Verhandl. DPG (VI) **33**, 337, P25.4 (1998).

663. *Reinmuth, J. and M. Donath:* Fe/W(110): eine Untersuchung mit spinaufgelöster Auftrittspotential-Spektroskopie. Verhandl. DPG (VI) **33**, 780, AM4.4 (1998).

664. *Rogers*, B.N., J.F. Drake*, W. Dorland* and A. Zeiler:* Phase Space of Tokamak Edge Turbulence, the L-H Transition, and the Structure of the Edge Pedestal. 17th IAEA Fusion Energy Conf., Yokohama 1998.

665. *Rohde*, D., H. Kersten*, W. Jacob and R. Hippler*:* Untersuchungen zum Sputtern von Kohlenstoffschichten. Verhandl. DPG (VI) **33**, 623, DS24.15 (1998).

666. *Roth, J.:* Chemical Erosion of Carbon Based Materials in Fusion Devices. 13th Int. Conf. Plasma Surface Interactions in Control. Fusion Devices, San Diego,CA 1998.

667. *Roth, J.:* Chemical Erosion of Carbon Based Materials under Divertor Relevant Conditions. 6th Europ. Fusion Phys. Workshop, Cadarache 1998.

668. *Roth, J.:* Materialprobleme in W7-X. Jülich-Greifswald Workshop on Plasma Edge Physics and Plasma-Wall Interaction, Jülich 1998.

669. *Roth, J.:* Modeling of Chemical Erosion. EU/JCT Meeting on Plasma-Wall Interaction, Garching 1998.

670. *Roth, J., W. Eckstein and K. Krieger:* Experimental Investigation of W Irradiation with C and CH_3 at Different Temperatures. 1st IAEA Co-ordination Meeting on "Plasma-Material Interaction Data for Mixed Plasma-Facing Materials in Fusion Reactors", Vienna 1998.

671. *Roth, J. and H.D. Pacher*:* Chemical Erosion of Carbon Based Materials - A Status Report. IEA Tritium Experience Workshop, PPPL, Princeton,NJ 1998.

672. *Ryter, F. and ASDEX Upgrade Team:* Recent H-Mode Threshold Studies in ASDEX Upgrade. 9th ITER Expert Group Workshop on Modelling and Database, Naka 1998.

673. *Ryter, F., J.P. Christiansen*, R. Budny*, J.G. Cordey*, J.C. Fuchs, M. Greenwald*, O. Gruber, A. Hubbard*, I. Hutchinson*, G. Huysmans*, P. Lomas*, C. Lowry*, T. Luce*, H. Meister, S. de Peña Hempel, C. Petty*, H. Salzmann, B. Schunke*, J. Schweinzer, J. Stober, W. Suttrop, K. Thomsen*, B. Tubbing* and S. Wolfe*:* Experimental Tests of Confinement Scale Invariance on JET, DIIID, ASDEX Upgrade and CMOD. Rapporteured Talk, 17th IAEA Fusion Energy Conf., Yokohama 1998.

674. *Ryter, F. and ITER Confinement and Threshold Database Working Group:* Status of the ITER Threshold Database. 9th ITER Expert Group Workshop on Modelling and Database, Naka 1998.

675. *Ryter, F., F. Leuterer, M. Beckmann, B. Brüsehaber, H. Bucher, G. Pereverzev, J. Schweinzer, W. Suttrop, ASDEX Upgrade Team and ECRH-Team IPF:* Expériences ECRH dans ASDEX Upgrade. Seminaire CRPP, Lausanne 1998.

676. *Ryter, F., R. Neu, R. Brückner, B. Brüsehaber, W. Suttrop and ASDEX Upgrade Team:* Non-Local Transport in ASDEX Upgrade. TTF Workshop on Non-Local Transport, Prague 1998.

677. *Ryter, F., J. Stober, W. Suttrop, J.C. Fuchs, O. Gruber, H. Meister, H. Murmann, S. de Peña Hempel, H. Salzmann, J. Schweinzer, ASDEX Upgrade Team, J.P. Christiansen*, G. Huysmans*, P. Lomas*, C. Lowry*, B. Schunke*, B. Tubbing* and JET Team*:* Dimensionally Similar Studies of Confinement H-Mode Transition in ASDEX Upgrade and JET. Rapporteured Talk, 17th IAEA Fusion Energy Conf., Yokohama 1998.

678. *Ryter, F., W. Suttrop, J. Schweinzer, J. Stober and ASDEX Upgrade Team:* Recent Threshold and LH Transition Results in ASDEX Upgrade. ITER Expert Group Combined Workshop on Confinement, Princeton,NJ 1998.

679. *Ryter, F., W. Suttrop, J. Stober, O. Gruber, H. Salzmann, J. Schweinzer and ASDEX Upgrade Team:* Report on Identity Experiments between ASDEX Upgrade and JET. ITER Expert Group Combined Workshop on Confinement, Princeton,NJ 1998.

680. *Sardei, F.:* Auf dem Weg zu generalisierten magnetischen Koordinaten für offene Feldstrukturen. Jülich-Garching-Arbeitstreffen, IPP Jülich 1998.

681. *Schalk*, B., U. Fantz* and K. Behringer:* Stoß-Strahlungsmodell für atomaren und molekularen Wasserstoff. Verhandlg. DPG (VI) **33**, 345, P29.14 (1998).

682. *Schill*, S., T. Baloui, G. Beikert, F. Gadelmeier*, K. Hübner* and B. Wolle*:* Messung und Simulation des Neutronenflusses in der Halle von W7-AS. Verhandl. DPG (VI) **33**, 344, P29.15 (1998).

683. *Schleußner, D., H. Maier, P. Franzen, R. Behrisch, M. Balden, ASDEX Upgrade Team, M. Perl*, W. Knapp* and C. Edelmann*:* Hydrogen Isotope Inventories in the ASDEX Upgrade Tungsten Coated Divertor Tiles. 13th Int. Conf. on Plasma Surface Interactions in Control. Fusion Devices, San Diego,CA 1998.

684. *Schleußner, D., M. Perl*, W. Knapp*, C. Edelmann*, P. Franzen, H. Maier, R. Behrisch, M. Balden and ASDEX Upgrade Team:* Hydrogen Isotope Inventories in the ASDEX Upgrade Tungsten Coated Divertor Tiles. 13th Int. Conf. on Plasma Surface Interactions in Control. Fusion Devices, San Diego,CA 1998.

685. *Schlögl, D., R. Neu, R. Dux and ASDEX Upgrade Team:* Absolutmessung von Fluor-Konzentrationen in ASDEX Upgrade mit Hilfe von Röntgenspektroskopie. Verhandl. DPG (VI) **33,** 321, P7.7 (1998).

686. *Schmidtmann, K., K. Behringer, J. Gafert, S. Günter, U. Schumacher* and ASDEX Upgrade Team:* Untersuchung von dichten Divertorplasmen im Tokamak ASDEX Upgrade. Verhandl. DPG (VI) **33**, 316, P3.1 (1998).

687. *Schneider, R., H.-S. Bosch, D.P. Coster, J.C. Fuchs, J. Gafert, G. Haas, A. Herrmann, M. Kaufmann, A. Kallenbach, J. Neuhauser, J. Schweinzer, U. Wenzel and ASDEX Upgrade Team:* Role of Divertor Geometry on Detachment and Core Plasma Performance in ASDEX Upgrade. 13th Int. Conf. on Plasma Surface Interactions in Control. Fusion Devices, San Diego,CA 1998.

688. *Schneider, R., D.P. Coster, A. Kallenbach, K. Borrass, H.-S. Bosch, J.C. Fuchs, J. Gafert, A. Herrmann, V. Mertens, J. Neuhauser, J. Schweinzer, U. Wenzel, B. Braams* and ASDEX Upgrade Team:* Test of the Predictive Capability of B2-EIRENE on ASDEX Upgrade. 17th IAEA Fusion Energy Conf., Yokohama 1998.

689. *Schweinzer, J., W. Sandmann, G. Haas, J. Neuhauser, H. Murmann, H. Salzmann, ASDEX Upgrade Team and NI Team:* Comparison of Scrape-off Layer Behaviour between DIV-I and DIV-II Operation on ASDEX Upgrade. 13th Int. Conf. on Plasma Surface Interactions in Control. Fusion Devices, San Diego,CA 1998.

690. *Scott, B.D.:* An Introduction to MHD. Summer Univ. Plasma Phys., Garching 1998.

691. *Scott, B.D.:* Anomalous Particle Pinch and Other Effects of Warm Ions. Verhandl. DPG (VI) **33**, 324, P14.1 (1998).

692. *Scott, B.D.:* Turbulence and Transport in the Plasma Boundary Region, A Theoretical Point of View. 6th Europ. Fusion Phys. Workshop, Cadarache 1998.

693. *Scott, B.D., F. Jenko, A.G. Peeters and A.C.-Y. Teo:* Self-Consistent Computation of Transport Barrier Foundation by Fluid Drift Turbulence in Tokamak Geometry. 17th IAEA Fusion Energy Conf., Yokohama 1998.

694. *Sergeev*, V.Yu., B.V. Kuteev*, S.M. Egorov*, L. Ledl, R. Burhenn and W7-AS Team:* Studies of Carbon Pellet Injection into W7-AS Plasmas. 26th Annual Conf. Plasma Phys. Control. Fusion of Russia, 1998.

695. *Shimada*, M., G. Janeschitz*, R.D. Stambaugh*, D. Post*, Yu. Igitkhanov*, G.W. Pacher*, H.D. Pacher*, M. Sugihara*, T. Fukuda*, A. Hubbard*, Y. Kamada*, B. LaBombard*, A.W. Leonard*, A. Loarte*, K. McCormick, T. Osborne*, G. Porter*, W. Suttrop, ITER Divertor Modeling and Database Expert Group and ITER Divertor Physics Expert Group:* Edge Database Analysis for Extrapolation to ITER. 17th IAEA Fusion Energy Conf., Yokohama 1998.

696. *Shishkin*, A.A., I.N. Sidorenko and H. Wobig:* Dynamic Control of Drift Resonances in Helias Configurations. 6th Ukrainian Conf. and School on Plasma Phys. and Control. Fusion, Alushta, Crimea 1998.

697. *Steltenpohl, A. and N. Memmel:* Wachstum von Pd auf Pd(111). Verhandl. DPG (VI) **33**, 866, O11.33 (1998).

698. *Steuer, K.-H.:* Energie aus Kernfusion. Woche der Forschung, Gymnasium Ottobrunn 1998.

699. *Steuer, K.-H.:* Energie durch Kernfusion. 4. Garchinger Umweltwoche, Garching 1998.

700. *Steuer, K.-H.:* Fortschritte in der Kernfusionsforschung. Workshop "Die Energiefrage", Papenburg 1998.

701. *Steuer, K.-H.:* Fusionsreaktoren, schnelle Brüter und Sonnenkraftwerke - Stand und Perspektiven bei der Erschließung neuer Energiequellen. 5 Schulvorträge, MPG Hauptversammlung, Weimar 1998.

702. *Steuer, K.-H.:* Kernspaltungs- und Kernfusionskraftwerke. Ferienakademie Cusanuswerk, Papenburg 1998.

703. *Steuer, K.-H.:* Stand und Perspektiven der Kernfusion mit magnetischem Plasmaeinschluß. Kolloquium, Univ. Gießen 1998.

704. *Steuer, K.-H.:* Thermodynamische Grundlagen von Energieumwandlungssystemen. Ferienakademie Cusanuswerk, Papenburg 1998.

705. *Stroth, U.:* Experimental Results from Stellarators. Summer Univ. for Plasma Physics, Garching 1998.

706. *Sünder, D. and P. Bachmann:* 1D-Mehrflüssigkeits-Plasmarandschicht-Modelle. Verhandl. DPG (VI) **33**, 321, P8.1 (1998).

707. *Suttrop, W., V. Mertens, H. Murmann, J. Neuhauser, J. Schweinzer and ASDEX Upgrade Team:* Operational Limits for High Edge Density H-Mode Tokamak Operation. 13th Int. Conf. on Plasma Surface Interactions in Control. Fusion Devices, San Diego,CA 1998.

708. *Suttrop, W., A.G. Peeters, F. Ryter, J. Stober and ASDEX Upgrade Team:* Physics and Scaling of the H-Mode Transition in ASDEX Upgrade. Invited Talk, Int. Congress Plasma Phys. and 25th EPS Conf. Control. Fusion Plasma Phys., Prague 1998.

709. *Suttrop, W., F. Ryter, V. Mertens, O. Gruber, H. Murmann, H. Salzmann, J. Schweinzer and ASDEX Upgrade Team:* H-Mode and Confinement Studies in ASDEX Upgrade. 17th IAEA Fusion Energy Conf., Yokohama 1998.

710. *Taglauer*, A., R. Niessner*, W. von der Linden, V. Dose and E. Taglauer:* Trace Metal Detection in Natural Water. 18th Int. Workshop on Maximum Entropy and Bayesian Methods, Garching 1998.

711. *Taglauer, E.:* Atomic Layer Epitaxy Investigations by Ion Scattering and Tunneling Microscopy. Europ. Science Foundation Comm. Meeting, Strasbourg 1998.

712. *Taglauer, E.:* Investigations of Surface Structure and Composition by Low-Energy Ion Scattering. Hunan Univ., Changsha 1998.

713. *Taglauer, E.:* Investigations of Surface Structure and Composition by Low-Energy Ion Scattering. Central South Univ. of Technol., Changsha 1998.

714. *Taglauer, E.:* Microprobe Applications for the Characterization of Catalyst Systems. 6th Int. Conf. on Nuclear Microprobe Technology and Applications, Stellenbosch 1998.

715. *Taglauer, E.:* Untersuchung von Adsorbatstrukturen mittels Ionenstreuung und Tunnelmikroskopie. Fritz-Haber-Institut, Berlin 1998.

716. *Taglauer, E., S. Labich, A. Kohl and H. Knözinger*:* Morphology and Surface Reactions on Supported Rhodium Model Catalysts. Symp. on Surface Science, Park City 1998.

717. *Tasso, H. and G.N. Throumoulopoulos*:* Axisymmetric Ideal Magnetohydrodynamic Equilibria with Incompressible Flows. Int. Sherwood Fusion Theory Conf., Atlanta 1998.

718. *Tasso, H. and G.N. Throumoulopoulos*:* Toroidal Magnetohydrodynamic Equilibria with Incompressible Flows. Invited Talk, Int. Congress Plasma Phys. and 25th EPS Conf. Control. Fusion Plasma Phys., Prague 1998.

719. *Ullrich, W., H.-S. Bosch, G. Haas und ASDEX Upgrade Team:* Messungen des Neutralgas Partialdrucks von He und D_2 in ASDEX Upgrade. Verhandl. DPG (VI) **33**, 346, P29.26 (1998).

720. *Vasquez, S.:* Amorphous Hydrogenated Carbon (a-C:H) Films on Polymer Foils Acting as Gas Permeation Barriers.1st Res. Coordination Meeting on Engineering, Industrial and Environmental Applications of Plasma Phys. and Fusion Technologies, Vienna 1998.

721. *Vollmer, O.:* RF Source for Negative Ions: Status and Plans. JDC Meeting, Garching 1998.

722. *Wagner, F.:* Der Weg zu ITER. Fachgespräch, Techn. Univ. Darmstadt 1998.

723. *Wagner, F.:* Einige ausgewählte physikalische Probleme der Fusion. Univ. Konstanz, 1998

724. *Wagner, F.:* Energieforschung aus Kernfusion. Musikalisch-wissenschaftliche Soiree, Techn. Univ. Ilmenau 1998.

725. *Wagner, F.:* Experimentelle Plasmaphysik I. Vorlesung, Techn. Univ. München, SS 1998.

726. *Wagner, F.:* Experimentelle Plasmaphysik II. Vorlesung, Techn. Univ. München, WS 1997/98.

727. *Wagner, F.:* Experimentelle Plasmaphysik II. Vorlesung, Univ. Greifswald, WS 1998/99.

728. *Wagner, F.:* Forschungswettlauf bei der Fusion - wie schädlich ist die antinukleare Haltung in unserem Land. Jahrestagung Kerntechnik '98, München 1998.

729. *Wagner, F.:* Fusionsenergie für das nächste Jahrhundert. VDI-TGA-Tagung, INTHERM Messe, Stuttgart 1998.

730. *Wagner, F.:* Neue Nukleartechnologien im Spannungsfeld von Naturwissenschaft und Ethik. Fachgespräch, Techn. Univ. Darmstadt 1998.

731. *Wagner, F.:* Physics at the Turn of the 21st Century. Status and Topics in Toroidal Confinement Int. Conf., St. Petersburg 1998.

732. *Wagner, F.:* Stand und Fortentwicklung der wichtigen magnetischen Einschlußkonzepte. Fachgespräch, Techn. Univ. Darmstadt 1998.

733. *Wagner, F.:* The Physics of Advanced Stellarators. 25th Annual IOP Plasma Phys. Conf., Oxford 1998.

734. *Wagner, F.:* Experimentelle Beiträge des Stellarators W7-AS zu den Bauprinzipien von W7-X. IPF Stuttgart, 1998.

735. *Wagner, F., M. Anton, J. Baldzuhn, J. Bleuel, R. Brakel, R. Burhenn, G. Cattanei, M. Endler, V. Erckmann, Y. Feng, S. Fiedler, J. Geiger, T. Geist, L. Giannone, P. Grigull, H.-J. Hartfuß, D.A. Hartmann, G. Herre, M. Hirsch, E. Holzhauer*, R. Jaenicke, M. Kick, J. Kisslinger, J.P.T. Koponen, G. Kühner, H.P. Laqua, H. Maaßberg, F. Sardei, U. Stroth, A. Weller, S. Zoletnik, J. Chatenet, D. Dorst, A. Elsner, C. Görner, H. Hacker, F. Karger, F. Knauer, R.W.T. König, H. Laqua, K. McCormick, H. Niedermeyer, C. Nührenberg, W. Ott, F.-P. Penningsfeld, A. Salat, F. Schneider, G. Theimer, H. Walter, C. Wendland, A. Werner, E. Würsching and P. Zeiler:* Overview on W7-AS Results with Relevance for Wendelstein 7-X and the Low-Shear Stellarator Line. 17th IAEA Fusion Energy Conf., Yokohama 1998.

736. *Walter, H., J. Bleuel, R. Burhenn, T. Geist, L. Giannone, H.-J. Hartfuß, J.P.T. Koponen, L. Ledl, G. Pereverzev and U. Stroth:* Recent Transient Transport Results from W7-AS. Transient Transport Meeting, Prague 1998.

737. *Walter, H., R. Burhenn, L. Giannone, H.-J. Hartfuß, L. Ledl and U. Stroth:* Störexperimente zur Bestimmung des Energietransports im Stellarator W7-AS. Verhandl. DPG (VI) **33**, 320, P6.3 (1998).

738. *Wehner*, S. and J. Küppers:* Abstraktion von adsorbierten H/D mit thermischen D/H Atomen auf Pt(111)-Oberflächen. Verhandl. DPG (VI) **33**, 900, O32.6 (1998).

739. *Weller, A., M. Anton, R. Brakel, J. Geiger, C. Görner, H.-J. Hartfuß, M. Hirsch, R. Jaenicke, C. Nührenberg, S.D. Pinches, D.A.Spong*, S. Zoletnik, W7-AS Team, NBI Group and ECRH GROUP (W7-AS):* Investigation of Equilibrium, Global Modes and Microinstabilities in the Stellarator W7-AS. 17th IAEA Fusion Energy Conf., Yokohama 1998.

740. *Weller, A., C. Görner and D. Gonda:* X-Ray Diagnostics on WENDELSTEIN 7-AS. 12th Topical Conf. on High Temperature Plasma Diagnostics, Princeton,NJ 1998.

741. *Wenzel, U., K. Behringer, K. Büchl, D.P. Coster, A. Herrmann, K. Schmidtmann and R. Schneider:* Characterization of the Hydrogen Emission in Divertor II of ASDEX Upgrade. 13th Int. Conf. Plasma Surface Interactions in Control. Fusion Devices, San Diego,CA 1998.

742. *Wienhold, P.*, H.G. Esser*, D. Hildebrandt, A. Kirschner*, K. Ohya*, V. Philipps*, M. Rubel* and J. von Seggern*:* Investigation of Erosion and Deposition on Wall Components of TEXTOR-94. 8th Int. Workshop on Carbon Materials, Jülich 1998.

743. *Wilhelm, R.:* Deposition, Properties and Applications of Carbon-Based Coatings. Workshop on Advanced Technologies Based on Wave and Beam Generated Plasmas. NATO ASI, Sozopol 1998.

744. *Wilhelm, R.:* ECR Plasmas for Thin-Film Deposition. Workshop on Advanced Technologies Based on Wave and Beam Generated Plasmas. NATO ASI, Sozopol 1998.

745. *Wilhelm, R.:* Plasmaphysik I. Vorlesung, Techn. Univ. München, WS 1998/99.

746. *Wilhelm, R. and W. Jacob:* Plasma Technology. Summer Univ. for Plasma Physics, Garching 1998.

747. *Wobig, H.:* Theoretische Plasmaphysik I. Vorlesung, Techn. Univ. München, WS 1998/99.

748. *Wobig, H.:* Theoretische Plasmaphysik II. Vorlesung. Techn. Univ. München, SS 1998.

749. *Wobig, H:* Theory of Advanced Stellarators. Tutorial Lecture, 25th EPS Conf. Control. Fusion Plasma Phys., Prague 1998.

750. *Wobig, H., J. Kisslinger, C.D. Beidler, E. Harmeyer and F. Herrnegger:* Power Balance in Stellarator Reactors. 17th IAEA Fusion Energy Conf., Yokohama 1998.

751. *Wolf, R.:* Experimental Results in Tokamak Physics. Summer Univ. Plasma Phys., Garching 1998.

752. *Wolf, R., O. Gruber, R. Dux, S. Günter, A. Kallenbach, K. Lackner, M. Maraschek, H. Meister, G. Pereverzev, F. Ryter, U. Seidel, S. Sesnic, J. Schweinzer, A. Stäbler, J. Stober, W. Ullrich and ASDEX Upgrade Team:* Advanced Tokamak Operation on ASDEX Upgrade. 17th IAEA Fusion Energy Conf., Yokohama 1998.

753. *Wolle*, B., R. Bätzner*, T. Baloui, G. Gonda, H. Klein*, B. Wiegel* and J. Wittstock*:* Special Absorber Neutron Detector Moderator Assembly (SANDMAN): A New Detector System for Flux Measurements of Collimated 2.5 MeV Neutrons. 12th Topical Conf. on High-Temperature Plasma Diagnostics, Princeton,NJ 1998.

754. *Wolle*, B., A. Weller, S. Schill*, F. Gadelmeier*, T. Baloui and G. Beikert:* Measurements and Simulations of the Neutron Production at W7-AS. 12th Topical Conf. High-Temperature Plasma Diagnostics, Princeton,NJ 1998.

755. *Zeiler, A.:* Phase Space of Tokamak Edge Turbulence, the L-H Transition, and the Formation of the Edge Pedestal. APS Conference, New Orleans,LA 1998.

756. *Zeiler, A.:* Turbulenz in Fusionsplasmen. Kolloquium, Univ. Ulm 1998.

757. *Zeiler, A., K. Hallatschek and D. Biskamp:* Electromagnetic η_i Mode Turbulence at the Plasma Edge. 17th IAEA Fusion Energy Conf., Yokohama 1998.

758. *Zolotukhin, A.V., C.D. Beidler, F. Herrnegger, J. Kisslinger and H. Wobig:* Guiding Center Studies for Highly Energetic Charged Particles in WENDELSTEIN 7-X. Verhandl. DPG (VI) **33**, 337, P25.3 (1998).

Internal Laboratory Reports

IPP 1/312 *Bosch, H.-S. and M. Jung (Eds.):* ASDEX Upgrade Results, Publications and Conference Contributions Period 1/97 to 12/97.

IPP 1/313 *Bosch, H.-S.:* Fusion Products Bibliography. Version 4.0.

IPP 1/314 *Lang, P.T., J. Neuhauser, K. Büchl, M. Kaufmann, R.S. Lang, A. Lorenz, V. Mertens, H.W. Müller, H. Salzmann and ASDEX Upgrade Team:* Controlled High Density Operation on ASDEX Upgrade by Pellet Refueling from the Magnetic High-Field Side.

IPP 1/315 *Herrmann, W.:* Confinement of Ripple-Trapped Slowing-Down Ions by a Radial Electric Field.

IPP 1/316 *Niemann, C.:* Zum Isotopenverhältnis H/D in ASDEX Upgrade.

IPP 1/317 *Lorenz, A., W. Beck, P. Cierpka, P.T. Hu, R.S. Lang, R.S. and G. Weber:* Optimised Pellet Guiding to the Magnetic High Field Side of ASDEX Upgrade.

IPP 1/318 *Bosch, H.-S., P. Franzen, O. Gruber, S. Günter, B. Heinemann, M. Kaufmann, K. Lackner, J. Neuhauser, G. Pereverzev, R. Riedl, C. Sihler, E. Speth, A. Stäbler, B. Streibl, O. Vollmer and R. Wolf:* Extension of the ASDEX Upgrade Programme: Tangential Neutral Beam Injection (TNBI) and Reactive Power Compensation (RPC). Application for Preferential Support, Phase I and II.

IPP 2/338 *Beidler, C.D., U. Stroth and H. Wobig:* Empirical Scaling Laws and Extrapolation to Helias Reactors.

IPP 2/340 *Shishkin*, A.A., I.N. Sidorenko and H. Wobig:* On Magnetic Islands and Drift Surfaces in Helias Configurations.

IPP 2/341 *Junker, J. and A. Weller:* Neutrons at W 7-X.

IPP 2/342 *Sünder, D. and H. Wobig:* Bifurcation of Temperature in 3-D Plasma Equilibria.

IPP III/225 W7-AS Contributions to the 24th EPS Conf. on Controlled Fusion and Plasma Physics, 9-13 June 1997, Berchtesgaden. - Joint Conf. of 11th Int. Stellarator Conf. and 8th Toki Conf. (ITC-8), 29 Sept.-3 Oct. 1997, Toki-city, Japan.

IPP III/229 *Häse, M.:* Untersuchung von Temperaturfluktuationen und deren Korrelation mit Dichtefluktuationen an W7-AS.

IPP III/230 *Görner, C.:* Tomographische Untersuchung von globalen Alfvén-Eigenmoden am Stellarator Wendelstein 7-AS.

IPP III/231 *Teo, A.C.-Y.:* One-Dimensional Model of Global Alfvén Eigenmodes in Tortus and Wendelstein VII-AS.

IPP III/233 *Fuchs, C.:* Messung des Cotton-Mouton-Effekts am Stellarator W7-AS.

IPP III/234 *Itoh, S.-I. and K. Itoh:* Statistical Theory of Subcritically-Excited Strong Turbulence in Inhomogeneous Plasmas.

IPP III/235 *Bleuel, J.:* Elektrostatische Turbulenz am Plasmarand des Stellarators Wendelstein 7-AS.

IPP III/236 *Itoh, S.-I. and Itoh, K.:* Statistical Theory of Subcritically-Excited Strong Turbulence in Inhomogeneous Plasmas (I).

IPP III/237 *Walter, H.:* Störexperimente zur Untersuchung des Energietransports im Stellarator W7-AS.

IPP 4/279 *Franzen, P., O. Vollmer and A. Stäbler:* Spectroscopic Determination of the Species Distributions of the ASDEX Upgrade Neutral Beam Injection System.

IPP 5/77 *Bosch, H.-S. and M. Jung (Eds.):* ASDEX Upgrade Results, Publications and Conference Contributions Period 1/97 to 12/97.

IPP 5/78 *Hallatschek, K.:* Beobachtung hochfrequenter kaskadierender Röntgenoszillationen mit Hilfe von Zeit-/Frequenztransformationen zur Erkennung von Ereignissen und Identifikation der Oszillationen als Tearing-Moden.

IPP 5/79 *Reinmüller, K.:* Emittierende Sonden und Entstehung von Hot Spots - Untersuchung des Kontakts zwischen Plasma und Elektronen emittierender Wand durch Teilchensimulation mit Modell für Stoßprozesse.

IPP 5/80 *Correa-Restrepo, D.:* Resistive Ballooning Modes near the Edge of Toroidal Configurations

IPP 5/81 *Pinches, S.D.:* Nonlinear Interaction of Fast Particles with Alfvén Waves in Tokamaks.

IPP 5/82 *Jenko, F.:* Numerische Modellierung von stoßfreier Driftwellenturbulenz.

IPP 6/348 *Spies, G.O.:* Comment on the Ideal Magnetohydrodynamic Continuous Spectrum in a Cylindrical Screw Pinch: A Question of Completeness.

IPP 8/13 *Bachmann, P. and D. Sünder:* 1D Mehrflüssigkeits-Plasmamodelle = 1D Multi-Fluid Plasma Models.

IPP 8/14 *Meyer, H.:* Analyse der Plasmarotation in einer linearen Magnetfeldkonfiguration = Analysis of the Plasma Rotation in a Linear Magnetic Configuration.

IPP 8/15 *Akbi, M., D. Hildebrandt, B. Jüttner, I. Kleberg and W. Schneider:* Deuterium Trapping in Divertor Tiles in ASDEX Upgrade.

IPP 9/117 *Eckstein, W.:* Sputtering, Reflection and Range Values for Plasma Edge Codes.

IPP 9/118 *Pecher, P.:* Quantitative Bestimmung der Teilchenflüsse aus Methan-ECR-Plasmen = Quantitative Determination of the Particle Fluxes Emanating from Methane ECR Plasmas.

IPP 9/119 *Reinmuth, J.:* Auftrittspotentialspektroskopie (APS) mit spinpolarisierten Elektronen an Mehrkomponentensystemen.

IPP 10/10 *Bosch, H.-S. and M. Jung (Eds.):* ASDEX Upgrade Results, Publications and Conference Contributions Period 1/97 to 12/97.

IPP 10/11 *Behringer, K.:* Escape Factors for Line Emission and Population Calculations.

IPP 11/1 *Krainz, G. and F. Schauer:* Gehäusekühlung der W7-X Hauptfeldspulen.

IPP 11/2 *Krainz, G.:* Preliminary Studies on Current Leads for Wendelstein 7-X.

IPP 11/3 *Niedermeyer, H.:* Jitter Measurements on PCs with a Real Time Operating System.

IPP R/46 *Lederer, H. and F. Hertweck:* Proc. of the 4th Europ. SGI/Cray MPP Workshop, 10-11 Sept. 1998, Garching.

Author Index

Teams

ASDEX Upgrade Team:, M.Balden, A.Bard, G.Becker, M.Beckmann, K.Behler, K.Behringer, A.Bergmann, M.Bessenrodt-Weberpals, D. Bolshukhin, K.Borrass, H.-S.Bosch, B.Braams*, M.Brambilla, R.Brandenburg*, F.Braun, H.Brinkschulte, R.Brückner, B.Brüsehaber, K.Büchl, A.Buhler, A.Carlson, D.Coster, L.Cupido*, S.De Peña Hempel, C.Dorn, R.Drube, R.Dux, S.Egorov*, W.Engelhardt, H.-U.Fahrbach, U.Fantz*, P.Franzen, P.Fu*, J.C.Fuchs, J.Gafert*, G.Gantenbein*, O.Gehre, A.Geier, J.Gernhardt, O.Gruber, E.Gubanka, A.Gude, S.Günter, G.Haas, J.-H.Han*, D.Hartmann, B.Heinemann, G.Herppich, A.Herrmann, W.Herrmann, F.Hofmeister, H.Hohenöcker, L.Hu*, D.Jacobi, A.Kallenbach, O.Kardaun, H.Kastelewicz, M.Kaufmann, A.Khudoleev*, H.Kollotzek, W.Kraus, K.Krieger, B.Kurzan, G.Kyriakakis*, K.Lackner, P.T.Lang, R.S.Lang, M.Laux, L.L.Lengyel, F.Leuterer, A.Lorenz, H.Maier, M.Manso*, M.Maraschek, M.Markoulaki*, K.-F.Mast, P.McCarthy*, D.Meisel, P.Meissner, H.Meister, R.Merkel, V.Mertens, J.P.Meskat*, H.W.Müller, M.Münich, H.Murmann, G.Neu, R.Neu, J.Neuhauser, J.-M.Noterdaeme, G.Pautasso, A.G.Peeters, G.Pereverzev, S.Pinches, G.Raupp, R.Riedl, V.Rohde, H.Röhr, J.Roth, F.Ryter, H.Salzmann, W.Sandmann, S.Schade, H.-B.Schilling, D.Schlögl, K.Schmidtmann*, R.Schneider, W.Schneider, G.Schramm, J.Schweinzer, S.Schweizer, B.D.Scott, U.Seidel, F.Serra*, S.Sesnic, C.Sihler, E.Speth, A.Stäbler, K.-H.Steuer, J.Stober, B.Streibl, W.Suttrop, P.Theodoropoulos*, C.Tichmann, W.Treutterer, M.Troppmann, N.Tsois*, W.Ullrich, M.Ulrich, O.Vollmer, U.Wenzel, F.Wesner, R.Wolf, R.Wunderlich, N.Xantopoulus*, Q.Yu*, D.Zasche, T.Zehetbauer, H.P.Zehrfeld, A.Zeiler, H.Zohm*.

ECRH Group (AUG): F.Leuterer, M.Beckmann, H.Brinkschulte, F.Monaco, M.Münich, F.Ryter.

ECRH Group (W7-AS): V.Erckmann, T.Geist, G.Grünwald, J.Hofner, F.Hollmann*, H.Laqua, F.Noke, F.Purps, U.Weber.

ICRH Group: W.Becker, F.Braun, H.Faugel, R.Fritsch, D.Hartmann, F.Hofmeister, J.-M.Noterdaeme, S.Puri, F.Wesner.

ITER Confinement and Threshold Database Working Group: D.Boucher*, G.Bracco*, T.N.Carlstrom*, A.Chudnovskij*, J.G.Cordey*, J.C.DeBoo*, W.Dorland*, T.Fukuda*, M.Greenwald*, G.Hammett*, G.Hoang*, S.-I.Itoh*, K.Itoh*, Y.Kamada*, O.Kardaun, S.M.Kaye*, A.Kus, Y.Martin*, T.Matsuda*, Y.Miura*, V.Mukhovatov*, J.Ongena*, E.Righi*, F.Ryter, D.P.Schissel*, H.Shirai*, J.Snipes*, T.Takizuka*, H.Tamai*, K.Thomsen*, K.Tsuchiya*, M.Valovic*.

NI Group: M.Ciric, P.Frank, P.Franzen, B.Heinemann, W.Kraus, W.Melkus, S.Obermayer; W.Ott, F.-P.Penningsfeld, F.Probst, R.Riedl, W.Schärich, E.Speth, A.Stäbler, R.Süß, O.Vollmer, K.Wittenbecher.

NI Team(W7-AS): W.Melkus, W.Ott, F.-P.Penningsfeld, F.Probst, E.Speth, R.Süß.

PSI Group: W. Bohmeyer, H. Grote, P. Kornejew, H.-D. Reiner.

W7-AS Team: M.Anton, S.Bäumel*, R.Balbin*, T.Baloui*, J.Bleuel, R.Brakel, H.Callaghan*, G.Cattanei, C.Christou, D.Darrow*, D.Dorst, O.Dumbrajs*, A.S.Egorov*, A.Elsner, M.Endler, K.Engelhardt, V.Erckmann, Y.Feng, S.Fiedler, S.Filchen'kov*, C.Fuchs, U.Gasparino, J.Geiger, T.Geist, L.Giannone, C.Görner, P.Grigull, O.Grulke*, H.Hacker, M.Häse, H.-J.Hartfuß, G.Herre, M.Heyn*, M.Hirsch, E.Holzhauer, J.K.Hübner, K.Itoh*, S.-I.Itoh*, R.Jaenicke, F.Karger, S.Kasilov*, M.Keller, M.Kick, A.Kislyakov*, T.Klinger*, J.Knauer, G.Kocsis*, C.Konrad, J.P.Koponen, H.Kroiss, G.Kühner, A.Kus, H.Laqua, L.Ledl, L.Lubyako*, H.Maaßberg, N.Marushchenko, K.McCormick, V.Moiseyenko*, S.Murakami*, I.Nomura, W.Ott, F.-P.Penningsfeld, W.Pernreiter, S.Reimbold*, M.Rodriguez, N.Ruhs, J.Saffert, M.Saffmann*, A.Salat, F.Sardei, S.Schill*, M.Schubert, V.Sergeev*, M.Shats*, E.Solano, E.Speth, U.Stroth, E.Suvorov*, W.Svendsen*, J.A.Tataronis*, G.Theimer, V.Tribaldos*, F.Volpe, F.Wagner, H.Walter, A.Weller, C.Wendland*, A.Werner*, E.Würsching, D.Zimmermann, M.Zippe, S.Zoletnik.

W7-X Team: S.Arndt, C.D.Beidler, R.Bünde, M.Drevlak, S.Gori, H.Greuner, G.Grieger, E.Harmeyer, C.Henning, F.Herrnegger, F.-W.Hoffmann, J.Junker, J.Kißlinger, A.Könies, P.Merkel, H.Münch, A.Nitsche, C.Nührenberg, J.Nührenberg, I.Ott, M.Pillsticker, F.Rau, H.Renner, J.Sapper, F.Schauer, I.Schönewolf, U.Schwenn, H.Strobel, E.Strumberger, M.Wanner, S.Weber, H.Wobig, R.Zille, A.V.Zolotukhin.

University Contributions to IPP Programme

LEHRSTUHL FÜR EXPERIMENTELLE PLASMAPHYSIK DER UNIVERSITÄT AUGSBURG

(Prof. Dr. Kurt Behringer)

PLASMA EDGE DIAGNOSTICS

(K. Behringer, U. Fantz, B. Heger, A. Kottmair, S. Meir, H. Paulin, B. Schalk and P. Starke)

1 Spectroscopic Diagnostics of Hydrogen Molecules

Investigations have been carried out for the determination of vibrational populations in the ground state of hydrogen molecules and molecular flux measurements in the divertor of ASDEX Upgrade. The developed diagnostic method for the vibrational population (U. Fantz, B. Heger, *Plasma Phys. Control. Fusion* **40** (1998), 2023 and Annual Report 1996, 1997) was improved. Using the collisional radiative model for H_2 the vibrational population in the ground state was calculated for divertor conditions and transferred in the upper Fulcher state considering vibrationally resolved excitation rate coefficients and the lifetimes of these levels (Fig. 1(a)).

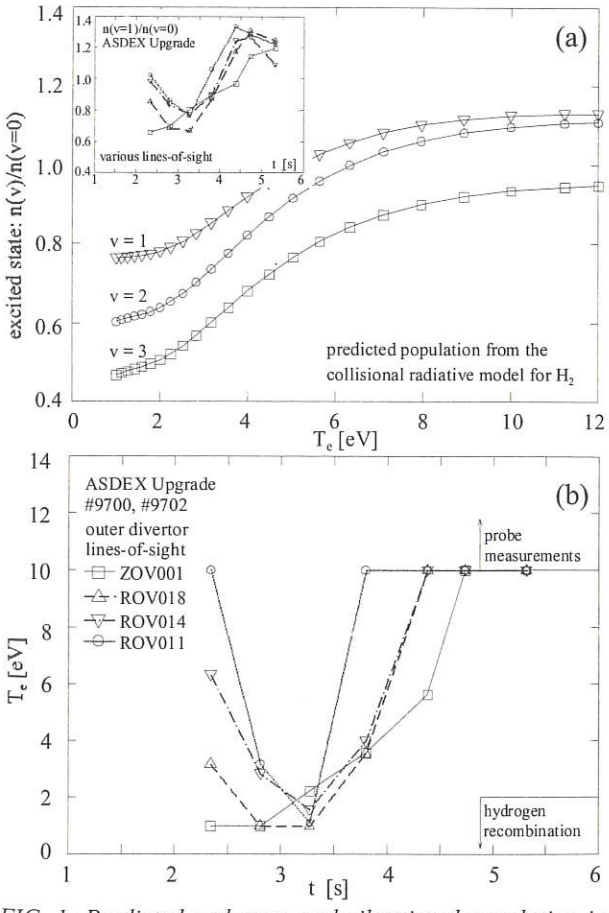

FIG .1: Predicted and measured vibrational population in the excited state of H_2 (a) and T_e derived from measurements (b).

The correlation between the vibrational population in the upper state (referred to v=0) and T_e is very sensitive in the range $2 < T_e < 10$ eV, especially the population in v=2.The measured v=1/v=0 ratios depend on line-of sight and time and are in good agreement with the predicted ones. Therefore, this can be used as a diagnostic tool for the T_e being a completion to other diagnostic methods in the divertor, such as probe measurements beyond 10 eV and the hydrogen recombination below 2 eV. The results (Fig.1(b)) show a weak dependence on the line-of-sight but a strong time dependence due to the transition from the attached to the detached plasma leading to low T_e. From the radiation of the Fulcher band the molecular hydrogen flux was determined using the $(S_{eff}+D_{eff})/XB_{Ful}$ ratio calculated with the collisional radiative model including the vibrational population (U. Fantz et al., *J. Nucl. Mater.* (1999), in print). Due to the sensitivity of this ratio on $T_e < 5$eV, the electron temperature has to be known in the plasma region where the molecular radiation originates from. Therefore, it is necessary to apply the method described above. The measured molecular fluxes are in the same order of magnitude as the ion fluxes, which were obtained from probe measurements. For making comparisons, calculations with the B2-Eirene code were carried out considering the vibrational states as distinct particles, leading to a smaller molecular hydrogen density. The Fulcher radiation, integrated over a line-of-sight, can be predicted by using the emission rate coefficient, which was taken from the collisional radiative model showing a density dependence. This leads to a good agreement of measurements and calculations.

The emission spectroscopy was extended in the vuv range and detailed investigations have been carried out in the continuum spectra of H_2, a transition which results in the repulsive triplet state leading to the dissociation of the molecule. A PC program was developed calculating this spectra. It turns out that the shape of the continuum represents the vibrational population of the upper state and the absolute value gives the T_e. The results for the population and the T_e are in good agreement with those obtained in the vis range. The program can also be used for computing Franck-Condon factors and transition probabilites for bound-bound transitions using potential curves and electronic transition moments.

2 Methane Plasmas and Chemical Erosion

Concerning methane plasmas, the densities of C and C_2 were derived from measured C-lines and the Mulliken C_2 band in the vuv range. Moreover, together with the diagnostics in the vis range, the dissociation model of methane can be further investigated including higher hydrocarbon.

The chemical erosion of cold hydrogen atoms and low energy ions ($\Gamma_{atoms}=10\cdot\Gamma_{ions}= 10^{21}m^{-2}s^{-1}$) on carbon surfaces has been further investigated in a planar inductively coupled RF plasma. The plasma parameters are well known showing a homogenous covering of the surface. The synergistic effect between the atoms and the ions was observed leading to a yield of one percent for hydrogen at 450 K and to a strong isotope effect (Annual report 1996,1997). With increasing bias at the substrate holder the isotope effect decreases. The absolute values of the yield are gained from weight losses, the variations were observed from the emission of the CH/CD band. For getting the erosion yield at room temperatur the cooling of the substrate holder is designed.

LEHRSTUHL FÜR EXPERIMENTALPHYSIK VI DER UNIVERSITÄT BAYREUTH

(Prof. Dr. Jürgen Küppers)

ELEMENTARY REACTIONS OF HYDROGEN ATOMS WITH ADSORBATES AND SOLID SURFACES

(C. Lutterloh, M. Kappel, A. Horn, Th. Zecho, A. Dinger, B. Brandner, A. Theobald)

IPP-University of Bayreuth cooperation is concentrated on investigating fusion-relevant plasma-wall interaction processes. Accordingly, the hydrogen atom surface chemistry on possible reactor wall materials is the primary research topic.

A considerable fraction of the species impinging on the first wall of a fusion experiment vessel are neutrals and ions in the kinetic energy range below about 10 eV. These particles are not capable of causing physical sputtering, but can induce several processes, such as chemical erosion, abstraction etc., by which the plasma is contaminated. It is therefore desirable to understand the elementary processes and mechanisms involved. Recent work of the IPP/UBT collaboration was concentrated on investigations of these issues. Since low-energy ions are neutralized in the immediate vicinity of a substrate by resonance neutralization, it is sufficient to study the low-energy atom-surface interaction. For experimental reasons the work utilized only thermal atoms with energies in the 0.1 eV range.

Reactions of atoms with adsorbates on solid surfaces are commonly addressed as Eley-Rideal reactions after a Nature paper of D.D. Eley and E.K. Rideal from 1940. The reaction of H atoms with an adsorbate X to form a gaseous HX molecule can be written as

$$H(gas) + X(ad) \rightarrow HX(gas).$$

The kinetics of formation of the gas phase product d[HX]/dt can be calculated if the reaction is performed in a specific way, i.e. if the H atom flux is switched on at t=0 and kept constant thereafter. The result is

$$d[HX]/dt = \sigma\Phi[X]_0 \exp(-\sigma\Phi t),$$

with σ as reaction cross-section, Φ as atom flux, t as time, and $[X]_0$ as concentration of X on the surface at reaction start. Our experiments on abstraction of D(ad) by H(gas) on Ni(100) surfaces have shown that the measured HD rates are at variance with the above expression. This result was confirmed by us on various Pt and Cu surfaces. Accordingly, the description of D abstraction from metal surfaces by H as an Eley-Rideal reaction is wrong. The same conclusion had to be drawn from experiments on methyl abstraction from adsorbed methyl iodide on metal surfaces towards methane. On metal surfaces, H atom reactions, e.g. abstraction, do not follow the kinetic laws deduced from the Eley-Rideal mechanistic description.

A mechanistic alternative for these reactions was proposed in 1981 by Harris and Kasemo. Footing on the strong atom-substrate potential and the inability of the incoming atom to channel its energy to the substrate due to the big mass mismatch between the in-atom and the substrate atoms, they proposed that in-atoms are captured in the potential well as hot atoms with considerable energy while moving across the surface. From this hot atom state they might react.

The consequence of this mechanism is that the kinetics of a gas phase product cannot be analytically expressed any more. The kinetics of the product will depend on probabilities for reaction and sticking of hot atoms and these are unknown. As a first approach, a model was developed by us in which two probabilities, p_r for reaction and p_s for sticking of hot atoms, were used to describe hot-atom reactions. Numerical calculations revealed that this simple model was capable of reproducing the essential kinetic characteristics measured in abstraction of D from Ni(100), P(111), and Cu(111) surfaces just by variation of one parameter, the ratio p_r/p_s. The kinetics measured in more complex reactions can be understood by virtue of this model.

Since the essential input of the hot-atom scenario is the strong adsorption well, one can speculate that the lifting of this strong attractive potential might induce an Eley-Rideal scenario. This was confirmed by us using a graphite-covered Pt surface (C/Pt) as substrate for an adsorbate which was used as target in an atom adsorbate reaction. By kinetic measurements it was shown that abstraction of CH_3 from CH_3I adsorbed on C/Pt towards methane precisely matches the expectations drawn from an Eley-Rideal mechanism. The same reaction proceeds on a Pt metal surface according to a hot-atom mechanism.

The methyl abstraction reaction on C/Pt substrates is the first proven example of an Eley-Rideal reaction. It could be shown that the more complex reaction of H with methylene iodide on C/Pt towards methane is a two-step reaction with two Eley-Rideal reaction steps. The kinetics measured is in perfect agreement with the analytical solution of the reaction kinetics

based on the assumption that Eley-Rideal mechanisms control the elementary steps in the reaction.

A further indication of the inapplicability of the Eley-Rideal mechanism at metal surfaces is given by the observation that abstraction of D from metals is structure-sensitive: for the kinetics it matters whether the substrate is a (111), (110), or (100) surface. Within a hot-atom scenario, this feature is expected since the sticking probability of a travelling hot atom should be affected by the structure of the underlying metal surface.

Publications:

Biederer, Th., Th. Kammler and J. Küppers: A Structural Effect in Direct Reactions: Kinetics of D Abstraction from Pt(110) 1x2 Surfaces with Gaseous H Atoms. Chem. Phys. Lett. **286**, 15 (1998).

Dinger, A., C. Lutterloh, J. Biener and J. Küppers: Hydrogen Atom Reactions with Monolayer Graphite Edges on Pt(111) Surfaces: Hydrogenation and H Abstraction. Surf. Sci. in print.

Dinger, A., C. Lutterloh, J. Biener and J. Küppers: Reactions of Gaseous H Atoms with Propylene Oxide Monolayers Adsorbed on Graphite Covered Pt(111) Surfaces. Surf. Sci. in print.

Dinger, A., C. Lutterloh, J. Biener and J. Küppers: Reactions of Gaseous H Atoms with Acetone Monolayers Adsorbed on Graphite Covered Pt(111) Surfaces. Surf. Sci. in print.

Horn, A., J. Biener and J. Küppers: A Dimerisation Reaction Induced by H Atoms: from $B(CH_3)_3$ Physisorbed on C/Pt(100) to $B_2H_2(CH_3)_4$. Surf. Sci. **414**, 290 (1989).

Ishi, S.-I. and J. Küppers: Numerical Analysis of TDS of H_2 from Hydrogenated Diamond Surfaces. J. Surf. Sci. Soc. Japan - Hyomen kagaku **19**, 37-38 (1998).

Kammler, Th., S. Wehner and J. Küppers: The Role of Sticking and Reaction Probabilities in Hot-Atom Mediated Abstraction Reactions of D on Metal Surfaces by Gaseous H Atoms. J. Chem. Phys. **109**, 4071 (1998).

Popp, V., R. Kladny, Th. Schimmel and J. Küppers: Structuring of Mica Surfaces with a Vibrating AFM Tip. Surf. Sci. **401**, 105 (1998).

Wehner, S. and J. Küppers: Abstraction of D Adsorbed on Pt(111) Surfaces with Gaseous H Atoms. J. Chem. Phys. **108**, 3353 (1998).

Wehner, S. and J. Küppers: Abstraction of H Adsorbed on Pt(111) Surfaces with Gaseous D Atoms: Isotope and Flux Effects. Surf. Sci. **411**, 46 (1998).

Wehner, S. and J. Küppers: Interaction of Gaseous D Atoms with CH_3I Adsorbed on Pt(111), H/Pt(111), and C/Pt(111) Surfaces: from Hot-Atom to Eley-Rideal Phenomenology. J. Chem. Phys. **109**, 294 (1998).

Wehner, S. and J. Küppers: Two Consecutive Eley-Rideal Reaction Steps in D Atom/Adsorbate Interaction: from Methylene Iodide via Methyl Iodide to Methane. Chem. Phys. Lett. **288**, 873 (1998).

Zecho, Th., B. Brandner and J. Küppers: Abstraction of D Adsorbed on Pt(100) Surfaces by Gaseous H Atoms: Effect of Surface Heterogeneity. Surf. Sci. **418**, L26 (1998).

Oral Presentations:

Biederer, Th., Th. Kammler and J. Küppers: Struktureinfluß bei der Deuteriumabstraktion durch thermische H Atome auf Pt(111) Flächen. Verhandl. DPG (VI) **33**, 900, O32.7 (1998).

Horn, A. and J. Küppers: Wechselwirkung von Neopentan mit thermischen Wasserstoffatomen. Verhandl. DPG (VI) **33**, 871, O11.67 (1998).

Kammler, Th. and J. Küppers: Adsorption, Absorption and Abstraction of Hydrogen on Cu(111) Surfaces. 45th AVS Symposium, Baltimore 1998.

Kappel, M., J. Biener and J. Küppers: Ionenstrahl-induzierte Gitterschädigung von Graphit. Verhandl. DPG (VI) **33**, 861, O10.4 (1998).

Küppers, J.: Atom-Adsorbate Reactions: Eley-Rideal and Hot-Atom Processes. Purdue Univ. 1998.

Küppers, J.: Atom-Adsorbate Reactions: Eley-Rideal and Hot-Atom Processes. Univ. of Massachusetts, Amherst 1998.

Küppers, J.: Atom-Adsorbate Reactions: Eley-Rideal and Hot-Atom Processes. Univ. of Washington, Seattle 1998.

Wehner, S. and J. Küppers: Abstraktion von adsorbierten H/D mit thermischen D/H Atomen auf Pt(111)-Oberflächen. Verhandl. DPG (VI) **33**, 900, O32.6 (1998).

Diploma Theses:

Biederer, Th.: Abstraktion von D(H) durch thermische H(D) Atome auf Pt(110)-Oberflächen. Univ. Bayreuth 1998.

Brandner, B.: Erosion von hydriertem Kohlenstoff (a-C:H) durch H Atome. Univ. Bayreuth 1998.

INSTITUT FÜR ANGEWANDTE PHYSIK DER UNIVERSITÄT HEIDELBERG

(Prof. Dr. Klaus Hübner)

Cooperation with IPP in the fields of CX and neutron diagnostics and transport studies was continued in 1998. This comprises CX and neutron measurements at W7-AS, investigations of fast particle confinement, numerical simulation of neutron transport as well as neutron diagnostics and charged particle diagnostics for W7-X.

1. NEUTRON TRANSPORT SIMULATION IN SUPPORT OF ACTIVATION MEASUREMENTS ON W7-AS

(T. Baloui, F. Gadelmeier, S. Schill, B. Wolle)

Information on the total neutron yields and the neutron fluence near fusion experiments or near the biological shield is of importance for radiological safety and neutronic compatibility of various plasma diagnostics. On the W7-AS stellarator extensive measurement campaigns using activation samples inside the vacuum vessel and at various positions in the experimental hall have been carried out in order to determine the total neutron yield and to measure fast and thermal neutrons. In order to determine neutron fluences, energy distribution and activation at the irradiation positions, neutron transport calculations have been performed using the MCNP code[1] with cross sections based on the ENDF/B-VI data. The accuracy of these neutronics simulations depends on the quality of the geometric model and the material composition of major structural components. Since structural components located close to neutron detectors have a strong influence on the local neutron field, they need to be modelled carefully in the numerical transport simulations. Based on machine drawings different models for the W7-AS device with a varying degree of structural details have been generated[2].

For the activation measurements three different activation materials viz. indium, copper and gold have been used. After irradiation the activated samples were counted on a remote well-shielded and absolute calibrated HPGe detector. In the high-energy region, the results of the MCNP simulations are in agreement with the measured neutron data. However, at various irradiation positions in the experimental hall, the measured low-energetic activations systematically deviate from the simulated ones. From the numerical results presently follows, that the discrepancies in the absolute values between simulations and measurements can only partly be explained by simplifications in the geometric model and material compositions used in the simulations.

2. CONFINEMENT AND LOSSES OF ENERGETIC IONS ON W7-AS

(S. Reimbold, B. Wolle)

On W7-AS the confinement and slowing-down of neutral-beam injected fast particles has been investigated. Information on the behaviour of the fast ions was obtained by combining local measurements of active neutral particle analysis (NPA) and the time evolution of the measured neutron rates. The NPA diagnostics is used to measure the velocity distribution of the fast particles in the plasma centre, while the volume integrated neutron production is dominated by beam-target fusion reactions and, hence, is strongly related to the fast particle velocity distribution.

In the analysis procedure, the experimental neutron rates are compared with theoretical results based on a relaxation-time model for the fast-ion velocity distribution. From the initial rising phase of the neutron signal at the beginning of the neutral beam heating as well as from the steady-state value of the neutron rate, the neutral-beam deposition power can be deduced. With this deposition power the time dependent neutron production is calculated.

From the available experimental results three different plasma scenarios could be identified. Firstly, there are plasmas with high density and high neutron rates where the predicted and measured neutron rates agree well throughout the discharges. Secondly, there are plasmas with low density and comparatively low neutron rates where the measured and predicted neutron rates tend to disagree. Finally, for a small number of plasmas discrepancies between measured and predicted neutron rates occur only during the rise phase of the neutron signals. Further analysis and comparison with results of other plasma diagnostics suggests that the observed effects in the neutron signals can be related to MHD activity which mostly is observed during neutral beam heating.

---

[1] J. F. Briesmeister (Ed.) report LA-12625-M, LANL, Los Alamos, 1993

[2] B. Wolle et al, Rev. Sci. Instrum. 70 (1999) 1197

LEHRSTUHL FÜR MESSTECHNIK (LMT) DER UNIVERSITÄT DES SAARLANDES

(Prof. Dr. Alexander W. Koch*)

The cooperation IPP - University of Saarland is concentrated on the development of speckle techniques to measure deformation, surface contour, surface roughness and surface structure changes, e.g. caused by erosion of technical, optically rough surfaces.

Spatial Phase-Shifting

(M. Jakobi*, P. Evanschitzky, J. Heinrich)

The current technical set-up for speckle interferometry is based on temporal phase-shifting using a single CCD camera. A laser illuminates the reference and the measurement object and the standard CCD camera records the speckle images, which are digitized by a frame grabber. The reference surface is moved by a computer-controlled piezoelectric transducer to introduce a phase difference between the reference and the measurement beam. Temporal phase-shifting is thus realized. Several speckle images are recorded sequentially and are distinguished by the phase shift. Reproducible results were achieved with a measurement distance of up to 6 m between measurement object and camera.

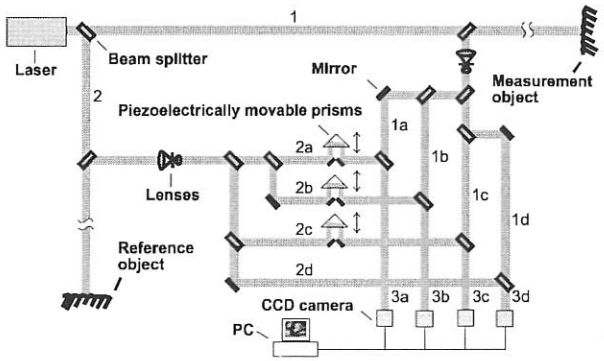

FIG. 1: Basic set-up of spatial phase-shifting (1: measurement beam, 2: reference beam, 3: phase shifted interference beams).

To set up the phase-shifting technique in a fusion-relevant environment without the use of a vibration-damped table the four phase-shifted speckle images are simultaneously acquired with four cameras.

Figure 1 shows the basic set-up of the spatial phase-shifting. After the first beam splitter (beams (1) and (2)) the laser light illuminates the reference and the measurement object. The light reflected by the measurement object is split into beams (1a), (1b), (1c) and (1d) and the light reflected by the reference object into beams (2a), (2b), (2c) and (2d). The measurement and the reference objects are imaged by lens systems. The necessary phase differences between the beams are realized by the path differences. Piezoelectrically movable prisms are integrated in beams (2a), (2b) and (2c). Beams (1a) and (2a) interfere to form beam (3a), and the other beams in the same manner. The pixel synchronous progressive scan CCD cameras allow simultaneous acquisition of four images, several interference figures, and parallel data transfer to a personal computer. The cameras are adjusted to record identical object areas. At different but known phases in the complex interferometer all necessary parameters can be determined to calculate the deformation, surface slope and/or erosion of the measurement object. This new laboratory set-up demonstrates the functionality and applicability of long-range speckle interferometry in experimental fusion devices.

Publications:

Koch, A.W., M. Ruprecht, O. Toedter, and G. Häusler: Optische Meßtechnik an technischen Oberflächen. ISBN 3-8169-1372-5. Expert Verlag, Renningen 1998.

Jakobi, M., P. Evanschitzky, and A. W. Koch: Erosionsmessung an rauhen Oberflächen mittels Streifenkontrast in der Speckle-Interferometrie. Proc. XII. Meßtechnisches Symposium des Arbeitskreises der Hochschullehrer für Meßtechnik e.V., Saarbrücken, S. 133-140, Sept. 1998.

Berger, E., W. von der Linden, V. Dose, M. Jakobi, and A.W. Koch: Reconstruction of surfaces from phase-shifting speckle interferometry: The Bayesian approach. Applied Optics (to be published).

Doctoral Thesis:

Ruprecht, M.: Ferndiagnostik technischer Oberflächen mittels Laser-Speckle-Verfahren. Univ. des Saarlandes 1998.

* Since 1.10.1998 with Lehrstuhl für Meßsystem- und Sensortechnik, TU München.

INSTITUT FÜR PLASMAFORSCHUNG (IPF) DER UNIVERSITÄT STUTTGART

(Prof. Dr. U. Schumacher)

The developments, measurements, and interpretation of heating and diagnostic systems are the basis of the long lasting close collaboration of Institute for Plasma Research (IPF) at Stuttgart University with MPI of Plasma Physics at Garching. The application of microwave heating, current drive, and diagnostics - in future mainly for W7-X - and the contributions to high resolution spectroscopy for bulk and divertor plasma diagnostics are of increasing importance.

1. PLASMA HEATING

(H. Z o h m , L. Empacher, W. Förster, G. Gantenbein, H. Hailer, M. Haug, E. Holzhauer, S. Klenge, W. Kasparek, H. Kumric, J. P. Meskat, G. A. Müller, B. Plaum, P. G. Schüller, K. Schwörer, D. Wagner)

In collaboration with IPP Garching and IAP Nizhny Novgorod.

1.1 Electron cyclotron resonance heating (ECRH)

The investigation of the application of ECRH to fusion plasmas was continued. On the technical side, the work on the W7-X ECRH system was the major part, although the support for W7-AS and ASDEX Upgrade was continued. In addition, studies of the MHD stability of ASDEX Upgrade high β discharges and the use of ECRH / ECCD to influence this stability became a major issue. Also, our general developments in the field of millimetre wave technology as well as the study of microwaves as a plasma diagnostic tool are reported here.

1.1.1 ECRH on W7-AS

In 1998, two 70 GHz/200kW systems were removed from W7-AS, to be replaced by one 140 GHz/500kW (DELTA) and a 70 GHz/500kW (BRAVO) gyrotron. The manufacturing of transmission components for both lines was finished, and low power tests at IPF showed high mode purity. At present, most parts for the lines are mounted. An optimised long-pulse dummy-load (cf Section *1.3.4*) which has inputs for two gyrotrons was built and integrated into the transmission system.

After the installation of the DELTA tube in summer, thermographic measurements of the output beam pattern were performed, and matching mirrors were designed and fabricated in collaboration with IAP. These mirrors produce a gaussian beam with high quality. Therefore, the transmission system could be commissioned without any problems, and plasma experiments were possible since November. The delivery of the 70 GHz gyrotron is expected in spring 1999.

With the ALPHA gyrotron, which operates with a depressed-collector, a new concept for the high voltage supply was tested. In this concept the cathode voltage as well as the body voltage is generated relative to the collector with the advantage that both supplies can be grounded there; however, a precise differential regulation is needed to keep the acceleration voltage (which is the sum of both voltages) constant. This principle was successfully demonstrated and will therefore be pursued for the power supplies for the ECRH system on W7-X.

Programs for improved calculation of the position, direction, and polarisation of the microwave beams being irradiated into the plasma depending on the position of the antenna and polariser mirrors were developed. Their integration into the existing control system together with a graphical user interface for control parameter setting and device survey will complete the microwave mirror control system.

1.1.2 ECRH system for ASDEX Upgrade

In 1998, the construction of the transmission lines for the 2 MW, 140 GHz ECRH system has been nearly completed. Two transmission lines have been used for high power experiments with the gyrotrons Zodiak 2 and 3. Two other gyrotrons have been delivered by the manufacturer, the corresponding transmission lines were built up and partially tested with high power.

Work has been concentrated on the improvement of the output beams of the gyrotrons. Since the gyrotron output radiation does not have a purely gaussian power distribution, unacceptable losses occur during transmission. Although these losses exist along the whole transmission path, they are predominantly located in the first mirror box directly after the gyrotron output window. With two special mirrors in this area it is possible to convert the gyrotron output beam into a fundamental gaussian mode appropriate for low loss transmission. The measurement of the radiation of four gyrotrons has been performed with a thermographic method. This method uses an IR-camera which records the thermal emission of a target which has been illuminated by the mm-wave beam at different distances from the output window. From these data the beam characteristics have been calculated in collaboration with IAP. The mirrors were manufactured on the basis of these data, installed, and tested. The results still show a significant deviation from the fundamental gaussian mode. Additional measurements have been performed to investigate this question for gyrotron Zodiak 3, and will be continued for the other gyrotrons.

1.1.3. ECRH system for W7-X

1.1.3.1 Multibeam transmission system

In 1998, the design of the transmission system for the ECRH facility on W7-X was matched to the modifications especially in the torus region. The optimisation of the surfaces of the multibeam waveguide was performed with extensive diffraction calculations. The results show that toroidal surfaces give better performance than the usual ellipsoids, and, for the geometry of the W7-X system, lead to negligible mode conversion loss (cf Section *1.3.3*). Design considerations of the launchers and calculations of the heat load of in-vessel components have been started.

The preparations for the installation of the prototype transmission system at IPF Stuttgart were continued. For the mounting of the mirrors stable supports were fabricated, and lens horns for the simulation of gyrotron beams as well as other test equipment were built and characterised. The alignment control, which is based on reflectometry from shallow gratings on the mirror surfaces, was successfully tested in a preliminary experiment using W7-AS components, and measures to integrate such a system into the prototype transmission line were taken. Measurements of the ohmic loss on typical metallic mirror surfaces were started.

The detailed design of mirrors and mounts was pursued. The main issue was the simulation of the deformation of the mirrors under thermal load using thermo-mechanical codes. The preferred model under investigation is a sandwich structure consisting of a 60 mm thick stable framework made from aluminum or stainless steel and a relatively thin (≈ 10 mm), highly reflecting copper layer with integrated cooling circuits (see **Fig. 1.1**). In spite of the stiff design, the calculations show that highly efficient cooling and further optimisations are necessary to guarantee low deformations of the mirror surfaces under all load conditions. First measurements on two small prototypes have been performed and mainly confirm the calculations.

Within the collaboration with FZK Karlsruhe modelling of the cavity and the output taper of the 140 GHz CW gyrotron under development for W7-X were performed, and the avoidance of parasitic resonances in the quasi-optic mode converter were studied.

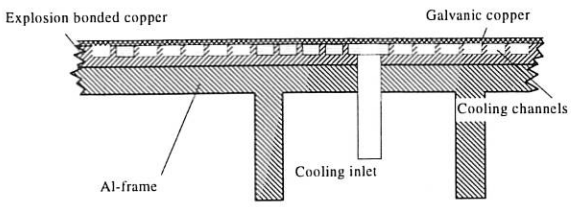

FIG. 1.1: Cross-section of a cooled mirror.

1.1.3.2 Development of gyrotron-specific power supplies

The 10 MW ECRH system of W7-X will require about 20 to 30 MW high voltage electrical power, depending on gyrotron efficiency. Therefore, the use of depressed collector gyrotrons with high efficiency is foreseen. These tubes may be equipped with a gun anode for flexible operation and with a collector coil for the reduction of the ohmic losses at the collector by sweeping of the electron beam. The developments of a complete set of auxiliary supplies, i.e. high voltage supply for the body of the gyrotron and gun anode as well as a supply for the heater of the gun, a current source for the collector coils and special snubber circuits for gyrotron protection have begun.

In 1998, a design for the gyrotrons was established, allowing for remote controlling by the W7-X control system, universal modular design, easy maintenance and high reliability. First components (thyratrons, design software) arrived at IPF for reliability tests.

1.1.4. ITER contributions

The ITER-tasks 'Optimisation of the in-vessel transmission system' and 'Study of alternate launcher concepts' were completed in 1998. A code to calculate the mode-conversion for deformation of the waveguides due to movements of the vacuum vessel was written. On this basis optimum combinations of waveguide length and diameter can be chosen which result in negligible mode conversion for all operational conditions in ITER. The results were confirmed by a slightly scaled experiment at 140 GHz

For the physics part in the study of alternate launcher concepts, several series of ray-tracing calculations were carried out. They confirm that the performance of the 50 MW ECW system does not drop strongly, if two antennas with fixed launcher angles (20° and 40°) are used instead of a steerable antenna. If, in addition, frequency tunability were possible, again a very flexible system is created which can cover all the applications of the ECW systems (central heating, on-axis and off-axis current drive, MHD mode stabilisation).

The technical part of the study identified the remote steering concept proposed by GA, San Diego, to be very promising. This scheme is based on the imaging properties of a rectangular corrugated waveguide which occur at length $L \approx 4a^2/\lambda$, where a is the width of the waveguide and λ is the wavelength of the radiation, and would allow the installation of the movable mirrors outside of the ITER vacuum vessel. To validate this concept, 8 meters of corrugated waveguide were fabricated. In collaboration with IAP low-power tests were performed injecting a gaussian beam into the waveguide with optimised length (6.72 m for a frequency of 142.4 GHz, 7.98 m for 168.8 GHz), and near- and far-field patterns were measured at the output. An example is shown in **Fig. 1.2**, where the output pattern at a distance of 1.7 m is measured for different input angles. The results confirm an available scanning range of ± 12° but show a breakdown of the principle at ± 15° as is expected from theory. This scanning range is essentially sufficient for the ITER application, however, due to the broad

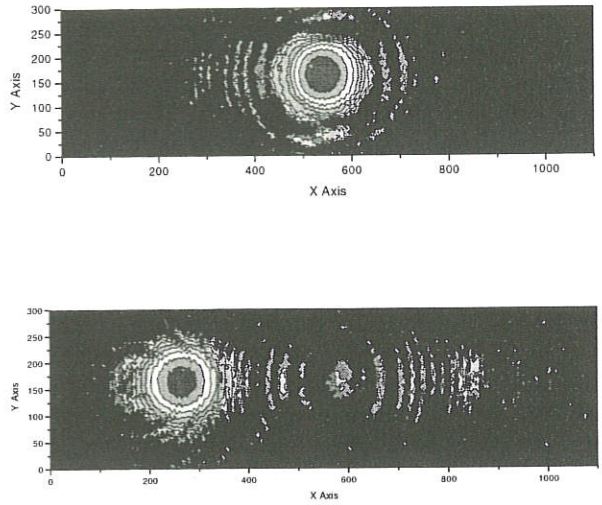

FIG. 1.2: Far field pattern at the output of the square corrugated waveguide (length 6.72 m, frequency 142.4 GHz) for input angles of 0° and 10°.

spectrum of applications of such antennas, numerical calculations and experiments were started to optimise the dispersion of the modes in corrugated waveguides to increase the scanning range.

1.2 MHD stability studies

The study of the MHD stability of fusion plasmas mainly concentrated on the formation of magnetic islands due to neoclassical tearing modes at the resistive β-limit. The possibility of removing these islands by small amounts of ECRH power is studied theoretically and experimentally in ASDEX Upgrade. In addition, ECE diagnostic is used on ASDEX Upgrade to infer details about the structure of the magnetic island.

1.2.1 Active control of neoclassical tearing modes using ECRH / ECCD

1.2.1.1 Experiments on ASDEX Upgrade

In 1998, first experiments on the stabilisation of neoclassical tearing modes were carried out on ASDEX Upgrade. The experiments were done in strongly NBI heated plasmas (P_{NBI} = 10 MW) where the achievable β is limited to β_N = 2.1 - 2.6 by neoclassical modes with mode numbers m = 3, n = 2. 800 kW of ECRH power were injected either phased into O- or X-point of the island ('AC-scheme') or continuously ('DC-scheme'). So far, we could only detect a clear effect with ECCD, i.e. with a finite toroidal launch angle of 15°. **Figure 1.3** shows an example where AC injection leads to a reduction of the size of the magnetic island and a concomitant increase of β. However, due to the reduction of the mode amplitude, the trigger signal

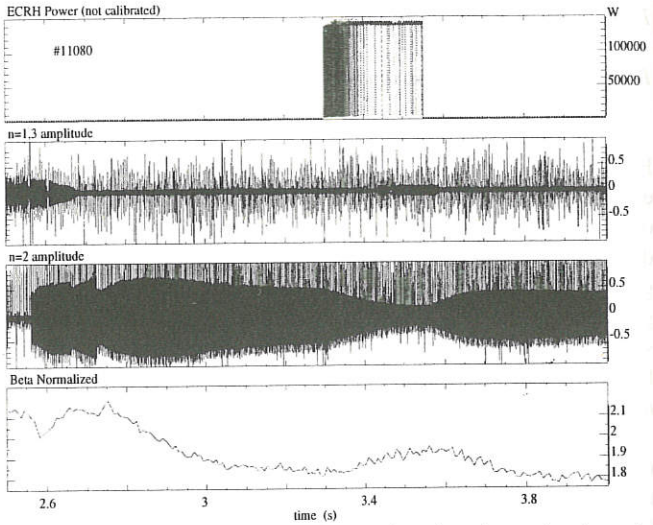

FIG. 1.3: Stabilisation experiment showing the reduction of a neoclassical tearing mode by a small amount of ECCD power.

generated from Mirnov coils stops after 50 ms, leading to DC injection. As can be seen, this is also effective in further reducing the mode amplitude.

These experiments suggest that both, AC and DC injection can be effective for stabilisation. This is consistent with experiments comparing AC O-point and X-point injection, where the O-point injection showed a stabilising effect, but the destabilising effect during X-point injection was weak, so that the sum of the two effects (corresponding to the DC-scheme) can be expected to be stabilising.

1.2.1.2 β-scaling of power requirement

The successful experiments on neoclassical tearing mode stabilisation led to the question, how the required ECCD current scales with β. Balancing the stabilising current I_{ECCD} against the bootstrap current $I_{BS} \propto \beta_p W$, where W is the island width and $W \propto \beta_p$ holds for a neoclassical tearing mode, one can see that two regimes of stabilisation exist, depending on the ECCD deposition width d:

- $d < W$: here, the full current I_{ECCD} contributes to stabilisation and thus, $I_{ECCD} \propto \beta_p W \propto \beta_p^2$, independent of d.
- $d > W$: here, only the fraction I_{ECCD} W/d contributes to stabilisation and we obtain a scaling $I_{ECCD} \propto \beta_p d$.

Thus, reducing d is favourable as long as $d > W$, but for $d < W$, the required current becomes independent of d. Conversely, when stabilising a neoclassical tearing mode with finite d, one will lose efficiency as soon as the island is reduced to $W < d$. However, the total power requirement is given by the absolute maximum in required current. For ITER parameters (β_p = 0.8), this is about 2-3 % of the total plasma current, leading to required ECCD power values well within the projected ITER capability of 50 MW.

1.2.2 *Analysis of the structure of magnetic islands*

For further work on active control of tearing-modes, detailed knowledge of tearing-mode behaviour and island structure is useful. Therefore, a new analysis method is being developed to infer island geometry, helical equilibrium flux, perturbation flux and hence the nonlinear stability parameter Δ' from electron cyclotron emission (ECE) data.

The ECE system of ASDEX Upgrade allows the evaluation of the plasma temperature profile with high temporal and spatial resolution. To relate these data to the magnetic structure of the island, a model of the helical equilibrium and perturbed flux is applied. Using the heat flux equation, the perturbed plasma temperature profile is obtained. The island geometry determines the Fourier spectrum of the temperature oscillation. By fitting the theoretically predicted temperature oscillation to the experimental data it is possible to determine the equilibrium flux and the perturbation flux. Further studies will focus on neoclassical islands and on the reliable determination of Δ'.

1.3 General developments in millimetre wave technology

1.3.1 *Scattering matrix analysis of corrugated rectangular waveguides*

Oversized rectangular corrugated waveguides have similar characteristics as cylindrical ones. When the corrugation depth approaches λ/4, the ohmic losses of the HE_{11} hybrid mode become minimal due to the almost vanishing tangential magnetic field at the waveguide walls. The field of such hybrid modes can be represented as a superposition of the TE and TM modes of the smooth waveguide.

The relative TE/TM eigenmode contents of hybrid modes in corrugated rectangular waveguides were calculated using a scattering matrix formalism. The waveguides have transversely corrugated top and bottom walls, while the side walls are smooth. Once the eigenmode mixture is found for a specific type of corrugation, the waveguide wavelength λ_w and the longitudinal wavenumber k_z can be computed from he phase variation of the total field over one corrugation period. Evaluating the eigenvalues of the HE_{1m} modes shows that for a corrugation depth of $d \approx 0.2\ \lambda$, the eigenvalues lie about equidistant, so that the mode mixtures created when injecting under an angle reproduce the original beam pattern for certain lengths. This effect has been used for the ITER antenna design presented in Section *1.1.4*.

1.3.2 *Optimisation of waveguide elements using a 'genetic code' approach*

The development of codes for the optimisation of waveguide components (especially bends) was continued. The aims of the optimisation are good broadband characteristics for plasma diagnostic applications and low ohmic losses for ECRH components. The mode conversion along the bends is

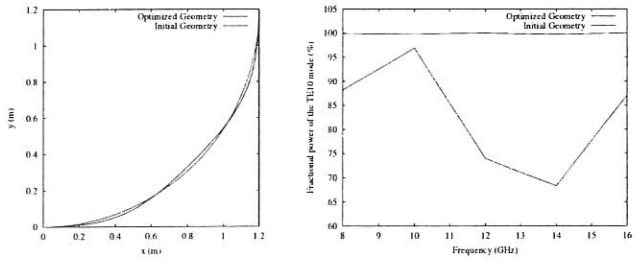

FIG. 1.4: Optimisation of a bent waveguide: Power of TE10 mode at the bend output before and after the optimisation (right) and initial and optimised bend geometry (left).

calculated. Given an initial mode mixture, the coupled mode equation can be integrated numerically. The code can take into account an arbitrary number of modes as well as ohmic losses.

The curvature is approximated by Chebycheff-polynomials. These coefficients as well as the corrugation-depth for corrugated waveguides are taken into account for the optimisation. The code works for rectangular and cylindrical waveguides. The optimisation is done with a genetic algorithm.

Figures 1.4 show the optimisation of a 90 degree bend of a broadband rectangular waveguide. The genetic algorithm was started with a population of 125 individuals originating from a bend with constant curvature. After 50 generations, the best individual had the properties shown in **Figs. 1.4**. As can be seen in the right-hand part, the output power in the TE10 mode is almost 100 % in the whole frequency range and noticeably improved with respect to the case with constant curvature. The optimised curvature has two maxima connected by an almost straight section (left-hand part). These studies will be continued by fabricating and testing optimised bends for various broadband diagnostic applications.

1.3.3 *Transmission characteristics of optical multibeam waveguides*

In multibeam waveguides, several independent beams or signals are transmitted parallel to the central beam in a quasi-optical beamline. Numerical diffraction calculations which had been performed for the design of the ECRH multibeam system for W7-X, showed a good beam quality at the end of the line. In 1998, these calculations were supported by the derivation of analytical formulae to predict the content of spurious gaussian modes. These modes are inevitably generated by focusing mirrors, but can be reconverted by a proper mirror-arrangement. The confocal arrangement of four identical mirrors as a zigzag or as a square, together with optional plane mirrors for the change of direction of the beams, has this favourable property. This is the case in a wide parameter range.

The optimised mirror shape is not the same as for single-beam transmission (off-axis ellipsoidal). When describing the surface by

$$z_s(x_s,y_s)=\frac{1}{4\sqrt{2}f}x_s^2+\frac{\sqrt{2}}{4f}y_s^2+\frac{p}{16f^2}\left(x_s^3+2x_sy_s^2\right),$$

one finds in the numerical as well as in the analytical calculations that the minimum of losses is near the symmetric case p=0, which corresponds to a toroidal mirror surface.

Owing to the good imaging characteristics, the compact design and the broadband property, the multibeam waveguide is interesting for many other imaging system as used, for example, in radio astronomy or for ECE.

1.3.4 Long-pulse load for high power gyrotron radiation

The development of loads for long-pulse high-power operation of gyrotrons was continued. For tests with the two transmission lines which are under construction at W7-AS (one 140 GHz and one 70 GHz line), a compact absorber load has been designed and built. A junction of both lines is connected to the load and, by a switch, it is possible to direct the microwave beams into the load. Thus, test operation of the gyrotrons or transmission lines can be performed without interruption of the routine operation of the plasma experiments.

Figure 1.5 shows a view of the opened load. The entire housing of the load is made of aluminum, and the absorbing walls consist of light-weight firebricks which showed good power loading capacity during high-power microwave material tests. For cooling of the absorbing material, air currents are drawn across the walls by a fan which is mounted outside of the load, visible in the left part of **Fig. 1.5**. The air streams out at the bottom of the load where it drives two turbines with metallic reflectors (one for each beam) which distribute the microwave power along the walls. These two reflectors can also be

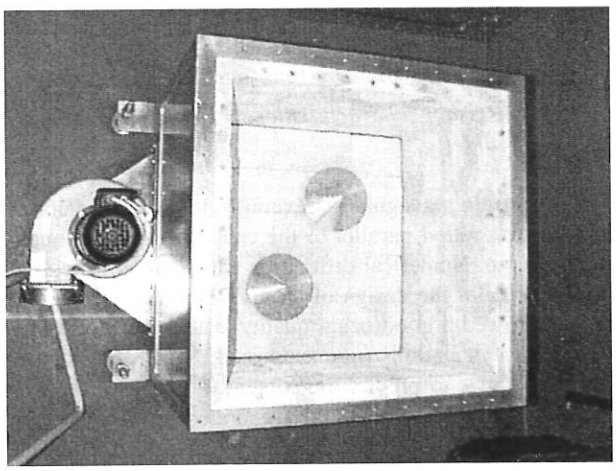

FIG. 1.5: A view into the opened long-pulse gyrotron load.

seen in **Fig. 1.5**. The structure of these special reflectors allows to superpose to the rotation an up and down movement of the reflected beam. Thus an enlargement of the absorbing surface is achieved which lowers the wall loading power density and allows higher power and/or longer pulses of the gyrotrons.

1.4 Millimetre wave diagnostics

1.4.1 Collective Thomson scattering on W7-AS

In collaboration with IAP, the experiments on collective Thomson scattering (CTS) with powerful gyrotron radiation were continued. The determination of the ion temperatures from thermal fluctuation spectra has been shown and the possibility to investigate the ion distribution function with respect to alpha particle measurements was demonstrated. The instrumentation for the scattering measurements has been continuously improved and matched to the needs. The backscattering systems used for experiments so far are still available. However, due to a major change in the gyrotron system, a new geometry with a reduced scattering angle became possible, which allows measurements with increased spatial resolution. In total, three possible scattering geometries are available now for further experiments.

In measurements of the thermal spectrum with the 90° geometry, where the ECR is within the scattering volume, the existence of the strong resonance near the ion-acoustic frequency was confirmed. A possible explanation is a high concentration of hot electrons in the heating zone which reduce the Landau damping of ion-acoustic waves. Other explanations assume a parametric decay of waves in the interaction zone.

The studies on the occurrence of a lower hybrid instability during the injection of energetic particles were continued. Theory shows, that the wave frequency mainly depends on the density and the concentration of the hydrogen ions in a plasma containing different ion sorts. An evaluation of the scattered spectra still showed high errors due to the bad spatial resolution of the back-scattering geometry used. It is expected, that these difficulties can be overcome with the new geometry.

Many scattering spectra showed fine structures with the periodicity of ion cyclotron harmonics, which also could be observed in signals from magnetic loop antennas. Investigations are planned to get a more solid theoretical and experimental basis for this effect and to clarify whether these results are relevant for plasma diagnostics.

1.4.2 Microwave reflectometry

On the stellarator W7-AS measurements with the existing tilted antenna (fixed tilt angle) were continued. A significant result is the observation that the width and frequency shift of the measured frequency power spectra can change dramatically in different confinement regimes. In addition, first measurements show that it should be possible to extract information about **E×B** plasma rotation from the asymmetric frequency shift in the frequency spectra. For future experiments, a new antenna system has been installed which allows to change the tilt angle continuously.

On ASDEX Upgrade tilted antennas have been installed in order to measure the poloidal and toroidal propagation velocity of density fluctuations. It is planned to operate a heterodyne reflectometer system which is currently built at IPF with these antennas to study the behaviour of the **E×B** velocity, with special emphasis on its role in the formation of transport barriers, both in H-mode and in advanced tokamak scenarios.

2. PLASMA EDGE DIAGNOSTICS

(U. S c h u m a c h e r, I. Altmann, G. Dodel, J. Gafert, K. Hirsch, E. Holzhauer, H. Jentschke, S. Klenge, H. Schmidt, K. Schmidtmann, and W. Schneider)

2.1 High resolution spectroscopy in the divertor of ASDEX Upgrade

Owing to changes of the ASDEX Upgrade divertor in 1998, the optical system with high spectral, temporal, and spatial resolution applied for the analysis of the ion dynamics in the divertor had to be renovated. The poloidal observation system consists of 105 lines of sight for the separate analysis of the strike-point regions of the inner and outer divertor. These chords are used to measure the temporal evolution of spatial emission profiles in front of the plates (e.g. C III radiation as a monitor for detachment) and to obtain divertor parameters (like n_e, T_e, T_i) from spectroscopic measurements. Owing to a negligible Doppler shift for ions they also supply the reference wavelength position. The system for toroidal observation of the inner and outer divertor consists of 20 lines of sight along the magnetic field direction and of 20 lines opposite to them. This system had to be completely new in construction, installation and adjustment due to the reconstruction of the ICRH antennae. Because of the opposite Doppler shifts the system allows reliable determination of flow velocities. The optimum line of sight arrangement was found on the basis of the B2-EIRENE predictive calculations and of the experience from the preceding experimental runs.

This line of sight arrangement was optimised to allow the observation of specific flow patterns of ions and neutrals. Among these flow reversal of impurities was predicted for a long time. Since this effect might strongly influence the plasma purity, methods for understanding and finally controlling this phenomenon have to be found. Flow reversal of impurities is expected to occur if the thermal forces due to the temperature gradient of the background plasma acting on the impurities are larger than the electric field, pressure, and friction forces directed towards the target. This is expected to occur only in a limited density range. For experimental verification of flow reversal a density ramp was performed. By using hydrogen as a working gas and successive increase of NBI heating power the discharge was kept in L-mode such that the spectra and their interpretation were not affected by ELMs. As sufficient CIII emission is required for flow reversal to be detected, this is only possible for C^{2+} ions during detachment and for one specific toroidal line of sight.

In **Fig. 2.1** the spectroscopic observation of flow reversal of the C^{2+} - ions is demonstrated for the above mentioned L-mode density ramp. Only in phases of detachment (cf increasing hydrogen radiation due to volume recombination in **Fig. 2.1c**) a second -oppositely shifted- component in the CIII spectrum is observed in the chord POU 004 (cf **Figs. 2.1a** and **2.1b**). **Figure 2.1d** summarises the results for the normal and for the reversed velocities of this discharge.

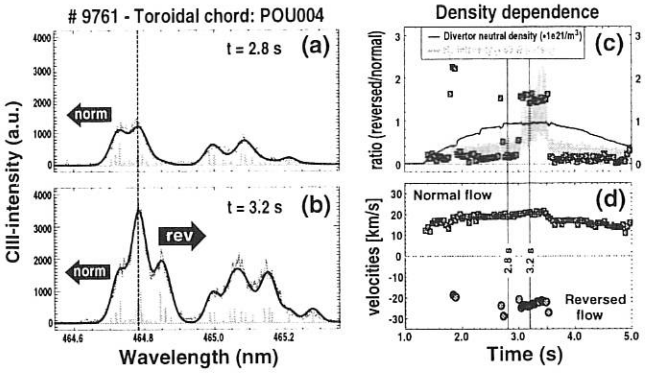

FIG. 2.1: Spectroscopic observation of C^{2+}-flow reversal in an L-mode density ramp discharge of ASDEX Upgrade: (a) blue-shifted CIII-spectrum (t=2.8s; attached), (b) superposition of additional red-shifted CIII-component (reversed flow) onto blue-shifted one (t=3.2 s; detached), (c) ratio (reversed / normal), divertor neutral density and H_β -emission in the outer separatrix as detachment monitor, and (d) resulting C^{2+}-flow velocities.

The plasma detachment, characterised by strong recombination radiation, is investigated separately by the analysis of the hydrogen spectrum. The electron temperature of these recombining plasmas is deduced from the absolute intensity step at the Balmer sprung at λ = 364 nm. Moreover, the Boltzmann plot is applied for temperature determination using the Balmer line intensities from quantum numbers n = 6 (λ = 410.2 nm) up to n = 10 (λ = 379.8 nm). While the temperature obtained from the Balmer step tends to higher temperature values and the weighting of the temperature determination from the Boltzmann plot is pronounced for lower temperatures, good agreement is found for taking the actual density and temperature distributions into consideration.

The electron density in the divertor region is measured by the Stark broadening of the Balmer line H_β (λ = 486.1 nm) and by the absolute Balmer continuum radiation. The electron density is determined by fitting profiles from model calculations (S. Günter) of the Stark profiles of H_β which take the ion dynamics and the static magnetic field into account to the measured spectra. Both methods yield electron densities of several 10^{20} m^{-3}.

2.2 CO_2-laser / HeNe-laser interferometer for ASDEX Upgrade

In collaboration with O. Gehre and J. Bönisch from IPP Garching further tests of the new electronic data acquisition system designed by G. Schramm for the two-wavelength-interferometer were performed and successfully finished. The

interferometer system was then installed and adjusted on ASDEX Upgrade. The central vertical chord is now nearly operational and can be used in 1999.

2.3 Erosion studies from emission and absorption spectroscopy

The measurement of erosion products and erosion rates is of major importance for tests of thermal protection materials for reusable space transportation systems and for plasma facing walls in thermonuclear fusion devices. These measurements are performed in plasma wind tunnels, i.e. with plasma jets interacting with targets of the material. One of the methods is to study the erosion of a C/C-SiC target in such a plasma jet by high resolution emission and absorption spectroscopy of Si I resonance spectral lines at 251 nm and 288 nm. The silicon is eroded by the plasma jet and forms a disc like radiating cloud in front of the target. High spectral resolution is obtained applying an Echelle spectrometer, whereas line integrals were measured with a 0.5m or 1m spectrometer and an gated ICCD camera for fluctuation and correlation investigation.

Different methods to determine the silicon neutral density from the absorption measurements are applied. The emission of self absorbing lines (Si I $3p^2\ ^3P$ - $3p4s\ ^3P^o$ multiplet) was investigated in detail (see Annual Report 1997) in the four manifestations like ratio of line intensities (centre and integral) and profile shape (half width and curvature in the centre). Agreement for the Si density was found for the two methods of line intensity ratios, whereas half width measurements tend systematically to lower values with less precision and the results from curvature evaluation were always significantly lower with large uncertainties.

Detailed investigations of the dynamic range as well as the limits of the methods and the corresponding signal to noise ratio (SNR) confirm these experimental results. For the Si multiplet chosen (251 nm) the detectable optical depth for the line intensity ratio measurements ranges from $0.5 \le \tau \le 20$, corresponding to densities $5\times10^{17}\ m^{-3} \le n_{Si} \le 10^{19}\ m^{-3}$. In **Fig. 2.2** the error (SNR^{-1}) of the optical depth for the strongest S I line at 251.6 nm is shown as a function of the Si density. The line intensity ratio methods for two central intensities and for the integral of all 6 lines achieve the same detectibility over the density range of interest. In the high resolution measurement ($\Delta\lambda \approx 1.2$ pm) the detector allows only two Si lines to be measured at the same time whereas the line integrals are registered for all 6 multiplet transitions simultaneously. This time correlated detection is indispensable because of the high fluctuation level. The half width measurement is less precise in this region but for larger optical depth ($\tau > 15$) or higher Si densities ($n_{Si} > 6\times10^{18}\ m^{-3}$) this evaluation could be advantageous.

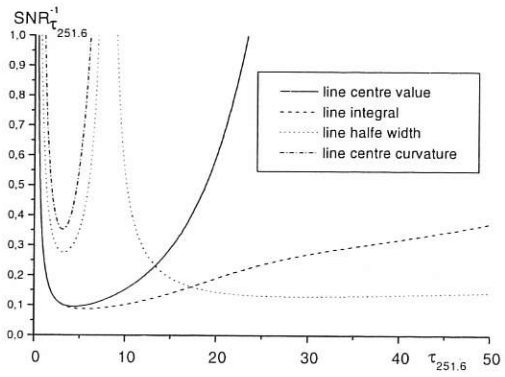

FIG. 2.2: Reciprocal signal to noise ratio of the 4 methods to measure the Si density by emission spectroscopy of absorbing multiplet lines (Si I $3p^2\ ^3P$ - $3p4s\ ^3P^o$) *as a function of the optical depth for the transition at 251.6 nm.*

PUBLICATIONS, CONFERENCE REPORTS, DIPLOMA THESES; AND SEMINAR TALKS

PUBLICATIONS

Günter, S., A. Gude, M. Maraschek, S. Sesnic, H. Zohm, and ASDEX Upgrade Team: Beta scaling for the onset of neoclassical tearing modes at ASDEX Upgrade. Nucl. Fusion **38** (1998) 1431-1434.

Heikkinen, J. A., T.P. Kiviniemi, A.G. Peeters, T. Kurki-Suonio, S. Sipilä, W. Herrmann, W. Suttrop, H. Zohm: Ion orbit loss current in ASDEX Upgrade. Plasma Phys. Contr. Fusion **40** (1998) 693-696.

Hirsch, M., P. Amadeo, M Anton, J. Baldzuhn, R. Brakel, J. Bleuel, S.Fiedler, T. Geist, P. Grigull, H. J. Hartfuß, E. Holzhauer, R. Jaenicke, M. Kick, J. Kisslinger, J. Koponen, F. Wagner, H. Wobig, S. Zoletnik and the W7-AS Team: Operational range and transport barrier of the H-mode in the stellarator W7-AS. Plasma Phys. Control. Fusion, **40** (1998) 631-634.

Holzhauer, E., M. Hirsch, T. Grossmann, B.Branas and F. Serra: Theoretical and experimental investigation of the phase-runaway in microwave reflectometry. Plasma Phys. Contr. Fusion **40** (1998) 1869-1886.

Idehara, T., Nishida, N., Yoshida, K., Ogawa, I., Tatsukawa, T., Wagner, D., Gantenbein, G., Kasparek, W., Thumm, M.: High frequency and high mode purity operations of gyrotron FU IVA. Int. J. Infrared Millimeter Waves **19** (1998) 919-930.

Jentschke, H., U. Schumacher, and K. Hirsch: Studies of silicon erosion in plasma-target interaction from optical emission and absorption spectroscopy. Contrib. Plasma Phys. **38** (1998) 501-512.

Jentschke, H., K. Hirsch, S. Klenge, and U. Schumacher: High resolution emission and absorption spectroscopy for erosion product analysis in boundary plasmas. Rev. Sci. Instrum. **70** (1999) 336-339.

Kass, T., H.-S. Bosch, F. Hoenen, K. Lackner, M. Maraschek, H. Zohm, and ASDEX Upgrade Team: The fishbone instability in ASDEX Upgrade. Nucl. Fusion **38** (1998) 807-819.

Ogawa, I., T. Idehara, A. Sakai, K. Yoshida, T. Tsuchida, K. Kawahata, A. Eijiri, H. Iguchi, K. Tanaka, K. Matsuoka, R. Akiyama, M. Osakabe, S. Okamura, T. Minami, C. Takahashi, and W. Kasparek: Production of an intense, well-collimated submillimetre wave beam and its application to plasma scattering measurements. Int. J. Infrared Millimeter Waves, **19** (1998) 727-736.

Ryter, F., W. Suttrop, B. Brüsehaber, M. Kaufmann, V. Mertens, H. Murmann, A.G. Peeters, J. Schweinzer, and H. Zohm: H-mode power threshold and transition in ASDEX Upgrade. Plasma Phys. Contr. Fusion **40** (1998) 725-729.

Suvorov, E.V., E. Holzhauer, W. Kasparek, A.B. Burov, Y.A. Dryagin, S.E. Filchenkov, A.A. Fraiman, L.V. Lubyako, D.A. Ryndyk, N.K. Skalyga, O.B. Smolyakova, V. Erckmann, T. Geist, M. Kick, N. Rust, W7-AS-team, and ECRH-team: Lower hybrid turbulence excited by a fast transverse ion beam in a magnetised plasma. Nucl. Fusion **38** (1998) 661-671.

Wagner, D., M. Thumm, G. Gantenbein, W. Kasparek, and T. Idehara: Analysis of a complete gyrotron oscillator using the scattering matrix description. Int. J. Infrared Millimeter Waves **19** (1998) 185-194.

CONFERENCE REPORTS

Frühjahrstagung der Deutschen Physikalischen Gesellschaft, Fachausschuß Plasmaphysik, Bayreuth, March 9-13, 1998

Schmidtmann, K., K. Behringer, J. Gafert, S. Günter, U. Schumacher und ASDEX Upgrade Team: Untersuchung von dichten Divertorplasmen im Tokamak ASDEX Upgrade. Verhandl. DPG (VI) **33** (1998) Fachvortrag P 3.1.

Gafert, J, K. Behringer, D. Coster, U. Schumacher und ASDEX Upgrade Team: Dynamik von Neutralen und Ionen im ASDEX Upgrade Divertor II. Verhandl. DPG (VI) **33** (1998) P 3.2.

Günter, S., A Könies, J. Gafert, A. Kallenbach, K. Schmidtmann und ASDEX Upgrade Team: Dichtebestimmung aus Wasserstoff-Linienprofilen in Divertorplasmen. Verhandl. DPG (VI) **33** (1998) P 29.05.

Klenge, S., K. Hirsch, H. Jentschke und U. Schumacher: Untersuchungen von Silizium mit Emissions- und Absorptionsspektroskopie bei der Plasma-Target-Wechselwirkung. Verhandl. DPG (VI) **33** (1998) P 29.20.

Schneider, W., K. Hirsch, H. Jentschke und U. Schumacher: Spektroskopische Untersuchung einer Radiofrequenz-Entladung in He, Ar und N_2. Verhandl. DPG (VI) **33** (1998) P 29.21.

Schinköth, D., G. Bauer, H. Jentschke, K. Hirsch und U. Schumacher: Bestimmung der Elektronendichte und Elektronentemperatur eines Freistrahlplasmas mittels Thomson-Streuung. Verhandl. DPG (VI) **33** (1998) P 29.22.

12th Topical Conference on High Temperature Plasma Diagnostics, Princeton, NJ, USA, June 7-11, 1998

Jentschke, H., K. Hirsch, S. Klenge, and U. Schumacher: High resolution emission and absorption spectroscopy for erosion product analysis in boundary plasmas.

25th EPS Conference on Controlled Fusion and Plasma Physics, Praha, Czech Republic, June 29-July 3, 1998

Zohm, H., G. Gantenbein, S. Günter, F. Leuterer, M. Maraschek, J. P. Meskat, A. G. Peeters, W. Suttrop, and D. Wagner: Experiments on MHD mode stabilisation by ECCD in ASDEX Upgrade. Europhys. Conf. Abstracts Vol. 22C

23rd International Conference on Infrared and Millimeter Waves, Colchester, U.K., September 7-11, 1998

Chirkov, A. V., G. G. Denisov, W. Kasparek, and D. Wagner: Simulation and experimental study of a wavebeam remote steering system. Proceedings (Eds. T J Parker and S R P Smith), ISBN 0 9533839 0 3 (1998), pp 250-251.

Empacher, L., G. Gantenbein, F. Hollmann, W. Kasparek, H. Zohm, V. Erckmann, and M. Weißgerber: Present developments for the 140 GHz transmission system for ECRH on the stellarator W7-X. Proceedings (Eds. T J Parker and S R P Smith), ISBN 0 9533839 0 3 (1998), pp 228-229.

Plaum, B., G. Gantenbein, W. Kasparek, M. Thumm, and D. Wagner: Mode conversion due to s-bend deformation of an oversized HE11 waveguide. Proceedings (Eds. T J Parker and S R P Smith), ISBN 0 9533839 0 3 (1998), pp 128-129.

Wagner, D., M. Thumm, and W. Kasparek: Calculation of eigenmode mixtures in oversized corrugated rectangular waveguides. Proceedings (Eds. T J Parker and S R P Smith), ISBN 0 9533839 0 3, (1998), pp 407-408.

20th Symposium on Fusion Technology (SOFT), Marseille, France, September 7-11, 1998

Erckmann, V., T. Geist, H. P. Laqua, M. Weissgerber, L. Empacher, W. Förster, G. Gantenbein, W. Kasparek, G. Müller, P. G. Schüller, and K. Schwörer: ECRH system for the W7-X stellarator. Proceedings (Eds. B. Beaumont, P. Libeyre, B. de Gentile, G. Tonon, Association EURATOM-CEA, Cadarache, France), Vol. 1, pp 299-302.

Gantenbein, G., L. Empacher, V. Erckmann, F. Hollmann, W. Kasparek, M. Weißgerber, and H. Zohm: Simulations and experiments on a multibeam waveguide ECRH transmission system. Proceedings (Eds. B. Beaumont, P. Libeyre, B. de Gentile, G. Tonon, Association EURATOM-CEA, Cadarache, France), Vol. 1, pp 423-426.

Müller, G. A., W. Förster, V. Erckmann, and H. Laqua: High voltage regulator for power modulation of a gyrotron with voltage depressed collector. Proceedings (Eds. B. Beaumont, P. Libeyre, B. de Gentile, G. Tonon, Association EURATOM-CEA, Cadarache, France), Vol.1, p. 877.

6th IAEA Technical Committee Meeting on H-mode Physics, Kloster Seeon, Germany, September 22-24, 1998

Zohm, H., Guest Editor of the collected papers in the special issue of Plasma Phys. Contr. Fusion **40** (1998) 531-861.

17th IAEA Fusion Energy Conference, Yokohama, Japan, October 19-24, 1998

Zohm, H., G. Gantenbein, S. Günter, F. Leuterer, M. Maraschek, J. P. Meskat, A. G. Peeters, W. Suttrop, D. Wagner, and Q. Yu: First experiments on neoclassical tearing mode stabilisation by ECCD in ASDEX Upgrade.

Workshop on Active Control of MHD Modes in Toroidal Devices, General Atomics, San Diego, November 22-24, 1998

Gantenbein, G.: Active control of neoclassical tearing modes by ECCD in ASDEX Upgrade.

DIPLOMA THESES

Klenge S.: Hochauflösende Emissions -und Absorptionsspektroskopie an Silizium in Randschichtplasmen. (High resolution emission and absorption spectroscopy on Silicon in plasma boundary layers.)

Schneider W.: Spektroskopische Untersuchungen an Molekülen zur Diagnostik einer Hochfrequenz-Plasmaquelle. (Spectroscopic investigations on molecules for the diagnostics of a RF plasma source.)

REPORTS

Barth, K.-L., K. Hirsch, and A. Lunk: In situ Diagnostik von Hitzeverbundwerkstoffen im Plasmawindkanal. Report IPF 3/98, Institut für Plasmaforschung, Universität Stuttgart, Germany.

Dodel, G.: On the history of far-infrared lasers: Thirty-five years of research and application. Report IPF 4/98, Institut für Plasmaforschung, Universität Stuttgart, Germany, submitted to Infrared Phys. Technol. (in print).

Hirsch, K., B. Roth, K.-L. Barth, H. Jentschke, A. Lunk and U. Schumacher: Plasma induced SiO_2 like protection layer formation on C/C-SiC heat shield materials for reentry vehicles. SFB-Report 1998/43, Institut für Plasmaforschung, Universität Stuttgart, Germany, submitted for publication in High Temperatures - High Pressures.

Hirsch, K., B. Roth, H. Jentschke, S. Klenge and U. Schumacher: Optical investigation of simulated reentry flows. SFB-Report 1998/44, Institut für Plasmaforschung, Universität Stuttgart, Germany, to be published.

SEMINAR TALKS

Dodel, G.: On the history of far-infrared lasers: Thirty-five years of research and application. Colloquium on Sources, Detectors, and Instruments in the FIR-Region, Institute of Space Sensor Technology, DLR, Berlin, October 2, 1998

Schumacher, U.: Hochauflösende Spektroskopie für Plasmatechnologie und Fusionsforschung. Universität Hannover, October 28, 1998

Schumacher, U.: Entwicklungsstand und Probleme des Fusionsreaktors. Elektrotechnisches Kolloquium, Universität Stuttgart,November 3, 1998

Zohm, H.: Active control of neoclassical tearing modes by ECCD in ASDEX Upgrade. Seminar, Association EURATOM-CEA, Centre d'Etudes Nucléaires de Cadarache, St. Paul lez Durance, France, October 7, 1998

Zohm, H.: Active control of neoclassical tearing modes by ECCD in ASDEX Upgrade. Seminar, Fukui University, Japan, October 26, 1998

How to reach
Max-Planck-Institut für Plasmaphysik, Garching

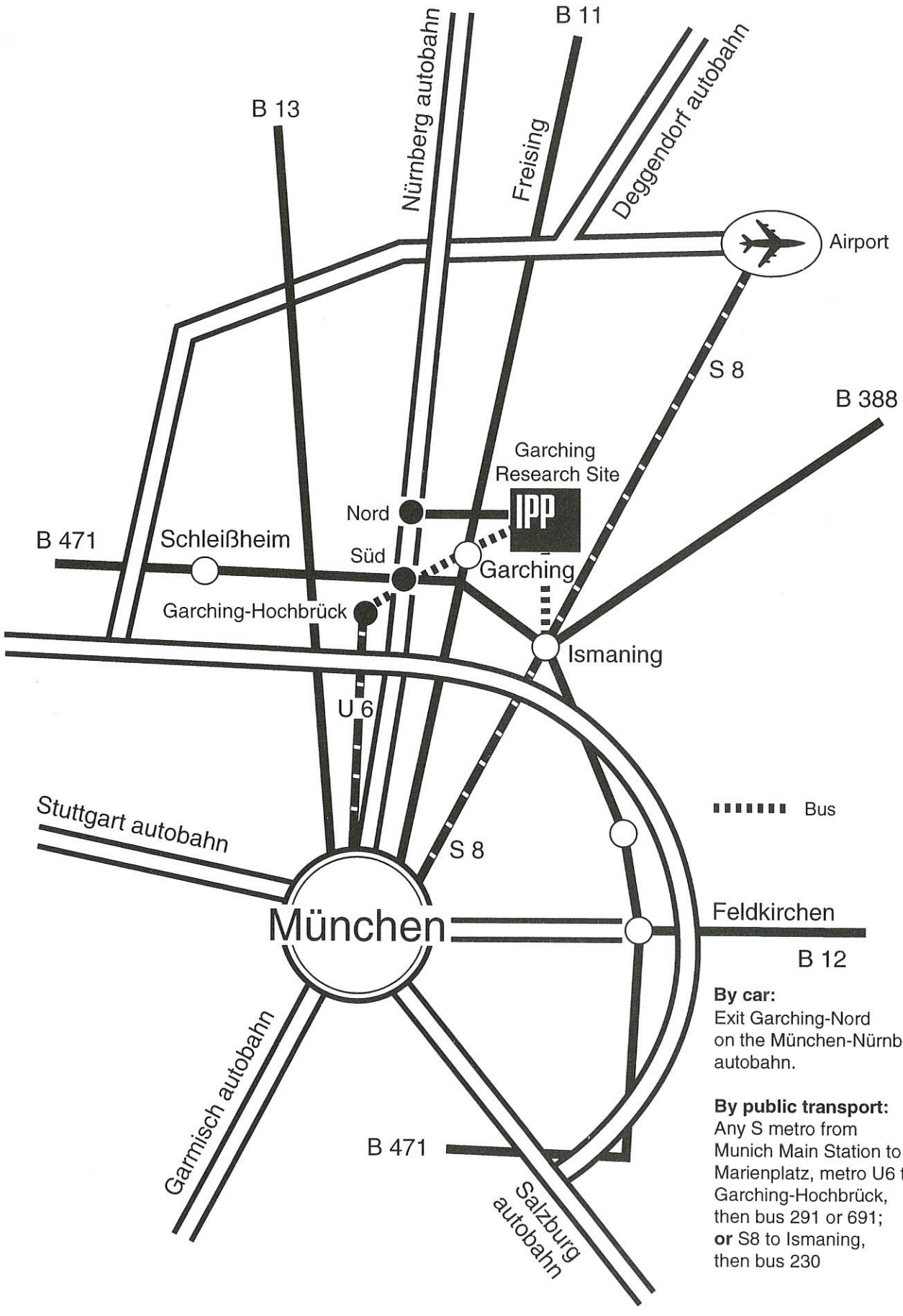

By car:
Exit Garching-Nord on the München-Nürnberg autobahn.

By public transport:
Any S metro from Munich Main Station to Marienplatz, metro U6 to Garching-Hochbrück, then bus 291 or 691; **or** S8 to Ismaning, then bus 230

How to reach Greifswald Branch Institute of Max-Planck-Institut für Plasmaphysik

Greifswald Branch Institute of
Max-Planck-Institut für Plasmaphysik
Walther-Rathenau-Strasse 49a
("Biotechnikum")
D-17489 Greifswald

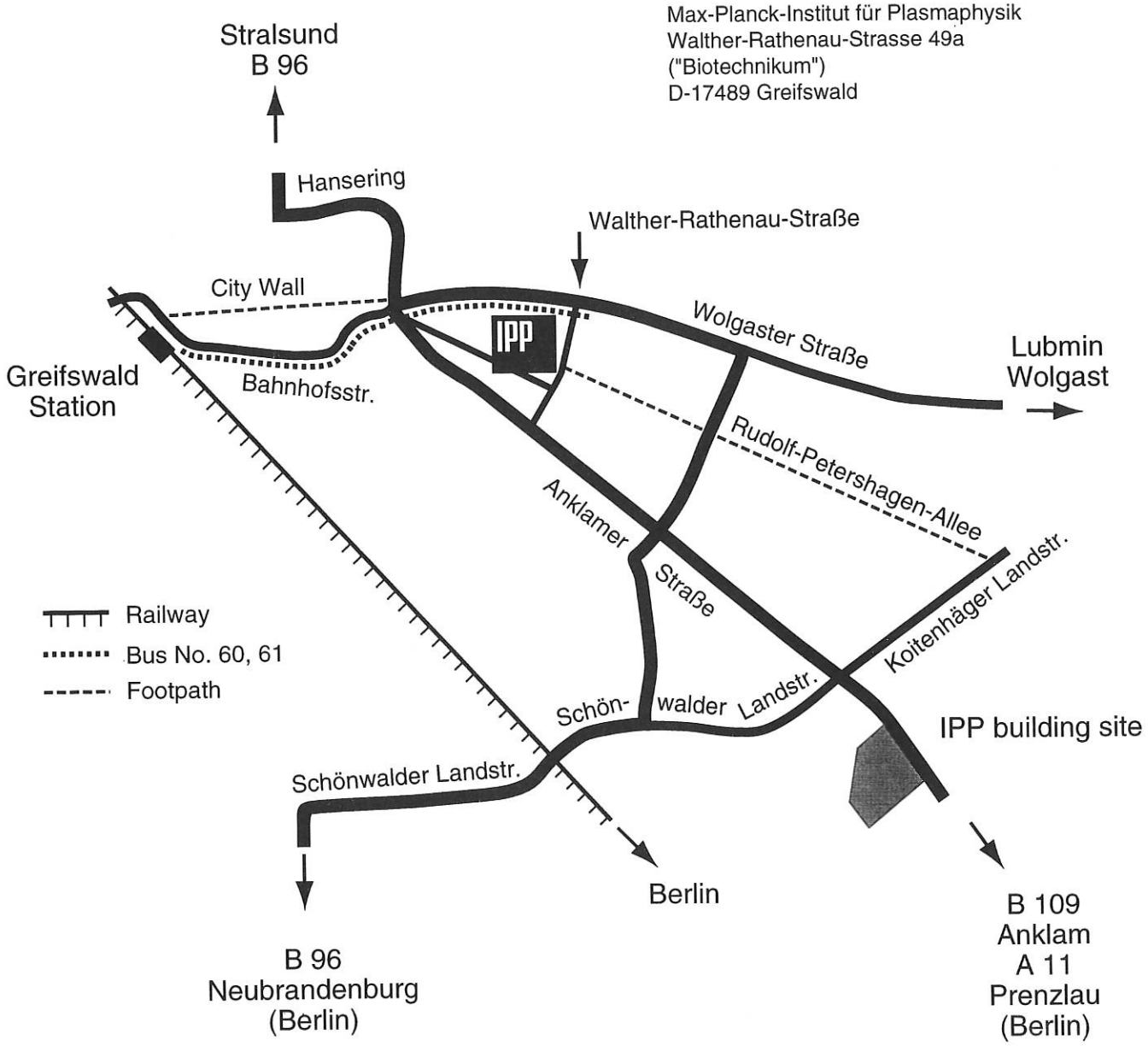

By air:
Via Berlin: from Berlin Tegel Airport by bus No. X9 to Zoologischer Garten, S-Bahn to Lichtenberg Station, by train to Greifswald **or**
Via Hamburg: from the airport to Main Railway Station, by train to Greifswald.

By car:
Via Berlin, Neubrandenburg to Greifswald **or** via Hamburg, Lübeck, Stralsund to Greifswald, in Greifswald follow the "Biotechnikum" signs.

By bus:
From Greifswald Railway Station by bus No. 60 or 61 to the "Am St. Georgsfeld"s stop.

On foot:
From Greifswald Railway Station 30 min by footpath on the City Wall (Stadtwall).

ANNUAL REPORT 1998

Max-Planck-Institut für Plasmaphysik (IPP) • 85748 Garching bei München
Telephone (0 89) 32 99-01 • Telefax (0 89) 32 99-22 00

Printing: Steinmeier, Nördlingen

Printed in Germany
ISSN 0179-9347

This work was performed under the terms of the agreement between Max-Planck-Institut für Plasmaphysik and the European Atomic Energy Community to conduct joint research in the field of plasma physics.

Max-Planck-Institut
für Plasmaphysik